BINARY SYSTEMS IN THE INFRARED

Eugenia Antonopoulou

B.Sc., M.Sc. (University of Athens)

Doctor of Philosophy

University of Edinburgh

1981

This thesis has been composed by me and consists entirely of my own work, except where specifically indicated in the text.

TABLE OF CONTENTS

ABSTRACT

Near infrared (JHKL) photometry of RS CVn-type binary systems has been carried out to search for any evidence of circumstellar material in these systems and also for the existence of light variations outside eclipse similar to those observed in the visual. No apparent infrared excess has been observed in fourteen randomly selected systems.

Infrared light curves of seven RS CVn binaries (HR 1099, UV Psc, SZ Psc, TY Pyx, AD Cap, HD 5303 and ER Vul) have been obtained, and nearly sinusoidal light variations outside eclipse have been detected for at least HR 1099, SZ Psc and TY Pyx. Irregular light variations have also been observed in the infrared as in the visual, and also a variation of the maximum brightness of HR 1099 and UV Psc. An estimate of the spectral types of the components of the seven extensively observed systems has been made using the current photometric data.

Taking into account the current and other observations, possible models have been discussed, with a preference for the spot model.

The active component has been shown to be a fast rotator.

Another part of this dissertation is near infrared photometry of Wolf-Rayet stars. The most interesting result of these observations was the discovery of an increase in brightness of HD 193793 (WC7+05) by $2^{m}.4$ in L' (λ_o = 3.8 μm) between June 1976 and August 1977. This has been attributed to the condensation of grains in the star's circumstellar shell.

CHAPTER I

INFRARED PHOTOMETRY

1.1 Infrared Wavelength Ranges

The infrared region of the electromagnetic spectrum covers the extensive wavelength range from the visual to radio wavelengths. For astronomical purposes it is convenient to divide the infrared spectrum into four regions. The division is based on the use of different observational techniques and on atmospheric limitations.

The region extending from visible wavelengths to 1 μm is known as the "photographic infrared region" or "Herschel" region for which it is possible to use photographic emulsions and image tubes. For wavelengths longer than 1 μm all the observations are based on photometry and photodetectors or bolometers must be used. Between 1 μm and 35 μm there are a number of atmospheric windows through which observations may be made from gound-based telescopes. This region is divided into two according to the different observational techniques used. Between 1 μm and 5 μm photoconductive (PbS) and mainly photovoltaic detectors at liquid nitrogen temperature are used. Bolometers may also be used but they are not as sensitive as the photodetectors at these wavelengths. From 5 μm to 35 μm bolometers, operating at liquid helium temperature, are used as detectors. Recently the use of intrinsic photoconductors extended up to 14 μm, while impurity photoconductors can be used for observations up to 24 μm.

Between 35 μm and 500 μm infrared observations are impossible from ground-based observatories and they are usually made using

airborne telescopes. Ground-based observations have been made only from dry and very high altitude sites through the partially transparent atmospheric windows at 346 μm and 460 μm. These windows are very sensitive to water vapour fluctuations, thus the observations are very difficult; ground-based observations at these wavelengths are however very important because they provide a link between the short-wavelength, high-resolution (a few arc seconds) ground-based observations and the long-wavelength, low-resolution (less than one are min) observations made from the air.

Longward of 500 μm ground-based observations are again possible, but they have been almost neglected. It is not yet very clear whether infrared or microwave instruments will be predominant in this region. In the present work the terminology "near infrared" is used for the 1 μm to 5 μm region.

1.2 Historical Review

The infrared region of the electromagnetic spectrum was discovered by Sir William Herschel, when he used a simple thermometer and prism to observe the infrared spectrum of the Sun. He published his work in a series of four papers in 1800.

The infrared technique was greatly improved in 1831 by L. Nobili and M. Melloni who introduced the thermocouple as a receiver of infrared radiation. The Astronomer Royal for Scotland, Piazzi Smyth (1858), made the first infrared observations in 1856 from an altitude of 2717 m on Tenerife, using the available thermocouple, which was developed by Nobili and Melloni. He was just able to detect the full Moon.

At the end of the 19th century S.P. Langley developed the first bolometer and so we have the first observations of the Sun and the Moon using bolometers and thermocouples operating at ambient temperature. More astronomers became involved in infrared observations (e.g. Rosse (1869) measured the Moon through its phases, Pettit and Nicholson (1928) made infrared observations of the Moon and of some bright stars). But until recent times infrared observations were very limited because of the lack of sensitive detectors and cryogenic techniques.

During and after the second world war there was rapid technological development in infrared astronomy, as in many fields. Kuiper et al. (1947) first used the lead sulphide (PbS) photoconductive detector for astronomical purposes, with which they observed the planets and some bright stars. At about the same time Golay (1947) published details of a new detector which is still used extensively in laboratory infrared work. In 1951 Fellgett developed and used the lead sulphide detector for stellar photometry.

In the early 1960's the development of cooled photoconductive and bolometric detectors and of cryogenic technology enabled astronomers to extend their observations to different objects at longer wavelengths in the infrared spectrum and to find and detect new faint sources. Helium cooled germanium bolometers were first developed for astronomical purposes by Low (1961). After the development of these bolometers infrared photometry extended to 10 and 20 μm (Low and Johnson 1964).

Another big step in infrared technology was the development of the indium antimonide (InSb) detector by Johnson (1962) who used this

detector, which was less sensitive than PbS at that time, in order to extend his photometry to longer wavelengths making observations through the 5.0 μm waveband established by him.

During the last twenty years there has been a rapid development of infrared astronomy. To a great extent this development is due to the advance of infrared detectors and the development of the required photometric techniques. Infrared techniques are continuously improving and the most sensitive detectors today enable astronomers to obtain accurate observations and to extend their data to even fainter limits. An indication of the sensitivity achievable today is given by the 3σ limit of $K \sim 17$ reached on the 3.8 m U.K. Infrared Telescope in 30 minutes' integration (Brand 1980, personal communication).

1.3 A Brief Discussion of the Present Available Infrared Photometric Instrumentation

Infrared instrumentation and techniques available at present for astronomical purposes have been widely discussed in a series of papers (e.g. Humphrey 1965; Low and Rieke 1974; Gillett, Dereniak and Joyce 1977; Lena 1978; Soifer and Pipher 1978; Barton and Allen 1980 and references therein). Quite a few books also give information about infrared detectors and associated apparatus (infrared filters, windows, beam splitters, cryogenics, electronics associated with infrared photometers), for instance "The Infrared Handbook" edited by Wolfe and Zissis (1978).

So in this section it is not intended to give an extensive description of infrared instrumentation and techniques but only to

discuss some aspects of an infrared photometer which will be useful for the discussion in Chapter III of the instruments used for the observations of this work.

1.3.1 A Brief Description of an Infrared Photometer

An infrared photometer consists mainly of two parts: (A) the optics and (B) the electronics.

A. The optics

1. Main photometer. Figure 1.3.1 shows the main body of an infrared photometer with a vibrating mirror chopping mode. The main photometer consists of: the chopping mechanism, which is discussed later in this section, the eyepiece, the wide angle eyepiece and the offset guider (in some cases). The main body of the photometer also has a mounting flange for the dewar-cryostat mounting.

2. The dewar. This consists of: (a) The container of the coolant (e.g. liquid nitrogen), which is isolated from the ambient temperature by a vacuum. (b) In good thermal contact with the container of the cryogenic liquid is a metal base on which the detector is mounted. On the same metal base are also (c) the filter wheel which is mounted on the filter assembly (d) the aperture slide or wheel and usually (e) a light pipe connecting the "window" with the filter assembly. (f) The window, which should be transparent in the infrared wavelength is made usually from zinc selenide, potassium bromide, sapphire, calcium fluoride, etc.

B. The electronics

1. The preamplifier. This is a current amplifier connected to the detector with its first stage mounted on the cold surface.

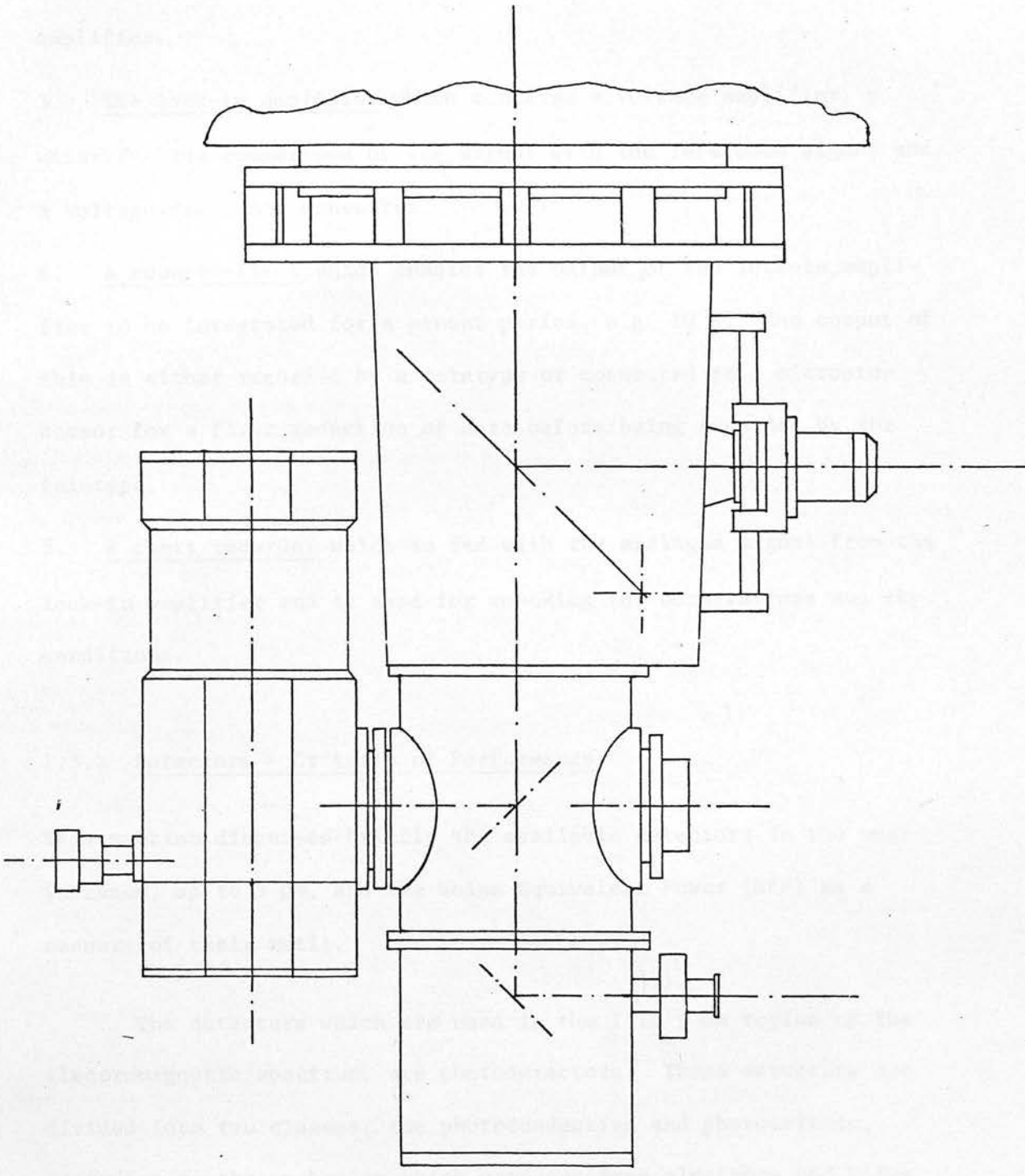

Figure 1.3.1 The main body of an infrared photometer with a vibrating mirror chopping mode (from the "Operating Notes" for the Greek photometer 1976)

2. The vibrator mirror servo loop which moves and controls the chopping mirror and provides the reference signal to the lock-in amplifier.

3. The lock-in amplifier which contains a voltage amplifier, a mixer for the comparison of the signal with the reference signal and a voltage-frequency converter.

4. A counter-timer which enables the output of the lock-in amplifier to be integrated for a preset period, e.g. 10 s. The output of this is either recorded by a teletype or connected to a microprocessor for a first reduction of data before being recorded by the teletype.

5. A chart recorder which is fed with the analogue signal from the lock-in amplifier and is used for checking the observations and sky conditions.

1.3.2 Detectors - Criteria of Performance

This section discusses briefly the available detectors in the near infrared, up to 5 μm, and the Noise Equivalent Power (NEP) as a measure of their merit.

The detectors which are used in the 1 to 5 μm region of the electromagnetic spectrum, are photodetectors. These detectors are divided into two classes, the photoconductive and photovoltaic, according to the mechanism which produces free electrons and holes. The operational characteristics of these detectors, their electrical properties in a wide range of frequency, temperature and background conditions are discussed in a number of articles (Humphrey 1965; Hall et al. 1975; Gillett et al. 1977 and references within these articles).

In the photoconductive detectors, when radiation of an appropriate wavelength falls on a photoconductor, it is absorbed, creating electron-hole pairs, and so the electrical conductivity changes, in other words the incident radiation causes the resistance of the detector to decrease. In these detectors, the free carriers are separated by a drift to the contacts under the influence of an externally applied field. The spectral response of a photoconductive detector depends on the energy gap, E, between the valence and the conduction band and it has a long wavelength cut off at $\lambda = \frac{hc}{E}$. Sometimes impurities are introduced in the semiconductive material in order to reduce the energy gap E and so photons with lower frequency become detectable. Because thermally excited carriers can change the conductivity of photoconductive detectors it is necessary to cool them below the temperature $T = \frac{E}{k}$, where E is the bandgap energy and k Boltzmann's constant, in order to reduce the number of thermally produced photons.

Until recently the most commonly used detector in the near infrared was lead sulphide (PbS), an intrinsic photoconductor. At liquid nitrogen operating temperature the usable response extends as far as 4.3 μm. An extensive discussion of the PbS detector, its electrical and photoconductive properties in a wide range of frequency, temperature and background conditions is given by Humphrey (1965).

The photovoltaic detector is a p-n junction area within the body of a semiconductor. In these detectors, when the incident radiation, with photons of wavelength sufficiently short to cause intrinsic excitation, falls on them it is absorbed by a very thin layer of the

order of 1 μm thick and produces hole-electron pairs. The photo-excited carriers diffuse towards the p-n junction where they are separated by the junction field. The measurable effect is a current change at zero-bias voltage, or a voltage change at zero current. Both of these are proportional to the number of incident photons per second and the quantum efficiency of the semiconductor. The spectral response of these detectors is set by the energy gap E, between the conduction and valence bands (photons with frequency $\nu > \frac{E}{h}$ can be detected and the detector temperature must be below E/k in order to avoid thermally produced photons).

At the present time the indium antimonide (InSb) detector, an intrinsic photovoltaic detector, has almost replaced the PbS photo-conductor for astronomical applications in the near infrared. In the absence of radiation, such a detector has the electrical characteristics of a normal diode. Incident radiation liberates carriers which are separated in the electrical field internally generated in the diode junction. The InSb detector has a high quantum efficiency ($n \cong 0.7$) at liquid or solid nitrogen temperatures (Gillet et al. 1977), and a long wavelength response limit of ~ 5.5 μm, as its energy gap is 0.23 eV at liquid nitrogen temperature. So this detector has the advantage of being usable at even longer wavelengths in the near infrared than the PbS detector. Another advantage of the InSb detector is that it is the fastest available detector in the near infrared.

Though the InSb detector was developed for use in infrared astronomy almost twenty years ago (Johnson 1962) and the advantages

of this detector were known, it only recently became extensively used among infrared astronomers after the optimisation of detector parameters and the development of new preamplifiers (Hall et al. 1975; Barton and Allen 1980) improved their sensitivity to the point where InSb is not only competitive with, but better than, the best PbS detectors.

The InSb detector is operated in the zero bias mode, so no current noise exists and the only noise the detector produces is Johnson noise. The equivalent current generator for the detector Johnson noise is

$$i_{Dn} = (4kT\Delta f)/R \qquad 1.3.1$$

where k is Boltzmann's constant, T is the operating temperature in K, Δf is the noise bandwidth and R_D is the impedance of the detector. Equation 1.3.1 implies that the Johnson noise is reduced when the impedance is increased. In order to improve the detector's impedance we briefly irradiate the detector with an intense light, usually through the J filter (this is discussed in Chapter III). Further noise reduction is achieved by lowering the operational temperature, by pumping on the liquid nitrogen or by using liquid helium instead (the latter however introduces difficulties by reducing the long wavelength response of the detector).

For an InSb detector the product of the detector area times the resistance is constant. The minimum size which has been achieved is as small as 0.1 mm while at present $R_DA \cong 2 \times 10^6\ \Omega\ cm^2$ at 77 K can be obtained. This yields a value of $2 \times 10^{10}\ \Omega$ for the impedance. By decreasing the detector's temperature, after pumping the liquid nitrogen and by "flashing" with 1.2 μm radiation for several

minutes, higher values of the impedance can be obtained and it becomes so high (up to 10^{12} Ω) that noise is determined by the feedback resistor which requires improvement of premplifiers.

1.3.3 Figures of merit of available detectors

The most widely used figure of merit of a detector, which is a measure of the minimum detectable signal capability from it, is the Noise Equivalent Power (NEP). Noise Equivalent Power is defined as the radiant power incident on the detector that produces a rms signal equal to the rms noise in 1 Hz electrical bandwidth. It follows from the definition of NEP that the merit of a detector increases as the NEP decreases. For astronomical purposes the most relevant basis for comparison is the minimum value of NEP under identical background conditions. So, in order to have meaningful comparison of several detectors the NEP must be measured under conditions as close as possible to the actual conditions under which the detectors will operate, namely, low background conditions and large f/number. The detector's NEP for a particular set of measurement conditions, is given by the equation:

$$\text{NEP} = \frac{F}{S/N(\Delta f)^{\frac{1}{2}}}$$

where F is the power incident on the detector, S/N is the signal-to-noise ratio, and Δf the electrical bandwidth through which the noise is measured.

Experimentally the NEP can be determined by measuring, for a known radiant input, the signal-to-noise ratio, where the signal is taken as the signal voltage and the noise as the noise voltage, in a

narrow electrical bandwidth. Then by extrapolation we find the power needed to give a signal-to-noise ratio equal to unity. In order to minimise the noise variations within the frequency interval over which the noise is measured, the amplifier bandwidth must be made as narrow as is practical.

For most detectors the NEP is proportional to the square root of the area of the detector. The detector sizes which have been achieved are as small as 0.1 mm (Soifer and Pipher 1978). Because for most detectors the NEP depends on the size of the detector another factor of merit has been introduced which removes the need to specify the area of the detector. This factor is known as D* or specific detectivity. This factor is the reciprocal of the NEP for a detector having unit area and used with an amplifier having a band-width of 1 Hz. So

$$D^* = A^{\frac{1}{2}}(NEP)^{-1} \quad (\text{cm Hz}^{\frac{1}{2}}/\text{Watt})$$

where A is the area of the detector measured in cm^2. But, as has been mentioned before, the NEP of different detectors is not strictly proportional to the area of the detector over the range of interest. So the use of D* as a factor of merit independent of the detector area may be misleading. For this reason the commonly used figure of merit for specified detectors is the NEP. Usually the NEP is followed by three numbers: the first gives the reference temperature of the detector (usually the operating temperature), the second the centre chopping frequency and the third the electrical bandwidth.

The NEP as a factor of merit of a detector has been introduced previously. A better specified factor is the NEP of the system used, including detector, filters, telescope, atmospheric conditions. This factor is given by the relation:

$$\text{"system NEP"} = 10^{-(10 + 0.4K)} D^2 \sqrt{2T} / \sigma$$

where K is the measured magnitude at 2.2 μm waveband in total integration time T when the S/N ratio is σ and the diameter of the telescope used is D in metres. As an example of the order of magnitude of a "system NEP" the figure of merit is given for the Kitt Peak system, with high-impedance Santa Barbara InSb detector, pumped LN_2 and flashed, on the 1.3 m telescope which is 3.3×10^{-16} W $Hz^{-\frac{1}{2}}$ (Smyth 1980, personal communication).

1.3.4 The chopping device and the nodding device - advantages and disadvantages of the available chopping systems

As will be mentioned in section 1.4 the sky is very bright in the infrared and typical sky radiation can be many orders of magnitude more intense than the majority of the observed objects. Thus a telescope, looking at a source, collects not only the photons coming from the source, but also the fluctuating power due to atmospheric emission. The cancellation of this emission is normally achieved by the chopping device. By means of this a signal from the source and the surrounding background and a signal from a nearby patch of sky are presented alternately to the detector and their difference is measured electronically. To reduce effects due to time sky variations a very high chopping frequency is desirable; however the S/N ratio of InSb detectors is optimised at some low frequency, which in practice dictates the chopping frequency. The separation of the two beams (source + sky, sky) should be as small as possible as this reduces the positional sky variation. It must be pointed out here that the chopping mechanism has been introduced in the infrared not

only for the cancellation of the continually changing sky emission, but also because an alternating signal can be more easily amplified than a direct one, and also because some detectors are better at detecting an alternating signal.

There are four mechanical techniques available for producing the chopped signal: one is by wobbling the secondary mirror and three are by using focal plane choppers. The focal plane choppers are the rotating segmented mirror, the vibrating single mirror, and the two-mirror vibrator. The advantages and disadvantages of these mechanisms for chopping infrared radiation are given in Table 1.3.1.

By applying the chopping device in the infrared observations the correction of the signal from the bright background would be accurate enough if the brightness of the background surrounding the star and of the nearby patch of sky were the same. But it is known that a gradient of the sky brightness may exist. That is why the nodding technique has been adopted. According to this, the telescope is moved back and forth, looking at two different patches of the sky (at two positions opposite to the source) minimising in this way the error introduced by the sky brightness.

1.4 Atmospheric transmission and emission - photometric bands

Ground-based observations are limited to several atmospheric "windows" because of atmospheric absorption and emission. The atmospheric attenuation of the signal is due primarily to the molecular absorption bands of H_2O vapour and CO_2, with minor contributions due to O_3, CO, N_2O and CH_4. The atmospheric transmission thus depends

TABLE 1.3.1

Available Chopping Systems

Type	Advantages	Disadvantages	References
Wobbling secondary	One reflection less, minimisation of flux loss, lower background. Uniform reflecting surface. No defocussing.		Low and Rieke 1974
Rotating segmented mirror	Large throws, suitable for observations of extended sources.	Non-uniform reflecting surface. High Background signal noticeable in longer wavelengths. Necessity of offset guider.	Becklin and Neugebauer 1968
Vibrating mirror	Uniform reflecting surface. Low background signal	Microphonics. Small throw. Problems of the vibrating system. Probable absorption at J and H, if dichroic. Defocussing.	Glass 1972a; Fahrbach et al. 1974
Two-mirror chopper	High frequencies with low mechanical power. Less mechanical problems. No focussing errors.	One extra reflection; beam moves across one of the mirrors during chopping.	Jorden, Long, MacGregor and Selby 1976

both on the weather conditions and on the site, attenuating the flux and limiting the observation to "window" regions. But the atmosphere does not only absorb the infrared radiation: another difficulty is the strong emission of the earth's atmosphere at these wavelengths. It has been found that in 1 μm bandwidth at 10 μm we collect from an area of the sky 5 arc seconds in diameter, a few nanowatts of radiation (and also a similar amount from the telescope). For comparison note that from an A0 star of zero magnitude we collect less than 10^{-11} Watt; three orders of magnitude down. The brightness (magnitude) versus the wavelength is given by Lena (1978).

Most emission of the sky is caused by H_2O, O_3 and CO_2. The emission from the ozone is independent of the altitude because ozone is distributed to very high altitudes in the atmosphere, somewhere about 30 km, but the emission from CO_2 decreases rapidly with increasing altitude. The atmospheric emission is however not a serious problem for observations at wavelengths shorter than 4 μm. The emission of the sky is not uniform. The non-uniform emission of the sky and atmospheric turbulence are responsible for fluctuations of the background radiation and give rise to a varying signal which is known as "sky noise". This is in addition to the photon noise of the "sky" background. One way to almost cancel the "sky noise" is to compare rapidly the emission of two very close sky "patches". This is the basis of the observing technique in the infrared known as chopping (discussed in section 1.3.3). If we do the chopping very fast the source moves in and out of the beam while the sky emission remains constant. A better result is achieved by operating in the two beam mode (nodding device).

As has been discussed before, ground-based infrared observations are made in the available atmospheric windows. For photometric observations the photometric bands have therefore been selected to match the regions of maximum atmospheric transmission. The photometric designations of the infrared windows, according to Johnson (1964), are I (λ_o = 0.9 μm), J (λ_o = 1.25 μm), K (λ_o = 2.2 μm), L (λ_o = 3.4 μm), M (λ_o = 5.0 μm) and N (λ_o = 10.2 μm) where λ_o is the effective wavelength defined as:

$$\lambda_o = \frac{\int_0^\infty \lambda\phi(\lambda)d\lambda}{\int_0^\infty \phi(\lambda)d\lambda}$$

where $\phi(\lambda)$ can be the product of the filter response function, the atmospheric transmission, windows, and the detector response. To a first approximation the observed flux levels behave like monochromatic flux levels at wavelength λ_o. Today, for the near infrared, the photometric bands J, H (λ_o = 1.65 μm), K and L and sometimes M have been adopted but generally individual observers or groups of observers choose and use their own restricted wavebands. We can say that the K passband with effective wavelength λ_o = 2.2 μm, is almost generally adopted; but the L passband with the Johnson's effective wavelength λ_o = 3.4 μm is not used as widely because the water absorption band has a very uncertain boundary near 3.4 μm. Thus today most infrared observers use filters with passbands with effective wavelengths at 3.6 μm (e.g. Low and Rieke 1974) or 3.8 μm (ROE infrared team).

The N window is a wide window 7.5-14 μm approximately, and it is firstly divided into two sections with designations O and P. Generally it is divided for photometric observations into three or four

parts, which is very useful for the study of dust features (silicate bump at 9.8 μm). The photometric designation for the window with λ_o = 21 μm is Q and Z for the window with λ_o = 35 μm.

1.5 Absolute Calibration - Photometric Standards

In order to give a physical meaning in the photometric measurements, a way must be found to interpret them in terms of absolute physical units. So it is necessary to find a way to estimate the flux of a star of known magnitude. This cannot be achieved directly, because it is not possible to observe through the earth's atmosphere to estimate the flux of, for example, a zero magnitude star, as the atmospheric extinction and the transmission of the telescope are difficult to estimate. Accurate absolute fluxes are available only for some planets at present because their angular diameters are accurately known and measurements which have been made from aircraft are free from atmospheric extinction. The planets are used for absolute calibration in the far infrared. For the near infrared the available absolute calibration is based on different model atmospheres.

Originally Johnson and Morgan (1953) and Johnson (1962) set up the zero points of their magnitude scales on the definition that the colour indices of normal AOV stars are zero. According to them, α Lyr, an AOV star and the basic standard in the near infrared, has zero magnitude at all wavelengths. A more critical examination of photometric results of different AOV stars (Johnson 1965a) showed that their colours differed from the accepted zero value. Johnson

(1965b) then established another way to calibrate his photometry. He measured the colours of different GV stars (similar to the Sun) at wavelengths up to 3.4 μm and estimated the average colours. He established his absolute calibration by accepting these colours as colours of the Sun and by using the available solar radiation data and the visual magnitude of the Sun.

Thomas et al (1973) introduced their infrared calibration by assuming that α Lyr is well represented by a model described in Schild et al. (1971). Then they normalised the measured V flux of α Lyr in order to have zero magnitudes at all wavelengths.

Low and Rieke (1974) revised Johnson's calibration on the basis of new data. The most important part of their work was the extension of the observations of GV stars to longer wavelengths, that is to the M and N wavebands. This permits a more accurate application of the method introduced by Johnson, which was discussed earlier in this section. Low and Rieke did not extend Johnson's method to obtain absolute calibration at Q waveband also, because the fluxes of the comparison stars were very small at this waveband.

Other workers have given absolute calibrations (Lee 1970; Gillett, Merrill and Stein 1972) which differ from one to the other. In connection with absolute calibration systems, several magnitude scales are available for comparison. As we mentioned before, the calibration systems introduced under different assumptions, differ among themselves. This causes uncertainty in the values of the standard stars in the infrared. Many observers established their own

magnitude scales, and it is worth mentioning here some photometric work on standard stars such as that done by Johnson et al. (1966), Lee (1970), Gehrz et al. (1974) in the Northern hemisphere and Glass (1974) and Thomas et al. (1973) in the Southern hemisphere, which are tied to Johnson's system. For the work presented here, Johnson's photometric standards have been used for the observations of the Northern hemisphere and Glass's (1974) for the Southern hemisphere as the other available system for southern standards by Thomas et al. is not accurate enough for near infrared photometry because they used a bolometer for their observations. The H and L' magnitudes of the standards were obtained by interpolation.

1.6 Infrared Surveys

At infrared wavelengths the sky has to be surveyed by scanning because imaging detectors are not yet available for $\lambda > 1$ μm. The first to make an infrared survey were Neugebauer and Leighton (1969). They undertook a survey of the Northern sky at 2.2 μm. This ground-based survey took them approximately six years to complete. "The Two-Micron Sky Survey" (NASA SP-3047), as it is called was published in 1969. It contains 5612 objects, all brighter than magnitude 3 at 2.2 μm with declinations between -33° and +80° and covers about three quarters of the sky. The objects are listed by 10° declination zones. Approximately one third of the sources are visible to the naked eye.

At the same time Price (1968) began a similar survey of the Southern sky, between -30° and -52° in declination. In his paper

"Results of an Infrared Stellar Survey" in 1968, he published a partial survey of 414 sources.

In 1976 Price and Walker published the "AFGL Four Color Infrared Sky Survey: Catalog of Observations at 4.2, 11.0, 19.8 and 27.4 μm" (AFGL TR-76-0208). This is a Rocket-borne Infrared Sky Survey and it contains 2363 sources detected in one or more of the survey colours and covers 90 percent of the celestial sphere at 11.0 μm. The catalogue is complete down to limiting magnitudes of [4.2] ≃ +1.3, [11.0] ≃ -1.1 and [19.8] ≃ -3.1. The observations were made during 1971 and 1974 in nine successful flights using a small cryogenically cooled telescope from above the atmosphere. This survey was conducted by the Air Force Geophysics Laboratory. This is an extended catalogue of the one which was carried out by the Air Force Cambridge Research Laboratory (Walker and Price 1975).

At wavelengths greater than 30 μm only a small part of the sky has been surveyed. A survey has been carried out at 100 μm, containing 72 sources (58 of which had not been previously detected). This survey covered 750 square degrees, most of the galactic plane, and was published in 1971 by Hoffmann, Frederick and Emery. The observations were made with a balloon-borne, 12-inch (30.5 μm) telescope.

Later on (in 1974) another survey with 100 sources was published by Hoffman and Aannestad. This survey is also at 100 μm. Recently (1978), Schnitz, Brown, Mead and Nagy published a Merged Infrared Catalogue (MIRC) which is a compilation of equatorial coordinates, spectral types, magnitudes and fluxes from five catalogues of infrared observations. It contains 11201 observations and is a record of all infrared observations from 1 μm to 100 μm of non-solar system

TABLE 1.6.1

Infrared Surveys

Catalogue	Wavelength (μm)	Type of observation	No. of objects	Author	Reference
Results of an Infrared Stellar Survey	2.2	ground-based	414	Price	1968, Astron. J. 73, 431
Two-Micron Sky Survey	2.2	ground-based	5612	Neugebauer and Leighton	1969, NASA SP-3047
100-Micron Survey of the of the galactic plane	100	balloon-borne survey	72	Hoffmann, Frederick and Emery	1971, Ap. J. 170, L89
	100	balloon-borne	100	Hoffmann and Aannestad	1974, NASA TMX-62, 367
AFCRL Infrared Sky Survey	4, 11, 20	rocket-borne		Walker and Price	1975, ARCRL-TR-95-0373
AFGL Four Colour Infrared Sky Survey	4.2, 11.0, 19.8, 27.4	rocket-borne survey	2363	Price and Walker	1976, AFGL-TR-76-0208
Merged Infrared Catalogue (MIRC)			11201	Schmitz, Brown, Mead and Nagy	1978, MIRC

objects. This Merged Infrared Catalogue was published by the National Aeronautics and Space Administration, Maryland. More comprehensive infrared surveys will be available in the coming decade from satellite data, for instance, the survey which will come from the Netherlands/United States/United Kingdom Infrared Astronomy Satellite (IRAS) project discussed by Aitken (1978). In Table 1.6.1 the best-known available Infrared Catalogues are summarised.

1.7 Principal Mechanisms Responsible for the Generation of Infrared Excess Flux

A star has excess radiation in a given infrared photometric band, if its radiation in this wavelength interval is above the radiation intensity expected from a blackbody with effective temperature corresponding to the star's spectral type. Many such objects have been detected in a wide variety of types, from cool carbon and M stars to O stars and HII regions, and a wide range of values of excess infrared radiation has been found. Neugebauer et al. (1971) in the first review article to appear on infrared sources, give an idea of the different objects which show excess at infrared wavelengths, while Allen (1975) in his book "Infrared, the New Astronomy", summarises the results of infrared observations of galactic and extragalactic sources up to the year 1975.

Generally speaking, there are two possible sources of infrared excess: first a circumstellar shell (this is extensively discussed later) and second a cool companion (Humphreys and Ney 1974a,b; Lockwood et al. 1975; Humphreys 1976) in the case of binary or multiple systems. In this section the principal mechanisms responsible

for the generation of infrared excess in the case of circumstellar shells, are discussed.

1.7.1 Thermal reradiation of starlight by a circumstellar shell

From the literature it is obvious that the most common mechanism producing infrared excess is thermal radiation from a circumstellar dust shell. Celestial objects with circumstellar dust shells emit at the infrared wavelengths, because the dust grains in the shell absorb the starlight, heat up, and re-emit the radiation at longer wavelengths.

Different objects, young or old, may have dust shells around them. The origin of the dust is different for different objects. In some cases, mass loss from the star is the origin of the dust shell. Thus dust shells may be formed from material ejected from central stars (Hyland et al. 1969; Geisel 1970; Burbidge and Stein 1970; Gehrz and Woolf 1971). In other cases, the shell may be the remnant of a protostellar dust cloud. Thus for many O, B and T Tauri stars which are found embedded in HII regions or dust clouds it is likely that the dust shell observed through the thermal reradiation is a remnant of the interstellar matter that has gravitationally collapsed to form stars.

Another origin of a dust shell is mass exchange between the components of a binary system during their evolution. As will be discussed in Chapter II, mass transfer from one component of a close binary system to the other constitutes the main difference between the evolution of a single star and that of a component of a binary system.

At this stage the influence of a dust shell at temperature T on the total radiation from a star-shell system in the case of plane parallel geometry will be discussed briefly. Let us assume a star which emits flux F_ν^* surrounded by a dust shell of constant temperature, T. The dust shell absorbs part of the stellar radiation and also itself emits radiation depending on its temperature. The total transmitted flux, at a given frequency ν, is then estimated as follows:

If k_ν and j_ν are the mass absorption and emission coefficients respectively for radiation of frequency ν, then the total emitted intensity of radiation, $dI_{\nu TOT}$, in a distance ds in the shell will be:

$$dI_{\nu TOT} = -k_\nu I_\nu^* + j_\nu$$

where I_ν^* is the intensity of the radiation from the star falling perpendicularly on the shell. But $j_\nu = kB_\nu(T)$ (Kirchhoff's law) where $B_\nu(T)$ is the Planck function representing the blackbody radiation of the dust shell at temperature T.

Then

$$dI_{\nu TOT} = -k_\nu I_\nu^* + k_\nu B_\nu(T)$$

If we integrate along the entire path length of the shell and convert into fluxes:

$$F_{\nu TOT} = F_\nu^* \exp(-\tau_\nu) + B_\nu(T)(1 - \exp(-\tau_\nu)) \qquad 1.7.1$$

where τ_ν is the optical thickness of the shell, of density , and is given by the relation:

$$\tau_\nu = \int_0^s k_\nu \rho \, ds$$

The optical depth of the shell is a very critical quantity for the total flux which passes through an isothermal dust shell, as can be seen from equation 1.7.1.

In an optically thick case ($\tau_\nu \gg 1$) the term that dominates in the second term of the equation 1.7.1 is $B_\nu(T)$; this means that the observed total thermal radiation from a star with an optically thick dust shell around it, has an energy distribution of a blackbody radiation at the temperature of the circumstellar grains. This temperature can be determined through Wien's Law, if the energy distribution is known, and it is independent of the type of grain.

In an optically thin case ($\tau_\nu \ll 1$), equation 1.7.1 is equivalent to:

$$F_{\nu TOT} = F_\nu^* \exp(-\tau_\nu) + \tau_\nu B_\nu(T).$$

The dust emission is proportional to the optical depth. In this case, if the size of the particles is smaller than the wavelength of the radiation involved, the flux spectrum has the characteristics of the specific grains of the shell.

1.7.2 Emission features

Infrared photometry and spectrophotometry of cool giants and supergiants, RV Tauri stars, Mira variables and S stars show that most of these stars have excess infrared emission in the N and Q windows. Woolf and Ney (1969) suggested that the emission feature they observed from o Cet, α Ori and μ Cep must be circumstellar and that the emission bump they observed resembles that predicted from mineral grains. Low and Krishna Swamy (1970) showed that α Ori had indeed a 20 μm emission bump. Woolf (1973) pointed out that M and S stars systematically show a double humped emission feature near 10 μm and 20 μm, whereas C stars show only the emission feature at 10 μm. These double emission features, which rise sharply against the

stellar continuum, are due to a silicate dust cloud which surrounds the star and reradiates the starlight. The silicate features are very characteristic, peaking at 9.7 μm and 20 μm. The emission peak at 9.7 μm declines rapidly towards short wavelengths and slowly towards long wavelengths. The silicate dust does not exist as solid particles at temperatures greater than 1500 K, at which temperature it evaporates (Gilman 1969). For cool stars, the variation of the silicate feature with spectral type has been well studied. It seems to arise in all stars later than a certain spectral type, which is luminosity class sensitive. This boundary is at GOIa^{+}, G8Ia, M1Iab, M5Ib and M6III, but there are exceptions, e.g. W Cephei (M2I) which does not show an excess, or RV UMa (M2-3III) which shows the silicate feature (Woolf 1973). Table 1.7.1 from Woolf (1973) gives a summary of the solids produced by evolved stars. Gehrz and Woolf (1971) have found a good correlation between the intensity of the silicate feature of late-type stars and the rate at which material escapes from them.

Spectra of certain stellar objects in the region 8-14 μm show infrared excess due to dust shells in which oxygen-rich or carbon-rich material dominates. The spectral features of these materials are not characteristic, as are the silicate features, as Thomas et al. (1976) deduced from their narrow band photometric observations of several interesting objects in the wavelength range 8 to 14 μm. Gilman (1969) discussed the materials that are expected in the atmospheres of oxygen-rich and carbon-rich stars and their condensation properties as a function of temperature and of oxygen-to-carbon ratio.

TABLE 1.7.1 (Woolf 1973)

Solids produced by evolved stars

Material	Types of star
Silicates	M and S stars
	G and K Supergiants
	RV Tauri stars (some)
	Solar Nebula (meteorites)
	Comets
Iron	Solar Nebula (meteorites)
	A and F unusual supergiants[b]
	Planetary nebulae[b]
	Be P Cygni and WR stars (some)[b]
	Novae and supernovae[b]
Carbon	R CrB stars
	Hot H deficient stars[a]
	C stars[b]
Si_3N_4	C stars[a]
Unknown dielectrics	RV Tauri stars (some)
	A and F unusual supergiants
	Planetary Nebulae[a]

[a] Spectral feature observed, identification in doubt.

[b] Black body like spectra, with negligible evidence for identification.

1.7.3 Dust emission features in evolved stars

As has been mentioned, circumstellar dust shells in evolved stars may be formed from the ejected material from the central star because an evolved star is usually a mass-losing star.

As has been mentioned before, Woolf (1973a), has established that all the cool evolved stars of types M, S and C, have silicate emission features, but the M and S stars show systematically a double emission feature near 10 μm and 20 μm, whereas the C stars show only the emission feature at 10 μm. Hackwell (1971) has also observed M, S and C stars and has drawn attention to the differences in their

energy spectra. Spectroscopic observations of M and S stars were made by Gillett et al. (1968), who found the characteristic 10 μm silicate emission feature in their spectra.

Another category of evolved stars which show dust emission features are the RV Tau pulsating variable stars (Gehrz 1971). The dust features in the spectra of these stars are not always the same; some of them such as U Mon and R Sge, show silicate features and some show unidentified features at 8-13 μm.

Generally speaking, infrared excess is expected from hot mass-losing stars due to free-free or free-bound radiation from ejected matter ionized by the star's light. But there is also observational evidence of hot stars, such as Be, Ae stars or Wolf-Rayet stars, in which the infrared excess is due to thermal reradiation of starlight by the circumstellar envelope (Gehrz and Hackwell 1974; Cohen et al. 1975; Williams et al. 1978). Planetary nebulae appear also to show emission features as has been shown by Gillett et al. 1972, Cohen and Barlow (1974), Jameson et al. (1974). Spectra of novae after their optical outburst first show infrared excess because of free-free emission from their surrounding ejected material and after some weeks because of reradiation of the starlight by a condensing dust shell, in other words if there are conditions suitable for condensations (Hyland and Neugebauer 1970; Geisel 1970). According to Woolf (1973) iron would be the most likely constituent to condense first. Not all novae, however, become thermal infrared sources. For example Nova V1229 Aquilae 1970 did (Geisel et al. 1970) while Nova V1500 Cyg 1975 did not (Gallagher and Ney 1976; Ennis et al. 1977). A model for the processes which might control grain formation in novae shells has been developed by Gallagher (1977).

1.7.4 Dust emission from young objects and protostars

As has been mentioned, dust shells are a characteristic not only of evolved stars undergoing mass loss, but also of young objects and protostars, remnants of the cloud which collapsed to form them. Evidence of dust has been observed in T Tauri stars: Mendoza (1966, 1968) found near infrared excess at wavelengths 1-3 μm from these stars. He suggested that the T Tauri stars are embedded in a dust cloud and that thermal reradiation of the starlight from the dust grains gives rise to the infrared excess. Later Rydgren et al. (1976) detected indications of the presence of silicates in some T Tauri stars. They found the 10 μm silicate bump in the spectra of some of the stars they observed and also the 20 μm feature, which was always stronger than that at 10 μm. The silicate features have also been detected in emission in the Trapezium region of the Orion Nebula by Stein and Gillett (1969). Woolf (1973) mentions that Ney has observed the same dust features in the O star Herschel 36 which is embedded in a dust cloud in M8. Cohen (1973a,b,c, 1974) has studied between 2 μm and 22 μm, a very large sample of young objects, and he found that beyond the 5-8 μm region the energy of nearly all the stars presents an excess which can be attributed to circumstellar dust environments. Similarly Cohen and Kuhi (1979) pointed out that infrared excess has been observed from stars in Taurus-Auriga, and in at least half of them this can only be explained by thermal emission.

Wynn-Williams and Becklin (1974) have established that dust grains are often physically associated with HII regions, and that heated dust grains cause the strong infrared emission that is observed. Theoretical aspects of this problem have been discussed by Panagia (1974).

1.7.5 Absorption features

The features of the silicate dust are observed not only in emission but also in absorption. The 9.7 μm silicate feature is seen in absorption in front of a large number of compact HII regions and protostars (e.g. Aitken and Jones 1973; Gillett et al. 1975; Willner 1976; Persson et al. 1976). Gillett and Forrest (1973) also found strong absorption features in the spectrum of the "Becklin-Neugebauer point source" in the wavelength regions 2-13.5 μm; the feature which has its maximum at about 10 μm is attributed to silicate grains. This observation is confirmed by Aitken and Jones (1973).

Another observed absorption feature occurs at a wavelength of about 3.1 μm which is compatible with one of the H_2O ice absorption bands. This ice absorption feature has been observed in different objects such as, for example,, in the source near the Rosette nebula by Cohen (1976). He suggested that this absorption feature was due tq pure, spherical ice grains, in accordance with laboratory experiments.

It is generally accepted that the emission features in the energy spectrum of an object give information about its circumstellar shell. The absorption features, however, are made up in general of contributions by the interstellar medium and by the absorbing cool dust cloud extending around the object as well as the warm emitting region itself, which produces, for example, the silicate extinction. In the latter case the observed flux, according to equation 1.7.1, should be given by the equation:

$$F_\nu^{obs} = \left[F_\nu^* \exp(-\tau_\nu) + B_\nu(T)[1 - \exp(-\tau_\nu)]\right] \exp(-\tau_\nu') \qquad 1.7.2$$

where τ'_ν is the optical depth of the absorbing dust cloud, while all the other symbols are the same as in section 1.7.1. If the circumstellar dust shell is very thick, so that $\tau_\nu \gg 1$, information can be obtained only on τ'_ν. In the opposite case, $\tau_\nu \ll 1$, it is possible to separate the shell flux term if a) the dependence of τ'_ν on the wavelength is smooth, and b) the shell emission term dominates (i.e. in the case of a very hot central source).

Absorption features independent of the observed object, must be of interstellar origin. Hackwell, Gehrz and Woolf (1970), for example, on the basis of double-humped absorption features at about 9.7 and 20 μm, suggested that there is silicate absorption in the direction of the galactic centre. Optical astronomers were the first to be involved in the understanding of the interstellar medium. In the past decade infrared and ultraviolet observations have contributed considerably to the study of the main components of solid interstellar matter.

1.7.6 Bremsstrahlung radiation; Free-free emission

This radiation arises in an ionised gas where electrons and positive ions coexist; as their paths frequently cross, the electrons lose energy and emit a photon of radiation, its wavelength depending on the temperature and the density of the gas. These free electrons possess no quantised energy levels, so their radiation is in the form of a continuous spectrum. The bremsstrahlung radiation is called free-free radiation when the charged particles producing it are unbound before and after the interaction.

Assume that k_ν is the absorption coefficient and j_ν is the corresponding emission coefficient in the direction of the observer. The absorption coefficient is given (Allen 1973) by the formula (for $h\nu/kT \ll 1$)

$$k_\nu = \frac{8}{3}\sqrt{\frac{\pi}{6}}\,\frac{e^6}{c(mkT)^{3/2}}\,\frac{z^2 g}{\nu^2}\,N_e\,N_i \quad (cm^{-1}) \qquad 1.7.3$$

where e and m are the electron charge and mass respectively, c is the speed of light, z the ion charge, T the kinetic temperature of the gas, k Boltzmann's constant, g the Gaunt factor, taken as unity in the infrared, representing the departure from Kramer's theory, ν is the frequency and N_e, N_i the number densities of electrons and ions. Knowing the free-free absorption coefficient, the emission coefficient can be estimated using the Kirchhoff's law:

$$j_\nu = k_\nu\, B_\nu(T_e)$$

where $B_\nu(T_e)$ is the intensity of the black-body radiation as given by Planck's law.

In order to discuss the spectrum of free-free radiation, assume an ionised gas cloud which is homogeneous in density and temperature. Assume also that the Rayleigh-Jeans approximation is valid ($h\nu \ll kT_e$) so that $B_\nu(T) = 2kT_e\,\nu^2/c^2$. Then the total transmitted flux, as in section 1.7.1 will be:

$$F_{\nu Total} = F_\nu^* \exp(-\tau_\nu) + B_\nu(T)[1 - \exp(-\tau_\nu)]$$

We are interested now in the second term of the second part of the equation, which is the term representing the emission from the cloud.

For an optically thick medium ($\tau_\nu \gg 1$) the second term is equal to $B_\nu(T)$. But $B_\nu(T) \propto \nu^2$. So for the optically thick region $F_\nu \propto \nu^2$.

In the optically thin case, $\tau_\nu \ll 1$, the second term is equal to $\tau_\nu B_\nu(T)$. But $B_\nu(T) \propto \nu^2$ and $k_\nu \propto \nu^{-2}$ (from equation 1.7.3). So for an optically thin cloud the F_ν is independent of the frequency.

Generally free-free emission can be expected to be the mechanism that produces infrared excess in an object, if there is a central source of sufficient excitation. This condition may be fulfilled if the star has a strong UV continuum. Possible candidates for free-free emission in the infrared are binary systems with a hot B or O star companion or stars that show strong Balmer emission lines (because Balmer emission lines and infrared radiation arise from interaction between atoms, ions and electrons). Gilman (1974) has suggested that it is also possible to have free-free emission from cooler stars if a different mechanism is responsible for the ionisation of the gas. For the K-excess of NML Tau he suggested a model in which the gas is ionised by the convection that occurs at the star's surface.

Free-free radiation appears to be the best interpretation of the infrared excess of Be stars, HII regions, and most Wolf-Rayet stars. Woolf et al. (1970) showed that the best model for the interpretation of their observational data from 3.5 to 11.5 μm of some Be stars is the free-free emission model from an ionised gas. They pointed out that Be stars exhibit a non-stellar component of infrared radiation which is approximately constant or diminishes slowly with increasing wavelength. Woolf et al. (1970) showed, taking ϕ Per as an example, that it is possible to derive the electron density and the size of the emitting region from the observed infrared spectrum of the star by comparing the relation given for the physical parameters of the

optically thin and thick parts of the spectrum. The derived values of the electron density and the size of the emitting region are similar to those obtained from studies of the Balmer emission lines.

Among the Wolf-Rayet stars the infrared excesses observed from the WN and most of the WC types, are explained by assuming free-free radiation from an ionised gas shell as the active mechanism (e.g. Allen et al. 1972; Cohen et al. 1975; Williams et al. 1977). Also in the 2 μm photometric band, most HII regions emit only free-free radiation from an ionised gas shell, as Glass (1972b) showed for the HII region 30 Doradus in the LMC.

The above objects are not the only ones showing infrared excess due to the existence of a hot gas shell. Many hot stars, single or components of binary systems, show the same behaviour, e.g. Jameson and Longmore (1976) explain their infrared observations of β Lyr by postulating a plasma cloud around the B4 star of the system. Dyck and Milkey (1972) discussed a free-free emission model and showed that it is possible to fit to this the observations of a number of hot stars.

Sometimes more than one mechanism is responsible for the infrared excess observed from different objects. Wallerstein (1971), suggested that objects with infrared excess can be placed in a sequence of stars running from Be, with pure free-free emission, to the other extreme of very late-objects like NML Cygni with pure dust shells and so with only dust emission. Objects of intermediate type could then be expected to show a combination of these two characteristics. In this way, Wallerstein explained the excess of infrared radiation from W Cep in terms of a contribution of free-free emission from a gas shell and of thermal reradiation from circumstellar dust.

1.8 The Objectives of Infrared Photometry

Astronomical measurements at infrared wavelengths are very important because infrared astronomy is the link between visual and radio astronomy. The information we get from it is valuable, as it gives us the opportunity to study the energy spectra of different objects over a large range of wavelengths. Infrared photometry is a very important tool in the hands of astronomers today. Interstellar extinction at infrared wavelengths is small compared with that in visual wavelengths and as a result infrared photometry enables astronomers to discover and observe highly obscured objects which may not have optical counterparts. Becklin and Neugebauer (1967) discovered the Becklin-Neugebauer source in the region of the Orion Nebula. The "Two Micron Sky Survey" (Neugebauer and Leighton 1969) contains a number of sources which are undetectable at visual wavelengths. Such a source is IC 2087 near the reflection nebula in the Taurus dark clouds (Allen 1972). Also Grasdalen et al. (1973) observed at 2.2 μm a number of sources in the Ophiuchus dark cloud which do not have optical counterparts.

Infrared photometry has become important also in studies of interstellar extinction (e.g. Smyth and Nandy 1978) and circumstellar matter. From observations at infrared wavelengths astronomers can discover a variety of mechanisms, thermal and non-thermal which are responsible for the infrared fluxes (e.g. Burbidge and Stein 1970) as well as the composition and the physical parameters of the circumstellar shells. From the energy spectrum it is possible to find out if the free-free radiation, the thermal radiation of a dust shell or synchrotron radiation gives the infrared fluxes and to calculate

the density, temperature and size of the circumstellar shells (Woolf et al. 1970; Cohen et al. 1975). In a series of papers (Woolf and Ney 1969; Humphreys et al. 1971; Gehrz 1972) the composition of the dust shells of different types of stars has been determined. Observations of novae in the infrared allow astronomers to study the birth and evolution of a dust shell. Wolf-Rayet stars are also very interesting infrared objects, as observations of them at infrared wavelengths give us useful information about mass loss (e.g. Wright and Barlow 1975) and also about condensation of shells which visual photometry is unable to detect (Williams et al. 1978).

Infrared photometry also plays a very important role in stellar evolution studies. Strom (1972) discusses the evolutionary problem in the light of infrared astronomy with particular reference to pre-main-sequence objects. Infrared observations of T Tauri stars may yield useful information on the early stages of planetary systems, while observations of HII regions and dense dark dust clouds, together with the study of molecular clouds, are providing completely new insight into the processes of star formation (Wynn-Williams 1977). Infrared observations are, however, also relevant in the later stages of stellar evolution; for example, in the case of planetary nebulae they have helped in the understanding of the nature and evolutionary stage of the planetary nebulae shell.

Also important is the contribution of infrared photometry to the study of the evolution of binary systems. It is generally accepted today (e.g. Plavec (1968), Paczynski (1971) and Thomas (1977)), that in some stages of the evolution of binary systems mass transfer from one component to the other and mass loss from the systems occur.

Mass transfer is the basic phenomenon in the evolution of binaries, and the main reason for differences in evolutionary paths between single stars and components of binary systems. Infrared photometry enables astronomers to study the phenomena of mass transfer and mass loss in close binary systems and to estimate the physical conditions and parameters, as well as the exact position of the emitting region and the processes which give rise to circumstellar emission (e.g. Jameson and Longmore 1976).

For all these reasons, and also because of its contribution to extragalactic studies and cosmology, infrared astronomy has undergone a rapid development in the past two decades and it is an extensively used and powerful branch of astronomy today.

CHAPTER II

RS CANUM VENATICORUM SYSTEMS

2.1 Binary Systems - Classification

Two stars form a binary system if they are gravitationally bound to each other, so that they revolve around the common centre of gravity. The systems discovered to be binaries spectroscopically, from variations in the radial velocities, are called spectroscopic binaries; if the orbital plane of a system is oriented so that the two components eclipse each other as seen from the earth then this is an eclipsing system.

There are several systems of classification of binaries. The older classification, adopted for many years, divides the systems according to the nature of the components, shape of the light curves, their periods and spectral types. Another introduced by Kopal (1955), is based on the ratio of the radii of the components to the radii of their Roche lobes (this is discussed later in this chapter). Another more recent classification, introduced by Sahade (1960), regards the binaries in the context of the evolutionary stage of the components. This aspect is also discussed in detail later in this chapter. A summary of these three classifications and the criteria used is given in Table 2.1.1.

The RS CVn systems, which are extensively studied later, belong to: a sub-class of Algol type according to the first classification, to detached type binary systems according to the Kopal classification, and to C_b or C_c (see Table 2.1.1) according to classification C. These are very rough classifications; the real classification of

TABLE 2.1.1

Classification of Binaries

	Classification A			Classification B		Classification C	
BASED ON	Shape of light curves, period, spectral types			Relative size of the components and their respective Roche lobes		Evolutionary stage of the components	
	according to prototype	according to GCVS	characteristics		characteristics		characteristics
TYPES	β Lyrae	EB	Sp: O-B9, $m_1/m_2 \simeq 1$ P = 1-12 days, successive minima unequal, no flat parts	detached	neither component fills up its Roche lobe	C_a	both components still gravitationally contracting
						C_b	both components V spectral class
						C_{b1}	similar components
						C_{b2}	dissimilar components
	Algol	EA	Sp: B8-M1(V + IV) $m_1/m_2 = 0.5$ P = 1-10 days, light curve with flat parts between minima	semi-detached	one component fills up its Roche lobe	C_c	spectral class of components V + IV or V + III
						C_d	spectral class of components III + III of IV + IV
						C_{d1}	similar components
	W UMa	EW	Sp: F5-M, $m_1/m_2 \simeq 1$, P < 1 day, continuous light variation, approximately equal minima	contact	both components fill up their Roche lobes	C_{d2}	dissimilar components
						C_e	systems with at least one component below M-S

RS CVn systems is much more complicated.

2.2 History

The history of the RS Canum Venaticorum-type binary systems as a group of stars with common properties starts in 1946 when Struve called attention to five eclipsing binaries with strong H and K lines of ionized calcium. These lines were much stronger than those observed in single stars of the same spectral class, so Struve suggested that they must be connected with the binary character of the stars. Also the components of these eclipsing systems were late G or early K.

One year later Hiltner (1947) collected all the scattered material of late-type variables with H and K CaII emission lines outside eclipse, and published a list of 13 binaries with periods distributed from 1.98 to 39.28 days. The spectral class of the components with emission varied from F2 to K2. In Hiltner's list the RS CVn system, the prototype of this group, was included. Gratton (1950) extended Hiltner's list by adding 6 more binaries with common characteristics (late-type components; H and K emission lines) but more luminous and with generally longer orbital periods. Plavec and Grygar (1965), in a study of the position of 266 eclipsing binary systems in the HR diagram, and so of the absolute dimensions of the systems, found that the H and K emission line binaries (named by them the AR Lac group) stood apart from the rest of the Algol-type binaries. Plavec and Grygar noticed that these systems have mass ratio quite close to unity and also that their primaries lie above the main

sequence and are classified as IV-V (RS CVn, Z Her) or directly as IV (WW Dra, AR Lac, SZ Psc). They pointed out also that the primaries are of relatively late spectral type - between F4 (RS CVn) and G5 (AR Lac). The next list of H and K emission line binaries was given by Popper (1970 table 2). The list consisted of 22 systems, though Popper suggested that there must be more in the Southern hemisphere. Here he mentioned the tendency for the mass ratio to be near unity and the evidence that the emission and absorption velocities are the same for any given star. Oliver, (1974) in his unpublished thesis, gave a comprehensive list of 24 binaries, all eclipsing, as possible candidates for this type of system. He created his list by adding two more stars to Popper's list (RT CrB and GK Hya) and he named these binaries as RS CVn systems, according to the name of the most studied star of this class. Oliver tried to interpret the peculiarities which are observed in the CaII emission binaries by using UBV photoelectric photometry. His extensive work has improved the observational data concerning the knowledge of these systems. Hall (1976) published in a review article on RS CVn stars a list of 25 binaries with strong H , H and K CaII lines in emission and with late spectral type components (hotter star is F or G, V or IV). He introduced as one of the main characteristics of the RS CVn binaries a limited range of orbital period of 1 day to 2 weeks. His list contained Popper's binaries except for three: two with periods less than one day (WY Cnc and UV Psc) and one with period more than two weeks. He included these systems, however, in two other groups (Hall 1976, tables 2 and 3) related to RS CVn binary objects. Hall started his list with the 24 binaries from Oliver's (1974) list, but he added some new RS CVn systems which had been reported recently, and ignored those which

have orbital period shorter than one day and longer than two weeks. Popper (1976) published a new list of H and K emission binaries containing the 22 stars of his old list (Popper 1970) and five additional ones which have been found to belong to this group. Owen and Gibson (1978) gave a list of RS CVn binaries comprising 29 members, the 26 of Hall's list plus five additions, newly discovered to be members of this class. Weiler and Stencel (1979) and Hearnshaw (1979) have proposed more extensive lists of candidates based on spectral classification summarised by Houk (1978) and Houk and Cowley (1975) in the Michigan Spectral Catalogue, the only criterion being the strong H and K CaII lines in emission.

Hall has shown that the space density of RS CVn binaries is high, over one star per million cubic parsecs, comparable to the figure for the abundant W UMa binaries. It seems likely that there could be many undetected members of RS CVn class. An ongoing programme in the southern hemisphere was initiated in 1977 at Mount John Observatory to discover additional members. The previously mentioned list suggested by Hearnshaw is a result of this programme.

It is obvious from the previous discussion that different criteria used by various workers to assign stars to the RS CVn class makes discussion of these systems difficult. In the present work the following criteria have been adopted to classify the RS CVn stars: binaries with abnormally strong CaII H and K emission (this is the only criterion common to all previous classifications), with the hotter component of spectral type F-GIV-V and with the cooler a near KOIV type star. The list of the stars observed for this project is given in Table 2.2.1.

TABLE 2.2.1

List of RS CVn Systems Observed

Star	HD	V_{max}	Orbital period (days)
HR 1099*	22468	5.8	2.8
UV Psc	7700	9.0	0.9
SZ Psc	219113	7.2	4.0
TY Pyx	77137	6.9	3.2
AD Cap	206046	9.7	3.0#
HD 5303		7.6	6.3#
ER Vul	200391	7.3	0.7
AR Lac	210334	6.9	2.0
λ' And	222107	4.8	20.5
Z Her	163930	7.3	4.0
HR 5110*	118216	5.0	2.6
HR 4665*	106677	5.4	64.4
RZ Eri	30050	7.4	39.3
GK Hya		8.8	3.6

* not eclipsing

estimated in the present work

2.3 Observed Characteristics and Peculiarities of RSCVn Systems

In the past several years this group of emission-line binaries has become very widely observed as these stars have been found to show interesting forms of activity in several wavelength regions. The observed characteristics can be divided into two: photometric and spectroscopic.

2.3.1 Spectroscopic characteristics

Abnormally strong H and K lines of ionized calcium in emission is a general characteristic of the class. Hα has also been observed in emission in most of the memebers of this group and actually it tends to be like the CaII emission lines, a common property of the RS CVn systems. An important point, which had been noticed in individual members before it was realised that they all belonged to the same group, is the variability of the H and K ionised calcium emission lines. This was first reported by Joy (1941) for the intensity of CaII emission lines of WW Dra and also confirmed by Struve (1946), who pointed out that the emission lines of RW UMa disappear altogether at secondary minimum. Later Hiltner (1947) reported that in RS CVn the emission lines disappear also at secondary minimum. Popper (1970) suggested that H and K emission is a photospheric feature which is pretty stable, allowing variations of 25% in emission. Recently the emission line variability has been established for most RS CVn systems not only in the case of H and K emission lines but also for Hα emission (Bopp 1976, Bopp and Fekel 1976, Weiler 1978a, Weiler et al. 1978, Bopp and Talcott 1978, 1980). Weiler (1976) found that the intensity of both H and K emission and H_α emission in

UX Ari, RS CVn and Z Her appeared to be correlated with orbital phase. His recent (Weiler 1978a) photoelectric spectrophotometry of the same emission lines in six systems (RS CVn, UX Ari, Z Her, AR Lac, LX Per, and SZ Psc) confirmed their variability and also demonstrated that the H and K lines of RS CVn did not disappear during secondary minimum as had been reported by Hiltner (1947). Nations and Ramsey (1980) observed that the equivalent width of the Hα emission line in HR 1099 seems to undergo modulations, being in antiphase with the photometric distortion wave of the system (this is discussed later in this section) while profile and/or intensity variations of Hα with time scales of a few days are also demonstrated for four RS CVn systems (UX Ari, HD 224085, AR Lac and SZ Psc). Fraquelli (1978), however, suggested that both the shapes and equivalent widths of Hα appear to correlate with their radio flux.

An important result of the spectroscopic observations of RS CVn systems was found by Popper (1970). He pointed out that the width of the emission lines corresponds to that of a photosphere synchronously rotating with the orbit as suggested by the period and radius. Also, spectroscopic observational evidence, asymmetries in Hα and velocity variations in MgII H and K, indicate mass flows in the system or from the system.

2.3.2 Photometric peculiarities

The most puzzling observational feature of RS CVn binaries, which seems to be related to other characteristics of this group, is the appreciable variations in their light curves. Two kinds of variation have been observed in the light curves of most of these

binaries. One is a nearly-sinusoidal wavelike variation, which migrates slowly towards decreasing (e.g. RS CVn, Catalano and Rodono 1974; RT Lac, Hall and Haslag 1976) or increasing (e.g. SS Boo, Hall and Neff 1979; HR 1099, Antonopoulou and Williams 1980) phases. The amplitude of the wave (from maximum to minimum) can be up to $0^{m}.2$ (Hall 1976, Table 1). This amplitude changes with time and sometimes the wave disappears; some examples are mentioned here: the amplitude of the wave observed in the light curves of RS CVn (the best studied system of this class) has been as large as $0^{m}.2$ and at times is almost unnoticeable (Hall 1972); the amplitude of the distortion wave of SS Boo also varies from $0^{m}.2$ to $0^{m}.05$ (Hall and Neff 1979), while that of SZ Psc varies from $0^{m}.2$ to $0^{m}.0$ (Eaton 1977). The period of the light variation is very nearly equal to the orbital period (Bopp et al. 1977; Landis et al. 1978; Weiler et al. 1978). The nature of the wave-like variations and the different characteristics are extensively discussed later in Chapter V (5.1).

The other type of light variation of RS CVn systems is the short-term irregular changes. These account for the overall level of brightness (usually over one or more cycles) and for short-timescale flaring. Photometry of RS CVn by Chisari and Lacona (1965) and that by Catalano and Rodono (1967), for instance, have revealed changes in the brightness level during primary eclipse over periods of a few orbital cycles. Such changes are also illustrated in the UBV photometry of UX Ari (Evans and Hall 1974; Landis et al. 1978), which indicates that the overall light level decreased by $0^{m}.1$ sometime between late 1972 and late 1974. Irregular variations in brightness in AR Lac have been reported by Babaer (1971). HR 1099 is another star of this group showing strong (probably the most pronounced)

irregular light variations in different regions of the spectrum; this is obvious from the published observations at visual (Bopp et al. 1977, Bartolini et al. 1978, Landis et al. 1978), infrared (Antonopoulou and Williams 1980), radio (Weiler et al. 1978, and references therein) and X-ray (White et al. 1978) wavelengths.

2.3.3 Orbital period variations

Another very common observational characteristic of the RS CVn systems is the tendency for the orbital period to be variable. This involves decreases, fluctuations or increases and occurs on short (AD Cap, AR Lac) or long (SZ Psc) timescales. It is well known that SZ Psc is a system with obviously decreasing period. This has been known since 1934 when Jensch suggested the possibility of variation in the period of SZ Psc from 19 determinations of primary minimum made between 1927 and 1933. Jakate et al. (1976) used all the available photometric data for the system and they calculated a rate of decrease of $P = -6.0 \times 10^{-8}$ days per day.

Another type of variation in period has been detected by Plavec (1960) for RS CVn, where fluctuations of orbital period around a mean value have been observed. Catalano and Rodono (1969) found that the fluctuations are around a mean period of 4.797865 days and have a cycle of about 4000 orbital periods. Hall (1972) pointed out that the orbital period of RS CVn undergoes large and seemingly erratic changes, both increases and decreases.

Sudden period changes have been observed by Plavec et al. (1961) for AR Lac. Photometric observations of AD Cap made by Popper (1980, personal communication) suggest a probable variable orbital period for the system.

Different mechanisms have been suggested to account for period changes in RS CVn systems. Plavec and Smetanova (1959) pointed out that the observed period variations of RS CVn cannot arise from the apsidal motion, as the resulting period and amplitude of the apsidal term are very different from the observed ones. They also considered the hypothesis of a third body, but this hypothesis was also excluded as the observed changes are not strictly periodic. Today it is believed that mass transfer from one component to the other, or mass loss from the whole system, are the only mechanisms that are capable of explaining the orbital period variations. But a problem arises concerning the mechanism producing mass loss from one component or both for detached systems, such as RS CVn binaries. Hall (1975) suggested that the mass loss mechanism must be related to the mechanism creating the wave-like light variations on account of the observed correlation between period changes and wave migration. He also attempted to demonstrate that for four systems (RS CVn, SS Cam, AR Lac and RT Lac) period decreases occur when the minimum of the wave is around orbital phase 0.25 and period increases occur when the wave is around phase 0.75. Hall (1972) and Arnold and Hall (1973) suggested that the changes of the orbital period can be explained by a mass ejection from the brighter hemisphere of the active star at a rate of 10^{-6} $M_{\odot}$ per year. This explanation was criticised by Catalano and Rodono (1974) who found it rather difficult to understand why the mass loss would occur from the brighter hemisphere and not from the spotted, active hemisphere. Another objection was the large amount of mass loss required.

There is photometric evidence for the existence of circumstellar matter in two known RS CVn systems, AR Lac and RT Lac (Catalano 1973,

Hall and Haslag 1976). This could be assumed to be a consequence of mass loss of one or both the components of the system. It has been suggested also (Ulrich 1976) that a mass loss of $10^{-9} M_{\odot}$ per year is expected from a KOIV component. Would this be capable of explaining the period changes observed in RS CVn systems?

Catalano and Rodono (1974) suggested a different origin of the short term period variations of RS CVn stars. They pointed out that the wave-like variation distorts the light curve of the system not only outside the eclipses but also within the primary eclipse, so as to make an observed time of minimum different from the time of conjunction. This generates spurious O-C period variations. Since the wave migrates, the O-C shifts will be correlated in time with the migration.

Hall et al. (1980) considered several possibilities to explain the detected changes of the period, but for the systems they examined a combination of mechanisms was found to be responsible for the period variations. They also pointed out that, if the system is in a mass exchanging state (without the whole system losing mass), the period change depends on the mass ratio, and a mass ratio near unity (typical of RS CVn systems) would not produce period changes. On the other hand, in the mass loss case, the period change depends not on the mass ratio but on the size of the corotating Alfvén radius.

From all the above it is obvious that the method of period variations has not been settled yet.

2.3.4 X-ray, Ultraviolet and Radio Observations

The RS CVn binaries have now been well established as a new class of X-ray sources (Walter et al. (1978a). Soft X-ray emission has been observed from several RS CVn systems, such as: HR 1099, UX Ari, RS CVn, AR Lac, HK Lac, RW UMa, LX Per, σ Gem, α Aur, UV Psc and SV Cam (Cash et al. 1978, Walter et al. 1978a, Walter et al. 1978b, Walter et al. 1978c, Agrawal et al. 1980). Walter et al. (1978a) suggested that the X-ray emission must have a coronal origin as the systems are known to be detached with no evidence for the presence of a degenerate component.

Ultraviolet observations with COPERNICUS of members of this class such as HR 1099, UX Ari, λ And and HR 4665, have shown variable Lyα and MgII emission lines with total fluxes over fifty times the level observed in the Sun (Weiler 1978b, Dupree et al 1980).

Oliver (1974) observed ultraviolet excess in the U-B colours of the cooler stars of some RS CVn binaries, but sometimes an excess was observed from the hotter components.

The emission of Lyα and MgII suggest a combination of active and variable chromospheric activity of these systems.

Another remarkable observational characteristic of RS CVn stars is the detection of strong and variable radio emission from several members. A number of large radio outbursts at 2.8 cm wavelength has been found from HR 1099, UX Ari, AR Lac, SZ Psc, and HR 5110 (Gibson and Hjellming 1974, Owen 1976, Spangler et al. 1977, Feldman et al. 1978b, Owen and Gibson 1978).

It is now established that the mechanism responsible for the radio emission from these binaries is non-thermal gyrosynchrotron radiation (Spangler 1977).

2.4 Characteristics of RS CVn Systems

It is worth summarising here the observational characteristics of the systems considered by the author to be RS CVn systems.

1. Abnormally strong H and K lines of ionised calcium in emission outside eclipse. This emission is displayed usually in the secondary component, but emission from both components or only from the primary has been observed.

2. The Hα line is also observed in emission from most of the members of this group and it tends to be a general characteristic of the class.

3. The intensity of both H and K emission and Hα emission is observed to be variable; this variability appears to be correlated with phases of the photometric wave-like distortions.

4. Variations are observed in the absorption line strengths but no correlation with the light curve variations is seen.

5. The hotter star of the system is usually an F or G main sequence or subgiant star and the cooler is around type KO subgiant.

6. The mass ratio of the two components is approximately equal to unity, except for RZ Eri ($m_1/m_2 = 1.3$), RT Lac ($m_1/m_2 = 2.13$) and AD Cap ($m_1/m_2 = 2.2$).

7. Regular and/or short-term irregular light variations are observed in the light curves of most systems: the regular variations usually have a quasi-sinusoidal wave form; this wave moves along the light curve towards increasing or decreasing phases.

8. Period changes occur, despite a detached-binary status, which are not strictly periodic.

9. Frequently there is an indication of ultraviolet excess caused usually by the secondary component but also sometimes by the primary or both.

10. Strong variable radio emission is observed from some RS CVn systems, while occasionally giant radio flares are exhibited.

11. Most of the systems, if not all, emit hard or soft X-rays, also variable chromospheric emission at Lyα and MgII H and K has been reported for two members (UX Ari and HR 1099) of the class.

2.5 Suggested Models

In order to explain the numerous observed photometric and spectroscopic peculiarities of RS CVn systems, especially the irregularities of their light curves, various models have been suggested. The proposed models belong to two different categories. The first one assumes intrinsic variability of one or both components to be responsible for the photometric behaviour of these systems, while the second is based on circumstellar absorption.

The intrinsic variability can be attributed to some sort of oscillations (pulsating model) or to non-uniform surface brightness

probably of the cooler star of the system (starspot model). With respect to pulsation, the cooler component is envisaged as undergoing a pulsation with a period approximately the same as the orbital period of the system. Oliver (1974), however, pointed out several problems with such a model. The first is connected with the position of the cooler component (usually a KOIV star) in the Hertzsprung-Russell diagram with respect to the position of the usual instability strip. The second problem is that the fundamental period of stellar radial oscillation, for example, for a KOIV star (the secondary of RS CVn), appears to be much less than the orbital period of the system. The oscillation period has been estimated from the relationship $P\beta^{\frac{1}{2}} = Q$, where β is the density of the star and Q is a parameter which has a value between 0.03 and 0.12. Popper (1977) suggested that non-radial oscillations of the cooler star may be a possible explanation for the changes of the light contribution of the cooler component, and he pointed out that this case is perhaps worth investigating. Eaton and Hall (1979) objected to the model of non-radial pulsation of the cooler star on the grounds that the observed amplitude of the distortion wave is large compared to that of the β Cephei or white dwarf stars, which, as has been shown, may be non-radial pulsators (Lesh and Aizenman 1978). Oliver (1974), as well as Eaton and Hall (1979), has not however taken into account the binary nature of RS CVn systems, which may affect the period and amplitude of the pulsation.

In order to explain the light variation outside eclipse, Catalano and Rodono (1967) suggested that one of the components must be surrounded by an extended equatorial ring tilted with respect to the orbital plane. According to them, the continuous variation of the

projected area of the disc during the orbital revolution would give rise to the observed wave-like variation of the system's luminosity outside the eclipses. A precessional motion of the rotational axis of the component with the equatorial ring would be the reason for the observed shift of the wave-like distortion. This model had been applied to RS CVn for which the theoretical period of precession of the equator, assumed to be inclined to the orbital plane, was in good agreement with the observationally determined period of the distortion wave of about 32 years (Catalano and Rodono 1967); this agreement supported their suggested ring model. Two years later, a new estimate of the migration period of the wave by Catalano and Rodono (1969), using observations obtained in 1967 and 1968, gave a value close to 10 years, very short compared with the theoretical one. This is the first reason for discrediting this model. Oliver (1974) discussed the model and found even stronger reasons for rejecting it, based on the difficulty of obtaining a sufficiently stable location of this ring. His arguments were that the location of the ring must be in the hot star's equatorial plane at a distance of 0.79a, where a is the separation of the two components, (this is the distance at which the Keplerian period for small particles equals the orbital period of the system). This places the ring completely outside the critical Roche lobe and at this distance there are no stable orbits. Also the cool star has a radius of 0.244a, and when the line of nodes of intersection between the ring's orbit and the orbital plane is aligned with the line joining the two stars, the ring will collide with the cool star. A recent new version of this approach is the model suggested by Castle (1977). According to this, a thin elliptical ring which surrounds the entire system is responsible for the

wave-like variation of RS CVn systems, while the apsidal motion would account for the migration.

The other suggested model, which is connected with intrinsic variability, is a model involving a surface of non-uniform brightness in one of the components, usually the secondary cooler one. This model was first introduced by Kron (1947) in order to explain the asymmetric light curve of AR Lac. He suggested spots unevenly distributed on the surface of the primary star, as the observed anomalous variations occurred only between minima and during secondary minimum, but not during primary minimum when the primary star was eclipsed. Since then the spot model has been widely used by different workers to explain similar brightness changes in red dwarfs, all of which are now known to be flare stars (Kron 1952; Chugainov 1966; Krzeminski 1969; Evans 1971; Torres, Ferraz Mello and Quast 1972; Bopp and Evans 1973; Bopp 1973; Mullan 1974). These workers worked extensively on this model for the flare stars, trying to find some characteristics of the spots such as size, location, temperature, strength of required magnetic field.

Hall (1972) proposed the spot model to explain the observed peculiarities of the RS CVn system, adopting the starspot hypothesis as a stellar activity analogous to that of the Sun, but on a much larger scale. The same model has been used since then by several other workers as an explanation of the observed peculiarities of different RS CVn type binary systems (Sadik 1979; Jakate 1980). A theoretical model of a binary system in which one of the components has spots on its surface has been recently discussed by Eaton and Hall (1979). They point out that the spot model gives significantly

better results than any competing hypothesis, such as pulsating of one of the components or circumstellar absorption of the light of the system. Though this model provides the easiest way to explain many of the observational events on these stars, the spot model gives rise to objections from different workers. The reasons are the very large spots (twenty or thirty per cent of the surface of the active star) required to explain the observed variations and also the physical difficulty of the origin and preservation of such large and long lived spots.

2.6 Evolution of Close Binary Systems - Evolutionary Status of RS CVn-type Systems

In order to discuss the evolutionary stage of the RS CVn-type binary systems a review of the general topic of close binary evolution is given. The term "close" is used for the systems in which mass exchange occurs between the components at some stage of their evolution, or in other words, if the evolution of one component is not independent of the evolution of its companion; this definition was suggested by Plavec (1967) and Paczynski (1967) independently at the Uccle Colloquium in 1966. It is based on the evolutionary status of the components and not on their dimensions as previously.

Let us first introduce some definitions which will be used in the following discussion.

Roche lobe: Consider a binary system whose components have masses m_1 and m_2; the distance between them is a and they travel in a circular orbit with their axis of rotation perpendicular to the

orbital plane. For each of the components there will be a surface outside of which particles of matter can no longer be retained by the gravitational attraction of the corresponding star. This surface is known as the zero-velocity surface or the critical Roche surface. The Roche surface consists of two lobes which surround the two components having a common point L_1 (inner Lagrangian point). The radius of each lobe is given by Paczynski (1971) in the following expressions:

$$r_1 = a\left(0.38 + 0.2 \log \frac{m_1}{m_2}\right) \qquad \text{for } 0.3 < m_1/m_2 < 20$$

$$r_1 = a\left(0.45224\left[\frac{m_1}{m_1 + m_2}\right]^{1/3}\right) \qquad \text{for } 0 < m_1/m_2 < 0.8$$

Critical radius R_{cr}: The most fundamental concept in the evolution of binaries is the assumption that there is mass transfer from one component to the other when the radius of one of the components of the system is equal to or greater than a critical radius R_{cr}. In the simplest case this means that R_{cr} must be equal to the radius of the Roche lobe of the corresponding component. This is correct only when the stellar rotation and the orbital revolution are synchronous and also when the surfaces of the stars are well defined. Otherwise mass transfer starts even when $R_{cr} < r$, as happens in ζ Aur and VV Cep (Batten 1970).

2.6.1 Evolutionary Tracks of Close Binary Systems

The evolutionary process of close binary systems is a very important topic, because binary stars are so common that it is not possible to develop a comprehensive theory of stellar evolution

without taking into account the duplicity of so many objects. A very brief discussion of the main points of the subject follows.

The evolution of close binary systems is influenced by mass transfer from one component to the other. This is believed to be the reason for differences in evolutionary paths between them and single stars. We cannot therefore regard stars in binary systems as evolving with constant mass. Let us assume two components of one binary system lying on the main sequence and both being well within their Roche lobes. As the more massive component (primary star) evolves its radius increases and eventually (the exact time being determined by the system mass ratio, the system separation and the mass of the primary star) it fills up its Roche lobe, or better its radius becomes equal to its critical radius, R_{cr}. Then mass transfer takes place from the primary star to its companion through the inner Lagrangian point L_1. Mass transfer stops when the mass ratio of the system has been reversed, or when the thermal equilibrium of the mass-losing star is restored.

Usually mass transfer proceeds in two stages: rapid mass exchange and slow mass exchange. If the primary has a radiative envelope, the first phase of mass outflow is due to thermal instability (Morton 1960). In this case the rapid mass exchange takes place on a thermal time scale, which is given by the formula

$$t = \frac{Gm_1^2}{r_1 \ell_1^2}$$

where m_1, r_1 and ℓ_1 are the mass, radius and luminosity of the primary at the onset of mass outflow. In the case in which the

primary has a deep convective envelope, it fills up its Roche lobe when dynamical instability (gravitational and pressure forces seriously out of balance) may set in (Paczynski 1965). Then transfer of a large fraction of the stellar matter takes place within a few hours or days, on a dynamical time scale, which is given by the formula

$$t_{dyn} = \left(\frac{2r_1^3}{Gm_1}\right)^{\frac{1}{2}}$$

Slow mass exchange may take place on a slow nuclear time scale.

There are three evolutionary stages in which the primary star expands and may fill up its Roche lobe. The first is connected with the hydrogen burning in the core of the primary, while the second and third are connected with the rapid contraction before the onset of helium and carbon burning in the core. Following Kippenhahn and Weigert (1967), the terminology case A, case B and case C is used for the type of evolution associated with the onset of mass exchange during the three stages of the expansion of the primary. Ziolkowski (1969) introduced also the case AB. This is the case when the mass exchange starts while hydrogen is burning in the core of the primary and continues during the hydrogen shell burning phase.

Much work has been done on the evolution of binaries for the different cases (A, B, C and AB) and many model computations have been performed. Most of these computations are based on the following assumptions:

a. the two components of the binary system are treated as spherically symmetric stars, even if they fill their Roche lobes;

b. conservation of the total mass and the total angular momentum of the system;

c. the mean radius of the Roche lobe is defined as the radius of the sphere which has the same volume as that of the Roche lobes;

d. the orbit of the system is circular.

Morton (1960) was the first to show that the mass flow from one component to the other should proceed on a thermal time scale, and to construct the first computational model for case A. Many workers followed him, and today there is a large number of models of the evolution of binaries under different conditions, initial masses, mass ratio, orbital period (Kippenhahn and Weigert 1967; Paczynski 1966; Plavec et al. 1969). For case B, binary models have been published for massive, $M > 15M_{\odot}$ (Kriz 1968, 1969; Kippenhahn 1969), low mass, $M < 3M_{\odot}$ (Kippenhahn et al. 1967; Refsdal and Weigert 1969), and intermediate mass systems (Van der Linden 1980). Numerical calculations of evolution of binaries have also been performed for case C (Lauterborn 1970) and case AB (Ziolkowski 1970; Horn 1970, 1971).

More sophisticated models, are now available, based not on the assumptions mentioned before, but allowing for non-spherical stars and non-conservation of mass and angular momentum (e.g. Flannery and Ulrich 1977).

The results of the study of the evolution of binary systems by various workers are summarised by Paczynski (1971), Van den Heuvel (1976) and Thomas (1977).

2.6.2 Evolutionary Status of RS CVn Systems

Plavec and Grygar (1965) realised the peculiarity of the RS CVn systems with regard to their evolutionary status and stated that "this group is likely to have its own history of evolution". Field (1969) analysed observational data of eighteen binaries having undersized subgiants as secondaries, to determine whether it is possible for these systems to be in a state of pre-main-sequence contraction. Among the binaries were four RS CVn systems; these systems did not fit into his pre-main-sequence contraction model. Hall (1972) considered the merits of pre- and post-main-sequence interpretation of the observed properties, and concluded that the first is the more probable. He pointed out that this evolutionary stage explains the fact that the cool component displays many of the youthful properties of T-Tauri stars. Huang (1973) suggested that the RS CVn-type binaries might be the progenitors of the W UMa binaries, if they are in the pre-main-sequence stage. An extensive discussion of the evolutionary problems of these systems is given by Oliver (1974). According to him they may occur in a mass-exchanging stage on a quiet nuclear time scale, and it is not easy to get any evidence of this. Biermann and Hall (1976) give several scenarios for the origin of these systems. They conclude that the most likely is that the RS CVn systems are in a thermal phase following the fission of a rapidly rotating main-sequence star. Popper and Ulrich (1977) contend that both components have evolved as single stars, a point of view supported by Morgan and Eggleton (1979). Hall (1975) has meantime favoured a post-main-sequence interpretation. From this brief review of the different workers' suggestions it is obvious that the problem is still unsolved.

2.7 Circumstellar Matter

The existence of circumstellar matter in a binary system was first discovered by Wyse in 1934 and confirmed later by Joy (1942), while Struve (1950) showed that it is a common phenomenon in close binary systems. Today the existence of circumstellar matter is connected with binary systems' evolution through the mass exchange process, as was mentioned in section 2.6.1. Circumstellar matter may be detected observationally in the following ways:

a. emission features in their spectra

b. changes of orbital period

c. distortion of the velocity curves

d. changes and anomalies of the light curves

e. possible infrared excess.

Batten (1970) introduced three elements in the discussion of circumstellar matter. These are: the stream, the disc and the cloud. The stream is the densest part of the circumstellar matter with particle density of about $10^{13}/cm^3$ and is confined to the orbital plane. It arises straight from the atmosphere of one of the components and flows to the other star of the system.

The disc usually surrounds one component (the more massive) but there is no reason why both components should not have discs. The disc is probably in contact with the star within, and extends to three or four times the stellar radius. It is probably fed by the stream and it is confined to the orbital plane.

The cloud, which is usually the least dense element of circumstellar matter, surrounds the entire system and is likely to extend

out of the orbital plane in spherical symmetry. The matter of the cloud comes from matter diffused out from the stream and disc.

The main characteristic that distinguishes the streams from the discs and clouds, in addition to their higher density, is the strongly directed motions, as the stream is directly moving from one component to the other. The most important distinction between the disc and the cloud is a kinematic one: the disc moves with the star but the stars move through the cloud. The particles in a disc are more predominantly under the influence of the star within, but the motions of the particles in a cloud are determined by both components.

2.8 Objectives of Observing RS CVn Systems in the Infrared

RS Canum Venaticorum binary systems have attracted the attention of observers of all regions of the spectrum in the past decade. The strong CaII and Hα emission lines in their spectra and their variability are the most important characteristics of the systems, while most of them have also been detected at radio wavelengths. Gibson and Hjellming (1974) suggested that the ultimate radio energy sources of these binaries is gravitational infall of matter transferred from one component to the other. Is this suggestion correct or is another mechanism responsible for the radio emission, and what is the reason for the strong emission lines and their variability?

Milone (1976) discovered infrared excess from RT Lac which reached the value of $0^{m}.7$ at K. He considered that circumstellar matter is the most likely source of the observed excess. Is infrared

excess a common characteristic of these systems and is distribution of mass in and around the Roche lobes of the components an observational fact? Are these systems in a mass-exchanging stage of their evolution or are they well within their Roche lobes?

The wave-like variation in the visual light curves of most of the systems (or probably all of them if accurate and extensive photometry were available) is the most fascinating characteristic and a puzzling observational fact. Does this variation occur at other wavelengths? What is its origin? Which is the best model to explain not only the asymmetries of the light curves but also as many observational characteristics of the systems as possible? In order to try and answer some of these questions a program of infrared photometric observations was undertaken and is described in the following chapter.

CHAPTER III

OBSERVATIONS

3.1 Instrumentation

The observations for the present work were made using three different telescopes at three different observatories: the Science Research Council 1.5 m flux collector on Tenerife, the Greek 1.2 m reflecting telescope in Kryonerion, and the South African 0.75 m reflecting telescope at Sutherland.

The bulk of the observations were made during October 1978 and September, November and December 1979 at the South African Astronomical Observatory (SAAO) at Sutherland, using the 0.75 m reflecting telescope, built by Grubb Parsons (Newcastle) in 1975. The telescope has a focal ratio f/15 giving a scale of 18.3 arc sec/mm. An infrared photometer, feeding a liquid nitrogen cooled photovoltaic indium antimonide (InSb) detector, was attached at the Cassegrain focus of the telescope. This photometer, built by the infrared team of the SAAO, is known as the MkII infrared photometer, and is similar to that described by Glass (1973). The main frame of the photometer is shown in Figure 3.1.1, taken from the "Operating Notes" for this photometer by Glass (1978).

A 2 mm aperture was used all the time. The chopper speed is 12.5 Hz and the integration time 10 seconds; both these parameters are fixed in this system. The rotating mirror device has been adopted for subtracting the sky background from the signal while an offset guider allows the observer to guide the star.

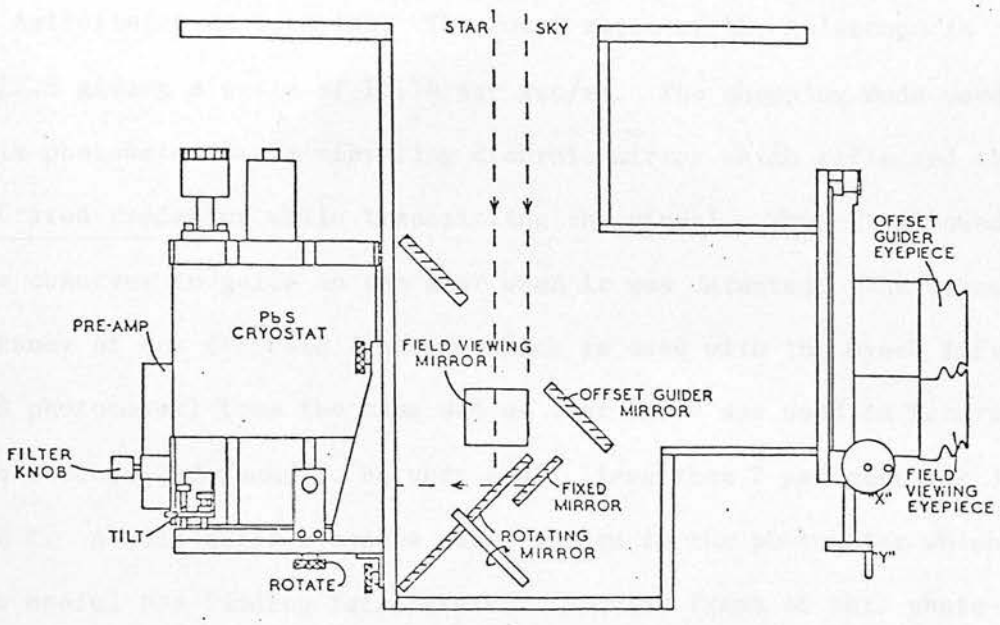

Figure 3.1.1 The main frame of the MkII photometer

At the beginning of this work, between October 1976 and August 1978, some observations were made using an infrared photometer built at the Royal Observatory Edinburgh (ROE infrared photometer), similar to that described by Williams et al. (1976). The photometer fed either a liquid nitrogen cooled InSb detector or a liquid helium cooled bolometer according to the needs of the other observers' projects. The photometer was attached on the Cassegrain focus of the SRC 1.5 m flux collector at the Cabezon Observatory of the Instituto de Astrofisica de Canarias. The focal ratio of the telescope is f/12.8 giving a scale of 10.74 arc sec/mm. The chopping mode used in this photometer was a vibrating dichroic mirror which reflected the infrared radiation while transmitting the visual. Thus it allowed the observer to guide on the star when it was detected. The transparency of one dichroic (the one which is used with the Greek infrared photometer) from the same set as that which was used in Tenerife was checked and found to be very small, less than 7 per cent for J, H and K. A wide angle eyepiece was attached to the photometer which was useful for finding faint stars. The main frame of this photometer is shown in Figure 1.3.1. With this photometer the integration time and the frequency of the vibrator mirror could be chosen. Usually 10 seconds integration time and 20 Hz frequency were used. A microprocessor was connected to the lock-in amplifier output via a voltage to frequency convertor which allowed the observer to obtain a first reduction of the data while observations were in progress. This was very useful as it enabled the observer to have an idea of the system behaviour, the weather conditions, and the number of integrations he ought to make in order to have a desirable statistical error. The microprocessor was useful also for changing filters and recording the sidereal time.

A few of the observations for this work were made in Greece using an infrared photometer built at the Royal Observatory Edinburgh but modified and tested by the author. This photometer is very similar to that used in Tenerife. The photometer was attached to the 1.2 m telescope of the Greek National Observatory at Kryonerion (Contopoulos and Banos 1976). The mounting flange of the photometer was designed to allow rotation of the photometer on the mounting flange of the telescope, allowing the sky chopping to be done in either right ascension or declination.

The filters used with the Greek photometer were from the same set as those used in Tenerife. It should be noted that the filters used with the ROE and the Greek infrared photometers have the same effective wavelengths as the filters used with the MkII photometer (SAAO). The J is from the same set, H and K have the same effective wavelength, but the L used in South Africa had effective wavelength $\lambda_0 = 3.4$ μm (as the Johnson filters) while the ROE and Greek have L' with $\lambda_0 = 3.8$ μm.

In the following Table 3.1.1 a summary is given of the different observational sessions, the telescopes and instruments used for carrying out the observations for the present work.

TABLE 3.1.1

Observing Sessions

Time	Site	Telescope diam. in m	Detector
1976 (10/10-20/10)	Tenerife	1.5	InSb or Bolometer
1977 (27/08-16/09)	Tenerife	1.5	InSb
1978 (02/05-16/05)	Kryonerion	1.2	InSb
1978 (04/08-17/08)	Tenerife	1.5	InSb
1978 (10/10-30/10)	Sutherland	0.75	InSb
1979 (18/09-01/10)	Sutherland	0.75	InSb
1979 (19/11-10/12)	Sutherland	0.75	InSb
1979 (18/12-31/12)	Sutherland	0.75	InSb

3.2 Observational Procedure

3.2.1 Methods for improving the detector's performance

The detectors of the three photometric systems used for obtaining the observational data of the present work were photovoltaic indium antimonide operating at liquid nitrogen temperature. A discussion of these detectors is given in chapter I (section 1.3.2).

As mentioned in chapter I (section 1.3.3), a measure of the merit of a detector is the Noise Equivalent Power (NEP), which is actually a measure of the minimum detectable signal capability of the system. According to Soifer and Pipher (1978) the theoretical NEP for an InSb detector as a function of wavelength λ (in μm), is given by the relation:

$$NEP = (9 \times 10^{-12})\ T^{\frac{1}{2}}\ n^{-1}\ R^{-\frac{1}{2}}\ \lambda^{-1}\ W\ Hz^{-\frac{1}{2}} \qquad (3.2.1)$$

where T (in K), R (in ohms) and n are respectively the operating temperature, the impedance and the quantum efficiency of the InSb detector. From the definition of the NEP (chapter I) the merit of the detector increases as the NEP decreases. From the equation 3.2.1 the only changes that can be made to improve the performance, for a given detector and at a given wavelength, are two:

a) to decrease the operating temperature

b) to increase the impedance.

The first is achieved by pumping on the liquid nitrogen and in this way temperatures as low as 55 K are reached. This procedure is commonly used today.

The second, to increase the impedance of the detector, is achieved by using a technique called "flashing" introduced by K. Matthews (Soifer and Pipher 1978). According to this technique, with the preamplifier switched off, a light is shone onto the InSb detector for a short period, usually through the J filter and the largest aperture. This technique is enough to improve the impedance by a factor of 10 (Soifer and Pipher 1978 give a factor or 10^4 by flashing and cooling the diode to $\sim$ 55 K, but this appears somewhat large).

It is known that the various types of InSb detectors react differently to flashing. In some the resistance does not change, e.g. for the InSb detector used in Tenerife in August 1978 it was found that the impedance did not increase after flashing. On the other hand, measurement of the impedance of the Greek detector before

and after flashing showed an improvement of a factor of 10. Glass (1979, personal communication) also reports improvement through flashing of the InSb detector of the MkII infrared photometer used in South Africa.

Flashing a photovoltaic detector not only increases its impedance but also improves the D.C. stability and lowers the noise voltage. Thus flashing improves the performance of an InSb detector. The physics of the "flashing" technique is not well understood yet, but its benefits have been used for some years.

3.2.2 Procedure for improved system

After the performances of the detector and the preamplifier have been checked and found satisfactory, the cryostat is attached to the main photometer which has been aligned.

A standard star is then acquired and an effort is made to maximise the received signal, usually through the K filter. This is achieved by:

a) re-adjusting the focus of the telescope

b) finding the right position of the x-wires

c) adjusting the cryostat

d) changing the phase of the lock-in amplifier.

Next a standard star is observed and the deflections in the different wavebands are compared with previous nights' observations. In this way the performance of the system and the weather conditions are noted.

3.2.3 Procedure for observations

When the observer is satisfied with the performance of the system the photometric observations can begin. The telescope is moved to place the object in one beam (usually named the "left"). The rotating or vibrating mirror (depending on the system used, section 3.1) chops at a given frequency (12.5 or 20 Hz) therefore the signal from the object results in a given frequency A.C. signal at the preamplifier of the detector. The preamplifier output is connected to a lock-in amplifier which is connected to the chopping reference signal. There are two outputs from the lock-in amplifier. One is directly connected to a chart recorder as D.C. voltage while the other, through a voltage to frequency convertor, to a counter. For the systems used for the observations the integration time was 10 seconds. When the integration was complete the counts were recorded on a teletypewriter and on paper tape. Then, according to the nodding scheme, the telescope was moved to place the object in the other beam usually named the "right"). The procedure was the same as previously described. If the two beams are named left (L), right (R) the observing procedure was LRRL to obtain a set. One or two sets were enough for the standard stars but as many as ten or more sets were necessary for faint stars ($K \sim 9$) in order to get an accuracy of the order of 0.05 mag. When the star is in the left beam, the output of the Lock-in amplifier is the difference between star (S) plus background (B) and background; when the star is in the right beam, the output is in the opposite sense.

Thus we have: left beam $(S + B) - B$

right beam $-(S + B) + B$

and by subtracting the counts from the two integrations (left-right)

we get:

$$(S + B) - B - [-(S + B) + B] = 2S$$

During the observations the observer has to keep a close eye on the teletype output and particularly on the chart recorder in order to check continuously the progress of the observations and the weather conditions. (This is the function of the chart recorder.)

While observing with the MkII infrared photometer (section 3.1), an identification number, the "run number", is entered in the data recording machine. Also a computer form is kept, recording the "run number", the name of the observed object, its coordinates, and the sidereal time at which each waveband is observed. This information will be used for the reduction of the data (section 3.4). The output of the teletype of this system gives the "run number", the counts of each integration, the filter and aperture used. The tape output is used for editing the data and for computer reduction.

When the ROE infrared photometer was used, the name of the star, the apertures used and the sidereal time (when the system was not interfaced to the sidereal clock) were kept while the filters used as well as the sensitivity gain were recorded automatically on the teletype output. The output of the teletype in this case gave also the number of integrations, the counts of each integration, the instrumental magnitude and the statistical error. This will be referred to later (section 3.4) when the "data reduction procedure" will be discussed.

3.3 Observational results

Observations were carried out during the years 1976 to 1979 and were made in the near infrared in the four colours J, H, K and L or L', with instruments and telescopes described in the previous section and given in Table 3.1.1. The effective wavelengths of the filters used at the different observatories are discussed at section 3.1. In Table 3.1.1 the periods of the observational runs are also summarised. Table 3.3.1 contains the stars extensively observed, which are discussed individually in Chapter V; Table 3.3.2 gives the infrared observations of the stars that were observed only for searching for infrared excess.

The results of the observations are given in Chapter V. Each observation is the average of a number of integrations which depends mainly on the faintness of the observed object. Standard stars were observed to calibrate the photometry.

Observations of the binary systems were alternated with observations of suitable comparison stars. During periods of expected changes in the light of the variable of interest to the author, the number of comparison star observations was reduced (once every three or four observations of the program star) to allow more frequent observation of the binary system. Unfortunately the alteration between the variable and the comparison star was slow; an average of three minutes was necessary to go from one star to the other, as almost all the observations were made by one observer and using the 30-inch telescope at Sutherland which does not have any automatic control mechanism.

TABLE 3.3.1

RS CVn Systems Extensively Observed

Star	Other names	Elements	Comparison star	Reference for elements
HR 1099	V711 Tau	2442766.069 + 2.83782E d	10 Tau	Bopp and Fekel 1976 Landis et al. 1978
UV Psc	HD 7700	2428038.555 + 0.861046E	HR 434	Huth 1959
SZ Psc	HD 219113	2442308.7671 + 3.96534286E	γ Psc	Jakate et al. 1976
TY Pyx	HD 77137	2443187.230 + 3.198584E	HR 3484	Surendiranath et al. 1978
AD Cap	HD 206046	2444142.291 + 2.985E	HR 8167	present work
HD 5303	BV 625	2444224.426 + 6.254E	HR 98	present work
ER Vul	HD 200391	2440182.3212 + 0.698082E	HR 7942	Al-Naimiy 1978

TABLE 3.3.2

Infrared Observations of other RS CVn Systems

Star	JD	J	H	K	L	L'
	2440000+					
AR Lac	3389.58	5.05	4.50	4.39		4.37
λ And	3401.54	1.93	1.20	1.10		1.24
HR 5110	3645.31	3.95	3.65	3.48		3.44
Z Her	3637.57	6.16	5.61	5.51		5.66
HR 4665	3645.33	4.28	3.67	3.55		3.41
RZ Eri	3801.51	6.16	5.71	5.57	5.25	
GK Hya	4204.60	7.97	7.66	7.59		

The selection of comparison stars is usually made with the following restrictions:

a) they should be in the neighbourhood of the variable star

b) they should be non-variable

c) they should have approximately the same magnitude and the same spectral type and class.

In selecting comparison stars for this work it was sometimes necessary to modify these criteria. A compromise between quality and quantity in the observations data had to be made. The quality of the photometric data was the main objective. On the other hand, as frequent observations as possible of the binary systems were necessary in order to reveal the expected variations outside eclipse, which was the main purpose for observing these binaries. If we had followed all the criteria for the comparison stars mentioned earlier we would have lost in quantity because observing comparison stars as faint as the program stars, 9 to 10 mag in V, would have occupied too much time. For this reason bright stars were used as comparison stars. Another reason for using bright comparison stars with colours different from the variable, was the following. Errors introduced in the differential photometry, at 7^m or 8^m in K, would be worse than those introduced because of the non-similarity of magnitudes and colours of standard stars to program binaries. Therefore the comparison stars were selected with the first two of the previously mentioned restrictions in mind (close to the variable, non-variable bright in infrared) and are listed in Table 3.3.3.

Since most of the photometry is differential not many standard stars need to be observed, unless a standard star was also a comparison star.

TABLE 3.3.3

Infrared Magnitudes of Comparison Stars

Star	J	H	K	L	L'	Note
10 Tau	3.25	2.98	2.91	2.88		average of 45 observations
HR 434	2.46	1.71	1.55	1.45		30
γ Psc	2.06	1.55	1.45	1.40		22
HR 3484	2.79	2.33	2.24	2.15		22
HR 8167	2.82	2.36	2.25	2.17		10
HR 98	1.70	1.39	1.32	1.30		10
HR 7942	2.46	1.92	1.84		1.76	15

The observing schedule was dictated by the coordinates of the stars and the predicted times of eclipses or other relevant parts of the light curves. Most of the observing time was devoted to the two main stars of this project, HR 1099 and UV Psc. These two stars are approximately two hours apart in right ascension, sufficiently close to observe them if necessary in the same run.

Chapter V contains discussion of all observations of each variable star. The comparison stars used for each variable are shown in Table 3.3.1.

3.4 Data Reduction

Photometric observations were made with two different systems (section 3.1), the MkII in South Africa, and the two similar infrared photometers built at ROE in Tenerife and Kryonerion. Two different procedures were used for the first part of the reduction of data.

The reduction of the raw observations using the MkII system, was carried out with the infrared photometry reduction program in Cape Town kindly provided by the SAAO staff. This program first reduced the data of the program stars and the standards to instrumental magnitudes and, comparing these with magnitudes of standard stars (Glass 1974) stored in the computer, gave the final magnitudes as output together with the statistical errors involved. These magnitudes are free of atmospheric extinction, as the program calculated the air mass and estimated the atmospheric extinction using the extinction coefficients stored in the computer ($J = 0^{m}.1$, $H = 0^{m}.06$, $K = 0^{m}.1$, $L = 0^{m}.15$ and $M = 0^{m}.28$ all per unit air mass). This program also gave the average instrumental sensitivity for each colour. The whole night's run was then reduced using these values.

As mentioned in section 3.1, in the photometric systems used in Tenerife and in Kryonerion the signal from the lock-in amplifier is connected to the input of a control system (microprocessor, type Motorola 6800) via a voltage to frequency convertor. The control system integrates the pulse train and also reads the sensitivity range switches. The results of the integration are logged to a teletype which gives both printed output and paper tape for further processing.

This control system also performs some data reduction on the results of the integration while the run is progressing. The reduction program in the microprocessor reduces the integration counts to instrumental magnitudes and evaluates the statistical errors involved. These reduced data are also given in the teletype's output.

After the first reduction of the data has been done, the atmospheric extinction is calculated and the zero point of the magnitude scale is established for each night.

3.4.1 Atmospheric Extinction

Atmospheric extinction arises because the light from a star passing through the earth's atmosphere suffers a loss depending on the zenith distance of the star. Let us assume that the magnitude of a star at a given wavelength outside the earth's atmosphere is $m_{o\lambda}$. Then the observed magnitude is given by the following relation:

$$m_\lambda = m_{o\lambda} + k_\lambda x(z) \qquad (3.4.1)$$

where k_λ is the extinction coefficient, which is a measure of the

light loss expressed in magnitudes for a star at the zenith, and x(z) is the path length expressed in units of air mass at the zenith. If we assume that the surface of the atmosphere and the earth are parallel planes then

$$x(z) = \sec z \qquad (3.4.2)$$

The evaluation of x(z) under these assumptions give a high degree of accuracy for the air mass. According to Hardie (1962) the error introduced by the inaccuracy of sec z is only 0.005 air mass at z = 60°. The value of sec z is given by the formula

$$\sec z = (\sin \phi \sin \delta + \cos \phi \cos \delta \cos h)^{-1} \qquad (3.4.3)$$

where ϕ is the observer's latitude while δ and h are the declination and the hour angle of the star. So the calculation of instrumental magnitudes free of atmospheric extinction is obtained by subtracting the product of the air mass (sec z) at the time of observation and the absorption coefficient at given wavelength. The absorption coefficients for all the near infrared wavelengths (J, H, K, L') are taken as equal to 0.1 mag/air mass (Williams 1976, personal communication), while the air mass is calculated from equation 3.4.3, using the sidereal time of observation and the coordinates of the star.

3.4.2 Interstellar Extinction

In the present work interstellar reddening corrections have not been applied to the observed magnitudes of RS CVn systems as the distances are not greater than 250 pc and for these distances the extinction at infrared wavelengths is negligible. But interstellar extinction has been taken into account and reddening corrections have

been applied to the observed magnitudes of the Wolf-Rayet system HR 193793 (Appendix 1, paper 1).

3.4.3 Magnitude Scale Zero Point

Standard stars were observed to calibrate the photometry. Having subtracted the contribution of the earth's atmosphere from the instrumental magnitudes of the standard stars, the zero point of the magnitude scale is found for each night, using the standards of Johnson et al. (1966) in the Northern hemisphere and those of Glass (1974) in the Southern hemisphere. The H and L' magnitudes of the standards were found from interpolation or extrapolation of their fluxes at the other infrared wavelengths or using Glass's (1974) relation which gives the H magnitude if the J and K magnitudes are known. The true magnitudes of the observed stars can then be obtained by comparing their extinction-free instrumental magnitudes to the zero point magnitude scale for the same night of observation. Of course, in the case of differential photometry, if the comparison stars are properly chosen (see section 3.3) this process is not necessary. One can obtain the same results by simply subtracting the two instrumental magnitudes (comparison minus variable).

3.4.4 Differential Photometry

The photometry of most of the present work is differential as it is photometry of binary systems. So the magnitudes and the colours of the binary stars are given as the difference of the magnitudes or the colours of the variable star minus the magnitudes or the colours of the comparison at the same wavelengths. A discussion of the

selection of the comparison stars for this project is given in Chapter 3.3. In Table 3.3.1 the comparison stars used for each observed binary system are listed.

3.4.5 Light Time Correction

The observation times of binaries are normally given in heliocentric Julian dates, which is the equivalent time of observation from the sun. In order to convert the Julian dates to heliocentric Julian dates the following correction must be applied:

$$R = 0^{d}.0058 \cos (\ell^* - \ell^{o}) \cos b^* \qquad (3.4.4)$$

where ℓ^*, b^* are the ecliptic longitude and latitude of the star and ℓ^{o} is the ecliptic longitude of the sun at the midpoint of the observing period. The correction factor R is added to the observed time to obtain the heliocentric time. From equation 3.4.4 this correction cannot be greater than 0.0058 days. This accuracy is within the limits of the time of each measurement which is of the order of 5 to 10 min. But in any case this uncertainty in time (maximum 8 min) does not introduce any difficulties in the study of the variations outside eclipse.

3.4.6 Calculation of Phases

The light curve of a binary system is a plot of the differential magnitudes against either the time, or the phase. The phase is

$$\phi(\text{phase}) = \frac{T(JD) - T_{o}(JD)}{P}$$

where $T(JD)$ and $T_{o}(JD)$ are the observation time and the epoch of the

primary minimum in Julian dates while P is the period of the system. The ephemerides used for the calculation of the phases of the individual system are given in Table 3.3.1.

CHAPTER IV

ANALYSIS OF DATA

In this chapter the general problems of the analysis of the infrared photometric data will be discussed. The results of the analysis for the individual stars will be discussed in the following chapter.

4.1 Estimation of the Spectral Types of the Components using the Observed Colours

The identification of the spectral types of the components of RS CVn type binary systems is still an open question. Blending problems in the spectra make an accurate luminosity classification impossible. An effort is made here to estimate the spectral types of the components of some RS CVn type systems from their observed colours. The colours used were the colours of the systems at maximum light in order to include the contribution of both stars to the observed magnitude. The available observed colours were: (B-V), (V-I), (V-J), (V-H), (V-K) and (V-L). In cases where one colour had not been observed an estimate was made by interpolation of the energy distribution.

A computer program was written to calculate the combined colours of all possible combinations of two stars belonging to spectral types F5V to K5V and G5IV to K3IV, assuming that the two stars of the observed system were normal. The program was based on simple definitions and equations. If it is assumed that $(V-\psi)_1$ and $(V-\psi)_2$ are

the V-ψ colours of stars 1 and 2 of a binary system, then the $(V-\psi)_{syst}$ colour of the system may be estimated as follows:

$$(V-\psi)_1 = 2.5 \log \frac{F\psi_1}{FV_1} - 2.5 \log \frac{F\psi_o}{FV_o} \qquad 4.1.1$$

where $F\psi_1$, FV_1 are the fluxes of star 1 at wavelengths ψ and V and $F\psi_o$ are the corresponding fluxes of a zero magnitude star.

Then similarly for star 2

$$(V-\psi)_2 = 2.5 \log \frac{F\psi_2}{FV_2} - 2.5 \log \frac{F\psi_o}{FV_o} \qquad 4.1.2$$

The second term of the right hand side of equations 4.1.1 and 4.1.2 is a constant; let it be equal to ε.

From equation 4.1.1

$$\frac{F\psi_1}{FV_1} = 10^{0.4[(V-\psi)_1 + \varepsilon]} \qquad 4.1.3$$

and from equation 4.1.2

$$\frac{F\psi_2}{FV_2} = 10^{0.4[(V-\psi)_2 + \varepsilon]} \qquad 4.1.4$$

Then the $(V-\psi)_{syst}$ colour of the combined system is:

$$(V-\psi)_{syst} = 2.5 \log \frac{F\psi_1 + F\psi_2}{FV_1 + FV_2} - \varepsilon \qquad 4.1.5$$

with ε as defined before.

Equation 4.1.5 can be written:

$$(V-\psi)_{syst} = 2.5 \log \left(\frac{\frac{F\psi_1}{FV_1} + \frac{F\psi_2}{FV_2}\frac{FV_2}{FV_1}}{1 + \frac{FV_2}{FV_1}} \right) - \varepsilon \qquad 4.1.6$$

The quantity $\frac{FV_2}{FV_1}$ is estimated from the equation:

$$(V_1 - V_2) = 2.5 \log \frac{FV_2}{FV_1} \quad \text{or} \quad \frac{FV_2}{FV_1} = 10^{0.4(V_1 - V_2)} \qquad 4.1.7$$

From the combination of the equationss 4.1.3, 4.1.4, 4.1.6 and 4.1.7 the V-ψ colour of the system is calculated, given the intrinsic colours and V magnitudes of the two components. The V magnitudes used are those given by Allen (1973) while the intrinsic colours of the single main-sequence stars are those by Johnson et al. (1968). For the subgiants, the intrinsic colours were estimated by interpolation from the intrinsic colours of giants (Johnson 1966) and main-sequence (Johnson et al 1968); the intrinsic V-H colours of giants were obtained using the empirical relation H = 0.19J + 0.81K given by Glass (1974). This way of obtaining intrinsic colours of subgiants introduces errors but the author is not aware of any published intrinsic colours of these stars.

This computer program compared the observed colours with those expected from different spectral combinations and using the χ^2 test yielded information about the most probable spectral types of the components of the system under study.

Having made a first approach to the problem of the spectral classification of the components, other aspects were taken into account before making a final decision. First, the spectroscopic results for the different systems were considered. For these systems we know that the absorption lines of both components are almost equal, so a combination of two very different components can be rejected. Another factor taken into account is the position of the system on the absolute magnitude-colour diagram. This is applied in cases where both components have about the same spectral type. Then the observed B-V colour can be meaningfully used as the colour of a

single star and M_V, the absolute visual magnitude of each component. The correction for duplicity was applied first, which is $0^m.75$, and afterwards the correction for the distance modulus. If m_V is the observed visual magnitude of the system, $M_V = m_V + 0.75 - 5\log r/10$ where r is the distance of the system.

For the eclipsing system, if the eclipses are total, one more criterion can be obtained for the spectral type of one of the components. If the primary eclipse is an occultation (in other words if the hotter star is the smaller), as in the case of UV Psc, the observed colours of the system during the primary eclipse are the colours of the cooler star. So by matching the observed colours during the occultation using the χ^2 test, the spectral type of the cooler component can be determined. In the case where the secondary minimum is an occultation, the observed colours during this eclipse can similarly contain information about the spectral type of the hotter component.

4.2 Searching for Infrared Excess from RS CVn-type Binary Systems

One of the main aims for undertaking the project of infrared observations of RS CVn systems was to search for infrared excess from them. Milone (1976) detected infrared excess in RT Lac, which was as great as $0^m.7$ in K near the secondary minimum. He suggested that this is evidence for the existence of circumstellar matter in the system. He gave the same explanation for the observed infrared

excess of two other RS CVn systems, the prototype of the group RS CVn and AR Lac which had been found to be infrared emitters by Atkins and Hall (1972).

4.2.1 Spectral-energy distribution

In order to investigate the existence of any infrared excess from selected RS CVn-type binary systems by a method which does not make use of the spectral classification (for the reasons that have been discussed earlier in this chapter), their energy distribution curves have been examined for evidence of circumstellar material. Log $\lambda F\lambda$ ($\lambda F\lambda$ in Watt cm^{-2}) has been plotted against log λ (λ in μm) for the observed systems; this is illustrated in Figure 4.2.1 for the little-observed systems (Table 3.3.2) and in Chapter V for the extensively observed systems, where they are discussed separately. For the calculation of the fluxes Johnson's (1966) absolute calibration has been adopted while the emitted flux at H and the flux at L' (λ_0 = 3.8 μm) have been calculated by interpolation and extrapolation. Reddening corrections have not been applied as the greatest distance of any of the observed systems is 250 pc. Thus any probable observed reddening must be circumstellar in origin.

As can be seen from Figure 4.2.1, and from the energy distribution of the systems given in Chapter V, the energy distribution of the observed RS CVn binaries is as expected from a blackbody at different temperatures which can be obtained from the relation $\lambda_p T$ = 3670 μmK, where λ_p is the wavelength at which the blackbody curve

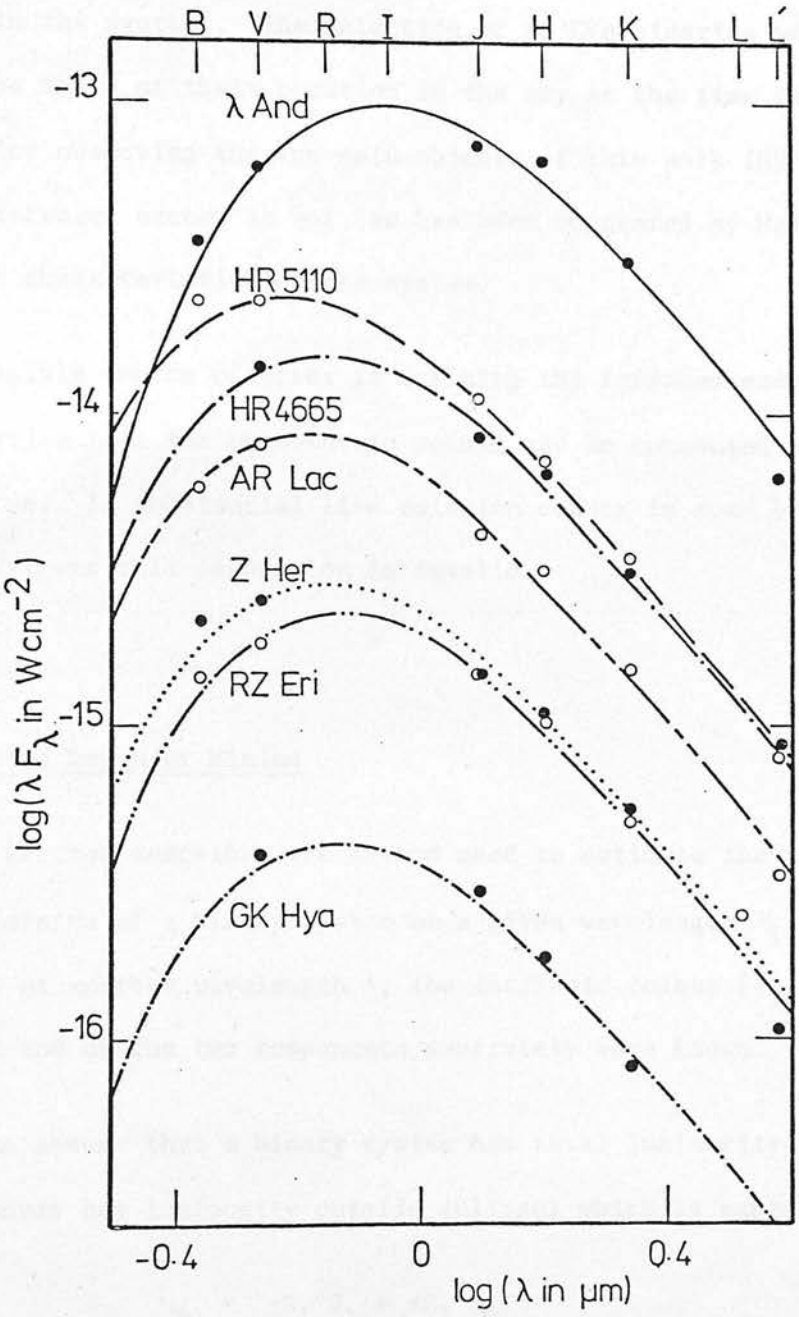

Figure 4.2.1 Energy distribution of the little-observed RS CVn systems

peaks in $\lambda F\lambda$ versus λ diagram. Thus there is no indication from the spectral energy curves of conspicuous excess radiation in the near infrared in the systems. The selection of RS CVn binaries was made only on the basis of their position in the sky at the time chosen as suitable for observing the two main objects of this work (HR 1099, UV Psc), so infrared excess is not, as has been suggested by Hall (1976), one of the characteristics of the system.

A possible source of error in defining the infrared excess is in the assumption that the photometric points may be connected by a smooth curve. If substantial line emission occurs in some broad bandpass filters this assumption is invalid.

4.3 Expected Depth of Minima

This section describes the method used to estimate the expected depths of minima of a binary system at a given wavelength λ_1, when the depths at another wavelength λ, the intrinsic colour $[\lambda_1]-[\lambda]$ of the system and of the two components separately were known.

Let us assume that a binary system has total luminosity L_T (or in other words has luminosity outside eclipse) which is expressed by

$$L_T = \pi R_1^2 S_1 + \pi R_2^2 S_2 \qquad 4.3.1$$

where R_1, R_2 are the radii of the components 1 and 2 and S_1 and S_2 are their surface brightnesses. During any of the eclipses (primary or secondary) the eclipsed area of one or the other star is the same, let us assume equal to AE. Then during the one eclipse the luminosity of the system is

$$L_1 = \pi R_1^2 S_1 + \pi R_2^2 S_2 - S_1 AE \qquad 4.3.2$$

while during the other eclipse it is

$$L_2 = \pi R_1^2 S_1 + \pi R_2^2 S_2 - S_2 AE \qquad 4.3.3$$

From equations 4.3.1, 4.3.2 and 4.3.3

$$L_1 = L_T - S_1 AE \qquad 4.3.4$$

$$L_2 = L_T - S_2 AE \qquad 4.3.5$$

and from equation 4.3.4, we have

$$AE = \frac{L_T - L_1}{S_1} \; ;$$

but AE is the same for both situations, thus

$$\left(\frac{L_T - L_1}{S_1}\right)_{\lambda_1} = \left(\frac{L_T - L_1}{S_1}\right)_{\lambda_2}$$

or

$$(L_T - L_1)_{\lambda_1} = \frac{S_{1_{\lambda_1}}}{S_{1_{\lambda_2}}} (L_T - L_1)_{\lambda_2} \qquad 4.3.6$$

But $\frac{S_{1_{\lambda_1}}}{S_{1_{\lambda_2}}} = \frac{F_{1_{\lambda_1}}}{F_{1_{\lambda_2}}}$ if F_1 is the flux from component 1 and equation 4.3.6 becomes

$$(L_T - L_1)_{\lambda} = \frac{F_{1_{\lambda_1}}}{F_{1_{\lambda_2}}} (L_T - L_1)_{\lambda_2}$$

or

$$L_{T_{\lambda_1}} \left(1 - \frac{L_1}{L_T}\right)_{\lambda_1} = \left(\frac{F_{1_{\lambda_1}}}{F_{1_{\lambda_2}}}\right) L_{T_{\lambda_2}} \left(1 - \frac{L_1}{L_T}\right)_{\lambda_2}$$

or

$$\left(1 - \frac{L_1}{L_T}\right)_{\lambda_1} = \left(\frac{F_{1_{\lambda_1}}}{F_{1_{\lambda_2}}}\right) \frac{L_{T_{\lambda_2}}}{L_{T_{\lambda_1}}} \left(1 - \frac{L_1}{L_T}\right)_{\lambda_2} \qquad 4.3.7$$

The quantity $\frac{L_{T_{\lambda_2}}}{L_{T_{\lambda_1}}}$ (the ratio of the total luminosity of the system in

two colours) is calculated by the relation:

$$\frac{L_{T_{\lambda_2}}}{L_{T_{\lambda_1}}} = 10^{-\frac{[\lambda_2] - [\lambda_1]}{2.5}} + C$$

where $[\lambda_1] - [\lambda_2]$ is the colour expected from the spectral types of the components of the system, and C is a zero-point constant that depends on the system of magnitudes used.

While the ratio of the fluxes of the eclipsed star in two colours $\frac{F_{1_{\lambda_1}}}{F_{1_{\lambda_2}}}$ is equal to

$$\frac{F_{1_{\lambda_1}}}{F_{1_{\lambda_2}}} = 10^{-\frac{[\lambda_2] - [\lambda_1]}{2.5}} - C$$

where the colour $[\lambda_2] - [\lambda_1]$ is the intrinsic colour of the eclipsed component and C is a constant as defined before, by the same process the relation giving the other minimum can be obtained using equation 4.3.5 instead of 4.3.4, which is analogous with equation 4.3.7. Thus the other minimum is given by the relation:

$$\left(1 - \frac{L_2}{L_T}\right)_{\lambda_1} = \left(\frac{F_{2_{\lambda_1}}}{F_{2_{\lambda_2}}}\right) \frac{L_{T_{\lambda_2}}}{L_{T_{\lambda_1}}} \left(1 - \frac{L_2}{L_T}\right)_{\lambda_2} \qquad 4.3.8$$

with the different quantities defined as before.

4.4 Estimation of the Period of some RS CVn Systems using Infrared Photometric Data

For some RS CVn systems, no accurate knowledge of their period exists, either because there are not enough observations, or because the period is probably variable. For stars observed for this project and belonging to this category, with continuous light variations, an

effort was made to determine the periodicity hidden in their observed brightness, using the author's infrared photometric data. A Fourier analysis program was applied to these data in order to find the fundamental frequency, or in other words the frequency that gives the best fit.

Several researchers have previously used the Fourier analysis technique to analyse the periodicities of variables (e.g. Barning 1963; Wehlau and Leung 1964; Valtier 1972; Gray and Desikachary 1973; Smyth et al. 1975; Stobie and Shobbrook 1976). Barning (1963) was the first to use this technique, which is in fact a "least squares" analysis of data, to determine the periodicities hidden in 12 Lac brightness observations. The "least squares" Fourier analysis has been described by Barning (1963) and also by Valtier (1972), so only some definitions that are connected with this analysis and will be used in the present work, are introduced.

Let us assume that M(t) is the observed data, to which it is desired to fit a trigonometric polynomial T(t), with unknown frequency and coefficients A and B given by

$$T(t) = A \cos 2\pi\omega t + B \sin 2\pi\omega t$$

For different frequencies ω, in a given frequency interval, it is possible to calculate values of A and B that lead to an optimum approximation of M(t) by T(t) in the "least squares" sense. So for each of the above pairs of A and B the least mean distance of M(t) from T(t) can be calculated:

$$X = \left[\sum [M(t) - T(t)]^2\right]^{\frac{1}{2}}$$

Reduction Factor R is then defined as

$$R = 1 - \frac{X}{[M(t)]^{\frac{1}{2}}}$$

which gives dominant frequencies in the form of peaks. From the optimum frequency (frequency with the largest Reduction Factor) the optimum periodicity of the brightness variation of the variable can be determined ($P = 1/\omega$). The amplitude C (which is equal to half the amplitude of the variation) can be estimated for each frequency in a given interval from the optimum A and B coefficients using the relation

$$C = (A^2 + B^2)^{\frac{1}{2}}$$

The "least squares" Fourier analysis was applied to AD Cap, which probably has a variable period, and to HD 5303 which has been observed very little and for which no accurate period is known. A discussion on this is given in Chapter V where these stars are discussed extensively.

4.5 Study of the Variations Outside Eclipse

For a better understanding of the variations outside eclipse observed at visual wavelengths, which is the most fascinating aspect of RS CVn binaries, some selected systems were extensively observed in the infrared, J, H and K wavebands mainly and occasionally in L. The aim was firstly to see if these variations exist also at infrared wavelengths and secondly to combine the infrared with published visible photometry and other observational data to model the systems.

4.5.1 "Least squares" Fourier analysis for estimation of amplitude and time of minima of the wave-like light variations

Another version of the method described in section 4.4 was applied to the current observations in order to obtain an unbiased measure of the time of minima and the amplitude of the observed light variations in the infrared of some selected RS CVn systems, knowing the period of the variation. The method is based on the following: It is known that if f(t) is a function that varies with time periodically with period p and $2\pi/p = \omega$ is the fundamental frequency, then f(t) can be analysed into an infinite sum of harmonic components at multiples of the fundamental frequency, which is known as a Fourier series expansion. So

$$T(t) = \sum_{n=0}^{\infty} \left(A_n \cos n\omega t + B_n \sin n\omega t \right)$$

In the present case the fundamental frequency of the periodic observed light variation M(t) is known. For this frequency, it is possible to estimate A and B which lead to an optimum approximation of T(t) to M(t) in a "least squares" sense. Then the amplitude of the variation can be determined ($C = (A^2 + B^2)^{\frac{1}{2}}$) and also the time of minimum.

For the current work the observed light variations of the non-eclipsing RS CVn system HR 1099, are periodic variations of sinusoidal type. In order to estimate the amplitudes of variation in different wavebands and the phase of the minima, the observed points were fitted with truncated Fourier series, knowing the fundamental frequency of the variation. A "least squares" Fourier analysis program was used in the ROE GEC 4082 computer in order to find the optimum A_n and B_n coefficients for the given frequency and also the time of minima of the variation; the results of this fit for the different

sets of observations of HR 1099 are given in section 5.1.

For eclipsing RS CVn systems for which the current infrared observations show light variations outside eclipse (SZ Psc, TY Pyx), the outside eclipse data were fitted to a truncated Fourier series in order to find the phase of minimum and the amplitude of the wave-like light distortion. In this case the period of the wave has been assumed to be equal to the orbital period of the system under study.

The same method has also been used to find the epoch of miminum light variation in two other RS CVn systems extensively observed for the current work, AD Cap and HD 5303, which also (like HR 1099) show continuous light variations.

In this chapter the extensively observed RS CVn systems are discussed individually. The list of these stars and also the ephemerides used to determine their phase and the comparison stars used for the observations are summarised in Table 3.3.1. Table 5.1 gives the available physical parameters of the systems discussed in this chapter.

5.1 HR 1099 (≡ V711 Tau ≡ HD 22468 ≡ ADS 2644A)

HR 1099 is a double-lined spectroscopic binary (Bopp and Fekel 1976) and a member of the class of RS CVn systems (Landis and Hall 1976) with strong and variable CaII and Hα emission lines (Wilson 1963, 1964; Bond 1976; Weiler et al. 1978). The observed light variations of the binary system in the visual (Bopp et al. 1977; Landis et al. 1978) have shown that HR 1099 does not eclipse; this is consistent with the orbital inclination of the system, $i = 34°$ or $38°$, given by Bopp and Fekel (1976). The light variation changes in amplitude and time of minima in the visual (Chambliss et al. 1978; Guinan et al. 1979), Because of these observational peculiarities, the system has recently been intensively observed in various spectral regions, especially after it was found to be a radio variable with frequent, strong radio outbursts (Owen 1976; Ryle 1976; Feldman et al. 1978a,b) and also with variable soft and hard X-ray emission (Walter et al. 1978d; White et al. 1978). Several campaigns on HR 1099 have been organised by different astronomers in order to search for correlations among the various observed phenomena: in September 1976 (Weiler et al. 1978; White et al. 1978), in October 1977 (Weiler

TABLE 5.1

Physical Parameters of RS CVn Binaries Chosen for Study

Star	M_h Solar Units		M_c	R_h Solar Units		R_c	Hα Emission		H and K Emission		Distance pc
HR 1099	1.1	(1)	1.3	3.0	(1)	3.0	V	(2)	both	(2)	35
UV Psc									both	(3)	125
SZ Psc	1.33	(4)	1.65	2.1	(5)	5.6	V	(6)	cool	(7)	100
TY Pyx	1.20	(8)	1.22	1.65	(8)	1.65			both	(8)	85
AD Cap	0.5	(4)	1.1						both	(3)	250
HD 5303							V	(9)	cool	(9)	
ER Vul	1.07	(10)	0.98						?	(11)	45

( ) = References

1 Bopp and Fekel
2 Wilson 1964
3 Popper 1969
4 Oliver 1974
5 Jakate et al. 1976
6 Weiler 1976
7 Bakos and Heard 1958
8 Andersen and Popper 1975
9 Hearnshaw and Oliver 1977
10 Northcott and Bakos 1967
11 Bond 1970

1977; Bartolini et al. 1978), and especially the one following the large radio outburst that started 20 September 1978 and lasted for almost two weeks, during which a series of outbursts was observed. An almost entire issue of the Astronomical Journal was devoted to the latter (Vol. 83, No.12, 1978), with all kinds of observations (photometric, spectroscopic, polarimetric) in a variety of spectral regions.

A discussion of the observational characteristics of HR 1099 in different regions of the electronomagnetic spectrum follows.

Since late 1976 Feldman and his collaborators have been engaged in a systematic program of monitoring the entire class of RS CVn systems north of -33° declination for radio emission in the centimetre region (2.8 cm), including HR 1099. The telescope they have been using is the 46 m telescope of the Algonquin Observatory. During their observing sessions they detected a series of very strong flares from the system. The most prominent radio flares observed by Feldman and his collaborators and also by other astronomers are summarised in Table 5.1.1. It is worth pointing out here that the radio flux density of quiescent HR 1099 is less than 20 mJy (1 Jy = 10^{-26} W m^{-2} Hz^{-1}) at the frequencies 1390 MHz and 2380 MHz (Mutel and Weisberg 1978).

No correlation was found between the radio activity and the orbital phase (Bartolini et al. 1978; Chambliss et al. 1978), while enhanced CaII, Hα and Lyα emission were observed during radio flares (Hobbs et al. 1978; Popper 1978; Bopp and Talcott 1978; Weiler et al. 1978). A correlation has however been found between the radio and X-ray activity of HR 1099. A three-hour X-ray outburst has been detected by the COPERNICUS 2.5-7.5 KeV detector, coincident with the

TABLE 5.1.1

Detected Radio Outbursts from HR 1099 since 1976

Time#	Frequency (in GHz)	Flux Density* (in Jy)	References
10 March 1976	8.085	0.179	Owen 1976, Owen et al. 1976
	2.695	0.134	Owen 1976
24 September 1976	8.085	0.190	Weiler et al. 1978
	2.695	0.120	Weiler et al. 1978
20 February 1978	15.50	1.040	Feldman et al. 1978a,b
	10.52	0.963	Feldman et al. 1978a,b
	7.87	0.980	Feldman et al. 1978a,b
	8.0	0.800	Aller et al. 1978
	14.5	0.820	Aller et al. 1978
	86.1	$\sim$ 0.5	Epstein and Briggs 1978
19 July 1979	10.76	1.2	Feldman et al. 1979
14 June 1980	10.48	0.2	

The time at which the radio flare was first detected.

* The peak flux density observed in the given flare outburst.

September 1976 (Table 5.1.1) large radio flare (White et al. 1978). Linsky et al. (1978) also obtained fluxes for several UV emission lines in the spectral range (1175-2000 Å) with the IUE during the last stages of the February 1978 radio outburst. Their observations showed that HR 1099 had line surface fluxes $\sim$ 100 times that of the quiet Sun, similar to those seen in solar flares. The mechanism responsible for the radio emission from HR 1099 is almost certainly nonthermal synchrotron radiation from mildly relativistic electrons as has been suggested by Owen et al. (1976) and Spangler (1977). Feldman et al. (1978b) gave the same explanation and also suggested that the radio radiation is emitted from a volume whose characteristic dimension is several times larger than the size of the active star but comparable with the separation of the two components. The nonthermal nature of the radio radiation is also supported by Epstein and Briggs' (1978) observations at millimetre wavelength (86.1 GHz) which yielded an upper limit for the flux density significantly less than would be expected if the spectrum were thermal. The suggested synchrotron radiation from mildly relativistic electrons as the emission mechanism of the radio radiation and not the fully relativistic synchrotron process is consistent with the high circular polarisation (up to 74% at 2380 MHz, Mutel and Weisberg 1978) occasionally observed, during large radio flares, from the system; in fully relativistic synchrotron emission and for a wide range of electron energy distribution no circular polarisation exceeding about 10% can be expected (Jones and O'Dell 1977a,b).

Another characteristic of HR 1099 observed at radio wavelengths is that the radiation of the system at these wavelengths is occasionally highly circularly polarised. No significant optical polarisation

has been observed (Weiler et al. 1978), while circular polarisation as high as 74% at 2380 MHz and 48% at 1390 MHz has been reported (Mutel and Weisberg 1978). Circular polarisation has also been observed by several other workers, e.g. Owen et al.(1976), Brown and Crane (1978), Gibson et al. (1978). The latter observed HR 1099 to be 20% right-hand circularly polarised at 4885 MHz during October 1977, which was a quiescent period for the system. No correlation of the flux density or the percentage polarisation with the phase of the system was found. They suggested as the most probably explanation of the observed polarisation the existence of a large-scale ordered magnetic field in HR 1099. But while HR 1099 is highly circularly polarised at radio frequencies, no linear polarisation has been detected. Mutel and Weisberg (1978) explained the absence of linear polarisation as the result of Faraday depolarisation of the radiation.

HR 1099 was first discovered to be an X-ray emitter by Walter et al. (1978d). Walter et al (1978b) discussed their observations of HR 1099, carried out with low energy detectors (energy range 0.2-2.8 KeV) on board the HEAO 1 satellite. They explained the observed quiescent X-ray emission from HR 1099, and also from other RS CVn systems, in terms of coronal emission at a temperature of $\sim 10^7$ K; according to them this very hot corona is driven by mass and energy ejection from the flares which have been frequently observed. HR 1099 is not only an X-ray emitter but also a variable X-ray emitter. As has been mentioned earlier, strong X-ray emission has been detected from the system during a large flare outburst (White et al. 1978).

Wilson (1963,1964) was the first to note the existence of strong H and K emission lines with a width of the order of 1 Å in the spectrum of HR 1099. He also pointed out that Hα, a rather strong

absorption line in such stars, is found to be in emission, having a width of 5 to 6 Å. More recently Bopp and Fekel (1976) studied the system spectroscopically and they found variations in the profile of Hα and also that the absorption lines from both components have approximately equal intensity, suggesting a similarity in the spectral classification of the two stars. The intensity of the emission lines appear however to be quite different, suggesting an active atmosphere for one component. Both Bopp and Fekel (1976) and Weiler et al. (1978) have shown that the hydrogen emission is associated with the cooler, more massive component. Bopp and Talcott (1978) have reported changes in Hα intensity on a time scale as short as 20 min during the large radio outburst in February 1978; they also pointed out the general strong enhancement of Hα during the previously mentioned radio flare, with a peak EW near 3 Å. A question now arises: are the CaII and Hα emission lines correlated with the light variation of the system, or in other words do the emission lines vary periodically with orbital phase? Bopp and Talcott (1978) found that during the February 1978 radio flare the mean Hα was nearly constant for a large fraction of the orbital phase (0.30-0.98). Weiler et al. (1978) reported equivalent width and profile variations of Hα emission from HR 1099 and also strong and not significantly variable CaII emission. Spectroscopic observations by Nations and Ramsey (1980) show the Hα equivalent width to undergo a modulation over the orbital period, in antiphase with the photometric distortion wave of the system. More observations are necessary to obtain a definite answer about the existence of a correlation between the light variation and the observed variation in Hα emission.

Strong and variable emission lines in the spectrum of HR 1099 have also been detected in the ultraviolet. HR 1099 has been found to exhibit strong and variable MgII h and k and Lyα emission lines. Observations with COPERNICUS show that Lyα emission seems marginally correlated with the orbital phase, with maximum emission occuring near the phase of photometric wave minimum, while the MgII emission line profiles usually match the velocity of the more active star (Weiler et al. 1978).

The last observational characteristic of HR 1099 to be discussed is its visual light variability, which seems to be closely correlated with the infrared light variations investigated in the present project. Cousins (1963) was the first to report the visual light variability of HR 1099; he reported an amplitude in V equal to $0^{m}.11$ from eight observations. 13 years after Cousins' report Landis and Hall (1976) confirmed the light variability of HR 1099 in V and published the first light curve of the system. Since then several visual light curves have been published, showing that the light variations of HR 1099 have variable amplitude and phase of minima and also that the system shows a variable maximum magnitude. In Table 5.1.2 the characteristics of the available visual light curves are given. It is worth mentioning here that the system is flaring in the visual as in radio wavelengths as has been reported by different observers (Landis et al. 1978; Bartolini et al. 1978; Guinan et al. 1979). The maximum observed increase of magnitude in V was at JD 2443054.76 - 2443054.81 when the differential magnitude brightened from $1^{m}.55$ to $1^{m}.40$ (Landis et al. 1978).

TABLE 5.1.2

Characteristics of the wave in the visual

Time of observations	Phase of minimum	Amplitude of variation	(μm)	References
1963.0	$0^{p}.654$*	$0^{m}.11$	0.55	Cousins 1963
1976.0	0.644#	0.111#	0.55	Bopp et al. 1977
1976.15	0.569#	0.078#	0.55	Bopp et al. 1977
1976.65	0.502#	0.129#	0.55	Landis et al. 1978
1977.83	0.680#	0.072#	0.55	Bartolini et al. 1978
1977.95 radio outburst	0.680	0.075	0.6563	Guinan et al. 1979
1978.20	0.74	0.078	0.55	Chamblis et al. 1978
1979.15 radio outburst	0.886+	0.21	0.55	Chambliss and Detterline 1979
1979.90	0.95	0.13	0.6563	Guinan et al. 1979

* Bopp et al. 1978

Antonopoulou and Williams 1980

+ as calculated in the present work

HR 1099 was the first and the most observed star in the present project. The reason was that HR 1099 is a non-eclipsing system, as mentioned earlier, and if an understanding could be reached, it would then be easier to understand the light variations outside eclipse of the eclipsing RS CVn systems.

HR 1099 has been followed in the infrared, J H K L L', since October 1976 in several observing sessions as is shown in Table 5.1.3. The main bulk of observations were made since October 1978 using the MkII infrared photometer of SAAO (section 3.1) using an indium antimonide detector on the 0.75 m telescope at Sutherland. The observations in Tables 5.1.4 and 5.1.5 have an accuracy of $\sim 0\overset{m}{.}05$, consequently they have not been used to determine the amplitude of the light variations (expected to be of the order of $0\overset{m}{.}1$ or less) and the time of their minima. However, the minimum of the light variation which is derived from the observations given in Table 5.1.5 is consistent with the results obtained from the more accurate data (accuracy $0\overset{m}{.}02$ or better). The September 1979 observations, Table 5.1.7, have not also been used for obtaining any information about the characteristics of the light variations, as they are not sufficient because of weather conditions during that observing run. The main sources for accurate scientific conclusions are the observations obtained in October 1978 (Table 5.1.6) and November-December 1979 (Table 5.1.8). In Table 5.1.9 the occasional H observations of HR 1099 during the November-December run are given. The system was observed occasionally at H in order to study only its colour.

The ephemeris used for the determination of the phases of the observations is:

$$T_o(JD) = 2442766.069 + 2\overset{d}{.}83782E$$

TABLE 5.1.3

Infrared Observations of HR 1099

Time	Comparison Star	Wavelengths	Telescope - Site	Detector	Note
10/10/76 - 24/10/76		K L'*	1.5 m - Tenerife	InSb/Bolo	Table 5.1.4
31/08/77 - 15/09/77	α Ari	J H K L'	1.5 m - Tenerife	InSb	Table 5.1.5
10/10/78 - 30/10/78	10 Tau	J H K L#	0.75 m - SAAO	InSb	Table 5.1.6
18/09/79 - 01/10/79	10 Tau	J H K	0.75 m - SAAO	InSb	Table 5.1.7
19/11/79 - 10/12/79	10 Tau	J H K L	0.75 m - SAAO	InSb	Table 5.1.8 Table 5.1.9

* L' λ_0 = 3.8 μm

L λ_0 = 3.4 μm

TABLE 5.1.4

HR 1099 - Infrared Magnitudes

JD 2440000 +	ϕ	K	L'	Detector
3062.60	0.492	3.40	3.28	InSb
3062.66	0.514	3.40	3.32	InSb
3063.57	0.834	3.30	3.20	InSb
3063.73	0.891	3.23	3.11	InSb
3064.65	0.216		3.29	Bolo
3067.63	0.265		3.21	Bolo
3067.70	0.290		3.34	Bolo
3068.58	0.600		3.55	Bolo
3068.68	0.635		3.33	Bolo
3072.57	0.006		3.52	Bolo
3072.60	0.016		3.35	Bolo
3072.69	0.048		3.32	Bolo

TABLE 5.1.5

HR 1099 - Differential Magnitudes*

JD 2440000 +	ϕ	ΔJ	ΔH	ΔK	$\Delta L'$
3387.71	0.056		3.90	3.84	3.82
3388.68	0.398		3.94	3.92	3.90
3388.73	0.415		3.93	3.93	3.85
3389.71	0.761	3.89	3.93	3.89	3.86
3389.73	0.768	3.86	3.90	3.88	3.82
3390.72	0.117	3.83	3.85	3.84	3.82
3391.74	0.476		3.90	3.86	3.83
3392.75	0.832		3.95	3.94	3.86
3393.69	0.163		3.92	3.93	3.89
3394.76	0.540		4.02	3.96	3.91
3395.68	0.864		3.92	3.90	3.84
3396.73	0.234	3.93	3.94	3.91	3.87
3396.80	0.259		3.89	3.88	3.88
3397.70	0.576	3.88	3.94	3.94	3.89
3397.75	0.594	3.96	3.98	3.95	3.91

* with respect to α Ari

TABLE 5.1.6

HR 1099 - Differential Magnitudes

JD 2440000 +	ϕ	ΔJ	ΔH	ΔK	ΔL
3792.50	0.697	0.73	0.41	0.33	0.24
3792.52	0.704	0.72	0.48	0.35	0.27
3792.58	0.721	0.74	0.48	0.34	0.26
3792.60	0.728	0.73	0.46	0.35	0.26
3792.63	0.744	0.72	0.42	0.31	0.22
3793.49	0.044	0.70	0.40	0.33	0.23
3793.51	0.054	0.70	0.40	0.34	0.24
3793.56	0.070	0.74	0.49	0.35	0.24
3793.58	0.074	0.72	0.41	0.34	0.28
3793.63	0.094	0.71	0.41	0.34	0.29
3794.50	0.401	0.65	0.36	0.29	0.23
3794.54	0.414	0.65	0.36	0.29	0.20
3794.56	0.424	0.68	0.39	0.30	0.15
3794.60	0.440	0.67	0.38	0.30	0.22
3794.62	0.444	0.68	0.37	0.30	0.26
3795.44	0.733	0.71	0.37	0.29	0.18
3795.46	0.736	0.72	0.37	0.31	0.24
3795.49	0.750	0.71	0.43	0.37	0.33
3795.51	0.754	0.96	0.62	0.51	0.47
3796.44	0.084	0.73	0.42	0.33	0.28
3796.46	0.094	0.72	0.41	0.34	0.28
3801.43	0.844	0.75	0.42	0.33	0.26
3801.46	0.854	0.74	0.45	0.36	0.30
3801.47	0.859	0.73	0.45	0.36	0.20
3801.58	0.894	0.72	0.44	0.34	0.30
3801.60	0.904	0.72	0.44	0.35	0.28
3801.62	0.910	0.75	0.44	0.36	0.30
3802.48	0.213	0.66	0.37	0.30	0.24
3802.49	0.217	0.67	0.37	0.30	0.21
3802.52	0.224	0.63	0.35	0.26	0.15
3802.54	0.234	0.65	0.36	0.30	0.18
3802.57	0.244	0.64	0.36	0.30	
3802.59	0.254	0.66	0.37	0.28	

TABLE 5.1.6 (cont'd)

JD 2440000 +	ϕ	ΔJ	ΔH	ΔK	ΔL
3802.61	0.259	0.64	0.34	0.27	
3806.44	0.609	0.67	0.40	0.33	
3806.45	0.614	0.67	0.39	0.33	
3806.47	0.620	0.72	0.37	0.30	
3806.50	0.630	0.67	0.37	0.28	
3806.55	0.647	0.68	0.41	0.31	
3806.57	0.655	0.70	0.40	0.30	
3807.55	0.984	0.74	0.44	0.36	
3807.57	0.004	0.73	0.46	0.36	
3807.59	0.014	0.72	0.44	0.37	
3807.60	0.024	0.73	0.45	0.35	
3809.38	0.645	0.70	0.42	0.36	
3809.42	0.659	0.68	0.41	0.33	
3809.54	0.694	0.69	0.41	0.31	
3809.56	0.704	0.67	0.40	0.31	
3809.58	0.714	0.69	0.42	0.32	
3810.46	0.024	0.71	0.43	0.34	0.25
3810.50	0.039	0.72	0.44	0.34	0.30
3810.52	0.044	0.72	0.43	0.33	0.32
3810.57	0.064	0.71	0.41	0.33	
3810.59	0.069	0.73	0.41	0.34	0.28
3810.61	0.074	0.72	0.41	0.33	0.26

TABLE 5.1.7

HR 1099 - Differential Magnitudes

JD 2440000 +	ϕ	ΔJ	ΔH	ΔK
4140.55	0.344	0.66	0.36	0.27
4140.56	0.347	0.65	0.36	0.27
4140.57	0.351	0.66	0.37	0.29
4140.58	0.355	0.65	0.36	0.28
4140.59	0.358	0.65	0.36	0.29
4140.60	0.362	0.67	0.36	0.28
4140.61	0.365	0.65	0.36	0.28
4140.62	0.369	0.64	0.35	0.27
4140.63	0.372	0.65	0.36	0.29
4143.57	0.408	0.64	0.35	0.29
4143.58	0.412	0.68	0.37	0.30
4143.59	0.415	0.66	0.34	
4143.60	0.419	0.64	0.35	0.28
4143.61	0.422	0.65	0.35	0.28
4143.62	0.426	0.65	0.34	0.28
4144.55	0.754	0.70	0.38	0.30
4144.56	0.757	0.70	0.38	0.30
4144.57	0.760	0.69	0.38	0.30
4144.59	0.768	0.68	0.38	0.30
4144.60	0.771	0.69	0.38	0.31
4144.61	0.775	0.69	0.39	0.31
4144.63	0.782	0.68	0.37	0.32
4146.59	0.472	0.66	0.37	0.30
4146.60	0.476	0.67	0.37	0.30
4146.60	0.478	0.66	0.37	0.29
4146.61	0.480	0.66	0.37	0.30
4146.62	0.483	0.67	0.37	0.29

TABLE 5.1.8

HR 1099 - Differential Magnitudes

JD	ϕ	ΔJ	ΔK	ΔL
2440000 +				
4200.45	0.452	0.66	0.29	0.22
4200.46	0.455	0.65	0.29	0.23
4200.47	0.459	0.67	0.30	0.20
4200.48	0.462	0.66	0.29	0.25
4200.51	0.473	0.68	0.32	0.28
4200.52	0.476	0.68	0.32	0.25
4201.42	0.793	0.71	0.32	0.20
4201.43	0.797	0.73	0.33	0.24
4202.49	0.171	0.72	0.32	0.26
4202.50	0.174	0.71	0.32	0.25
4202.51	0.177	0.71	0.32	0.26
4202.52	0.181	0.70	0.32	0.28
4203.45	0.509	0.67	0.29	0.21
4203.45	0.509	0.67	0.29	0.24
4203.46	0.512	0.67	0.30	0.22
4203.47	0.516	0.67	0.29	0.23
4203.49	0.523	0.67	0.31	0.24
4203.50	0.526	0.67	0.30	0.25
4204.43	0.856	0.75	0.35	0.32
4204.44	0.858	0.75	0.35	0.29
4204.45	0.861	0.75	0.35	0.29
4204.46	0.865	0.73	0.35	0.27
4206.45	0.566	0.68	0.31	0.25
4206.46	0.570	0.68	0.31	0.23
4206.47	0.573	0.69	0.31	0.26
4206.48	0.577	0.69	0.31	0.25
4206.50	0.584	0.69	0.30	0.24
4206.51	0.587	0.68	0.29	0.24
4207.42	0.908	0.74	0.34	0.29
4207.43	0.911	0.73	0.33	0.30
4207.44	0.915	0.73	0.34	0.30
4207.45	0.918	0.76	0.36	0.30
4207.46	0.922	0.76	0.35	0.32

TABLE 5.1.8 (cont'd)

JD 2440000 +	ϕ	ΔJ	ΔK	ΔL
4207.48	0.929	0.75	0.35	0.28
4207.49	0.933	0.75	0.35	0.29
4207.50	0.936	0.76	0.36	0.30
4209.37	0.595	0.65	0.30	0.26
4209.38	0.599	0.65	0.31	0.26
4209.39	0.602	0.65	0.31	0.28
4209.42	0.613	0.66	0.30	0.30
4211.45	0.328	0.68		
4212.43	0.673	0.68	0.30	0.27
4212.44	0.677	0.69	0.30	0.26
4212.45	0.680	0.69	0.30	0.25
4212.46	0.684	0.68	0.30	0.25
4212.47	0.687	0.68	0.30	0.25
4212.48	0.691	0.68	0.31	0.24
4212.49	0.694	0.69	0.30	0.25
4213.44	0.029	0.74	0.35	0.28
4213.45	0.033	0.75	0.35	0.27
4213.48	0.043	0.74	0.36	0.27
4213.49	0.047	0.76	0.35	0.26
4213.49	0.049	0.74	0.34	0.28
4213.50	0.052	0.74	0.34	0.33
4216.37	0.062	0.73	0.35	0.26
4216.43	0.085	0.73	0.35	0.25
4216.44	0.086	0.73	0.35	0.26
4216.45	0.09	0.73	0.35	0.27
4216.46	0.093	0.73	0.35	0.27
4216.49	0.104	0.72	0.33	0.27
4216.49	0.104	0.71	0.33	0.28
4217.42	0.432	0.66	0.30	0.21
4217.43	0.435	0.66	0.29	0.22
4217.44	0.439	0.65	0.29	0.21
4217.48	0.453	0.67	0.30	0.24
4217.49	0.456	0.66	0.30	0.25
4217.50	0.460	0.66	0.29	0.23

TABLE 5.1.8 (cont'd)

JD 2440000 +	ϕ	ΔJ	ΔK	ΔL
4217.51	0.463	0.66	0.30	0.24
4218.43	0.788	0.70	0.33	0.26
4218.44	0.791	0.69	0.33	0.28
4218.45	0.795	0.70	0.31	0.26
4218.46	0.798	0.69	0.33	0.23
4218.47	0.802	0.70	0.33	0.28
4218.48	0.805	0.70	0.34	0.27
4226.39	0.539	0.68	0.31	0.24
4226.40	0.596	0.69	0.32	0.24
4226.41	0.600	0.69	0.33	0.23
4226.42	0.603	0.69	0.33	0.24
4226.44	0.610	0.68	0.30	0.28
4226.45	0.614	0.68	0.31	0.26
4227.39	0.945	0.75	0.36	0.26
4227.40	0.948	0.74	0.36	0.28
4227.41	0.952	0.75	0.37	0.30
4227.42	0.956	0.75	0.36	0.32
4227.42	0.956	0.75	0.36	0.33
4227.43	0.959	0.75	0.38	0.34
4228.41	0.304	0.68	0.30	0.23
4228.41	0.304	0.67	0.30	0.19
4228.42	0.308	0.67	0.30	0.21
4228.42	0.308	0.68	0.30	0.26
4228.45	0.318	0.67	0.28	0.24
4228.46	0.322	0.67	0.28	0.26
4230.39	0.002	0.73	0.36	0.32
4230.40	0.006	0.74	0.36	0.33
4230.41	0.009	0.74	0.37	0.31
4230.41	0.009	0.75	0.38	0.31
4231.39	0.354	0.68	0.31	0.25
4231.40	0.358	0.68	0.31	0.26
4231.41	0.361	0.69	0.31	0.31
4231.42	0.365	0.69	0.31	0.27
4231.43	0.369	0.65	0.30	0.23

TABLE 5.1.8 (cont'd)

JD 2440000 +	ϕ	ΔJ	ΔK	ΔL
4231.44	0.372	0.65	0.30	0.22
4231.45	0.376	0.66	0.29	0.24
4232.40	0.710	0.69	0.31	0.27
4232.41	0.714	0.70	0.32	0.26
4232.42	0.717	0.71	0.33	0.26
4232.42	0.717	0.72	0.35	
4233.29	0.024	0.75	0.36	0.23
4233.30	0.027	0.75	0.37	0.29
4233.31	0.031	0.76	0.37	0.28
4233.32	0.035	0.76	0.38	
4233.33	0.038	0.75	0.37	0.24
4233.34	0.042	0.73	0.36	0.25
4233.35	0.045	0.75	0.36	0.25
4234.36	0.401	0.66	0.29	0.22
4234.37	0.405	0.66	0.29	0.22
4234.38	0.408	0.66	0.29	0.22
4234.39	0.412	0.65	0.29	0.21
4234.41	0.419	0.66	0.28	0.25
4234.41	0.419	0.66	0.30	0.26
4234.42	0.422	0.66	0.29	0.26
4234.43	0.426	0.66	0.29	0.25
4235.36	0.755	0.70	0.32	0.26
4235.38	0.760	0.70	0.31	0.25
4235.39	0.764	0.69	0.31	0.25
4235.39	0.764	0.69	0.30	0.22
4235.41	0.771	0.70	0.31	0.24
4235.41	0.771	0.69	0.32	0.24
4235.42	0.775	0.70	0.32	0.28
4236.36	0.106	0.73	0.34	0.31
4236.37	0.109	0.73	0.34	0.31
4236.38	0.113	0.72	0.33	0.27
4236.39	0.116	0.71	0.33	0.26
4236.39	0.116	0.70	0.32	0.32
4236.40	0.120	0.72	0.33	0.25
4236.41	0.123	0.72	0.33	0.28
4236.41	0.123	0.72	0.33	0.26

TABLE 5.1.9

HR 1099 - Differential Magnitudes

JD 2440000 +	ϕ	ΔH	JD 2440000 +	ϕ	ΔH
4230.39	0.002	0.43	4234.41	0.419	0.37
4230.40	0.006	0.43	4235.36	0.750	0.40
4231.39	0.354	0.42	4235.41	0.771	0.39
4231.43	0.369	0.38	4236.36	0.106	0.43
4232.40	0.710	0.38	4236.38	0.113	0.42
4233.29	0.024	0.43	4236.39	0.116	0.42
4233.34	0.042	0.43	4236.40	0.120	0.42
4234.36	0.401	0.38	4236.41	0.123	0.41
4234.39	0.412	0.37			

where the period is spectroscopically determined by the Bopp and Fekel (1976) orbital period while the zero phase corresponds to conjunction with the more active component in front. As it is known the more active component of the RS CVn type binary systems is the cooler component, so this conjunction is the one where the primary eclipse would occur if HR 1099 were an eclipsing system. The ephemeris given by Bopp and Fekel (1976) had the zero phase at periastron while the one given by Bopp et al. (1977) had zero phase at minimum light as of 1976.0. The photometric measures included both the components of the visual pair ADS 2644. The observations obtained in October 1978 are illustrated in Figure 5.1.1, and the November-December observations in Figure 5.1.2. In Figure 5.1.2 the September 1979 data are also shown; these seem to match the 1979 observations, but around phase 0.4 they suggest that the system was probably brighter in September. In the Figure 5.1.3 the colour curves $\Delta(J-K)$ for the 1978 and 1979 observations are given.

In order to obtain unbiased measures of the light and colour ($\Delta(J-K)$) variations of HR 1099 the October 1978 and the November-December 1979 observations are fitted with a truncated Fourier series (section 4.5.1) using the orbital period as the period of the light variation. The results of this analysis are given in Table 5.1.10. In the same Table the weighted average phases of minima for the two different epochs are also given. The weighted average of the data points is given by the relation

$$\mu = \frac{\Sigma(x_i/\sigma_i^2)}{\Sigma(1/\sigma_i^2)}$$

where each data point x_i is weighted inversely by its own variance σ_i^2 in the sum, while the uncertainty of the mean σ_μ is given by the

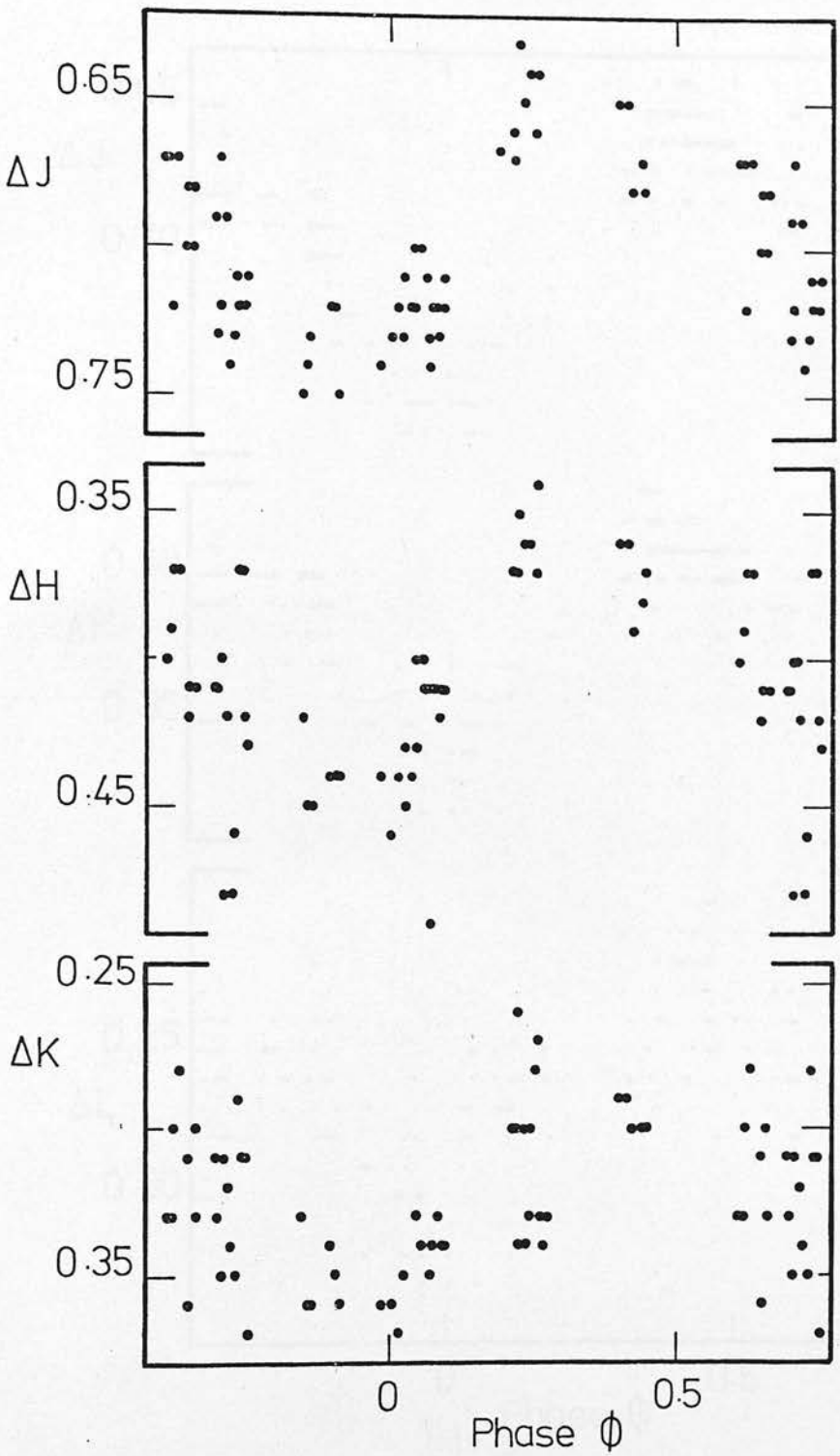

Figure 5.1.1 HR 1099 - Differential light curves; October 1978 observations

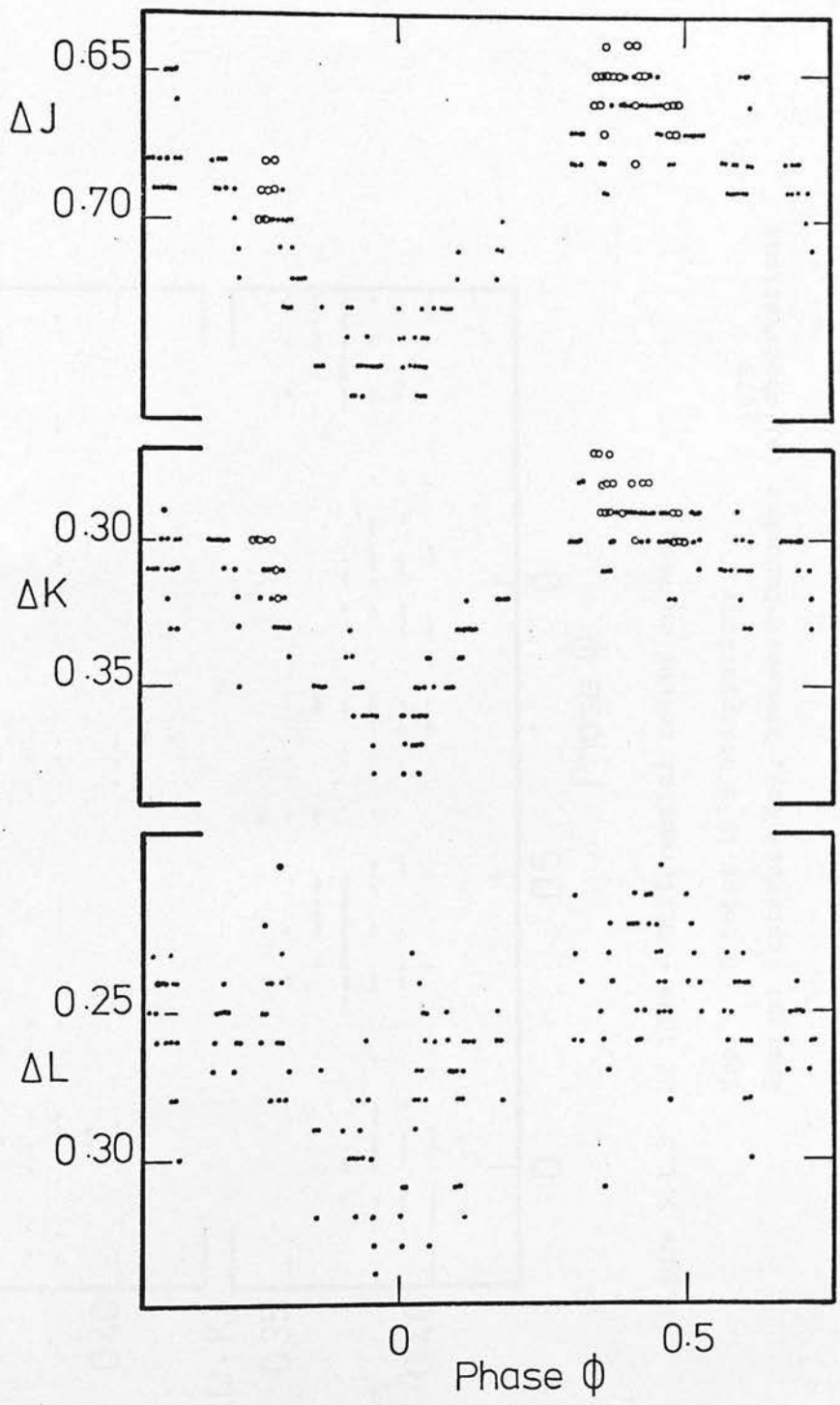

Figure 5.1.2 HR 1099 - Differential light curves; September 1979(o) and November-December 1979(•) observations

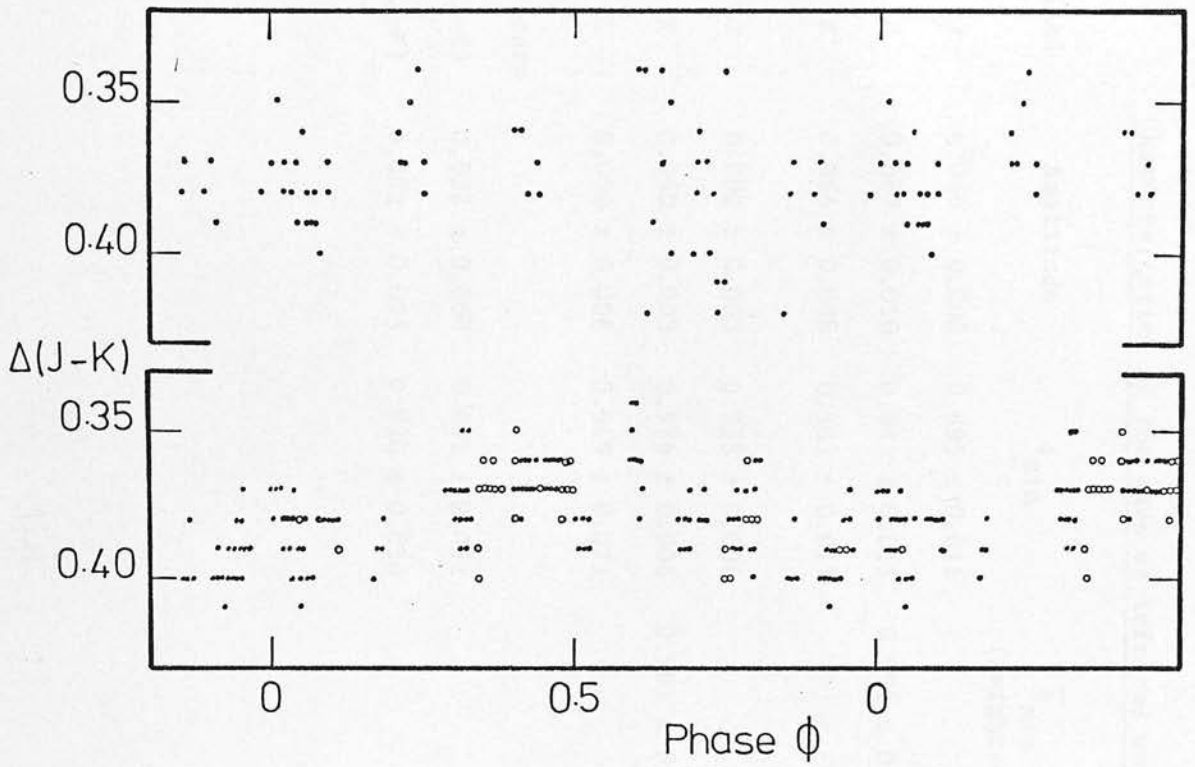

Figure 5.1.3 HR 1099 - Differential colour curves

Top: October 1978 observations

Bottom: September (o), November-December (•) 1979 observations

TABLE 5.1.10

Characteristics of the wave at infrared wavelengths

Band	Amplitude	ϕ_{min}	$\overline{\phi}_{min}$ (weighted)	Time of observations
J	$0^{m}.086 \pm 0.008$	0.895 ± 0.011		
H	0.087 ± 0.010	0.885 ± 0.015	0.894 ± 0.008	October 1978
K	0.064 ± 0.008	0.903 ± 0.015		
J	0.082 ± 0.003	0.953 ± 0.006		
K	0.060 ± 0.003	0.976 ± 0.008	0.961 ± 0.005	Nov-Dec 1979
L	0.050 ± 0.006	0.949 ± 0.021		
colours				
Δ'(J-K)	0.022 ± 0.008	0.862 ± 0.052		October 1978
Δ(J-K)	0.022 ± 0.003	0.980 ± 0.020		Nov-Dec 1979

formula

$$\sigma_{\mu}^{2} = \frac{1}{\Sigma(1/\sigma_{i}^{2})}$$

Comparison of Figure 5.1.3 with Figures 5.1.1 and 5.1.2 shows that the light and colour variations of HR 1099 for both epochs (October 1978 and November-December 1979) are in phase and that the minima of light and colour curves are coincident. This is also obvious from the "least squares" Fourier analysis result for these curves given in Table 5.1.10.

From Table 5.1.10 also it may be noted that between October 1978 and November-December 1979 the wave has changed a little in amplitude for the different colours and in phase of minimum. The amplitude seems to be a little smaller in late 1979, while the wave appears to migrate towards increasing phase (Chapter VI). The observed change in phase of minimum is 0.067 ± 0.013 in 13.5 months. This implies a migration period of the wave (towards increasing phase) equal to 16.8 ± 2.7 years. But if the visual phases of minima, derived from observations made in the time between the 1978 and 1979 infrared observations, are taken into account for the determination of the migration period of the wave (Chapter VI) then a different period is found. All the observed phases of minima of the wave and also the calculated migration period P of the wave for each period between two observed phases of minima are given in Table 5.1.11.

In Figure 5.1.4 the phase of minima of the wave-like light variations (Table 5.1.2 and 5.1.10) and the amplitude of the wave in V (Table 5.1.2) are plotted against phase. From this Figure it can be seen that only marginal anticorrelation exists between phase of minima and amplitude of variation while from Table 5.1.11 the migration

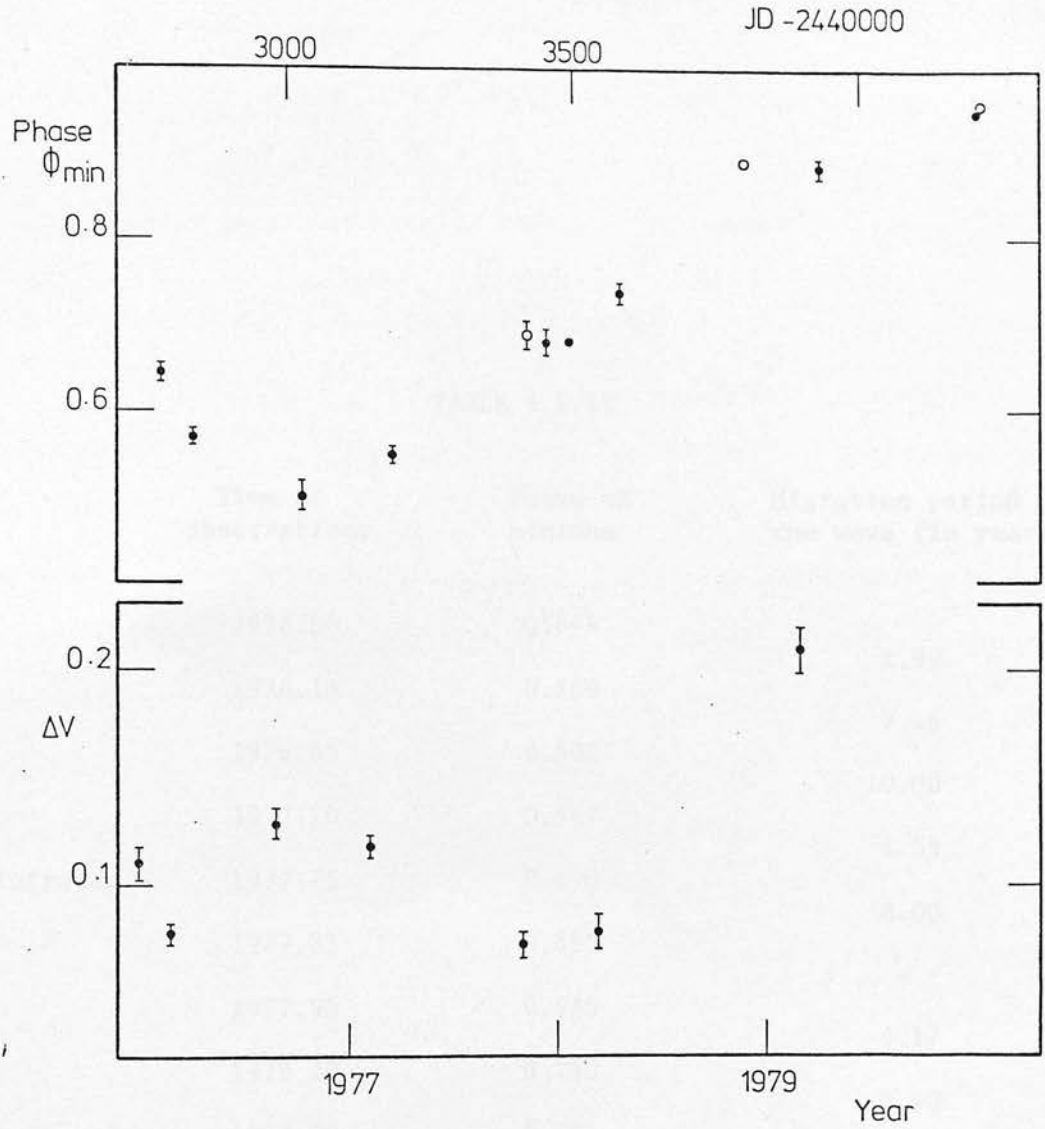

Figure 5.1.4 Top: The calculated phase of minima against epoch

Bottom: The calculated amplitude of light variation in V against epoch

(The filled circles denote the visual and the open circles the infrared observations.)

TABLE 5.1.11

	Time of observations	Phase of minimum	Migration period of the wave (in years)
	1976.00	$0^{P}.644$	
	1976.15	0.569	1.99
	1976.65	0.502	7.46
	1977.10	0.547	10.00
infrared	1977.75	0.690	4.55
	1977.83	0.680	8.00
	1977.95	0.680	-
	1978 20	0.740	4.17
infrared	1978.80	0.894	3.90
	1979.15	0.886	43.75
	1979.90	0.950	11.72
infrared	1979.95	0.961	4.54

period seems to be correlated marginally with the amplitude of the variation. From Figure 5.1.4 and also from Table 5.1.11 it is obvious that with the available data it is not meaningful to speak of migrating cycles of the wave, but it seems that the wave is migrating towards increasing or decreasing phases with a variable speed.

To determine the colours of HR 1099 the comparison star 10 Tau was tied to Glass's 1974 standards. 10 Tau's infrared magnitudes are given in Table 3.3.3. Simultaneous visual and infrared observations were made at phases of maximum light. The visual colours V-R, V-I, were transformed to Johnson's system using the relations given by Bessell (1979). The average colours of several observations were corrected for the contribution of the third component as all the observations made included the visual companion ADS 2644B. Eggen's (1968) UBV photometry of ADS 2644B indicates that it is an unreddened star of type between K2V and K5V, in keeping with Wilson's (1964) type of K3V. The estimated visual magnitude and colours for HR 1099 are then

V	B-V	V-R	V-I	V-J	V-H	V-K	V-L
5.83	0.93	0.77	1.38	1.86	2.43	2.58	2.65

The spectral types of the components of HR 1099 are uncertain but, as was observed by Bopp and Fekel (1976), the two components have about the same type. The energy distribution of the system (Figure 5.1.5) suggests a combination of KOV and K2IV components (from Johnson's 1966 temperature scale). According to the observed colours of HR 1099, using the method described in section 4.1 and the previously mentioned criteria (spectroscopic evidence of about the same spectral types and energy distribution) the most probable combination of the two

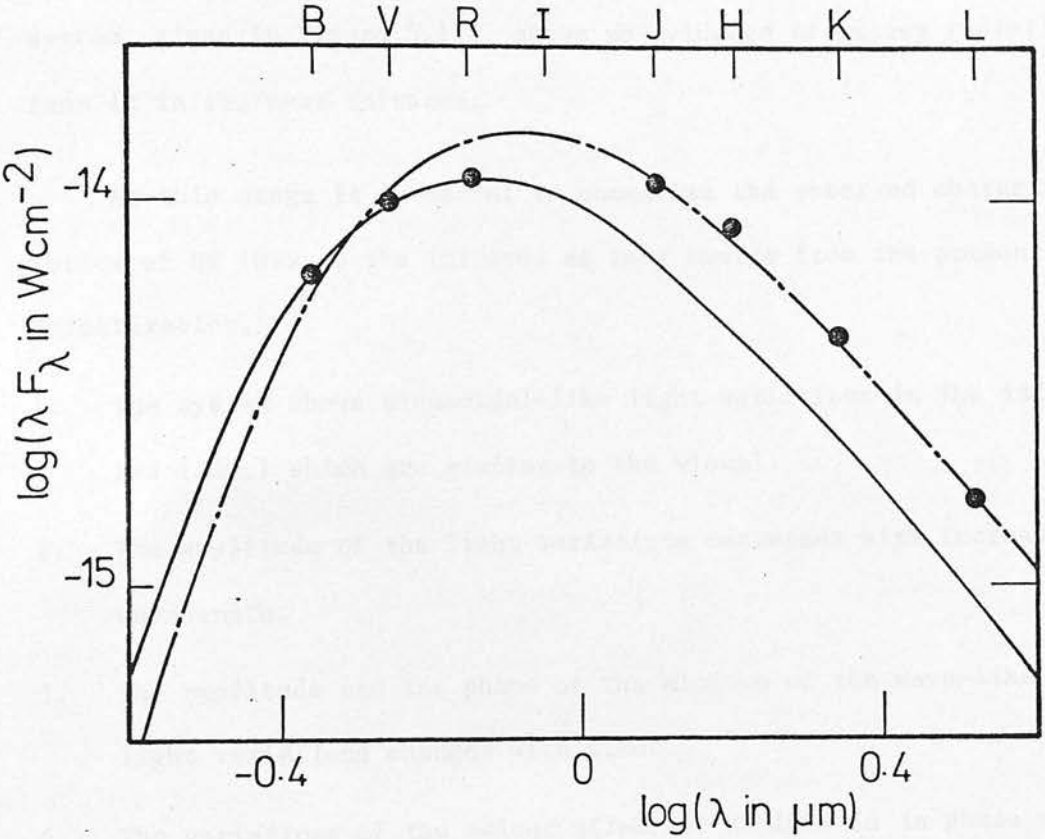

Figure 5.1.5 HR 1099 - Energy distribution

components of HR 1099 is K0V for the hotter star and K3IV for the cooler companion; the χ^2 test gives a value of 0.051 for this combination of components (section 4.1). The energy distribution of the system, given in Figure 5.1.5, shows no evidence of excess radiation from it in the near infrared.

At this stage it is useful to summarise the observed characteristics of HR 1099 in the infrared as they emerge from the present investigation.

1. The system shows sinusoidal-like light variations in the infrared (JHKL) which are similar to the visual.
2. The amplitude of the light variations decreases with increasing wavelength.
3. The amplitude and the phase of the minimum of the wave-like light variations changes with time.
4. The variations of the colour $\Delta(J-K)$ of HR 1099 is in phase with its light variations, or in other words the system is redder in its brightness minimum.
5. The wave seems to migrate towards increasing phases at least since October 1977.
6. The speed of the migration of the wave is variable.
7. No conspicuous infrared excess, attributable to circumstellar emission, has been observed from the system.
8. Sudden changes of the system's brightness in all observed colours (JD 2443795.51, Table 5.1.6); similar variations have been observed in the visual.

5.2 UV Piscium

UV Psc, also designated HD 7700, BV 149 and BD +6°0189, was discovered from photographic plates to be an eclipsing system by Strohmeier et al. at the Remeis-Bamberg Observatory in Germany in 1957. It was reported to be $9^m.6$ at its maximum light and to have a primary minimum $0^m.7$ deep. Strohmeier et al. (1957) also reported five times of minimum from photographic studies and one time of minimum has been announced by Nikulina (1958) from visual observations. Huth (1959) published in the "Mitteilungen über veränderliche Sterne" a light curve of UV Psc made by Strohmeier from 348 photographic plates. The elements given in this report are 2428038.555 + $0^d.861046E$, while the magnitude range of the system is reported to be $9^m.6$–$10^m.5$. One year later Strohmeier and Knigge (1960) published a new light curve, again photographic observations, which gave the maximum brightness of the star as $0^m.3$ brighter than the last time and the primary minimum $1^m.05$ deep. The first photoelectric observations of the system were reported by Carr (1967) in his unpublished thesis. He observed UV Psc in B and V filters and analysed the light curves in order to determine the orbital elements. From his UBV photometry he concluded that the system is made up of two main sequence stars of spectral classes G5V and dK2. More photoelectric observations were published by Oliver (1974) who obtained a light curve, incomplete outside minima, in the visual region. His light curve does not show any evidence of asymmetries while the one observed by Carr, less than half a year earlier, shows a depression around phase 0.75 while the depths of the minima are very similar in both light curves, $0^m.85$ at primary minimum and $0^m.2$ at secondary. Oliver suggested that the most probable spectral classification for the system's components according

to the visual observed colours are G2V and K0IV or G2IV and K0IV. Recent visual observations of UV Psc were made in 1977 by Sadik (1979). His light curves in B and V show that asymmetries at their maxima exist; Sadik suggested that a locally hotter region is possibly responsible for the irregularities.* The only spectroscopic observations known to the author are by Popper (1969), showing emission of both components present at H and K. UV Psc has been found to be a flaring radio source at 6 cm by Spangler et al. (1977) while Agrawal et al. (1980) observed a flaring X-ray emission from the system in the energy range 0.18 to 3 KeV.

Infrared observations of UV Psc were carried out in October 1978 (Table 5.1.2), September 1979 (Table 5.2.2), and November-December 1979 (Table 5.2.3), using the 0.75 m telescope at Sutherland and InSb detector. Thus all the observations were made using the same photometer, detector, filters and telescope. HR 434 was adopted as comparison star; its infrared colours are given in Table 3.3.3. The observations were made in JHK and rarely in L as the photometer and the telescope used were not suitable for accurate (error less than $0^m.05$) L observation for objects fainter than 5^m in K. The phases of the observations were calculated from the ephemeris given by Huth (1959)

$$T_o(JD) = 2428038.555 + 0^d.861046E$$

and they are given in Tables 5.2.1, 5.2.2 and 5.2.3 where the differential magnitudes are summarised; the light curves defined by the observations in J, H and K are illustrated in Figures 5.2.1 (October 1978 and September 1979 observations) and 5.2.2 (November-December

---

* His observations also indicate that the depth of the primary minimum at V is equal to $0^m.85$ and that of the secondary is $0^m.35$.

TABLE 5.2.1

UV Psc - Differential Magnitudes

JD 2440000 +	ϕ	ΔJ	ΔH	ΔK
3792.43	0.206	5.16	5.51	5.59
3792.45	0.229	5.16	5.50	5.55
3793.44	0.379	5.19	5.52	5.55
3794.41	0.505	5.53	5.92	5.98
3794.45	0.540	5.41	5.75	5.80
3794.48	0.575	5.19	5.52	5.56
3795.36	0.609	5.18	5.49	5.55
3802.39	0.773	5.17	5.51	
3802.43	0.820	5.15	5.47	5.52
3809.32	0.830	5.12	5.48	5.53
3809.34	0.840	5.12	5.51	5.58
3809.35	0.860	5.15	5.50	5.55
3809.45	0.970	5.21	5.62	5.72
3809.46	0.980	5.45	5.88	6.07
3809.48	0.007	5.77	6.10	6.19
3809.52	0.054	5.53	5.90	6.04
3810.38	0.053	5.38	5.65	5.63
3810.40	0.076	5.20	5.51	5.57
3810.41	0.088	5.17	5.50	5.56

TABLE 5.2.2

UV Psc - Differential Magnitudes

JD 2440000 +	ϕ	ΔJ	ΔH	ΔK
4137.44	0.890	5.14	5.51	5.54
4137.45	0.893	5.13	5.51	5.55
4137.45	0.905	5.13	5.49	5.55
4137.46	0.916	5.12	5.51	5.56
4137.46	0.916	5.13	5.50	5.54
4137.47	0.927	5.13		
4141.47	0.580	5.18	5.47	5.54
4141.48	0.585	5.14	5.47	5.54
4141.49	0.597	5.15	5.52	5.53
4141.50	0.610	5.15	5.51	5.58
4141.51	0.620	5.19	5.56	5.56
4143.38	0.792	5.13	5.49	5.52
4143.39	0.800	5.12	5.49	5.56
4143.40	0.815	5.13	5.50	5.54
4143.41	0.826	5.13	5.51	5.54
4143.42	0.838	5.15	5.51	5.55
4143.43	0.850	5.14	5.51	5.54
4143.45	0.873	5.13	5.49	5.55
4143.46	0.885	5.12	5.50	5.54
4143.47	0.896	5.14	5.48	5.56
4143.48	0.901	5.14	5.47	5.57
4143.49	0.920	5.14	5.50	5.56
4143.52	0.954	5.13	5.51	5.55
4143.53	0.966	5.18	5.57	5.64
4143.54	0.977	5.28	5.66	5.75
4143.55	0.989	5.36	5.77	5.84
4144.44	0.023	5.77	6.11	6.12
4144.45	0.034	5.77	6.04	6.01
4144.46	0.046	5.61	5.89	5.87
4144.46	0.050	5.48	5.77	5.73
4144.47	0.057	5.36	5.67	5.65
4144.48	0.069	5.29	5.59	5.60
4144.49	0.080	5.18	5.54	5.57

TABLE 5.2.2 (cont'd)

JD 2440000 +	ϕ	ΔJ	ΔH	ΔK
4144.50	0.092	5.17	5.53	5.54
4144.51	0.104	5.16	5.54	5.56
4144.52	0.116	5.17	5.52	5.56
4144.53	0.127	5.19	5.54	5.55
4144.54	0.139	5.17	5.53	5.57
4145.41	0.149	5.16	5.49	5.51
4145.42	0.160	5.15	5.49	5.53
4146.40	0.299	5.12	5.44	5.55
4146.41	0.310	5.12	5.43	5.52
4146.42	0.322	5.12	5.43	5.54
4146.43	0.333	5.11	5.46	5.54
4146.44	0.345	5.10	5.47	5.50
4146.45	0.357	5.10	5.49	5.54
4146.46	0.369	5.10	5.56	5.55
4146.47	0.380	5.09	5.51	5.53
4146.48	0.392	5.12	5.49	5.53
4146.51	0.427	5.14	5.56	5.58
4146.52	0.438	5.17	5.52	5.57
4146.53	0.450	5.15	5.49	5.55
4146.54	0.455	5.22		5.61
4146.55	0.462	5.22	5.58	5.67
4146.56	0.470			5.75

TABLE 5.2.3

UV Psc - Differential Magnitudes

JD 2440000 +	ϕ	ΔJ	ΔH	ΔK
4201.38	0.152	5.15	5.50	5.52
4201.39	0.163	5.18	5.50	5.53
4201.40	0.175	5.15	5.50	5.54
4202.31	0.232	5.13	5.47	5.53
4202.32	0.243	5.12	5.48	5.56
4202.33	0.255	5.12	5.48	5.53
4202.33	0.261	5.13	5.50	5.54
4202.34	0.266	5.15	5.50	5.56
4203.32	0.405	5.15	5.52	5.55
4204.33	0.578	5.20	5.54	5.56
4204.34	0.589	5.17	5.52	5.57
4204.35	0.600	5.17	5.50	5.55
4204.36	0.613	5.15	5.50	5.54
4204.37	0.624	5.15	5.50	5.56
4206.29	0.854	5.15	5.48	5.53
4206.30	0.865	5.17	5.50	5.53
4206.31	0.877	5.16	5.51	5.56
4206.32	0.889	5.17	5.52	5.55
4206.33	0.900	5.19	5.52	5.54
4206.34	0.912	5.20	5.51	5.58
4206.34	0.918	5.19	5.51	5.58
4206.35	0.929	5.21	5.52	5.60
4206.36	0.941	5.21	5.55	5.58
4206.37	0.947	5.23	5.54	5.58
4206.38	0.958	5.25	5.58	5.67
4206.39	0.970	5.32	5.66	5.72
4206.40	0.982	5.39	5.74	5.81
4206.41	0.993	5.53	5.88	6.00
4206.42	0.005	5.66	6.00	6.05
4210.32	0.534	5.50	5.87	5.90
4210.33	0.546	5.42	5.75	5.79
4210.34	0.558	5.30	5.63	5.67
4210.35	0.569	5.24	5.59	5.64

TABLE 5.2.3 (cont'd)

JD 2440000 +	ϕ	ΔJ	ΔH	ΔK
4210.37	0.592	5.18	5.51	5.58
4210.39	0.616	5.20	5.52	5.58
4210.39	0.621	5.20	5.51	5.58
4211.28	0.649	5.16	5.50	5.56
4211.29	0.661	5.17	5.51	5.58
4211.30	0.672	5.17	5.51	5.58
4211.32	0.696	5.17	5.51	5.57
4211.33	0.707	5.17	5.51	5.56
4211.34	0.719	5.17	5.53	5.56
4211.35	0.731	5.17	5.51	5.57
4211.37	0.754	5.16	5.49	5.56
4211.38	0.765	5.17	5.50	5.55
4211.39	0.777	5.15	5.51	5.56
4211.40	0.789	5.16	5.53	5.56
4212.27	0.799	5.14	5.51	5.58
4212.28	0.811	5.14	5.50	5.56
4212.29	0.822	5.13	5.49	5.54
4212.30	0.834	5.13	5.50	5.54
4212.31	0.845	5.14	5.51	5.54
4212.32	0.857	5.14	5.50	5.55
4212.33	0.869	5.16	5.50	5.55
4212.34	0.880	5.15	5.50	5.54
4212.35	0.892	5.14	5.50	5.54
4212.36	0.904	5.16	5.49	5.55
4212.37	0.915	5.16	5.53	5.57
4212.38	0.927	5.16	5.51	5.56
4212.39	0.938	5.14	5.53	5.56
4212.40	0.950	5.17	5.50	5.56
4213.26	0.949	5.14	5.50	5.55
4213.28	0.972	5.18	5.57	5.64
4213.28	0.972	5.25	5.68	5.71
4213.29	0.989	5.37	5.79	5.87
4213.30	0.995	5.58	5.98	5.92
4213.31	0.007	5.68	6.05	6.09

TABLE 5.2.3 (cont'd)

JD 2440000 +	ϕ	ΔJ	ΔH	ΔK
4213.32	0.018	5.74	6.06	6.09
4213.33	0.030	5.74	6.06	6.09
4213.33	0.030	5.70	5.98	6.01
4213.34	0.042	5.59	5.86	5.84
4213.35	0.053	5.42	5.71	5.72
4213.36	0.065	5.29	5.61	5.62
4213.37	0.077	5.19	5.54	5.55
4213.38	0.088	5.13	5.50	5.54
4213.39	0.100	5.13	5.50	5.56
4213.39	0.106	5.13	5.50	5.56
4213.40	0.111	5.14	5.50	5.54
4213.41	0.123	5.12	5.47	5.57
4214.30	0.157	5.16	5.51	5.54
4214.31	0.168	5.16	5.49	5.54
4214.32	0.180	5.16	5.51	5.56
4214.33	0.191	5.16	5.51	5.58
4214.33	0.191	5.16	5.51	5.55
4214.34	0.203	5.16		
4216.39	0.584	5.19	5.51	5.55
4216.40	0.596	5.16	5.55	5.64
4216.41	0.607	5.31	5.75	5.92
4217.32	0.664	5.17	5.53	5.57
4217.33	0.676	5.18	5.50	5.56
4217.34	0.687	5.16	5.51	5.57
4217.35	0.699	5.16	5.49	5.55
4217.36	0.710	5.14	5.49	5.55
4217.37	0.722	5.14	5.48	5.53
4217.38	0.734	5.15	5.46	5.57
4218.30	0.802	5.15	5.49	5.53
4218.31	0.814	5.15	5.49	5.51
4218.32	0.825	5.14	5.49	5.50
4218.32	0.825	5.16	5.50	5.52
4218.33	0.837	5.14	5.48	5.52
4218.34	0.849	5.14	5.48	5.50

TABLE 5.2.3 (cont'd)

JD 2440000 +	ϕ	ΔJ	ΔH	ΔK
4218.35	0.860	5.15	5.49	5.51
4218.36	0.872	5.15	5.50	5.50
4218.37	0.883	5.16	5.45	5.52
4218.37	0.889	5.14	5.49	5.51
4218.38	0.895	5.13	5.50	5.52
4218.39	0.907	5.14	5.47	5.52
4218.39	0.907	5.17	5.49	5.54
4226.30	0.092	5.24	5.52	5.57
4226.32	0.116	5.17	5.50	5.59
4226.33	0.128	5.17	5.52	5.56
4226.35	0.151	5.18	5.52	
4227.32	0.278	5.14	5.50	5.55
4227.32	0.284	5.14	5.51	5.55
4227.33	0.284	5.13	5.51	5.55
4227.34	0.301	5.16	5.50	5.56
4227.35	0.313	5.19	5.51	5.58
4227.36	0.324	5.19	5.52	5.56
4230.34	0.785	5.16	5.48	5.54
4230.35	0.797	5.17	5.52	5.56
4230.36	0.808	5.18	5.51	5.58
4230.36	0.808	5.19	5.54	5.61
4230.37	0.820	5.22	5.61	5.74
4231.30	0.900	5.16	5.52	5.58
4231.31	0.912	5.18	5.52	5.57
4231.32	0.923	5.18	5.51	5.56
4231.32	0.923	5.20	5.49	5.58
4231.33	0.935	5.17	5.49	5.55
4231.34	0.946	5.16	5.47	5.55
4231.34	0.946	5.11	5.50	5.55
4231.35	0.958	5.16	5.49	5.54
4231.36	0.970	5.17	5.54	5.61
4231.37	0.976	5.22	5.60	5.75
4234.28	0.361	5.16	5.50	5.57
4234.29	0.373	5.18	5.54	5.57

TABLE 5.2.3 (cont'd)

JD 2440000 +	ϕ	ΔJ	ΔH	ΔK
4234.30	0.384	5.17	5.53	5.57
4234.31	0.396	5.17	5.54	5.59
4234.32	0.407	5.20	5.53	5.55
4234.33	0.419	5.23	5.56	5.62
4236.32	0.730	5.15	5.50	5.56
4236.33	0.742	5.17	5.51	5.54
4236.33	0.742	5.14	5.49	5.55
4236.34	0.753	5.13	5.48	5.54
4238.33	0.065	5.35	5.63	5.65
4238.34	0.076	5.23	5.60	5.63
4239.29	0.179	5.15	5.49	5.54
4239.30	0.191	5.17	5.50	5.56
4239.31	0.203	5.16	5.49	5.57
4239.32	0.214	5.14	5.49	5.56
4239.32	0.214	5.15	5.51	5.56
4239.33	0.226	5.15	5.49	5.54

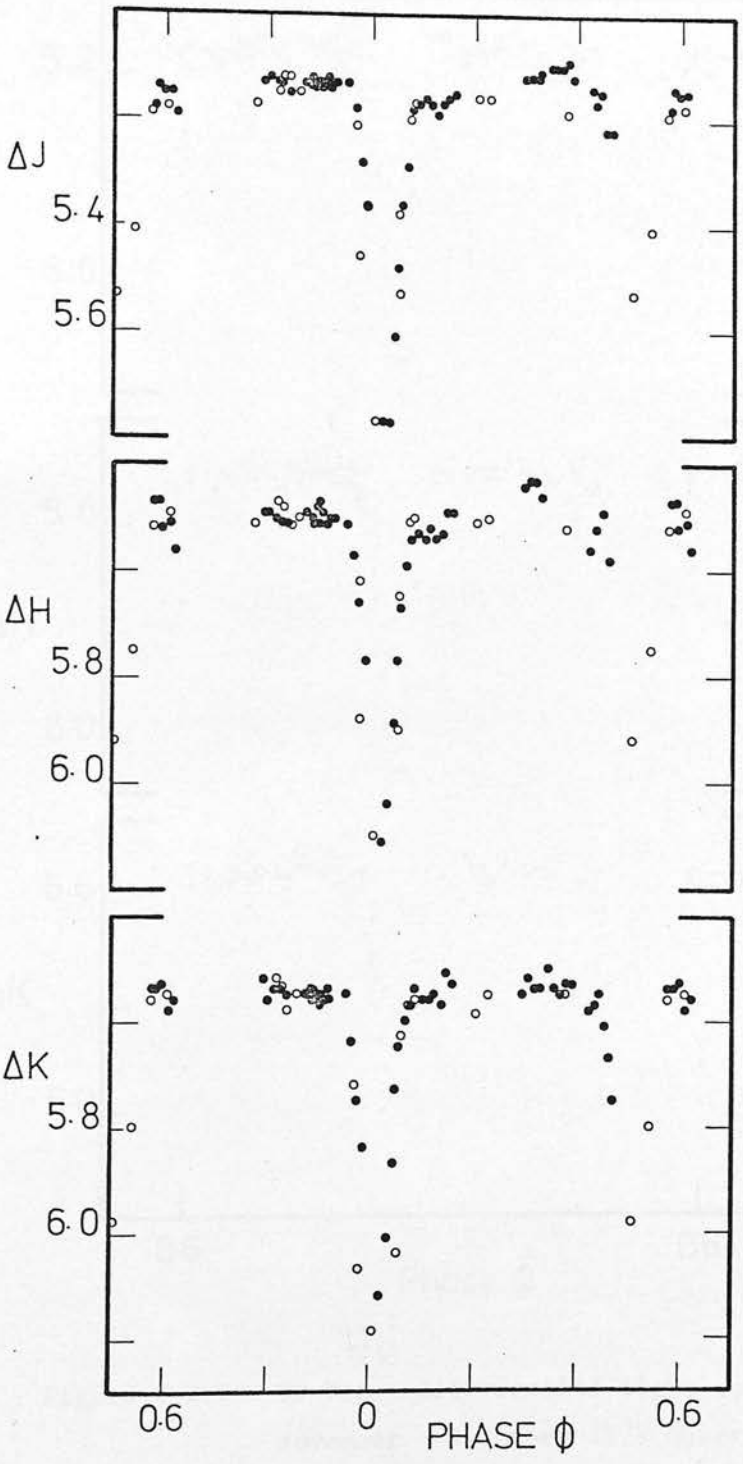

Figure 5.2.1 UV Psc - Differential light curves; October 1978(o) and September 1979(•) observations

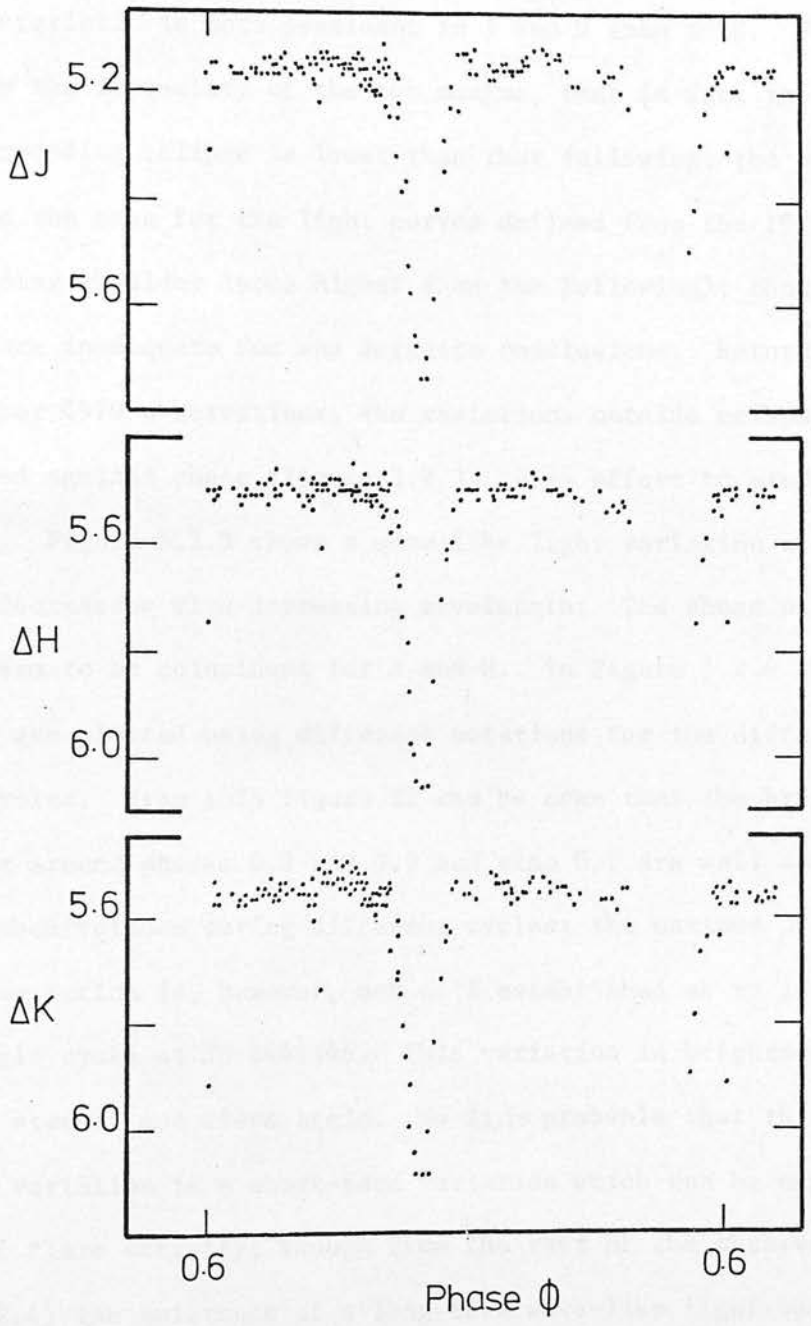

Figure 5.2.2 UV Psc - Differential light curves; November - December 1979 observations

1979 observations). The infrared light curves obtained in the present work indicate that the system shows long and short time scale variations. The September 1979 observations show unequal maxima; this characteristic is more prominent in J and H than in K. Figure 5.2.1 shows the inequality of the two maxima, that in fact the shoulder preceding eclipse is lower than that following; the opposite seems to be the case for the light curves defined from the 1978 data (the preceding shoulder looks higher than the following); though the 1978 data are inadequate for any definite conclusions. Returning to the September 1979 observations, the variations outside eclipse have been plotted against phase (Figure 5.2.3) in an effort to study these variations. Figure 5.2.3 shows a wave-like light variation with an amplitude decreasing with increasing wavelength; The phase of maxima does not seem to be coincident for J and H. In Figure 5.2.4 the same variations are plotted using different notations for the different observed cycles. From this figure it can be seen that the brightness of the star around phases 0.8 and 0.9 and also 0.1 are well established by observations during different cycles; the maximum of the wave-like variation is, however, not well established as it is derived from a single cycle at JD 2444146. This variation in brightness drops very steeply and rises again. So it is probable that this particular variation is a short-term variation which can be explained in terms of flare activity; though from the rest of the observations (Figure 5.2.4) the existence of a long-term wave-like light variation with amplitude decreasing with increasing wavelength is certain. The characteristics of this wave cannot be estimated because of the lack of adequate observations. Another prominent characteristic of the September 1979 infrared light curves is the difference in the height

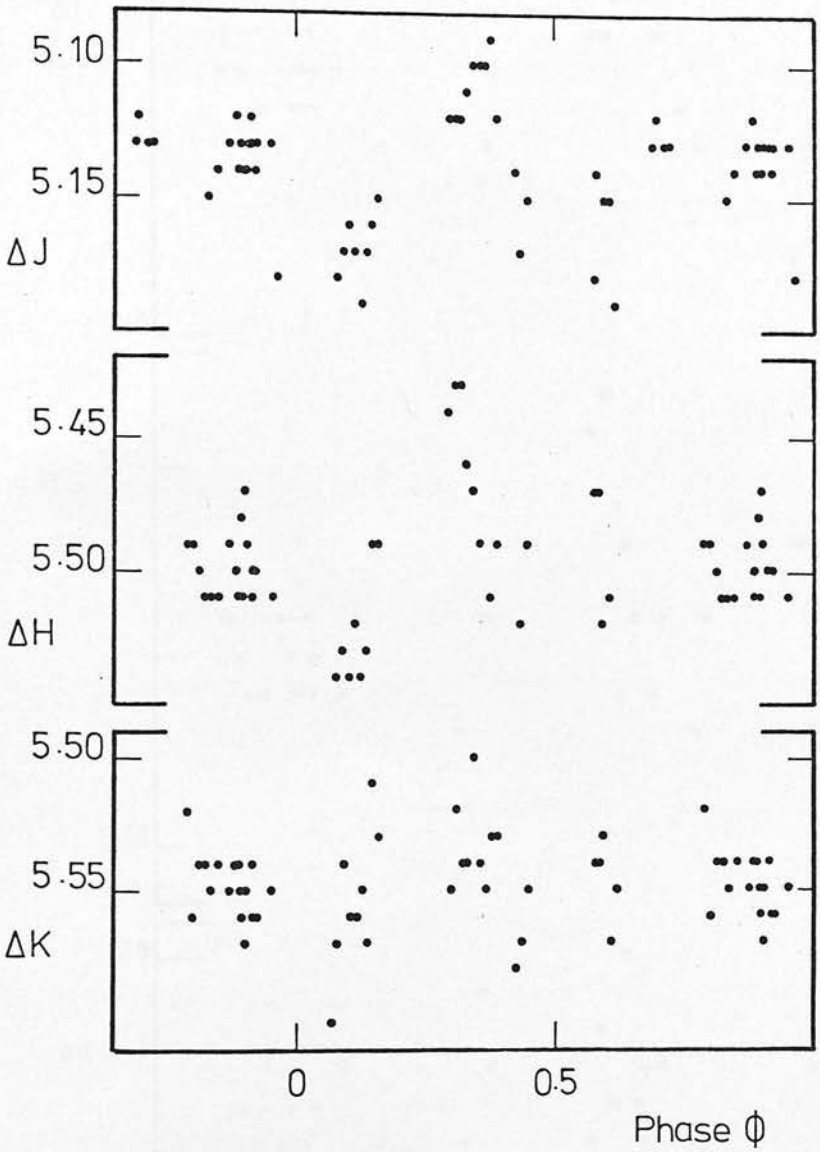

Figure 5.2.3 UV Psc - Light variations outside eclipse

September 1979 observations

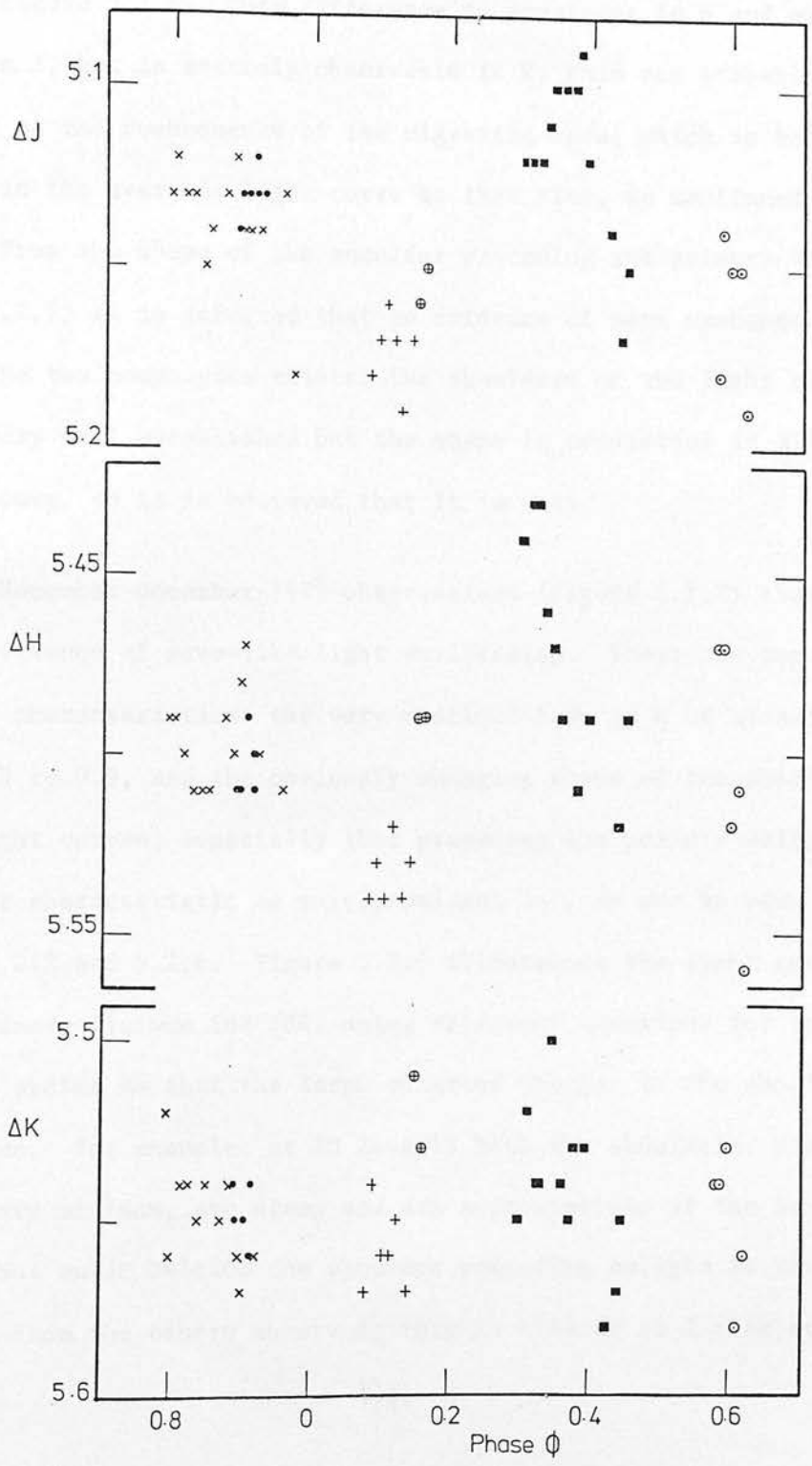

Figure 5.2.4 UV Psc - Light variations outside eclipse, September 1979 observations.

Notations used for the different cycles:
JD 2444137 (●), 2444141 (⊙), 2444143 (x), 2444144 (+), 2444145 (⊕), 2444146 (■).

of the pre- and post-primary eclipse part of the light curves, as is shown in Figure 5.2.5. This difference is prominent in H and even more so in J, but is scarcely observable in K; this can probably be explained as the consequence of the migrating wave, which is believed to exist in the system's light curve at that time, as mentioned before. From the shape of the shoulder preceding the primary eclipse (Figure 5.2.5) it is inferred that no evidence of mass exchange between the two components exists; the shoulders of the light curves are not very well established but the shape is consistent in all three colours, so it is believed that it is real.

The November-December 1979 observations (Figure 5.2.2) show no obvious evidence of wave-like light variability. There are two prominent characteristics: the very distinct bump in K at around phases 0.8 to 0.9, and the obviously changing shape of the shoulders of the light curves, especially that preceding the primary eclipse. The latter characteristic is more prominent in J as can be seen from Figures 5.2.2 and 5.2.6. Figure 5.2.6 illustrates the light curve around primary minimum for JHK, using different notations for the different cycles so that the large observed changes in the shoulders can be seen. For example, at JD 2444213 both the shoulders, pre- and post-primary minimum, are steep and are approximately at the same height. But on JD 2444206 the shoulder preceding eclipse is very different from the others observed; this is clearer at J than at H and K.

From the current data the primary minimum has been well established, but not the secondary. Figure 5.2.7, which illustrates the primary minimum for the three different observing epochs, shows that

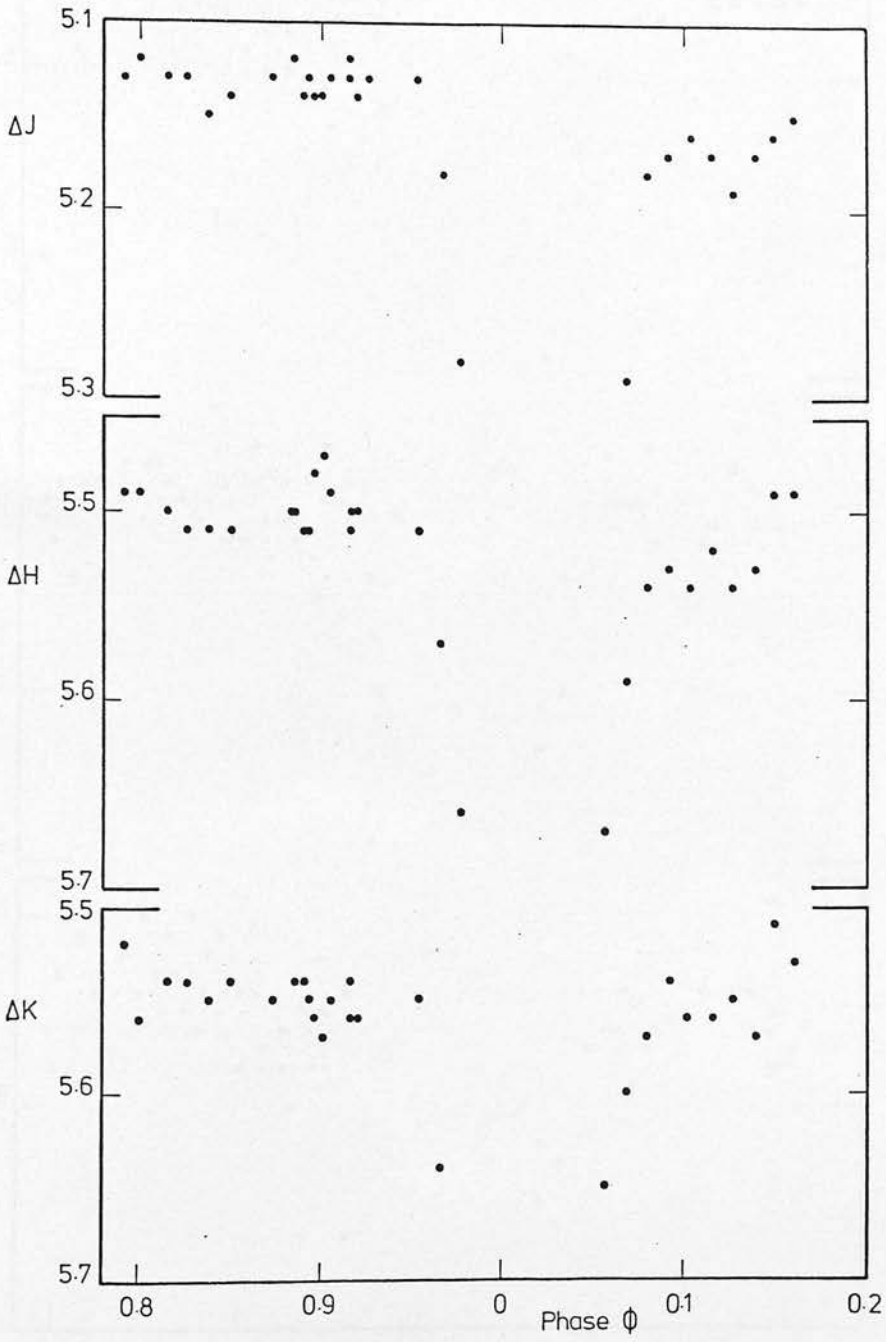

Figure 5.2.5 UV Psc - September 1979 observations around primary minimum

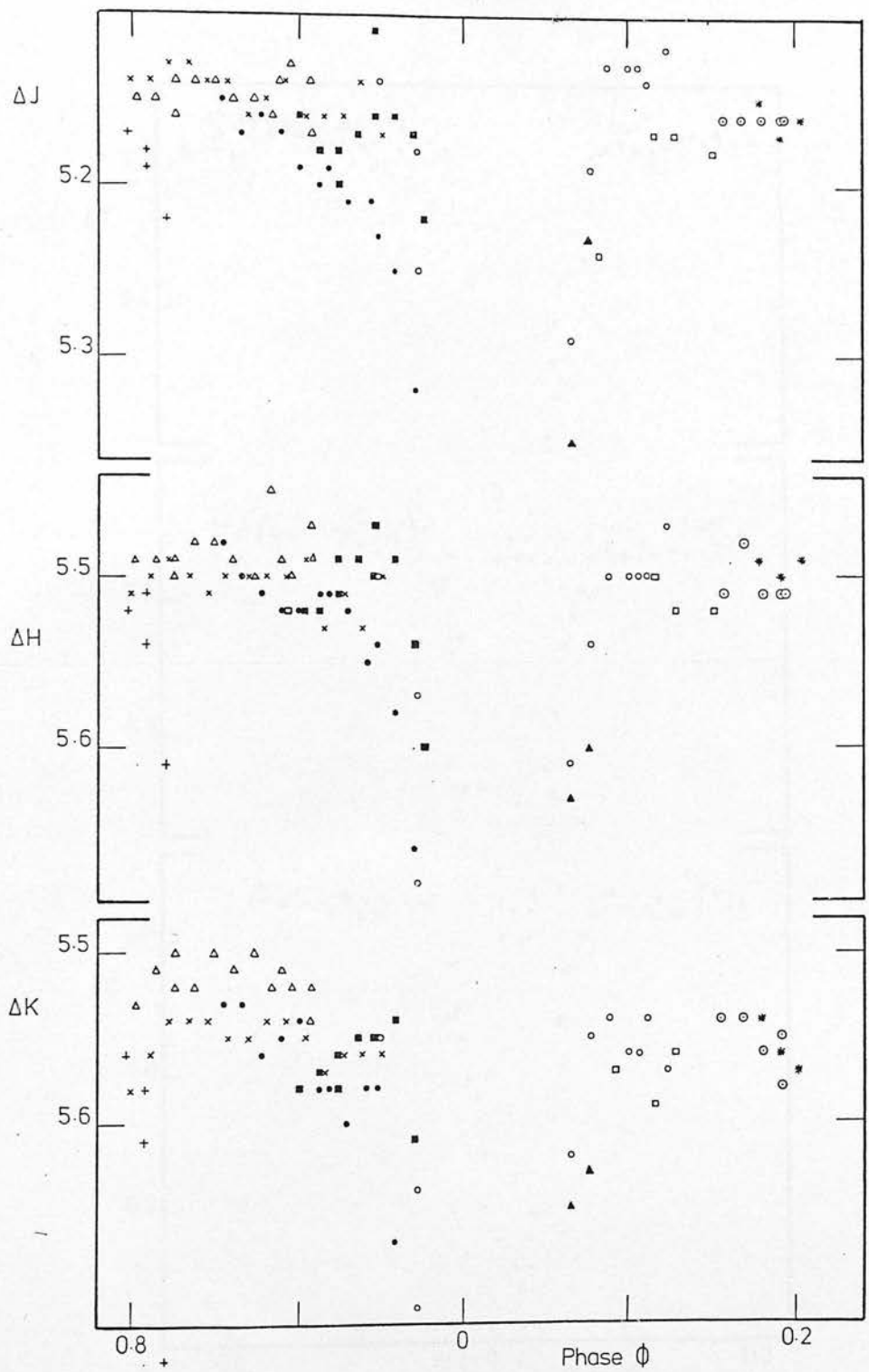

Figure 5.2.6 UV Psc - Differential magnitudes aroung primary minimum, November-December 1979 observations.

Notations used for the different cycles:
JD 2444206 (●), 2444212 (x), 2444213 (o), 2444214 (⊙), 2444218 (Δ), 2444226 (□), 2444230 (+), 2444231 (■), 2444238 (▲) and 2444239 (*).

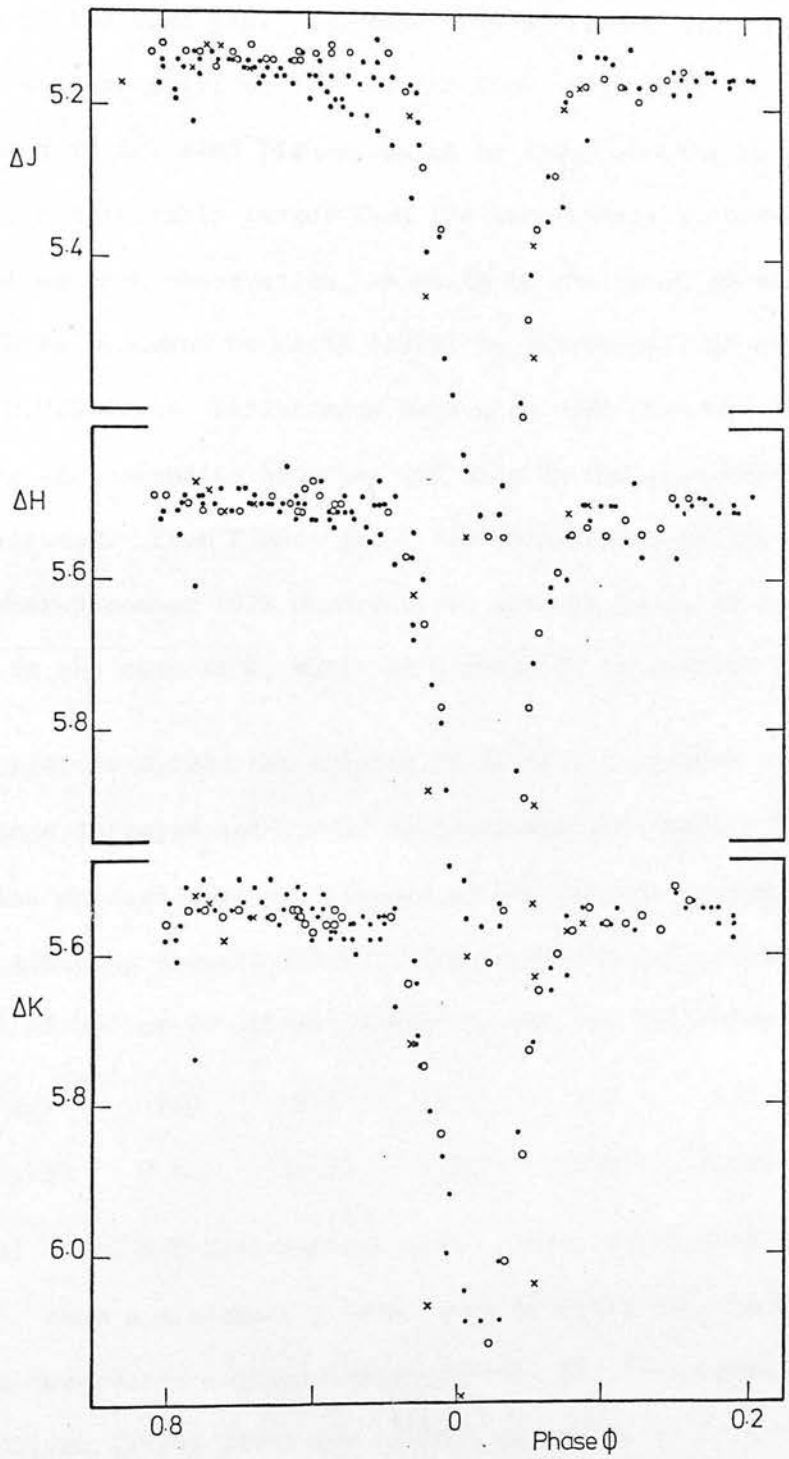

Figure 5.2.7 UV Psc - Primary minimum

October 1978 (x), September 1979 (o) and November-December 1979 (•) observations

the depth of the primary minimum seems to be variable. The minimum observed in November-December 1979 seems to be shallower than that in September of the same year, and this even shallower than that observed in 1978. A phase shift of 0.02 in the time of primary minimum can also be seen in the same figure, which in terms of time is 0.023 days or 33 min, considerably larger than the uncertainty introduced by the time spent on each observation. A shift in the epoch of zero phase has also been observed by Sadik (1979) in the visual; he gives a shift of 0.016 days. Differences have also been observed in the descending and ascending branches and also in the shoulders of the primary minimum. From Figure 5.2.7 the shoulder preceding eclipse in the November-December 1979 observations appears lower at J, but the opposite is the case at K, while at H there is no obvious separation.

In order to obtain the colours of UV Psc at maximum light, simultaneous infrared and visual observations were made. The V-R and V-I Cousins colours were transformed to the Johnson system using the formulae given by Bessell (1979). The resulting colours and visual magnitude of UV Psc in Johnson's system, are the following:

V	B-V	V-R	V-I	V-J	V-H	V-K	V-L
9.00	0.730	0.633	1.079	1.370	1.800	1.890	2.050

The visual V and B-V observations given above, which were made in late 1979, show a discrepancy from those of Sadik made in November 1977; his observations give outside-eclipse (V, B-V) equal to (9.22, 0.81). Oliver (1974) gives the maximum magnitude in V equal to 9.06 while Huth (1959) gives photographic magnitude 9.6. The system seems to have a variable maximum at V. The energy distributions of the system during primary minimum and outside eclipse are illustrated in

Figure 5.2.8. From this figure it is obvious that no apparent infrared excess exists in the system. The colours can therefore be used to estimate the spectral types of the two components

An uncertainty arises for the components' spectral types. Carr (1967) suggests two main sequence stars of spectral types G5 and K2. Oliver's (1974) photometric observations suggest a combination of G2V and KOIV or G2IV and KOIV. In an effort to shed some light on this uncertainty the current infrared and visual colours given above, during the system's maximum, were used in order to estimate the spectral types of the two components (section 4.1). The results obtained were combined with the spectral types of the cooler component which can be derived from the colours of the system during primary eclipse as this is an occultation (Oliver 1974, and also from Figure 5.2.2); the spectral types suggested for the cooler component are K3V or K2IV. Another consideration which has been taken into account for the estimation of the spectral types of UV Psc components is its energy distribution (Figure 5.2.8); this can be fitted by a combination of two blackbodies of temperatures, derived from the relation $\lambda_{max}T = 3670$ μmK, of about 5800 K and 4600 K; using the spectral type-temperature scale given by Johnson (1966), the spectral types suggested by the energy distribution are G2V and K2IV. Having all the above mentioned criteria in mind, the most probable combinations of spectral types suggested by the current data for the components of UV Psc are G2V and KOIV or G7V and K3V. The former classification is in keeping with one of two probable classifications given by Oliver according to his UBV photometry.

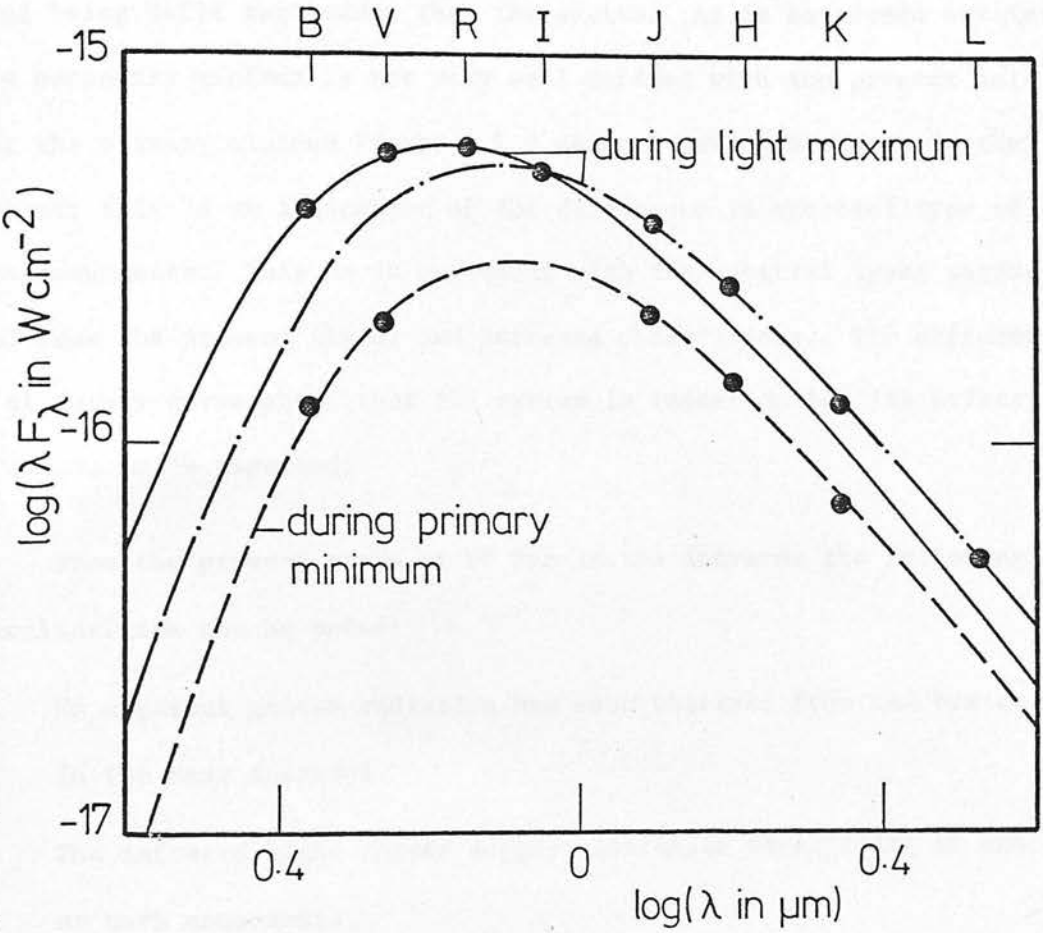

Figure 5.2.8 UV Psc - Energy distribution

In Figure 5.2.9 the absolute values of the differential colours $|\Delta(J-K)|$ are plotted against phase. This is done because the differential colours of the system $\Delta(J-K)$ are negative, the comparison star used being K4III and redder than the system. As is mentioned earlier, the secondary minimum is not very well defined with the present data. For the primary minimum Figure 5.2.9 shows a definite change in the colour; this is an indication of the difference in spectral type of two components. This is in agreement with the spectral types suggested from the present visual and infrared observations. The differential colour curve shows that the system is redder during its primary minimum, as is expected.

From the present study of UV Psc in the infrared the following peculiarities can be noted:

1. No apparent excess radiation has been observed from the system in the near infrared.
2. The infrared light curves suggest intrinsic variability of one or both components.
3. Wave-like light variation has probably been observed in October 1978 and September 1979. No obvious long-term variation has been detected in the November-December light curves of UV Psc, but sudden, short-term variations have been observed.
4. In November-December 1979 the system was systematically brighter in K than in September 1979, October 1978. The opposite occurs in J.
5. The system was found to be brighter by about $0^{m}.03$ in K at JD 2444218. The increase in brightness is not obvious in J and H.

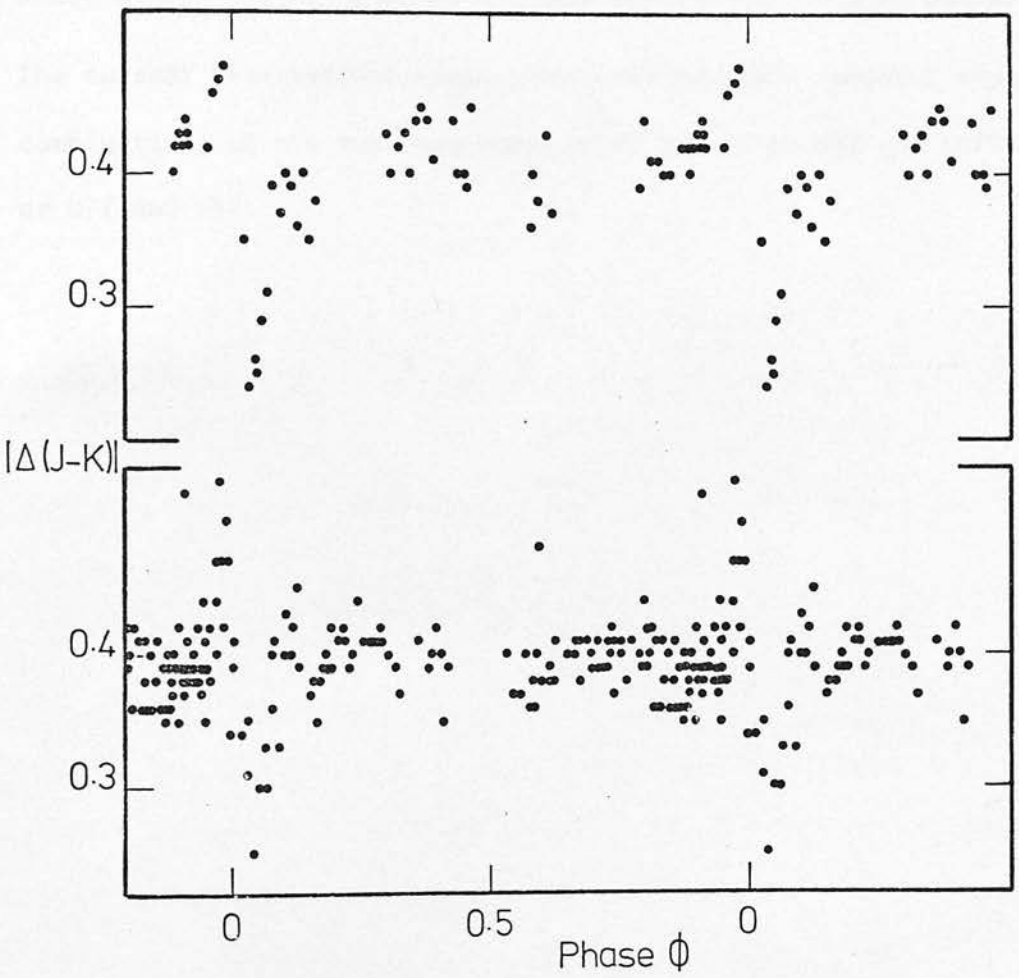

Figure 5.2.9 UV Psc - Differential colour curves

Top : September 1979 observations

Bottom : November-December 1979 observations

6. The shoulders of the primary minimum show large changes from cycle-to-cycle, especially the shoulder preceding the minimum.

7. Indications of unequal primary minima exist (the secondary minima are not completely covered).

8. Shift of the primary minimum has been observed by 0.02 in phase.

9. The current observations suggest the most probable spectral type combinations of the two components of UV Psc to be G2V and K0IV or G7V and K3V.

5.3 SZ Piscium

SZ Psc (≡ HD 219113 ≡ BD +01°4695) is a double-lined spectroscopic binary and an eclipsing system with an Algol-like light curve; it is a very interesting member of the RS CVn-type binary class as it is known to show large period and light variations, thus it has become a system of singular interest for studying mass exchange. It has, however, received scant attention as the period of SZ Psc (∿ 4 days) has prevented a full light curve from being obtained. Thus few observations exist in the literature and only very recently SZ Psc has attracted the attention of different observers. Bakos and Heard (1958) reported the preliminary results of two-colour photometric and spectroscopic observations of the system and suggested intrinsic variations of one of the components. These variations have been confirmed by Fernie and Marlborough from their 1962 observations (Head and Bakos 1968). A part of SZ Psc's light curve has been obtained by Oliver (1974). Those observations are enough to show a shift of the secondary minimum as it was detected at approximately phase 0.30. Oliver also reported that Popper's observations obtained in 1969 indicated primary minimum occuring about 0.18 early in phase, which is in agreement with the position of the expected primary minimum from his data, providing that the orbit is circular.

Jakate et al. (1976) discussed the photometry and spectra of this object. Their spectroscopic observations show that the spectra of both stars are visible and yield the classifications of F8V and K1IV; the two components have almost equal masses, the secondary being slightly more massive. They also reported the existence of strong H and K emission lines in the spectrum of the K component but

they have not attempted any study of possible variation in the emission with phase as their spectra were poorly exposed in this region. From the photometry of Jakate et al., the late-type star has (V, B-V, R-I) equal to (7.65, +0.99, +0.415) mag from the apparently total eclipse leaving (8.15, +0.35, +0.1) mag for the F star. Jakate et al. also confirmed the non-constancy of the system's period and they found its rate of decrease ($\dot{P} = -(6.0 \pm 0.5) \times 10^{-8}$ days/day) by comparing their photoelectric data with previous photographic photometry. They were also able to confirm the intrinsic variability of the system, on short (at least of the orbital period) and long (of the order of a decade) time scale; they suggested the possibility of the system being in a mass-exchanging stage as an explanation for their observations. Radio observations (at 2695 and 8085 MHz) suggested that SZ Psc is a variable radio source (Owen and Gibson 1978).

Photoelectric spectrophotometry by Weiler (1976, 1978a) and spectroscopic observations by Bopp and Talcott (1978) showed peculiarities at Hα; these observers found random variation in Hα which is in emission up to seventy per cent of the continuum around phase 0.80. More data are probably needed to establish if this is an effect always seen at this phase. Weiler also looked for any variations of CaII emission lines and found them to be relatively stable.

Photometric observations made by Eaton (1977) showed sinusoidal light variations outside eclipse with an amplitude of $0^{m}.075$ in the visual. Thus the sinusoidal wave observed by Bakos in 1957 ($0^{m}.2$ amplitude), which was absent in his 1974 data, has been re-established.

All these conclusions were doubted recently after Jakate's announcement that HD 219018, which had long been used as comparison star for the system, is a variable on a scale of about $0^m.1$. Photometric observations of HD 219018 made by Fernie (1979) contradicted Jakate's report; Fernie suggested the variability of Jakate's check star as the most probable explanation for the observed variability of HD 219018. Also Fernie pointed out that "it does not seem likely that the earlier conclusions regarding SZ Psc were vitiated by variability in HD 219018". This suggestion by Fernie turned out to be true; recent visual observations of SZ Psc by Okazaki (1979) and Tümer et al. (1980), using a different comparison star (they avoided using the probable variable HD 219018), confirmed the unequal minima in B and V light curves. Tümer et al. (1980) also showed a displacement of 0.05 in phase of the primary minimum, compared with the value given by Eaton.

Thus the visual observations show a decrease of the orbital period, a non-permanent sinusoidal wave with varying amplitude, and also a displacement in phase of the minima. All these observational facts made SZ Psc a promising interesting object in the infrared and its observations were undertaken during several observing sessions.

Infrared observations were made up of several series: one in August 1978 using the 1.5 m flux-collector in Tenerife; and three different runs using the 0.75 m telescope in Sutherland (October 1978, September and November-December 1979). The observations were made mainly at JHK wavebands and occasionally at L, using InSb detectors. Most of them were made using the same telescope and the same filters. γ Psc was used as the comparison star; its infrared magni-

tudes, which are the mean magnitudes of 25 observations, are given in Table 3.3.3. The differential magnitudes of SZ Psc are given in Table 5.3.1 and are illustrated in Figure 5.3.1. The colour curve is shown in Figure 5.3.2. The phase of each observation was computed using the ephemeris given by Jakate et al. (1976):

$$T_o(JD) = 2442308.7671 + 3^d.96534286E$$

These elements (according to Jakate et al.) provide representation to an accuracy measured in minutes over more than 4000 cycles, thus over almost half a century. The period was obtained by least squares analysis of the available times of minima. The standard error of the observations is of the order of $0^m.03$ while the error goes down to $0^m.02$ and $0^m.01$ in the 1979 data. At JD 2444210.30 the system was found to be brighter by $0^m.28$ in all three wavebands. A possible explanation of this sudden brightness increase of the system is flare activity of one of the components, as has also been observed in other RS CVn systems (e.g. HR 1099, section 5.1; TY Pyx, section 5.4). Another random, short scale intrinsic variability of the system has been observed at JD 2444227.30 when the system became fainter by $0^m.12$ in K and also bluer. These short scale light variabilities of SZ Psc have also been extensively observed in visual wavelengths (Jakate et al. 1976).

As can be seen from Figure 5.3.1 none of the minima has been well identified. An estimation of the predicted minima of SZ Psc in the infrared wavelengths at the time of the current observations of the primary minimum, using the method described in section 4.3, is not possible, as simultaneous visual observations are required since the depth is variable (Jakate et al. 1976). For the present infrared

TABLE 5.3.1

SZ Psc - Differential Magnitudes

JD 2440000 +	ϕ	ΔJ	ΔH	ΔK	ΔL
3733.72	0.352	3.46	3.50	3.42	
3733.74	0.357	3.50	3.49	3.44	
3734.71	0.601	3.53	3.55	3.47	
3735.70	0.851	3.41	3.43	3.42	
3735.74	0.861	3.48	3.47	3.39	
3792.27	0.117	3.55	3.66	3.87	
3792.29	0.122	3.60	3.86	4.03	
3792.30	0.125	4.04	3.91		3.89
3792.38	0.145	3.48	3.49	3.46	
3793.33	0.385	3.46	3.44	3.41	3.30
3793.35	0.390	3.47	3.46	3.43	3.37
3801.38	0.415	3.44	3.45	3.40	3.30
3806.30	0.655	3.50	3.48	3.40	
3806.32	0.660	3.46	3.46	3.41	
3807.29	0.905	3.41	3.46	3.41	3.43
3807.32	0.914	3.47	3.46	3.40	3.29
4140.38	0.905	3.55	3.49	3.44	
4140.39	0.908	3.51	3.48	3.42	
4140.40	0.910	3.51	3.47	3.44	
4141.355	0.151	3.50	3.48	3.44	
4141.37	0.155	3.50	3.48	3.43	
4141.38	0.158	3.48	3.47	3.44	
4141.39	0.160	3.48	3.47	3.43	
4141.40	0.163	3.48	3.46	3.43	
4141.43	0.170	3.49	3.47	3.43	
4141.44	0.173	3.50	3.48	3.43	
4143.33	0.649	3.50	3.47	3.43	
4143.34	0.651	3.49	3.47	3.43	
4143.35	0.654	3.48	3.47	3.43	
4144.39	0.917	3.51	3.48	3.43	
4144.39	0.917	3.51	3.48	3.44	
4144.40	0.919	3.52	3.49	3.44	
4144.41	0.922	3.52	3.48	3.44	

TABLE 5.3.1 (cont'd)

JD 2440000 +	ϕ	ΔJ	ΔH	ΔK	ΔL
4145.37	0.164	3.43	3.43	3.39	
4145.37	0.164	3.45	3.43	3.39	
4146.35	0.411	3.50	3.47	3.43	
4146.36	0.413	3.50	3.47	3.43	
4146.37	0.416	3.50	3.49	3.43	
4201.28	0.263	3.46	3.45	3.41	3.38
4201.29	0.266	3.50	3.47	3.42	3.47
4204.28	0.020	3.65	3.58	3.53	3.51
4202.30	0.025	3.66	3.60	3.54	3.51
4207.30	0.782	3.48	3.44	3.41	3.34
4207.31	0.784	3.48	3.45	3.42	3.42
4209.28	0.281	3.48	3.45	3.42	
4209.30	0.286	3.47	3.46	3.42	3.34
4210.28	0.533	3.62	3.60	3.56	3.51
4210.30	0.538	3.34	3.32	3.27	
4214.27	0.539	3.59	3.58	3.52	
4214.28	0.542	3.61	3.58	3.52	3.60
4217.27	0.296	3.46	3.44	3.41	3.33
4217.29	0.301	3.48	3.44	3.41	3.44
4218.27	0.548	3.58	3.54	3.52	3.51
4218.28	0.551	3.58	3.55	3.52	
4227.29	0.823	3.51	3.47	3.44	
4227.30	0.825	3.57	3.57	3.56	
4231.28	0.829	3.53	3.48	3.44	
4231.29	0.831	3.53	3.49	3.45	

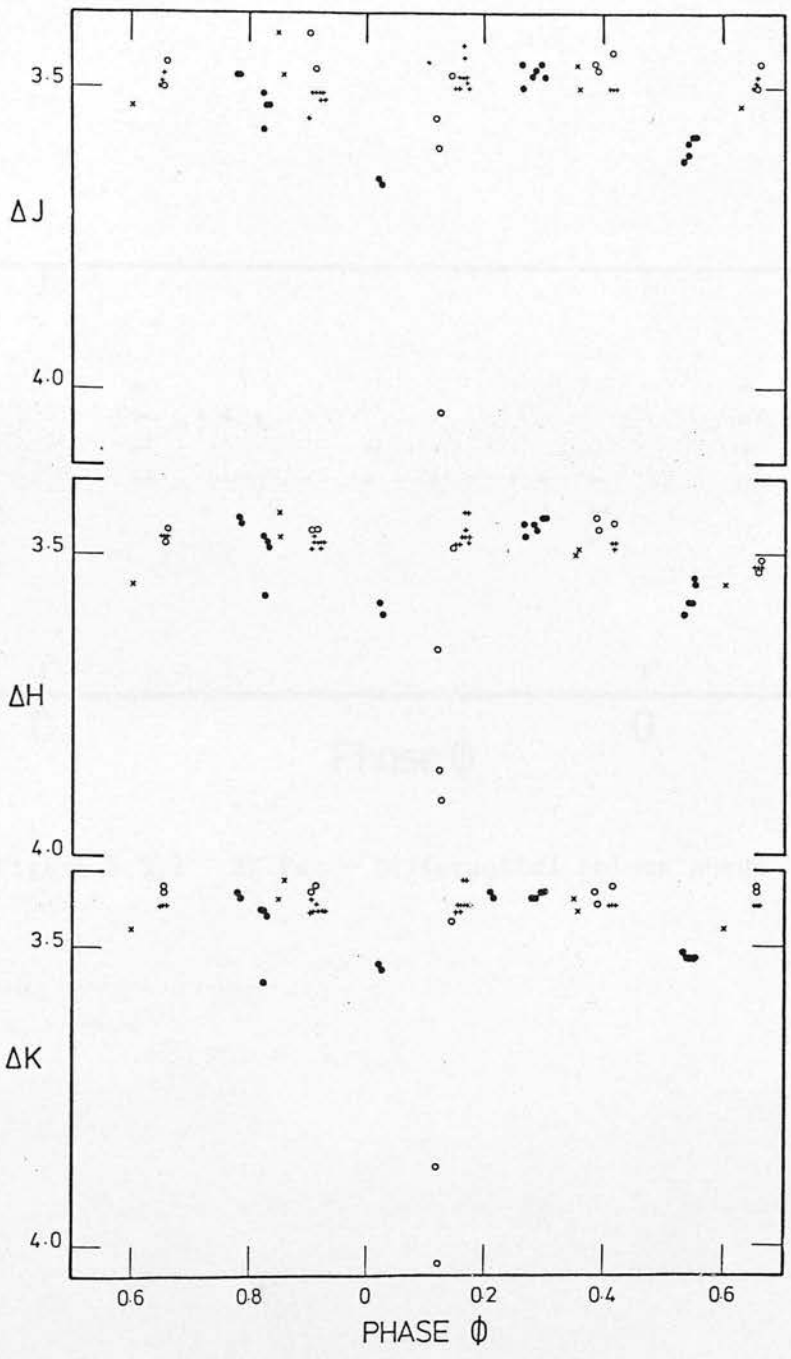

Figure 5.3.1 SZ Psc - Differential light curves; August 1978 (x), October 1978 (o), September 1979 (+) and November-December 1979 (•) observations

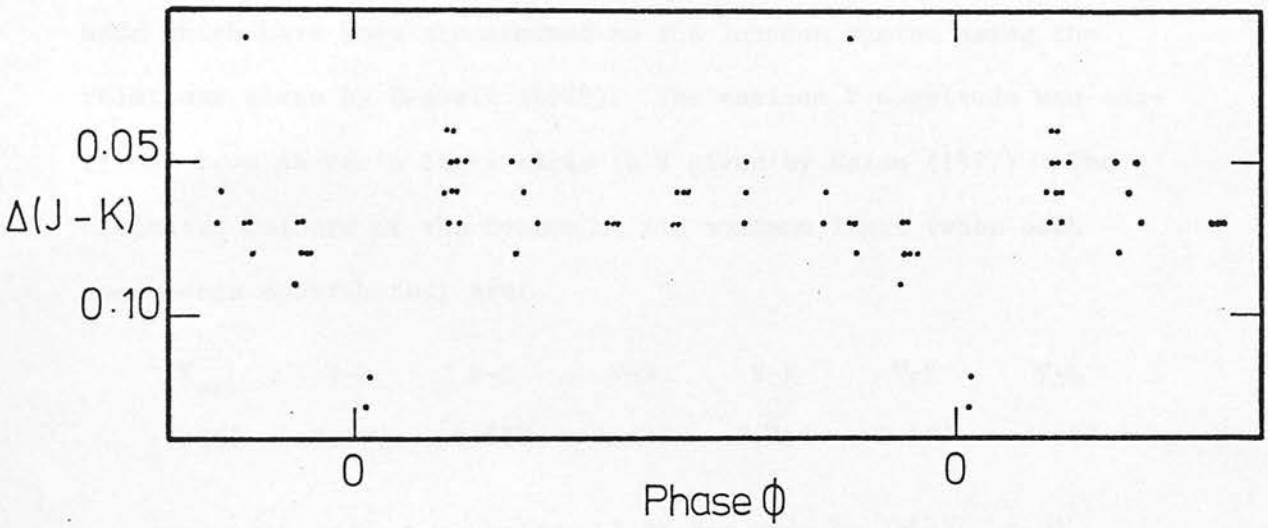

Figure 5.3.2 SZ Psc - Differential colour curve

observations of the secondary minimum, simultaneous visual observations exist but the minimum is not well defined (Tümer et al. 1980).

In order to estimate the colours of the system, the average of its maximum values were tied to the comparison stars (its infrared magnitudes are given in Table 3.3.3). During light maximum, and especially at JD 2444141.45, simultaneous visual observations were made which have been transformed to the Johnson system using the relations given by Bessell (1979). The maximum V magnitude was confirmed from SZ Psc's light curve in V given by Eaton (1977). The estimated colours of the system at its maximum light (when both components contributed) are:

V_{max}	V-R	V-I	V-J	V-H	V-K	V-L
7.267	0.730	1.270	1.727	2.257	2.387	2.487

Spectroscopic observations of SZ Psc made by Jakate et al. (1976) showed that the spectra of both components were visible and yielded the classification K1IV and F8V. The combined intrinsic colours of a system with components K1IV and F8V are:

B-V	V-I	V-J	V-H	V-K	V-L
0.862	1.121	1.461	1.927	2.043	2.138

The small discrepancy between the observed and intrinsic values of (B-V) of $0^m.026$ can be attributed to observational or spectral classification errors. The infrared colour excesses are:

E(V-I)	E(V-J)	E(V-H)	E(V-K)	E(V-L)
0.149	0.266	0.330	0.344	0.349

This small observed infrared excess can be explained in terms of line

emission as is suggested from the system's emission line spectrum. The infrared colours (H-K) = 0.13 and (K-L) = 0.10 do not point to any contribution of free-free radiation from a circumstellar gas shell (cf. D.A. Allen, 1973, Figure 1).

In Figure 5.3.3 the energy distribution of SZ Psc is given. This seems to consist of a combination of two blackbody distributions of different temperatures; one of about 5600 K($\lambda_{max}T$ = 3670 Kμm, in a $\lambda F\lambda$ versus λ in μm diagram) the second of 4350 K. The estimated temperatures have a departure from the temperatures appropriate to the system's spectral types F8V + K1IV (6000 K and 4840 K, Johnson 1966) which, of course, is expected as a consequence of the redder observed colours.

In Figure 5.3.4 the data obtained in September and November-December 1979 are plotted against phase. These data are plotted on a larger scale than the whole set of data observed in an effort to search for wave-like light variations outside eclipse, similar to those which have been reported to exist in the visual (Jakate et al. 1976; Eaton 1977; Tümer et al. 1979). As the observations were made over an inteval of about four months (from September to end December), most of the light curve is covered.

A careful study of Figure 5.3.4 shows that a distortion wave exists in the infrared light curves of SZ Psc obtained for this investigation, whose amplitude decreases with increasing wavelength. The wave is clearly visible in J where its amplitude seems to be of the order of $0^{m}.05$ and its period equal or approximately equal to the orbital period.

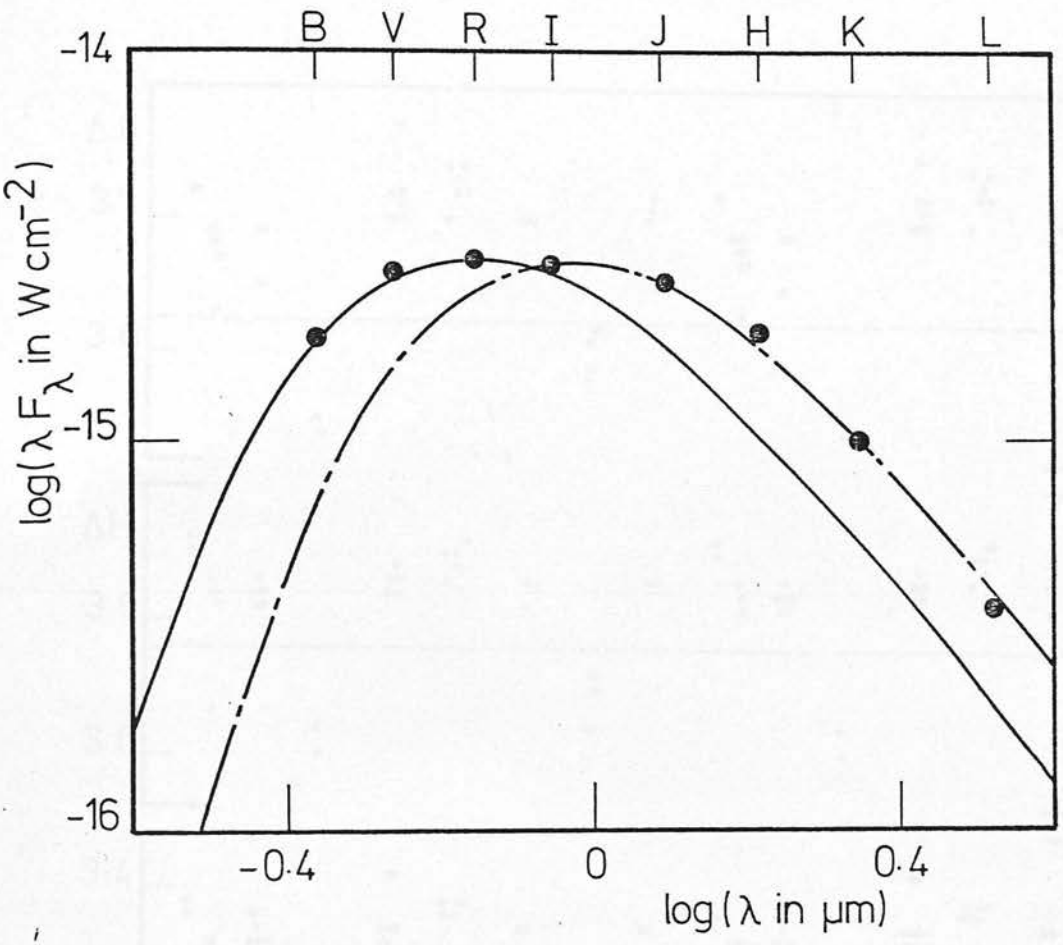

Figure 5.3.3 SZ Psc - Energy distribution

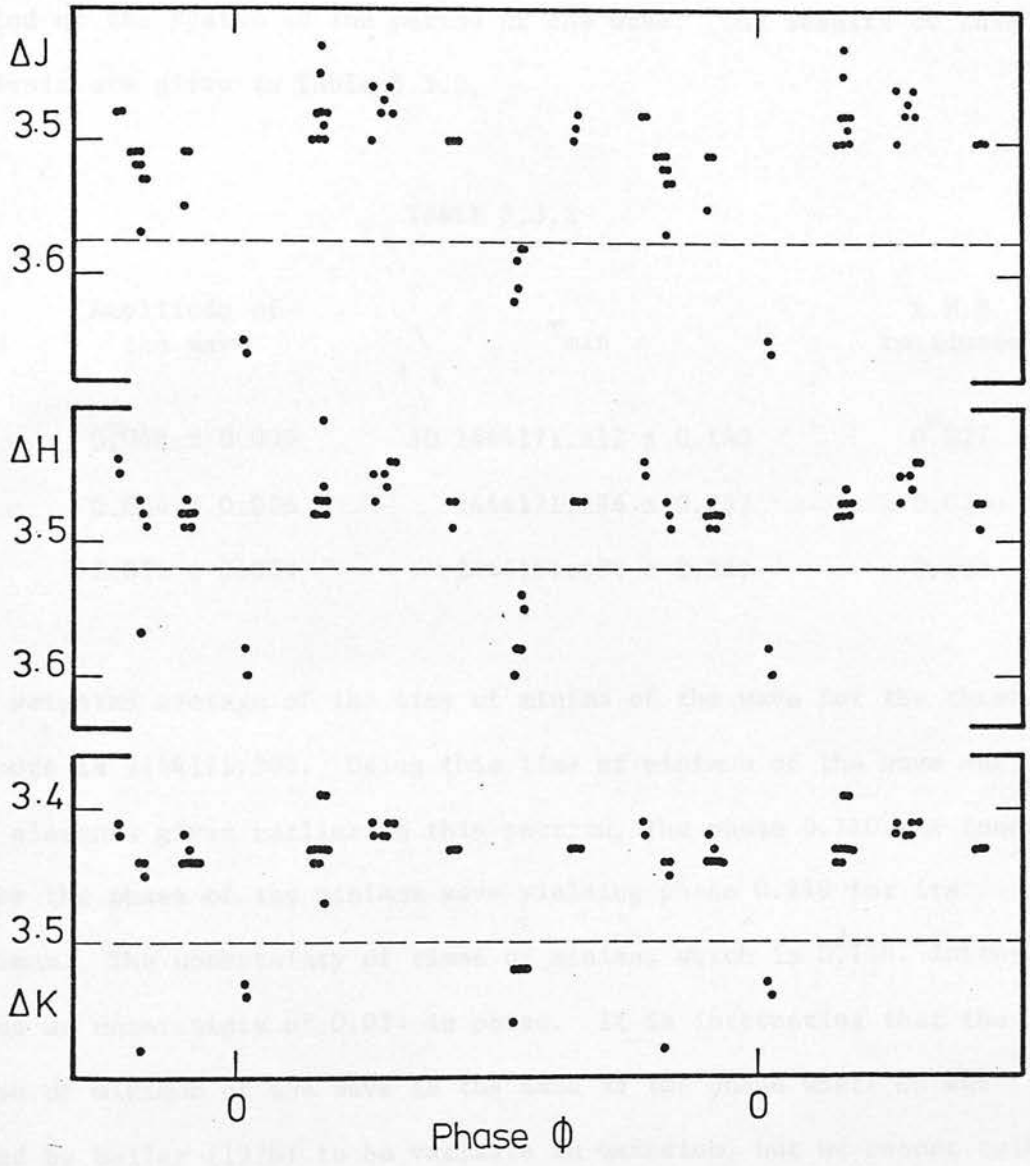

Figure 5.3.4 SZ Psc - September, November-December 1979 observations. The dashed line separates the out of eclipse observations.

In order to get an unbiased measure of the amplitude and the phase of minima of the distortion wave in J, H and K light curves of SZ Psc, the technique of least squares Fourier Analysis was used to fit the 1979 observations outside eclipse, adopting the orbital period of the system as the period of the wave. The results of this analysis are given in Table 5.3.2.

TABLE 5.3.2

Band	Amplitude of the wave	T_{min}	R.M.S. residuals
J	$0^m.048 \pm 0.006$	JD 2444171.312 ± 0.180	$0^m.027$
H	0.034 ± 0.006	2444171.186 ± 0.257	0.029
K	0.032 ± 0.009	2444171.538 ± 0.360	0.037

The weighted average of the time of minima of the wave for the three colours is 2444171.309. Using this time of minimum of the wave and the elements given earlier in this section, the phase 0.710 was found to be the phase of the minimum wave yielding phase 0.210 for its maximum. The uncertainty of times of minima, which is $0^d.136$, introduces an uncertainty of 0.034 in phase. It is interesting that the phase of minimum of the wave is the same as the phase where Hα was found by Weiler (1976) to be variable in emission, but we cannot talk about correlation of these two results as the observations were made at epochs five years apart.

In Table 5.3.2 the amplitude of the wave is also given. As can be seen in Table 5.3.3, the amplitude is decreasing with increasing wavelength; this also has been observed in HR 1099 (section 5.1).

TABLE 5.3.3

Characteristics of the wave

Time	Filters	ϕ_{min}	Migration Period (in years)	Reference
1974.8	V	0.95		Fernie (Jakate et al. 1976)
			4.2	
1976.9	B,V	0.45		Eaton 1977
			2.86	
1977.75	uvbyI	0.15		Eaton and Hall 1979
1977.95	B,V	0.15		Eaton and Hall 1979
			3.57	
1979.85	J,H,K	0.71		present work

The above estimate of amplitude and phase of the distortion wave in the infrared light curves of SZ Psc was made on the assumption that the period of the light variations outside eclipse is equal to the orbital period of the system. This assumption has a logical basis, since this has been observed in other RS CVn systems (Hall 1972; Bopp et al. 1977). The "least squares" Fourier analysis for determining the hidden periodicity of these light variations was not applied, as the system is eclipsing with unequal minima.

In Table 5.3.3 the characteristics of the wave-like light variations observed in the visual and infrared (present work) light curves of SZ Psc are summarised. The wave seems to be migrating towards increasing or decreasing phases (Figure 5.3.5) and it is more likely that the wave in this system is moving in a full cycle; it seems that this wave is behaving differently from the wave observed in HR 1099 (Table 5.1.10, Figure 5.1.4). From Table 5.3.3 it can be seen also that, for the case of the wave moving towards increasing phases, the migration period of the wave in SZ Psc is not constant but does not show the variation observed in HR 1099 wave's migration period. It is probably meaningful to talk about migration cycles of the wave in the case of SZ Psc. More observations are needed before a definite decision is made.

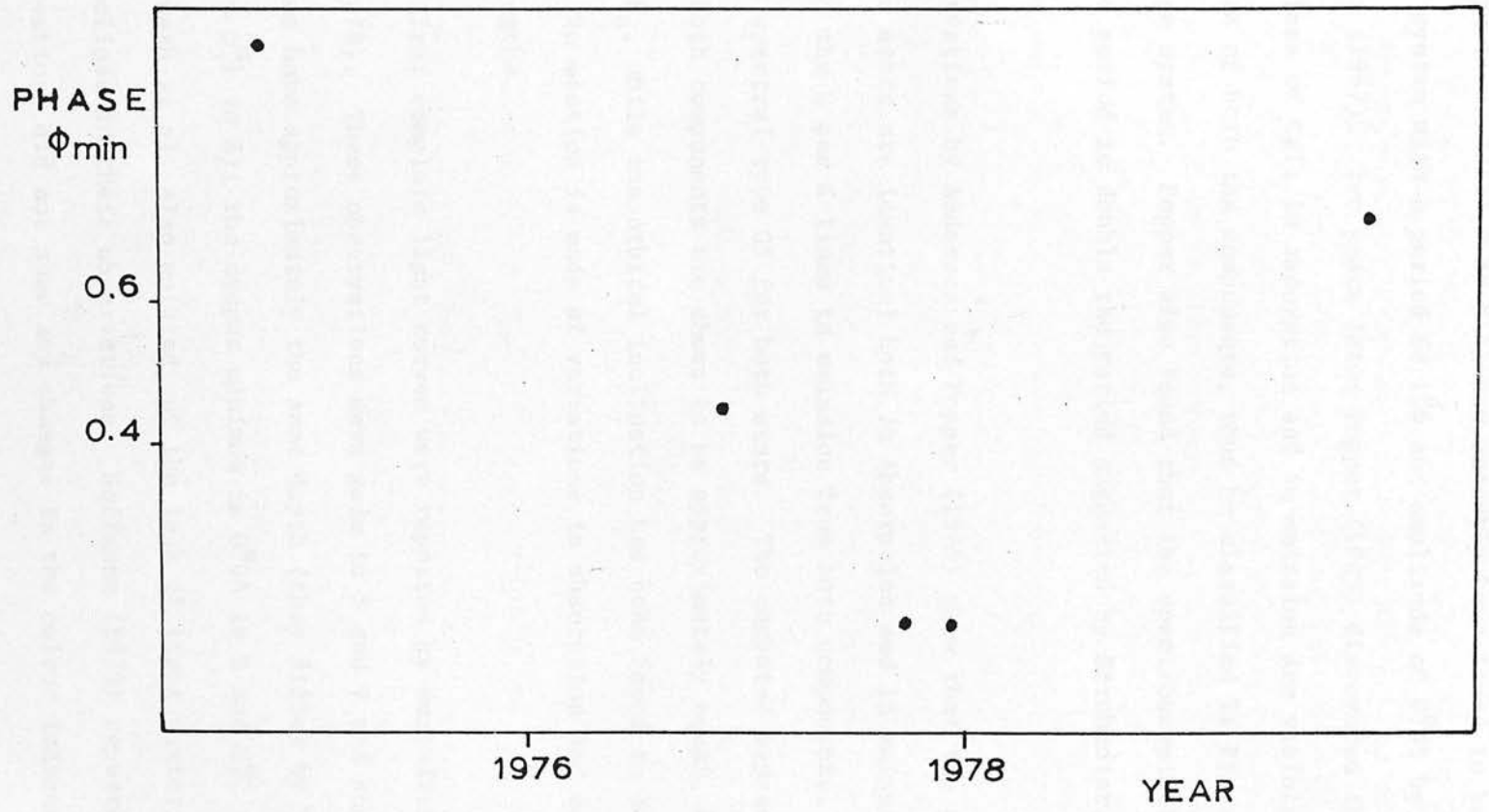

Figure 5.3.5 The calculated phase of minima of the wave against epoch

5.4 TY Pyxidis

TY Pyx (≡ HD 77137 ≡ BV 811) has recently been found to be an eclipsing system with a period of $1^{d}.6$ and amplitude of $0^{m}.55$ by Strohmeier (1967). Two years later Popper (1969) discovered that the H and K lines of CaII in absorption and in emission are visible in the spectra of both the components, thus he classified TY Pyx as an RS CVn type system. Popper also found that the spectroscopically determined period is double the period suggested by Strohmeier, as is now known.

Observations by Andersen and Popper (1975) show that the spectra of the two stars are identical both in absorption and in emission lines with the H and K lines in emission from both components. They suggested spectral type G5 for both stars. The computed masses and radii of both components are shown to be approximately equal, 1.2 $M_{\odot}$ and 1.65 $R_{\odot}$, while the orbital inclination has been found to be $i = 88°$. No mention is made of variations in absorption and emission line strengths.

The first complete light curves were reported by Surendiranath et al. (1978). These observations were made in B and V and show that both minima have approximately the same depth (they differ by $\sim 0^{m}.05$ in V and $\sim 0^{m}.1$ in B); the deeper minimum is $0^{m}.65$ in V and $0^{m}.7$ in B. Surendiranath et al. also pointed out the lack of light variations outside eclipse in their observations. Hoffmann (1978) reported that his observations did not show any changes in the colour indices of the system and he concluded that no star spot activity was visible at the time of the observations. The system is not detectable at 2695 and 8085 MHz (Owen and Gibson 1978).

In the present work JHK and occasionally L photometric observations were carried out at the South African Astronomical Observatory in November-December 1979. The comparison and check star was HR 3484; its infrared magnitudes are given in Table 3.3.3. The differential magnitudes are plotted in Figure 5.4.1 and the data are tabulated in Table 5.4.1. The phase of each observation was calculated from the ephemeris given by Surendiranath et al. (1978),

$$\text{JD } 2443187.230 + 3^{d}.198584E \ ,$$

where the epoch of the deeper minimum has been adopted as the epoch of primary minima. There were 120 usable observations in each of the colours. The statistical error is less than $0^{m}.03$. On JD 244213.55 the system was found to be brighter than usual at the same phase by $0^{m}.3$ in the JHK. This can be explained in terms of flare activity in the system, which is quite a common phenomenon in RS CVn type binary systems in different spectral regions (Weiler et al. 1978; Feldman et al. 1978; White et al. 1978).

The light curves for TY Pyx at J, H and K are quite well defined by the present observations, except the region 0.2-0.4 in phase. The secondary minimum has been clearly identified while the primary has been shown to be approximately equal in depth to the secondary (about $0^{m}.6$ for JHK) as has been observed in the visual colours also. The two components are almost identical, as has been found by spectroscopic observations. This also explains the equality of the minima at the different wavelengths. From equation 4.3.7 it can be seen that the depth of minima (caused by the eclipse of the same star) at two different wavelengths can be the same only if $\frac{F_{1_{\lambda 1}}}{F_{1_{\lambda 2}}} = \frac{L_{T_{\lambda 1}}}{L_{T_{\lambda 2}}}$ (the symbols are defined in section 4.3). This can happen if the

TABLE 5.4.1

TY Pyx - Differential Magnitudes

JD 2440000 +	ϕ	ΔJ	ΔH	ΔK	ΔL
4204.52	0.044	2.95	3.04	3.03	3.12
4204.54	0.050	2.90	3.02	3.02	3.12
4204.55	0.053	2.89	3.01	3.02	3.08
4206.55	0.678	2.86	3.01	3.00	3.00
4206.57	0.685	2.86	3.00	3.00	2.92
4206.58	0.688	2.84	3.00	2.99	
4206.59	0.691	2.85	3.01	3.00	
4207.54	0.988	3.23	3.40	3.43	3.41
4207.56	0.994	3.35	3.50	3.53	
4207.57	0.997	3.39	3.56	3.68	
4207.58	0.000	3.44	3.65	3.59	
4210.54	0.926	2.85	3.02	3.02	3.04
4210.55	0.929	2.85	3.03	3.03	
4210.57	0.935	2.85	3.04	3.03	
4210.57	0.935	2.85	3.02	3.05	
4210.58	0.938	2.86	3.02	3.03	
4212.52	0.545	2.89	3.04	3.04	
4212.53	0.545	2.89	3.05	3.06	3.03
4212.55	0.554	2.90	3.06	3.07	3.03
4212.56	0.554	2.92	3.04	3.04	3.05
4212.58	0.564	2.88	3.03	3.02	3.09
4213.55	0.867	2.55	2.71	2.73	2.81
4213.56	0.870	2.87	3.02	3.03	
4213.57	0.873	2.86	3.02	3.04	
4213.57	0.873	2.86	3.02	3.04	2.94
4213.58	0.876	2.86	3.00	3.03	
4213.59	0.879	2.87	3.00	3.02	2.98
4215.52	0.483	3.17	3.33	3.28	3.39
4215.53	0.486	3.26	3.44	3.37	
4215.54	0.489	3.33	3.49	3.44	
4215.55	0.492	3.42	3.57	3.51	3.64
4215.57	0.498	3.49	3.62	3.59	
4215.58	0.500	3.54	3.62	3.55	

TABLE 5.4.1 (cont'd)

JD 244000 +	ϕ	ΔJ	ΔH	ΔK	ΔL
4215.58	0.500	3.47	3.60	3.52	
4216.53	0.800	2.86	3.01	3.02	
4216.54	0.802	2.86	3.02	3.03	
4216.55	0.805	2.86	3.02	3.04	
4216.56	0.808	2.89	3.03	3.04	
4216.57	0.811	2.89	3.07	3.10	
4217.54	0.114	2.86	3.02	3.03	
4217.55	0.118	2.87	3.02	3.03	
4217.56	0.121	2.87	3.02	3.03	
4217.57	0.124	2.87	3.02	3.03	
4217.57	0.124	2.86	3.03	3.04	
4217.58	0.127	2.86	3.02	3.03	
4217.59	0.130	2.87	3.03	3.04	
4218.51	0.418	2.89	3.04	3.03	
4218.52	0.421	2.89	3.04	3.04	
4228.48	0.535	2.92	3.05	3.05	
4228.49	0.538	2.90	3.05	3.04	
4228.50	0.541	2.90	3.04	3.05	
4228.51	0.544	2.91	3.04	3.06	
4228.51	0.544	2.91	3.04	3.03	
4228.52	0.547	2.92	3.05	3.05	
4230.46	0.154	2.86	3.01	3.00	
4230.47	0.157	2.88	3.02	3.01	
4230.48	0.160	2.89	3.02	3.01	3.05
4230.49	0.163	2.86	3.02	3.00	
4230.49	0.163	2.86	3.01	3.01	
4230.52	0.172	2.87	3.03	3.01	
4230.53	0.176	2.87	3.03	3.02	
4230.53	0.176	2.88	3.03	3.02	
4230.54	0.180	2.86	3.03	3.02	
4231.47	0.469	2.95	3.11	3.13	
4231.48	0.472	2.99	3.16	3.17	
4231.48	0.472	3.02	3.19	3.20	
4231.49	0.476	3.04	3.21	3.24	

TABLE 5.4.1 (cont'd)

JD 244000 +	ϕ	ΔJ	ΔH	ΔK	ΔL
4231.50	0.479	3.13	3.27	3.31	
4231.51	0.482	3.17	3.32	3.34	
4231.51	0.482	3.21	3.36	3.39	
4231.52	0.485	3.26	3.40	3.42	
4231.53	0.488	3.29	3.45	3.47	
4231.54	0.491	3.33	3.50	3.54	
4231.54	0.491	3.38	3.52	3.55	
4231.55	0.496	3.41	3.57	3.58	
4231.56	0.499	3.42	3.58	3.59	
4231.57	0.500	3.43	3.59	3.58	
4231.57	0.500	3.42	3.58	3.58	
4231.58	0.504	3.40	3.55	3.53	
4231.58	0.504	3.36	3.52	3.50	
4231.59	0.507	3.33	3.48	3.47	
4231.60	0.510	3.30	3.45	3.44	
4231.61	0.512	3.27	3.42	3.40	
4234.45	0.401	2.89	3.04	3.05	3.14
4234.46	0.404	2.90	3.05	3.06	
4234.47	0.407	2.91	3.06	3.06	
4234.48	0.410	2.91	3.07	3.06	
4234.49	0.414	2.90	3.07	3.07	
4234.49	0.414	2.90	3.08	3.06	
4234.50	0.417	2.90	3.08	3.09	
4234.51	0.420	2.91	3.07	3.06	
4235.44	0.710	2.85	3.02	3.02	
4235.45	0.714	2.83	3.01	3.01	
4235.46	0.717	2.83	3.01	3.00	
4235.46	0.717	2.83	3.01	3.01	
4235.47	0.720	2.83	3.00	3.00	
4235.49	0.726	2.86	3.03	3.02	
4235.49	0.726	2.87	3.01	3.02	
4235.50	0.729	2.87	3.01	3.02	
4235.51	0.732	2.87	3.01	3.02	
4235.51	0.732	2.86	3.01	3.03	

TABLE 5.4.1 (cont'd)

JD 244000 +	ϕ	ΔJ	ΔH	ΔK	ΔL
4235.52	0.736	2.89	3.01	3.02	
4235.53	0.739	2.86	3.01	3.02	
4235.54	0.745	2.86	3.02	3.02	
4236.44	0.023	3.08	3.22	3.20	
4236.45	0.026	3.04	3.19	3.15	
4236.46	0.029	3.00	3.16	3.16	
4236.47	0.033	3.00	3.16	3.09	
4236.48	0.036	2.95	3.11	3.09	
4236.48	0.036	2.94	3.10	3.08	
4236.49	0.039	2.94	3.09	3.06	
4236.50	0.042	2.91	3.06	3.06	
4238.44	0.648	2.87	3.03	3.03	
4238.45	0.650	2.88	3.03	3.04	
4238.46	0.655	2.89	3.03	3.05	
4238.46	0.655	2.89	3.05	3.05	
4238.48	0.661	2.89	3.05	3.05	
4238.48	0.661	2.89	3.05	3.06	
4238.49	0.664	2.89	3.05	3.05	

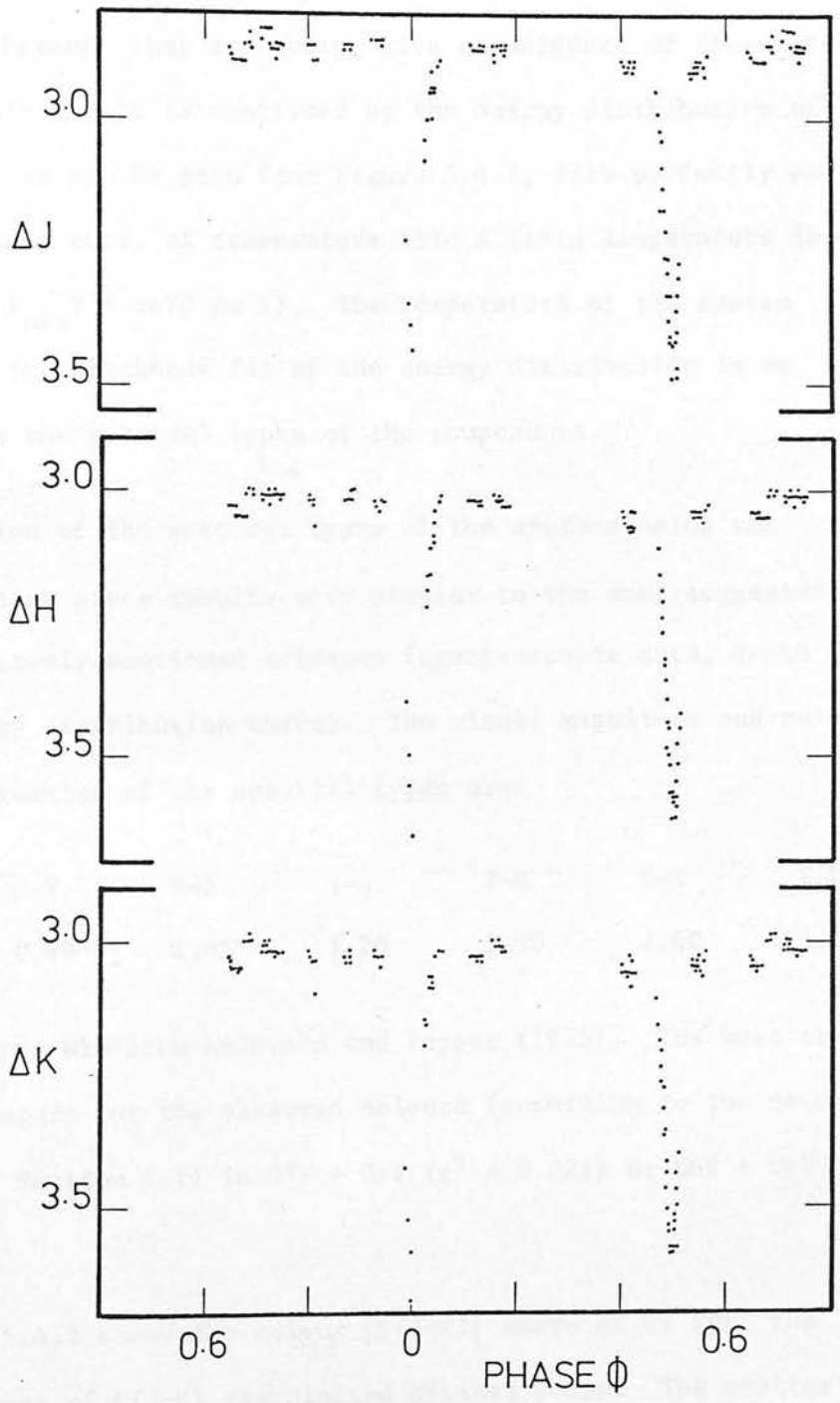

Figure 5.4.1 TY Pyx - Differential light curves

colour index $[\lambda_1]-[\lambda_2]$ of one star is equal to the colour index of the system which is satisfied when the two components are of the same spectral type and luminosity class, as is the case for TY Pyx. The minima also, because they are sharp, give no evidence of circumstellar material. This result is confirmed by the energy distribution of the system which, as can be seen from Figure 5.4.2, fits perfectly well with a blackbody curve at temperature 5550 K (this temperature is derived from $\lambda_{max}T$ = 3670 μm K). The temperature of the system suggested by the blackbody fit of the energy distribution is as expected from the spectral types of the components.

Estimation of the spectral types of the systems using the observed colours gives results very similar to the ones suggested by all the previously mentioned evidence (spectroscopic data, depth of minima, energy distribution curve). The visual magnitude and colours used for estimation of the spectral types are:

V	B-V	V-I	V-J	V-H	V-K	V-L
6.87	0.69	1.05	1.20	1.50	1.60	1.67

The visual data are from Andersen and Popper (1975). The best combination of stars for the observed colours (according to the method described in Section 4.1) is G5V + G7V (χ^2 = 0.021) or G6V + G6V (χ^2 = 0.018).

Figure 5.4.3 shows the colour $|\Delta(J-K)|$ curve of TY Pyx; the absolute values of $\Delta(J-K)$ are plotted against phase. The scatter of the points around primary and secondary minima is larger than in other phases. The most probable reason for this is that the observations in J and K are not completely simultaneous, so that large, fast

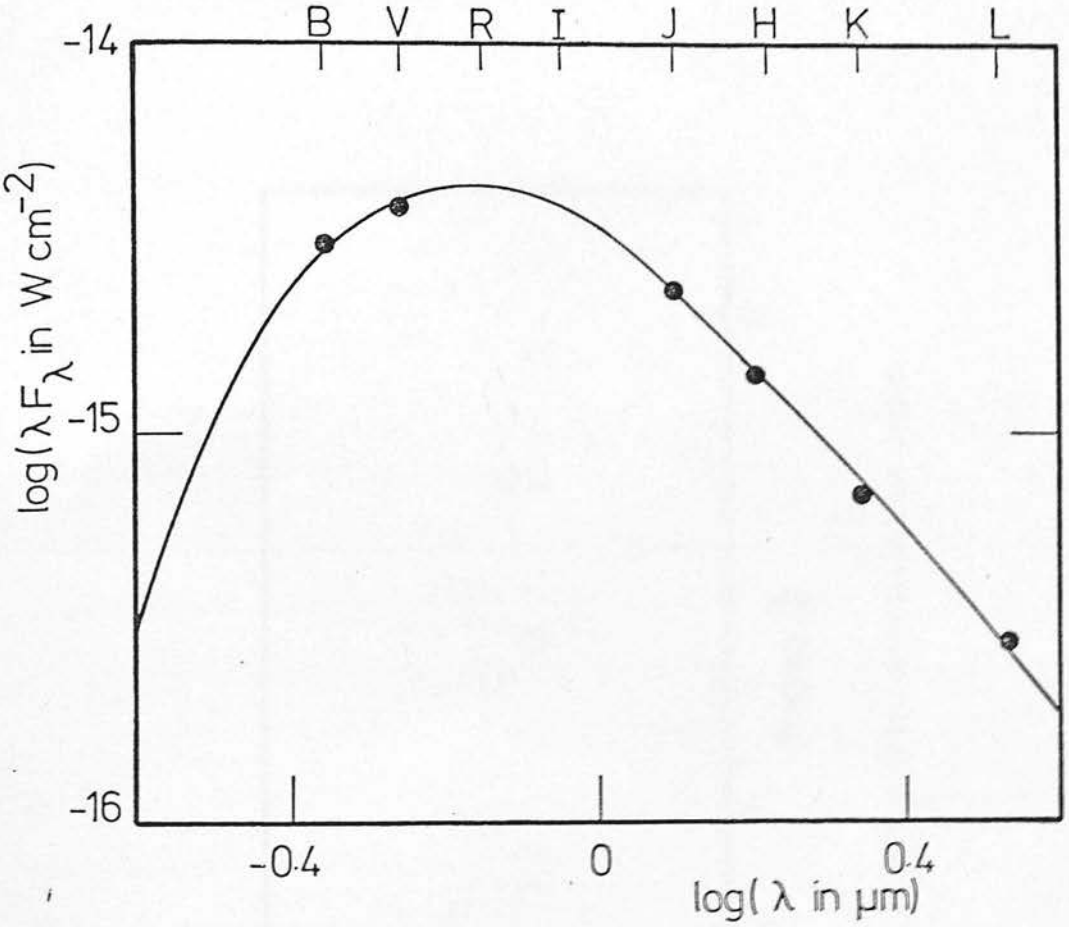

Figure 5.4.2 TY Pyx - Energy distribution

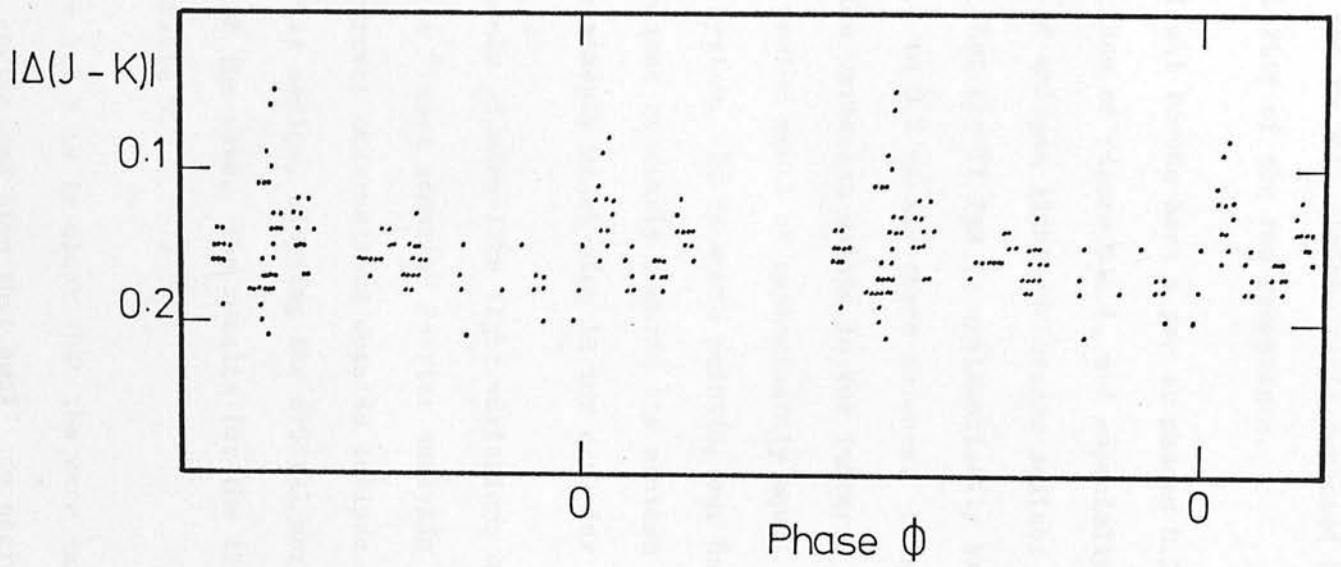

Figure 5.4.3 TY Pyx - Differential colour curve

changes in magnitude at minima and around them create the observed colour scatter. The colour curve shows continuous variation with minimum around phase 0.8 and maximum around phase 0.3. This means that TY Pyx is redder at phase 0.3 and bluer at phase 0.8. The observed colour changes are probably connected with wave-like light distortion, the wave being bluer during its maximum. The system looks equally red in both minima, as is expected because of the spectral similarity of the two components.

The JHK light curves have a gap at phases 0.2 to 0.4. However a careful inspection of Figure 5.4.1, and especially of Figure 5.4.4 where the out of eclipse light variations against phase are illustrated, shows that the TY Pyx is systematically brighter over the phase range 0.7 to 0.2 in all three colours. This is an indication that a wave-like variation exists in the infrared light curves of TY Pyx which has period equal or approximately equal to the orbital period of the system. It is worth pointing out here that the light variation decreases gradually towards its minimum (Figure 5.4.4) and then increases steeply which also is the case for HR 1099.

The existence of wave-like light variations outside eclipse was stressed using a "least squares" Fourier analysis method (section 4.5.1). The current observations outside eclipse were fitted to a truncated Fourier series, adopting the orbital period of the system as the period of the wave. The results for the three wavebands are summarised in Table 5.4.2.

From Table 5.4.2 is is clear that the wave exists in the TY Pyx infrared light curves and also that amplitude decreases with increasing wavelength. The weighted average of the time of minima of the

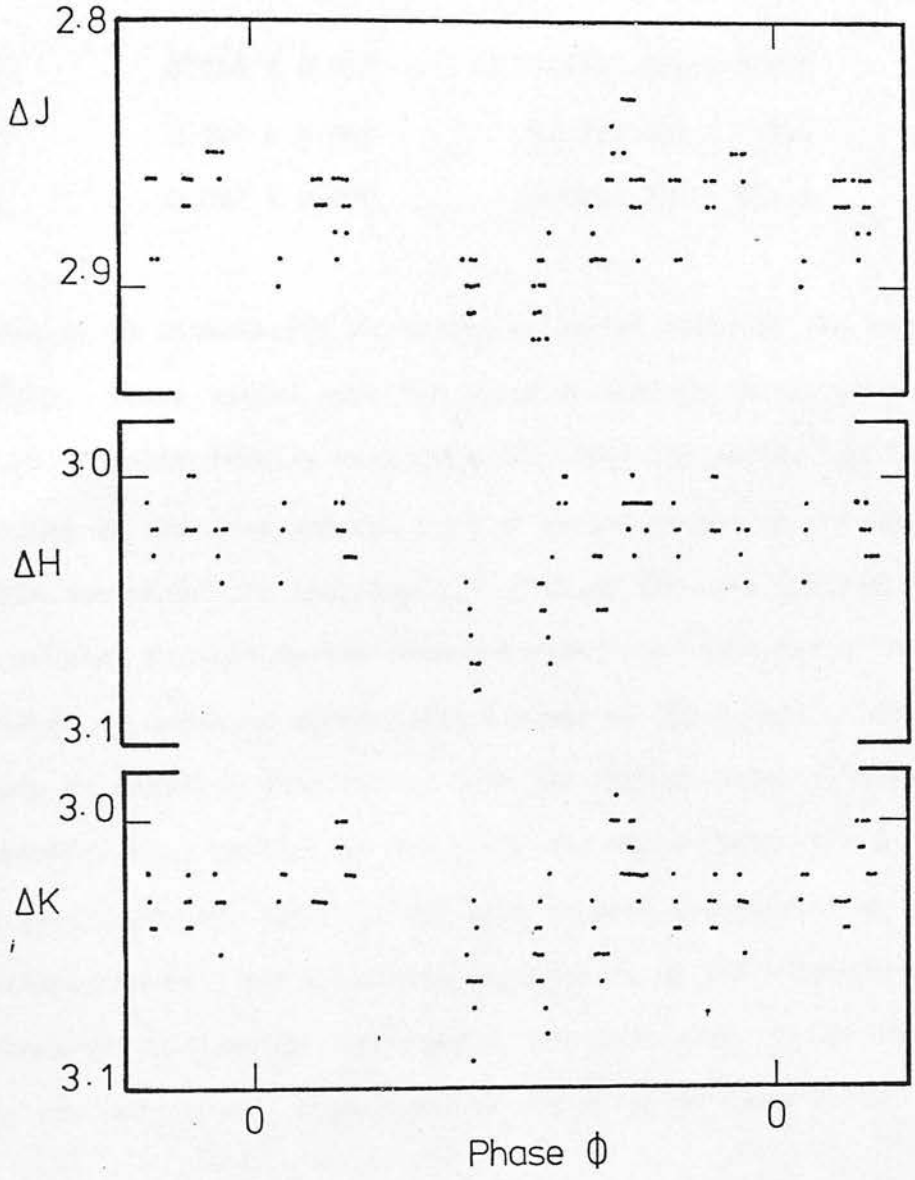

Figure 5.4.4 TY Pyx - Out of eclipse light variations

TABLE 5.4.2

Band	Amplitude of the wave	T_{min}	R.M.S. Residual
J	$0^m.048 \pm 0.003$	JD 2444224.846 ± 0.070	$0^m.020$
H	0.040 ± 0.002	2444224.892 ± 0.054	0.015
K	0.027 ± 0.003	2444224.990 ± 0.118	0.020

wave is JD 2444224.879 while the estimated error of the mean is $0^d.040$. These values give the phase of minimum of the wave as 0.409 ± 0.013. These results were obtained under the assumption that the period of the wave and the orbital period of the system are equal. This assumption is legitimate as this is the case (period of the wave = orbital period) in the observed wave-like light variations in visual or infrared wavelength of other RS CVn systems. An effort was made to estimate this period from the current data, although they are insufficient, as they do not cover the whole light curve. The J and H data were only used (as the wave is more outstanding at these wavebands) to find the hidden periodicity of the brightness variations of the system. The results are promising, though their accuracy is not very high. These results are given in Table 5.4.3. The

TABLE 5.4.3

Band	Frequency	C	Reduction factor
J	0.309	0.024	0.392
	0.312	0.023	0.354
H	0.309	0.021	0.425
	0.312	0.020	0.424

frequencies obtained by this method (section 4.4) are very similar to the ones yielding from the systems orbital period (f = 0.3126), while the amplitudes of the wave, being equal to 2C, are the same as the ones given in Table 5.4.2.

It is mentioned earlier that the colour curve of TY Pyx (Figure 5.4.3) shows that the system is redder at about phase 0.3. This suggests that the system is redder at the wave's minimum; the discrepancy between the phase of wave's minimum and phase at which the system is redder can be explained as a result of the errors in these estimations. More observations are needed to study the out of eclipse light variations of TY Pyx.

5.5 AD Capricorni (≡ HD 206046 ≡ BD −16° 5909)

The only available light curve of this system is given by Tsesevich (1954) who observed AD Cap between 1942 and 1944. Tsesevich reported that, though his observations have a great scatter, there is no doubt that the system is a β Lyrae type variable with slight light variation, of amplitude hardly exceeding $0^m.4$, and a period of 6.11826 days. More photometric data were given by Oliver (1974), but not enough to yield any scientific results. Spectroscopic observations made by Popper (1969, 1976) show H and K emission from both components. Popper also suggested G5 as the spectral type of the primary component; he gave provisional minimum masses of the two stars of the system (0.5 $M_\odot$ for the hot component and 1.1 $M_\odot$ for the cool) and he also revised the period of the system to 3 days instead of 6.12 days.

Recent observations of AD Cap by Popper (1980, personal communication) show that the light appears to be continuously variable with a range of about $0^{m}.2$ in V, without showing any true eclipses. He points out that the period of the system derived from his observations is variable.

AD Cap was observed at J, H, K, wavebands on one night in October 1978 and six nights in September 1979. The comparison star was HR 8167; its infrared magnitudes, which are the average of ten observations, are given in Table 3.3.3. In order to calculate the phases of the observations, an estimate of the period of the system is required, as this is variable, as mentioned above. So an effort was made to estimate the frequency which fits the 1979 infrared observations, using Fourier analysis as described in Section 4.4. The results of this analysis, giving reduction factors greater than 0.7 for the three infrared colours, are summarized in Table 5.5.1.

TABLE 5.5.1

Band	Frequency	C	Reduction Factor
	0.670	0.137	0.847
J	0.302	0.117	0.731
	0.335	0.130	0.702
H	0.335	0.130	0.790
	0.670	0.120	0.748
K	0.335	0.110	0.768
	0.670	0.100	0.721

From the above results it is obvious that the most probable frequencies to fit the JHK data are 0.335 and 0.670; the latter is double the first frequency. Thus the frequency which has been adopted is 0.335, yielding a period for the system of 2.985 days.

In order to find the epoch of minimum for the present observations, the JHK photometric data were fitted to a truncated Fourier Series (Section 4.5) using the period mentioned above. The times of minima for the three colours are given in Table 5.5.2

TABLE 5.5.2

Band	Amplitude	T_{min}	R.M.S. Residual
J	$0^m.268 \pm 0.032$	JD 2444142.338 ± 0.048	$0^m.050$
H	0.300 ± 0.016	2444142.293 ± 0.021	0.022
K	0.260 ± 0.016	2444142.277 ± 0.024	0.022

From the above Table is is obvious that the weighted average of the time of minimum for the three colours is 2444142.291 ± 0.015. Then the following ephemeris is suggested for AD Cap:

$$T(o)JD = 2444142.291 + 2^d.985E$$

where phase 0.0 corresponds to minimum light as at September 1979. This ephemeris was used to calculate the phases of the observations given in Table 5.5.3; in the same Table the differential magnitudes (ΔJ, ΔH, and ΔK) are also given. Figure 5.5.1 illustrates the differential infrared magnitudes against phase, while in Figure 5.5.2 the $\Delta(J-K)$ differential colour curve is shown. As can be seen from Figures 5.5.1 and 5.5.2 the colour curve has it minimum in phase with the minimum of the infrared light curves.

TABLE 5.5.3

AD Cap - Differential Magnitudes

JD 2440000 +	ϕ	ΔJ	ΔH	ΔK
3801.27	0.757	5.02	4.87	
3801.31	0.770	5.02	4.90	4.87
4140.33	0.342	4.99	4.92	4.87
4140.34	0.345	5.00	4.88	4.85
4140.35	0.348	5.01	4.93	4.86
4140.36	0.352	5.00	4.85	4.83
4141.31	0.670	5.04	4.84	4.86
4141.32	0.673	5.01	4.92	4.86
4143.26	0.323	5.01	4.89	4.85
4143.27	0.327	5.00	4.85	4.83
4143.28	0.330	4.98	4.87	4.83
4143.29	0.331	5.01	4.87	4.87
4144.29	0.668	5.04	4.87	4.86
4144.30	0.672	5.02	4.90	4.93
4144.31	0.674	5.03	4.90	4.90
4144.32	0.677	5.02	4.90	4.92
4144.33	0.683	5.02	4.89	4.86
4144.34	0.684	4.99	4.90	4.90
4145.27	0.996	5.25	5.12	5.08
4145.29	0.002	5.26	5.11	5.05
4145.30	0.006	5.25	5.12	5.06
4145.31	0.009	5.25	5.10	5.06
4146.26	0.328	5.00	4.87	4.86
4146.27	0.333	5.00	4.88	4.84
4146.28	0.334	5.02	4.86	4.86
4146.29	0.338	5.01	4.87	4.90

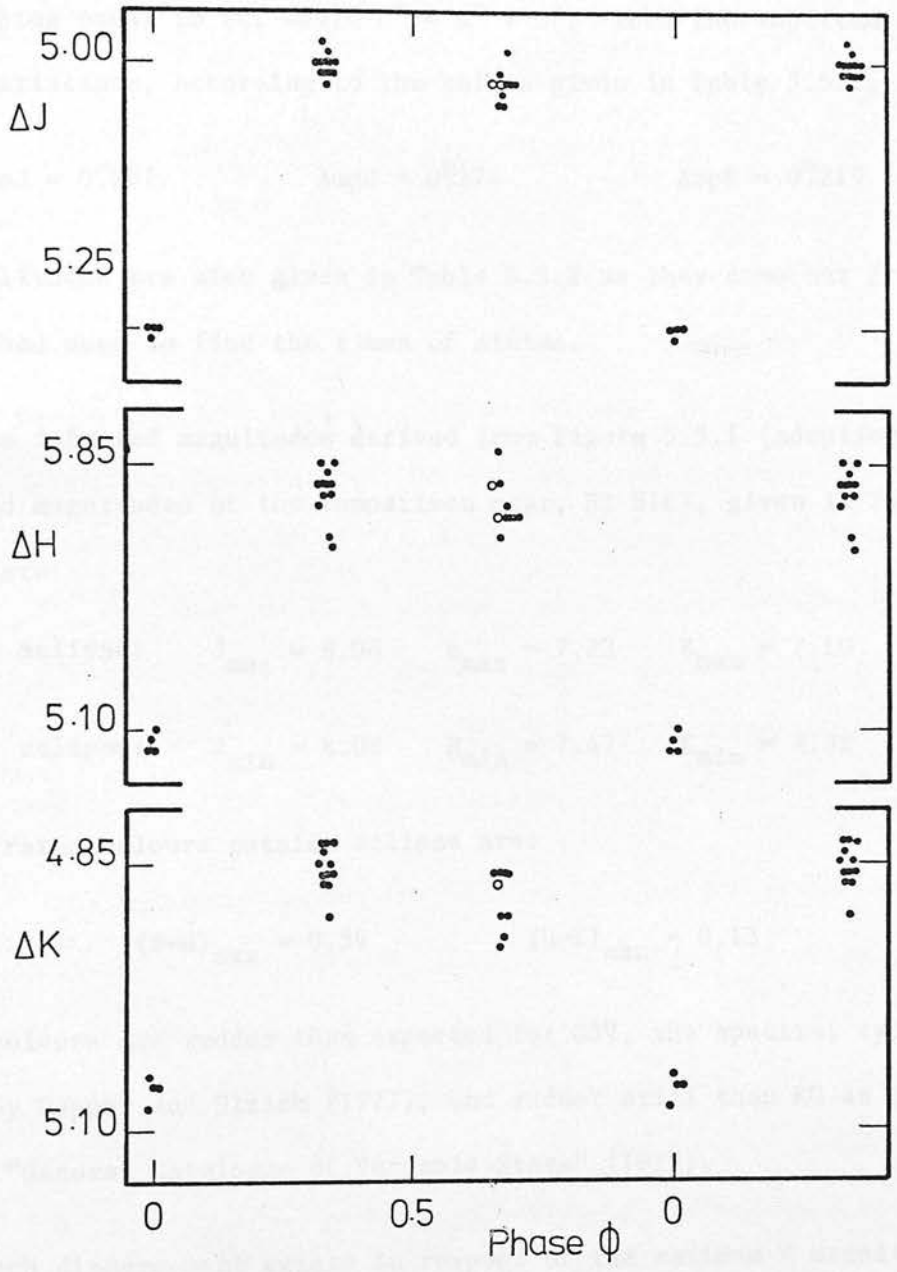

Figure 5.5.1 AD Cap - Differential light curves

The amplitudes of the infrared variations for J, H and K wavebands have been calculated using the same Fourier analysis program used to find the frequency that fits the observations, these amplitudes being equal to 2C, where $C^2 = A^2 + B^2$. Thus the amplitudes of light variations, according to the values given in Table 5.5.1, are:

AmpJ = $0^m.261$ AmpH = $0^m.274$ AmpK = $0^m.219$

The amplitudes are also given in Table 5.5.2 as they came out from the method used to find the times of minima.

The infrared magnitudes derived from Figure 5.5.1 (adopting the infrared magnitudes of the comparison star, HR 8167, given in Table 3.3.3) are:

outside eclipse: $J_{max} = 8.08$ $H_{max} = 7.23$ $K_{max} = 7.10$

during eclipse: $J_{min} = 8.08$ $H_{min} = 7.47$ $K_{min} = 7.32$

The infrared colours outside eclipse are:

$$(J-H)_{max} = 0.59 \qquad (H-K)_{max} = 0.13$$

These colours are redder than expected for G5V, the spectral types given by Popper and Ulrich (1977), and redder still than K0 as given in the "General Catalogue of Variable Stars" (1979).

Much disagreement exists in respect of the maximum V magnitude of the system and of the amplitude of the light variation in V. In the GCVS the V magnitude varies from $9^m.3$ to $9^m.9$. Oliver (1974) gives a magnitude of $8^m.7$ while according to Popper and Dumont (1977) the V magnitude outside eclipse is $9^m.77$. What is the reason for this discrepancy? Is it due to real variability or to observational errors?

In order to obtain the colours of AD Cap the V magnitude outside eclipse given by Popper and Dumont (1977) has been adopted. Then the colours of the system, outside eclipse are:

U-B	B-V	V-I	V-J	V-H	V-K
0.58	1.00	1.64	1.95	2.54	2.67

These colours are redder than the colours expected for a system of G5 stars, while the energy distribution (Figure 5.5.3) fits well with the energy distribution of a blackbody of temperature 4150 K, which is the temperature of K5V star. In the recent version of "A Finding List for Observers of Interacting Binary Systems" (Wood et al. 1980) a K0 spectral type is given for the star eclipsed at primary minimum. The energy distribution of AD Cap does not show evidence of infrared excess. All the above evidence suggests later spectral types for the system. The estimated spectral types, using the photometric data as described in Section 4.1 are K4V + K5V; for this combination χ^2 has its minimum value which is equal to 0.023.

The infrared observations (Figure 5.5.1) show continuous light variations with amplitudes larger than those observed by Popper in the visual (see above). Is the amplitude in the visual always smaller than in the infrared or is the range of the light variation as variable as it is in HR 1099 (Section 5.1)? Several sets of simultaneous observations at visual and infrared wavelengths are required in order to give an answer to the above questions.

The infrared observations in 1978 seem to fit well with those in 1979. Though the 1978 observations are very few and no definite decision can be made about the variability of the system in the infrared, it is likely that the system does not change much in one

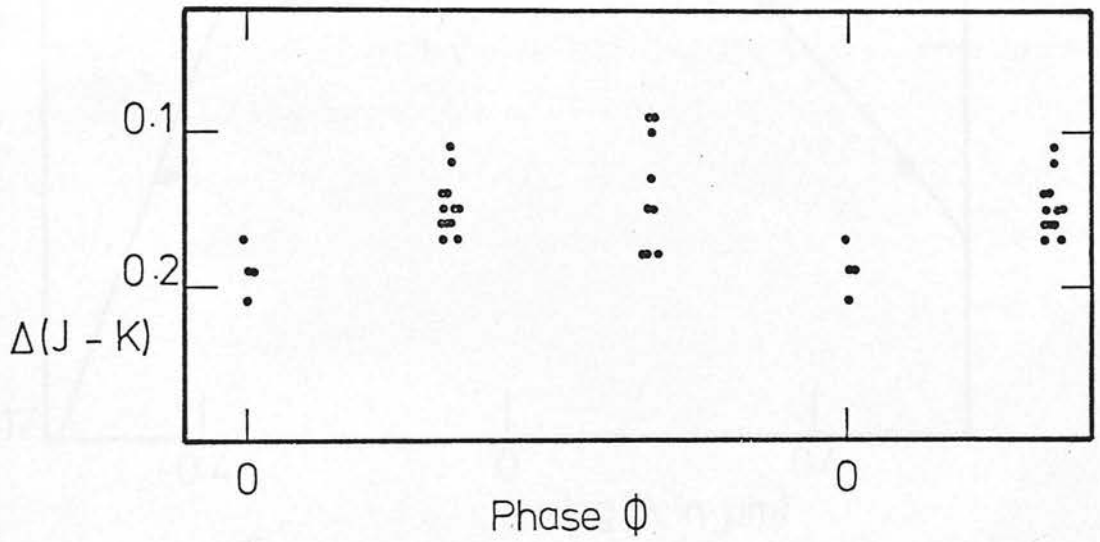

Figure 5.5.2 AD Cap - Differential colour curve

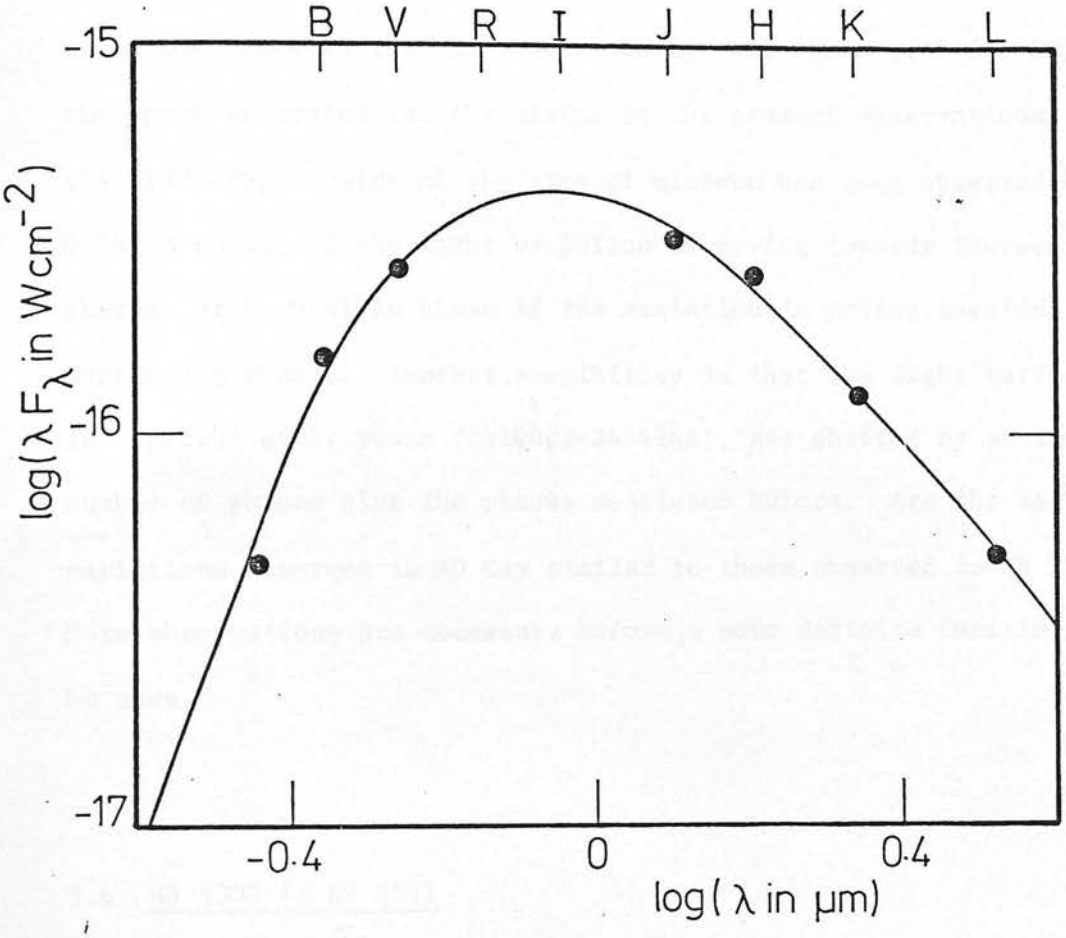

Figure 5.5.3 AD Cap - Energy distribution

year. It is worth pointing out here that the system does not show any true eclipses, as has been mentioned for the visual.

Tsesevich (1954) gives the epoch of the minimum for his observations made between 1942 and 1944. Using this epoch (2430603.55) and the epoch suggested for the minima of the present observations (2444142.295) a shift of the time of minimum has been observed by 0.39 in phase, if the light variation is moving towards increasing phases, or by 0.61 in phase if the variation is moving towards decreasing phases. Another possibility is that the light variation, in a period of 37 years (2430603-2444142), has shifted by an integer number of phases plus the phases mentioned before. Are the light variations observed in AD Cap similar to those observed in HR 1099? More observations are necessary before a more definite decision can be made.

5.6 HD 5303 (≡ BV 625)

HD 5303 was found by Strohmeier et al. (1965), from plates of the Bamberg southern station, to be a variable with amplitude $A_{pg} = 0^{m}.3$. The star is listed as a southern H and K emission line object in the objective prism survey of Bidelman and MacConnell (1973). It is also noted as having H and K emission by Houk and Cowley (1975), who classified the system as G2/G5V + F0. Concerning the spectral types of the system, Kelly (1980, personal communication) suggested, using objective prism plates, that the spectral type of the hotter component must be about G0V and it could not be later than G5V, in keeping with the classification of Stoy (1963) and Strohmeier et al. (1965). The

strong H and K emission nature of HD 5303 was confirmed from the spectra taken by Hearnshaw and Oliver (1977). They also reported that the H and K lines from the cooler component and the hydrogen lines from its companion give equal velocity amplitudes of about 130 km/s, and hence the mass ratio is approximately unity. The author is not aware of any published light curves of HD 5303 or of any further available observational material; it seems that this star is almost completely neglected, probably because of its position in the extreme south.

Infrared observations of HD 5303 were made on eight nights in November-December 1979. These observations show it to be a variable in the infrared as it has been reported to be in the visual (Strohmeier et al. 1965). HR 98 has been used as comparison star; its infrared magnitudes, the average of eight nights' observations, are given in Table 3.3.3.

The infrared data disagree badly with the phases computed from the period given by Hearnshaw and Oliver (1977). This implies either that the period of HD 5303 is variable or that the period given by Hearnshaw and Oliver is incorrect. Recently Hearnshaw (1979) gave a revised period of 2.798 days, but even using the new period the phases do not agree with the infrared data. An effort was made to re-estimate the period of HD 5303 by applying Fourier analysis, as described in section 4.4, to the present data. The results of this analysis with the highest reduction factor for the three colours are summarised in Table 5.6.1.

TABLE 5.6.1

Band	Frequency	C	Reduction Factor
	0.1599	0.100	0.825
J	0.3597	0.105	0.776
	0.3254	0.089	0.764
	0.1599	0.089	0.747
H	0.3254	0.076	0.747
	0.8449	0.078	0.742
	0.1599	0.083	0.866
K	0.3254	0.068	0.757
	0.8449	0.071	0.728

From the above Table it is obvious that the most probable frequency to fit the JHK data is 0.1599 yielding a period of 6.254 days. The time of minimum and the amplitudes of variation for the three colours, found by fitting the infrared data with truncated Fourier series (section 4.3) using the above period, are summarised in Table 5.6.2.

TABLE 5.6.2

Band	Amplitude	T_{min}	R.M.S. Residual
J	$0^m.201 \pm 0.012$	JD 2444224.483 ± 0.054	$0^m.019$
H	0.178 ± 0.010	2444224.450 ± 0.056	0.020
K	0.165 ± 0.008	2444224.350 ± 0.053	0.018

The amplitudes of variation given in Table 5.6.2 are the same as those calculated from the parameter C given in Table 5.6.1 (Amplitude

= 2C). The weighted average of the time of minima for the three colours is JD 2444224.426 ± 0.031. Thus the suggested ephemeris for the system HD 5303 is the following:

$$T_o(JD) = 2444224.426 + 6^d.254E$$

This ephemeris was used to compute the phases of the infrared observations given in Table 5.6.3. The JHK light curves are illustrated in Figure 5.6.1, while the colour ($|\Delta(J-K)|$) curve is shown in Figure 5.6.2.

It is obvious from Figure 5.6.1 that the infrared observations do not show any true eclipses but a continuous light variation similar to that observed in the non-eclipsing system HR 1099 (present work, section 5.1). This is strong evidence that HD 5303 is a non-eclipsing binary system. Another similarity of HD 5303 to HR 1099 is the fact that the amplitude of the light variation decreases with increasing wavelength; but the observed amplitudes of HD 5303 (Table 5.6.2) are larger, more than double, those observed in HR 1099.

If the phase of 0.0 at JD 2443022.716 (Hearnshaw and Oliver 1977) corresponded to minimum light, then the phase of minimum has shifted. If it is assumed that the period of HD 5303 is not variable, then the phase of minimum has shifted by 0.11 in phase in 3.292 years, in the case where the light variation is moving towards increasing phases, or by 0.89 in phase in the opposite case. The first hypothesis implies a migration period of the light variation of 29.94 years while the second implies one of 3.7 years. More observations in visual and infrared wavelengths are needed in order to confirm and study the light variations of this system.

In order to determine the colours of the system the absolute infrared magnitudes were calculated adopting infrared magnitudes for the comparison star, HR 98, as given in Table 3.3.3. Then the magnitudes of HD 5303 at maximum light are: J = 5.89, H = 5.40, K = 5.28, L = 5.17. The magnitude in V was found by Strohmeier et al (1965) to be $7^m.8$ while Stoy (1963) gave $7^m.6$. We assume that the magnitude given by Stoy is the maximum magnitude of the system (this is in keeping with the observed variation of $0^m.3$ and the magnitudes given by other workers as mentioned before) and this magnitude has been adopted in order to find the colours of HD 5303 at its maximum. Then the colours are:

V-J	V-H	V-K	V-L
1.71	2.2	2.32	2.43

These colours are different from the expected combined colours of the system if we adopt the spectral classification given in the Michigan Spectral Catalogue. For a system G2V + F0 the expected colours are:

V-J	V-H	V-K	V-L
0.643	0.847	0.868	0.923

obviously very different from the observed colours.

The infrared magnitudes of the system at maximum light, as given before, have been combined with the visual magnitude (V = 7.6) to produce the energy distribution of the star, illustrated in Figure 5.6.3. As can be seen from Figure 5.6.3 the observed fluxes of HD 5303 fit very well with a blackbody curve of temperature about 4600 K ($T\lambda_{max}$ = 3670 μmK in $\lambda F\lambda$ (in W cm^{-2}) versus λ (in μm) diagram). The energy distribution of the system shows no indication of infrared excess. The estimated temperature (4600 K) is also much less than

TABLE 5.6.3

HD 5303 - Differential Magnitudes

JD 2440000 +	ϕ	ΔJ	ΔH	ΔK	ΔL
4203.28	0.619	4.17	4.00	3.96	3.87
4203.29	0.620	4.18	3.99	3.95	
4203.34	0.628	4.17	4.00	3.95	
4203.35	0.630	4.17	4.00	3.94	
4203.37	0.633	4.17	4.00	3.95	
4204.40	0.798	4.24	4.06	4.00	3.93
4204.41	0.799	4.25	4.07	3.99	
4207.35	0.270	4.22	4.02	3.96	3.86
4207.37	0.273	4.22	4.02	3.95	
4207.38	0.274	4.22	4.02	3.96	
4207.39	0.276	4.21	4.02	3.96	
4228.31	0.621	4.19	4.01	3.95	
4228.32	0.623	4.20	4.01	3.96	
4228.33	0.624	4.19	3.99	3.96	
4228.34	0.625	4.19	4.01	3.95	
4228.35	0.628	4.19	4.00	3.95	
4228.35	0.628	4.19	4.00	3.95	
4228.36	0.629	4.18	4.00	3.96	
4228.37	0.631	4.19	4.01	3.96	
4228.37	0.631	4.20	4.00	3.96	
4228.38	0.632	4.19	4.01	3.95	
4230.29	0.938	4.35	4.16	4.11	
4230.30	0.939	4.37	4.17	4.10	
4230.31	0.941	4.36	4.15	4.10	
4230.32	0.942	4.36	4.15	4.09	
4235.27	0.734	4.27	4.08	4.01	
4235.28	0.735	4.28	4.08	4.02	
4235.28	0.735	4.29	4.09	4.02	
4235.29	0.737	4.29	4.09	4.03	
4235.30	0.739	4.29	4.08	4.01	
4235.30	0.739	4.25	4.06	4.02	
4235.31	0.739	4.27	4.06	4.00	

TABLE 5.6.3 (cont'd)

JD 2440000 +	ϕ	ΔJ	ΔH	ΔK	ΔL
4235.32	0.741	4.27	4.06	4.01	
4235.32	0.741	4.27	4.05	4.01	
4235.33	0.742	4.28	4.07	4.01	
4236.27	0.892	4.33	4.13	4.06	
4236.28	0.894	4.32	4.13	4.06	
4236.29	0.896	4.32	4.12	4.05	
4236.29	0.896	4.31	4.10	4.05	
4236.30	0.897	4.31	4.12	4.08	
4238.27	0.212	4.31	4.10	4.03	
4238.28	0.214	4.32	4.11	4.02	
4238.29	0.215	4.33	4.12	4.04	
4238.30	0.217	4.34	4.12	4.04	
4238.30	0.217	4.33	4.13	4.04	
4238.31	0.219	4.30	4.11	4.04	

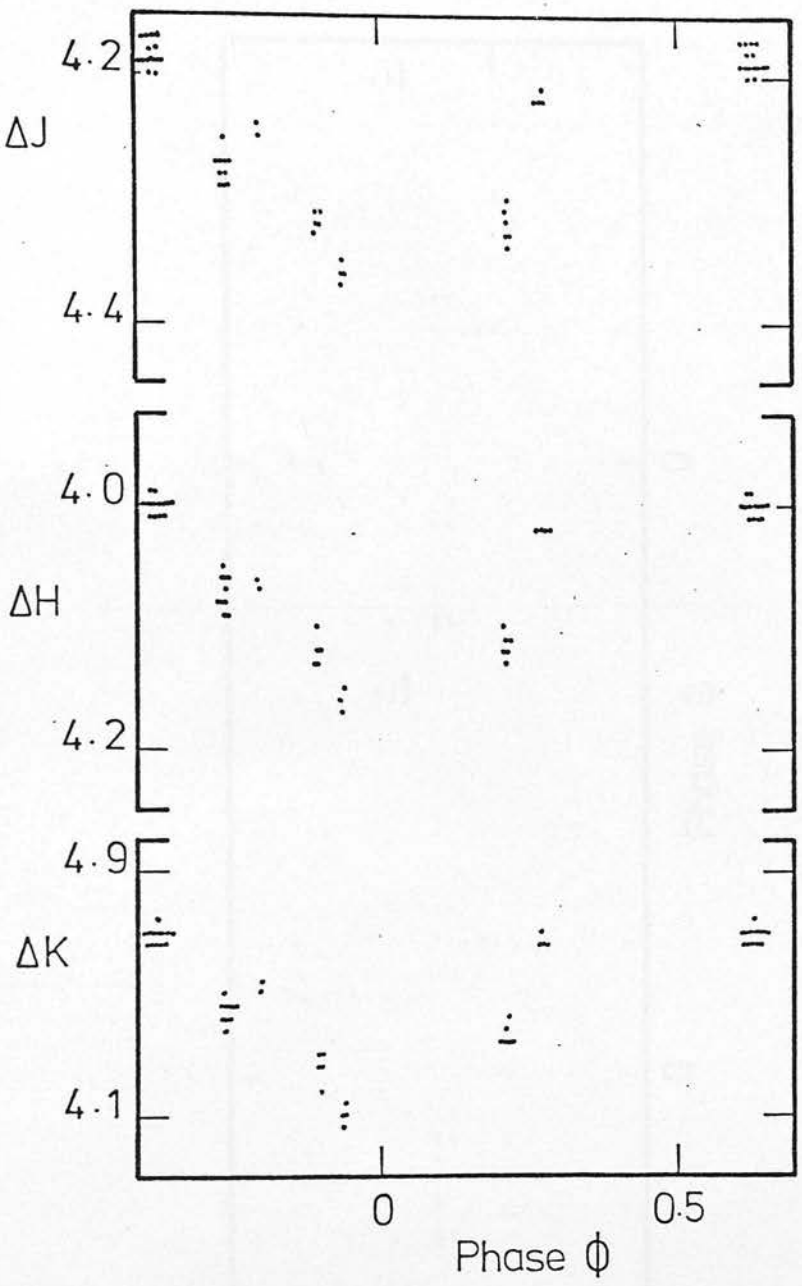

Figure 5.6.1 HD 5303 - Differential light curves

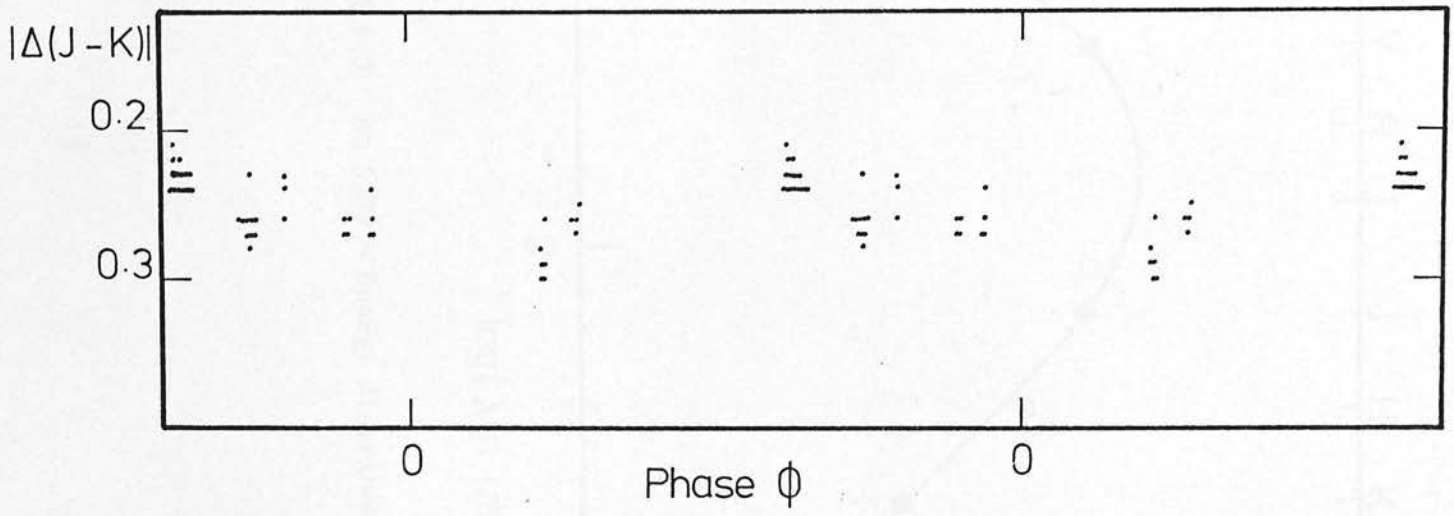

Figure 5.6.2 HD 5303 - Differential colour curve

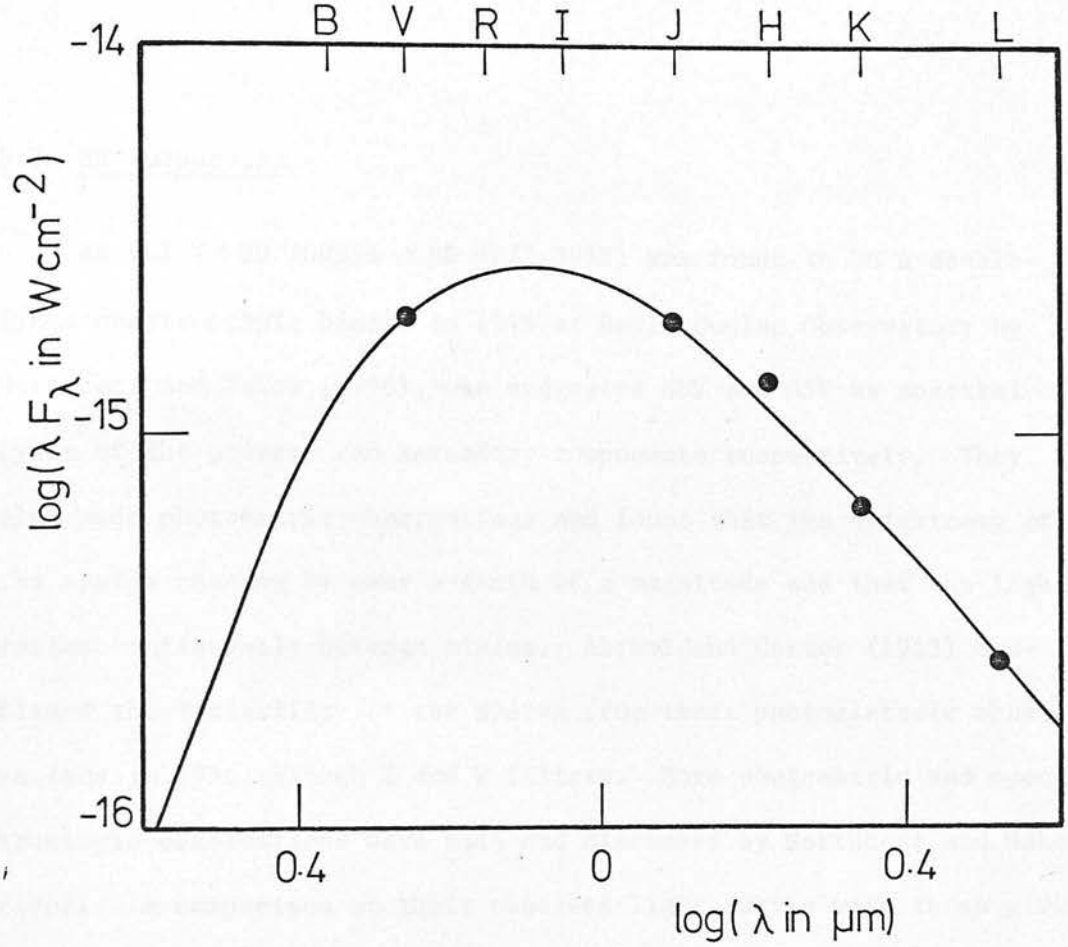

Figure 5.6.3 HD 5303 - Energy distribution

the temperature of the system if the spectral types of the components are G2/5V + F0 (Johnson 1966). These results suggest a possible misclassification of the system. A re-examination of the spectral type of the system is most desirable.

5.7 ER Vulpeculae

ER Vul (≡ HD 200391 ≡ BD +27° 3952) was found to be a double-lined spectroscopic binary in 1946 at David Dunlap Observatory by Northcott and Bakos (1956), who suggested G0V and G5V as spectral types of the primary and secondary components respectively. They also made photometric observations and found that the brightness of the system changes by over a tenth of a magnitude and that the light varies continuously between minima. Abrami and Cester (1963) confirmed the variability of the system from their photoelectric observations in 1956 through B and V filters. More photometric and spectroscopic observations were made and discussed by Northcott and Bakos (1967). A comparison of their observed light curves with those given by Abrami and Cester shows changes in the depth of the primary minima and in the shape of the maxima. Northcott and Bakos suggested that the irregular variations in the B and V light curves of ER Vul could be explained by the presence of a gaseous cloud of variable brightness situated at the inner Lagrangian point and extending to one side. But their spectroscopic observations showed no evidence of this cloud. Spectroscopic observations by Hill et al. (1975) suggested that the spectral type of the brighter component is G2V with nebulous (i.e. broad) lines in its spectrum. Recent photometry by Al-Maimiy (1978) showed that the previously observed irregularities

in B and V light curves appeared to be present in his 1978 (July-August photometric observations. He pointed out that the peculiarities are mainly a great variability in the brightness outside eclipse and in the depth of the secondary minimum. From the visual observations it can be shown that the period of the system is decreasing (Northcott and Bakos 1967; Abrami and Cester 1963; Al-Maimiy 1978).

Infrared photometric observations of ER Vul were made using the 1.5 m flux collector in Tenerife, at the same time as the visual observations of the system were made by Al-Maimiy. ER Vul was observed on seven nights in August 1978 using an InSb detector. The comparison star was HR 7942, whose infrared magnitudes are given in Table 3.3.3. The light curve was obtained in four colours (J H K L'; L' 0 3.8 μm). The observations of ER Vul are listed in Table 5.7.1 and plotted in Figure 5.7.1. The differential colours, (J-K), are illustrated in Figure 5.7.2. The phases were computed from the light elements

$$T_o(JD) = 2440182.3212 + 0^d.698082E$$

given by Al-Naimiy (1978) where phase 0.0 corresponds to minimum light. (The light elements given in the "Rocznik Astronomiczny, 1980" are in error. The value of the period given is not that given by the reference.) The observed infrared light curves are similar to those in the visual. The light appears to be continuously variable with a range of about $0^m.15$ in K. The light variation seems to be larger at longer wavelengths (amplitude in L bigger than amplitude in J), while the light variation seems to have the smallest amplitude in H. The infrared observations indicate irregular light curve variations similar to those reported in B and V (Abrami and Cester 1963, Northcott and Bakos 1967; Al-Naimiy 1978).

TABLE 5.7.1

ER Vul - Differential Magnitudes

JD 2440000 +	ϕ	ΔJ	ΔH	ΔK	ΔL
3727.57	0.556	3.73	4.02	3.97	3.95
3727.59	0.585	3.72	3.93	3.96	3.95
3727.60	0.599	3.71	3.90	3.86	3.95
3727.62	0.628	3.73	3.86	3.98	4.00
3727.63	0.642	3.71		3.98	
3733.59	0.180	3.82	3.97	4.01	4.05
3733.60	0.194	3.82	3.99	4.07	4.13
3733.64	0.252	3.73	3.92	3.95	4.01
3733.68	0.309	3.77	3.97	3.89	3.97
3734.56	0.569	3.75	3.94	3.97	4.04
3734.57	0.591	3.75	3.91	3.99	4.01
3734.61	0.640	3.76	3.88	3.96	3.93
3734.63	0.670	3.75	3.93	3.99	3.99
3735.50	0.916	3.68	3.99	3.90	
3735.54	0.973		4.03	4.07	
3735.56	0.002	3.84	3.97	4.07	
3735.58	0.030	3.83	3.97	4.06	4.04
3735.60	0.060	3.81	3.97	4.06	4.10
3735.61	0.074	3.82	3.94	4.00	4.10
3735.64	0.117	3.76	3.93	3.98	3.96
3736.62	0.528	3.86	4.00	4.03	4.05
3736.63	0.542	3.82	4.02	4.01	
3736.65	0.563	3.76	3.93	3.97	4.00
3737.50	0.781	3.69	3.88	3.89	3.88
3737.51	0.795	3.67	3.87	3.92	3.88
3737.52	0.810	3.69	3.87	3.95	3.92
3737.58	0.896	3.73	3.89	3.90	3.91
3737.59	0.910	3.71	3.89	3.96	3.99
3737.62	0.953	3.70	3.89	3.93	3.94
3737.630	0.967	3.78	3.99	4.02	3.99
3738.48	0.185	3.72	3.98	4.00	4.06
3738.49	0.199	3.74	3.94	3.95	4.15
3738.50	0.214	3.13	3.95	3.96	3.98
3738.53	0.257	3.72	3.92	3.94	3.97
3738.54	0.271	3.65	3.90	3.90	3.97

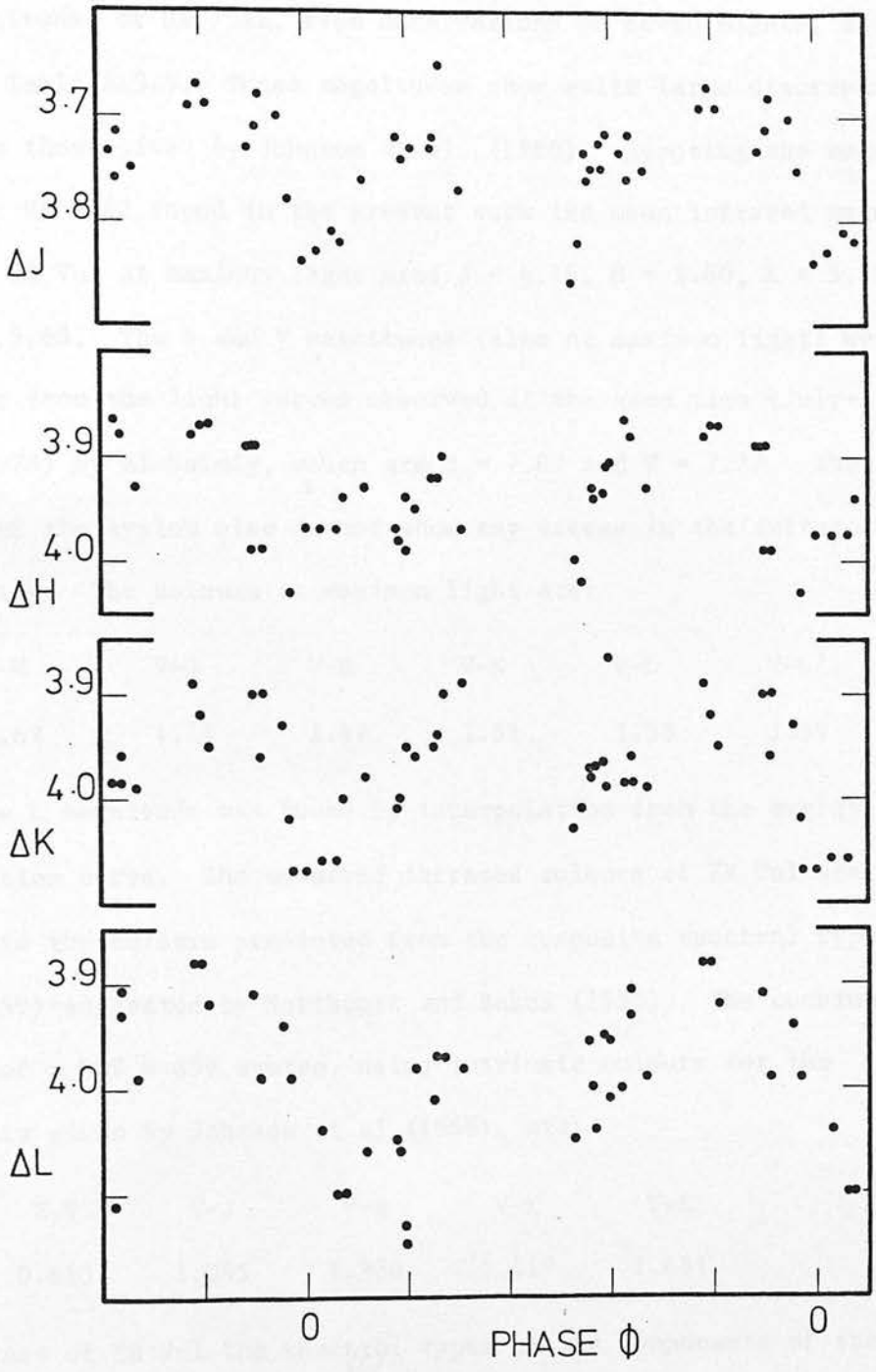

Figure 5.7.1 ER Vul - Differential light curves

To determine the colours of ER Vul, the comparison star HR 7942 was tied to α Lyr which was assumed to be $0^m.0$ at all wavelengths. The mean magnitudes of HR 7942, from observations on seven nights, are given in Table 3.3.3. These magnitudes show quite large discrepancies from those given by Johnson et al. (1966). Adopting the magnitudes for HR 7942 found in the present work the mean infrared magnitudes of ER Vul at maximum light are: J = 6.16, H = 5.80, K = 5.76 and L' = 5.68. The B and V magnitudes (also at maximum light) were estimated from the light curves observed at the same time (July-August 1978) by Al-Naimiy, which are B = 7.89 and V = 7.27. The colours of the system also do not show any excess in the infrared wavelengths. The colours at maximum light are:

B-V	V-J	V-H	V-K	V-L	V-L'
0.62	1.11	1.47	1.51	1.58	1.59

where the L magnitude was found by interpolation from the energy distribution curve. The observed infrared colours of ER Vul are very similar to the colours predicted from the composite spectral type (G0V + G5V) suggested by Northcott and Bakos (1956). The combined colours of a G0V + G5V system, using intrinsic colours for the components given by Johnson et al (1968), are:

B-V	V-J	V-H	V-K	V-L
0.615	1.065	1.360	1.419	1.481

In the case of ER Vul the spectral types of the components of the system estimated spectroscopically (Northcott and Bakos, 1956) and photometrically give similar results; the χ^2 test gives a value of = 0.037 for the combination G0V + G5V. But the best combination for the observed colours seems to require a later spectral type for the cooler component; the combination G0V + K2V (χ^2 = 0.001) seems to be

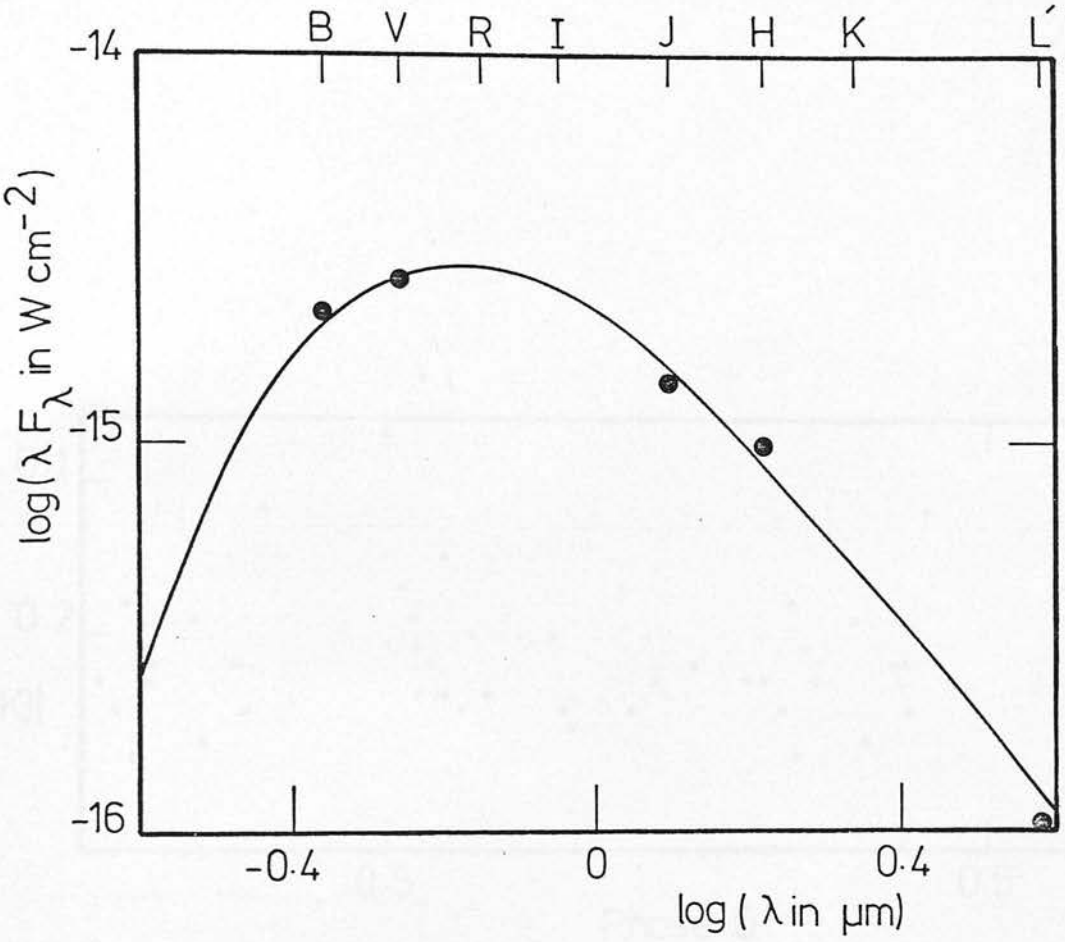

Figure 5.7.3 ER Vul - Energy distribution

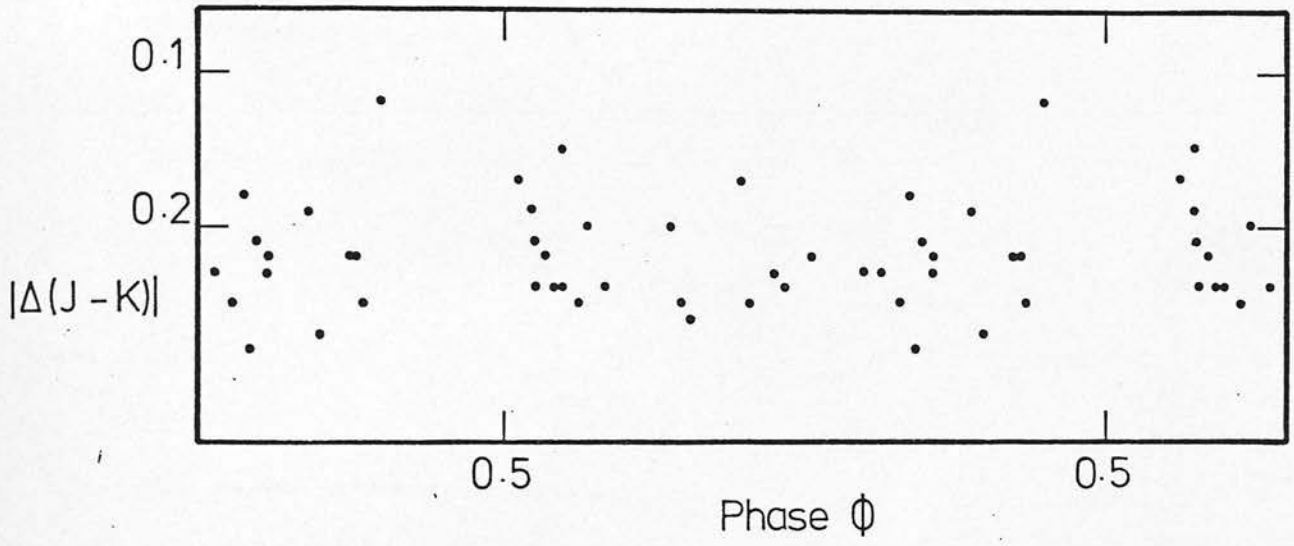

Figure 5.7.2 ER Vul - Differential colour curve

the best according to the photometrically determined spectral types method.

The energy distribution of ER Vul is illustrated in Figure 5.7.3 and does not show any evidence of near infrared excess; the observed fluxes fit perfectly well with a blackbody curve of temperature of about 5000 K.

CHAPTER VI

GENERAL DISCUSSION - CONCLUSIONS

In the previous chapter the observational results for each binary system of the present project have been analysed, and many similarities suggest themselves. Although each system has individual characteristics, as shown in the discussion in Chapter V, their common properties will be discussed here for their relevance to characteristics of the RS CVn class, and a simple model is suggested for the systems which explains the observational facts.

The most fascinating result of this project is the discovery of the wave-like infrared light variation outside eclipse for three of the systems that have been extensively observed. For two of these systems, HR 1099 and SZ Psc, similar photometric asymmetries in their light curves have been detected in the visual, as seen in sections 5.1 and 5.3, where the systems are discussed individually. For the third star, TY Pyx, the distortion wave outside eclipse has probably been detected in the visual by Oliver (1974a). The amplitudes of the wave-like infrared light variations for the three systems are summarised in Table 6.1. For HR 1099, for which simultaneous visual observations were made, the infrared variations are in phase with the visual. The same wave seems to exist in the September 1979 light curve of UV Psc, but inadequate data do not allow definition of the wave's characteristics (amplitude, phase of minimum); this light distortion outside eclipse in the UV Psc light curve is not detectable in the November-December 1979 observations. The two program stars, AD Cap and HD 5303, show continuous light variations, but the systems have been observed very little hitherto, in fact they have been almost completely

neglected; therefore it is not clear if the observed continuous variations are similar to those observed in HR 1099 or similar to the W UMa type stars. The amplitudes of the light variations observed in HD 5303 and AD Cap are of the order of $0^m.15$ to $0^m.30$ (Tables 5.5.2 and 5.6.2), while the observed variations in the previously mentioned systems (HR 1099, SZ Psc and TY Pyx) are less than $0^m.10$ (Table 6.1). A common characteristic of the distortion wave in all three systems (HR 1099, SZ Psc, TY Pyx) that exhibit this wave in the infrared is that the amplitude of the wave decreases with increasing wavelength (Table 6.1). This is the opposite of Oliver's conclusion (Oliver 1974, Table 43), where the amplitude of the wave in UBV seems to increase with increasing wavelength for four of the six systems in which wave-like light variations have been detected. These systems are different from those studied in the current project.

For HR 1099, for which the wave has been observed in more than one epoch, the wave seems to show variations in the amplitude and time of minima. For the systems in which the distortion wave exists in their light curves, the wave-like light variation is in phase with the colour variation, in other words the minimum of the colour curve is coincident with the minimum of the wave. From Figures 5.1.1, 5.1.2, 5.3.4 and 5.4.4 it is obvious that another common characteristic of the systems that show measurable wave-like light variations is the shape of the wave. For all three systems the wave clearly decreases slowly to its minimum while it rises steeply.

A common characteristic of the seven systems discussed in Chapter V is the irregular light variability. In fourteen RS CVn systems the current infrared observations do not show any apparent infrared excess (Chapter IV).

The similarities in the characteristics of the RS CVn systems investigated in the present work are:

1. Wave-like light variations in the infrared similar to those in the visual.
2. The amplitude and phase of minimum of the wave for a given wavelength varies with time. For a given epoch the amplitude of the wave decreases with increasing wavelength.
3. The wave-like light variations, in all the three systems where they were clearly detectable, seem to decrease slowly while rising steeply.
4. Irregular light variations have been observed in the infrared as in the visual.
5. The maximum brightness of the systems varies in the visual and apparently also in the infrared.
6. No apparent infrared excess has been detected in fourteen RS CVn systems observed in the infrared in the present project.

TABLE 6.1

The Characteristics of the Observed Wave-like Light Variations in the Infrared

Star	J	H	K	L	ϕ_{min}	Time of Observations (years)
HR 1099	$0^m.086$	$0^m.087$	$0^m.064$		0.894	1978.85
HR 1099	0.082		0.060	0.050	0.961	1979.95
SZ Psc	0.048	0.034	0.032		0.710	1979.85
TY Pyx	0.048	0.040	0.027		0.409	1979.95

The suggested models for the RS CVn systems have been discussed in Chapter II (section 2.5). The pulsating model could be a possible explanation. With respect to pulsation, the cooler component is envisaged as undergoing a pulsation with a period approximately the same as the orbital period of the system. As has been discussed earlier (section 5.2) this model has been rejected because the position of the cooler component (usually a K0IV star) is not near the usual instability strip in the Hertzsprung-Russell diagram and also because the oscillation period and amplitude of variation expected from the several types of pulsators do not agree with the observed period and amplitude of light variations of RS CVn systems. The above mentioned reasons for rejecting the pulsating model are probably not very critical, as the period and amplitude of light variations and also the position of the cooler component in the Hertzsprung-Russell diagram would be expected to be different from those for single pulsators; the binary nature of the RS CVn should affect all these parameters in the case where the cooler components are pulsators. But there are more observational facts that cannot be explained on the basis of the pulsating model. The flare activity observed from the RS CVn systems in different regions of the electromagnetic spectrum and also the indirect observation of strong magnetic fields in the systems (through the detection of polarised light from some RS CVn binaries) are indications that the hypothesis that one of the components is a pulsator has its weak points.

Another possible model for the RS CVn systems is that which attributes the sinusoidal-like light variations outside eclipse to the existence of a cloud or ring around the whole system or around the cooler component. The possibility of a ring around the secondary

has been discussed in section 2.4 and has been rejected as dynamically unstable. For the case of an asymmetrical cloud or a ring around the entire system, let us consider the sources of continuous opacity (as absorption lines have not been detected spectroscopically, and also it is unlikely to affect all the visual and infrared broad photometric bands where the wave-like light variations have been detected).

Sources of continuous opacity are: Thomson scattering by electrons, which is independent of wavelength; Rayleigh scattering due to neutral hydrogen, which is proportional to λ^{-4}; and absorption by the negative hydrogen ion (H^-) whose wavelength dependence is given by C.W. Allen (1973). The first is rejected because the observed light variations are wavelength-dependent. The wavelength dependence of Rayleigh scattering does not agree with the observed dependence (e.g. assuming the October 1978 observations of HR 1099 (Table 5.1.10), and that $\Delta m = K/\lambda^4$, K constant, for the observed ΔJ amplitude the expected ΔH and ΔK amplitudes are $0^m.028$ and $0^m.0896$, very different from those observed). The absorption by the negative hydrogen ion, which explains the amplitude dependence on wavelength in UBV observed by Oliver (1974), does not seem to explain the current observations. According to Allen (1973) the absorption coefficient in this case has its minimum at the H waveband; thus the expected minimum amplitude of the light variation would be expected in the H band (Figure 6.1). The observations however (Tables 5.1.10, 5.3.2 and 5.4.2) show a continuous decrease of the amplitude of the wave with increasing wavelength. Thus this model is not applicable.

Combining the above mentioned infrared observational facts, as derived from the present project, with other observers' work in other regions of the electromagnetic spectrum, the spot model seems to be

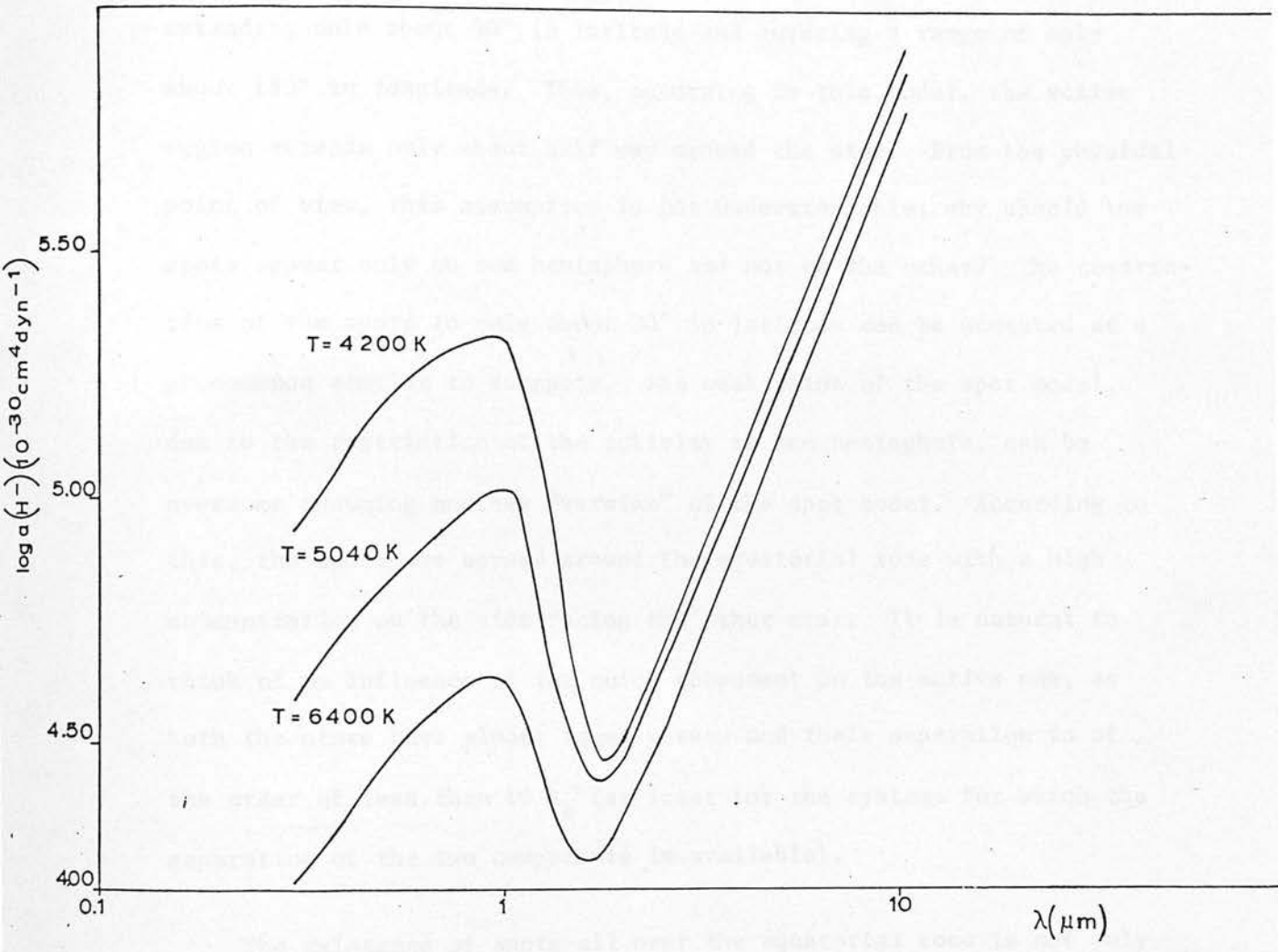

Figure 6.1 H^- absorption coefficient plotted against wavelength

the most plausible model for the RS CVn-type binary systems. According to this model, one of the components of the RS CVn-type binary systems carries a spot complex (analogous to sunspots). As has been suggested by Hall, the spots are confined to the equatorial region, extending only about 30° in latitude and covering a range of only about 180° in longitude. Thus, according to this model, the active region extends only about half way around the star. From the physical point of view, this assumption is not understandable; why should the spots appear only on one hemisphere and not on the other? The restriction of the spots to only about 30° in latitude can be accepted as a phenomenon similar to sunspots. The weak point of the spot model, due to the restriction of the activity to one hemisphere, can be overcome assuming another "version" of the spot model. According to this, the spots are spread around the equatorial zone with a high concentration on the side facing the other star. It is natural to think of an influence of the quiet component on the active one, as both the stars have almost equal masses and their separation is of the order of less than 10 $R_\odot$ (at least for the systems for which the separation of the two components is available).

The existence of spots all over the equatorial zone is not only physically more understandable but also it explains the magnitude variation observed at maximum light (Guinan et al. 1980). Let us suppose that A is the ratio of the area of the concentrated spot complex to the whole effective area of the stellar disk, and that the spot temperature is T_s, while the temperature of the surrounding photosphere of the star with spot activity is T_*. It is assumed that the spotted star and the spots themselves radiate like black bodies at temperatures T_* and T_s respectively. A relation between the effective

area of the spot A and its temperature T_s can be derived using simple blackbody formulae. The observed amplitude of the wave-like light variations Δm for a given wavelength λ is given by the relation:

$$\Delta m = 2.5 \log \frac{F(T_*)}{AF(T_s) + (1 - A)F(T_*)}$$

$$\Delta m = 2.5 \log \frac{\frac{c}{e^{c_2/\lambda T_*} - 1}}{(1 - A)\frac{c}{e^{c_2/\lambda T_*} - 1} + A\frac{c}{e^{c_2/\lambda T_s} - 1}}$$

$$\Delta m = 2.5 \log \frac{e^{c_2/\lambda T_s} - 1}{[(1 - A)e^{c_2/\lambda T_s} - 1] + [A(e^{c_2/\lambda T_*} - 1)]}$$

$$\Delta m = -2.5 \log [(1 - A) + AB] \qquad 6.1$$

where $B \equiv \frac{e^{c_2/\lambda T_*} - 1}{e^{c_2/\lambda T_s} - 1}$

From equation 6.1

$$\log [(1 - A) + AB] = -0.4\Delta m \qquad \text{or}$$

$$1 - A + AB = 10^{-0.4\Delta m} \qquad \text{or}$$

$$A = \frac{10^{-0.4\Delta m} - 1}{B - 1} \qquad 6.2$$

Equation 6.2 gives a relation between the effective area of the spot and its temperature T_s, knowing the temperature of the surrounding photosphere (from the spectral type, Johnson 1966) and the observed amplitude of the variation Δm at a given wavelength λ. In order to

find an exact estimate of the effective area and the temperature of the spot, synchronous observations at more than one wavelength are required. From equation 6.2, knowing the relation between temperature and spot area for a given Δm at wavelength λ, the expected amplitudes of the light variation Δm_i at any other wavelengths λ_i can be estimated for any combination A, T_s which satisfies the above relation. The above have been applied to HR 1099 which is a non-eclipsing RS CVn system and the most observed system for this project; the results are given in Figure 6.2. The relation between the effective area A of the concentrated spot complex (as a fraction of the whole area of the stellar disk) and $\Delta T = T_* - T_s$, for a given amplitude $\Delta m = 0^m.13$ at wavelength $\lambda = 0.6563$ μm (Guinan et al. 1979) from observations synchronous with our November-December 1979 infrared observations, is given in Figure 6.2a. In Figure 6.2b the expected amplitudes of the light variations in J, K and L for temperature and area of the spots which fit the visual light curve are given. Figure 6.2b shows that a huge spot which covers 35 percent of the stellar disk and with temperature difference between the temperatures of the spot and the photosphere ($\Delta T = T_* - T_s$) of the order of 700 ± 100 K, can explain our November-December 1979 observations. These results emerge, taking into account that the active component of HR 1099 is a K3IV star, as appeared from the present investigation using the current photometric colours of the system (section 5.1). A spot complex with a temperature only some hundreds of degrees cooler than the surrounding photosphere would have to be very large in order to produce the observed amplitude ($\Delta m = 0^m.13$ at $\lambda_o = 0.6563$ μm), as is shown in Figure 6.2a. Such a spot complex would produce not only the observed amplitudes of the light variations in the infrared, but also the sinusoidal-like shape

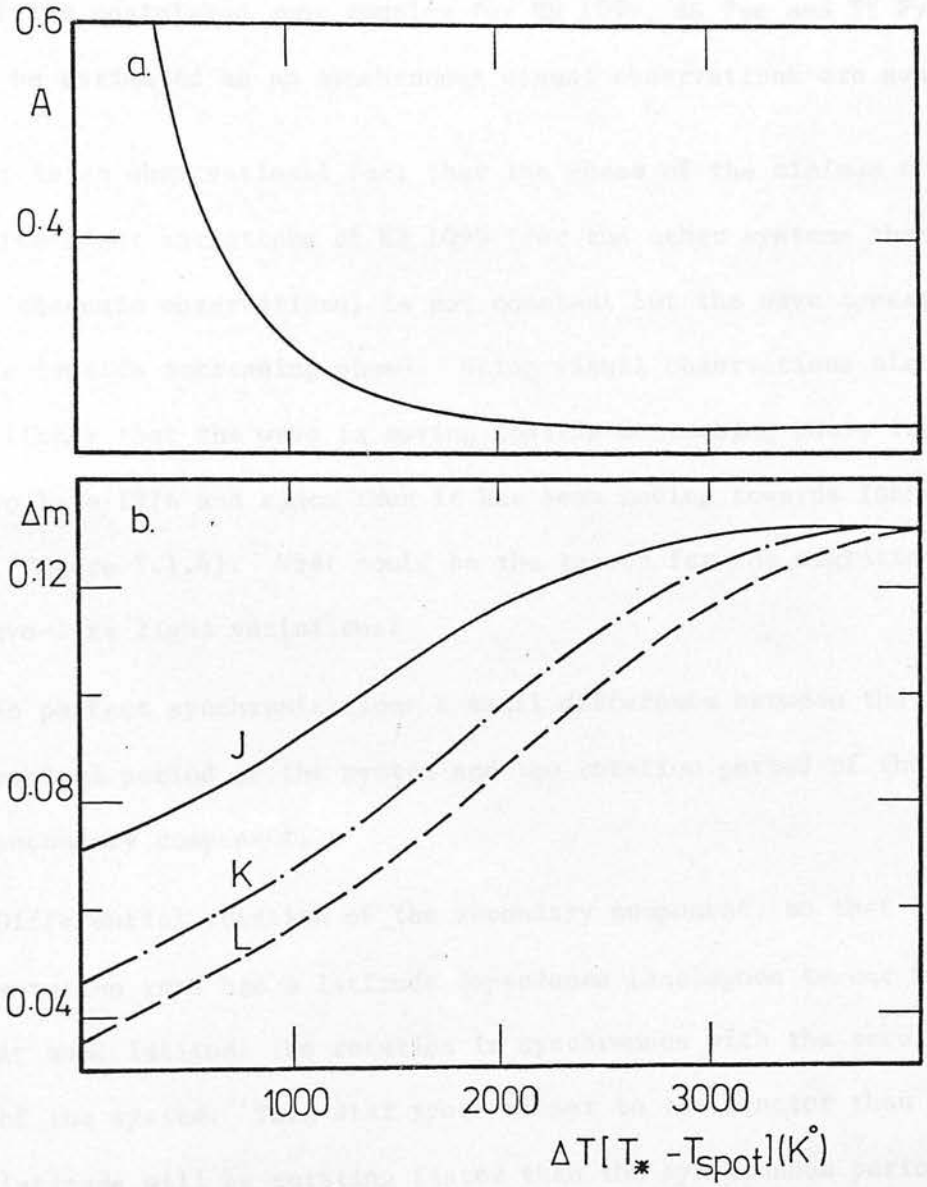

Figure 6.2 Top: Relation between the fraction of the projected area of the stellar disk occupied by spots and the temperature difference ($\Delta T = T_* - T_{spot}$) which satisfies the optical light curve.

Bottom: The expected amplitudes of the light variations in J K L corresponding to these values of A and ΔT.

of the visual and infrared light curve of HR 1099; no flat parts at the top of the light curve have been observed. The temperature and area of the postulated spot complex for HR 1099, SZ Psc and TY Pyx cannot be estimated as no synchronous visual observations are available.

It is an observational fact that the phase of the minimum of the wave-like light variations of HR 1099 (for the other systems there are no adequate observations) is not constant but the wave appears to migrate towards increasing phase. Using visual observations also it seems likely that the wave is moving towards decreasing phase from 1975 to late 1976 and since then it has been moving towards increasing phase (Figure 5.1.4). What could be the reason for the migration of the wave-like light variations?

1. No perfect synchronisation: a small difference between the orbital period of the system and the rotation period of the secondary component.

2. Differential rotation of the secondary component, so that the rotation rate has a latitude dependence (analogous to our Sun). At some latitude the rotation is synchronous with the revolution of the system. Then star spots closer to the equator than this latitude will be rotating faster than the synchronous period and the asymmetry in the light curve due to the star spots in this area would shift towards earlier phase. The opposite would happen if the spotty areas were at latitudes closer to the poles than the latitude where the rotation is synchronous; in this case the wave-like light variation shifts towards increasing phase. Thus for HR 1099, where the wave is migrating towards increasing or decreasing phase, this would be explained in terms of the position of the spots on the secondary component.

3. The reason for the migration is probably related to the movements and the dynamical condition of the atmosphere of the spotted star.

The second explanation seems more plausible.

The existence of a cool spot on the disk of one of the stars explains also the wavelength dependence of the observed amplitudes of the wave-like light variations. As has been mentioned earlier, for all the three systems HR 1099, SZ Psc and TY Pyx for which the light variation has been confirmed in the infrared wavelength also, the amplitude of the variation decreases with increasing wavelength (Table 6.1). The results of Oliver's (1974) UBV photometry are different for four of six observed RS CVn systems. For four systems (which are different from the RS CVn systems of the present project) he found that the wave increases with increasing wavelength while for the other two the amplitude is independent of wavelength. Oliver's observations cannot be explained in terms of the given spot model (Figure 6.3). Probably Oliver's stars are not spotty stars. Infrared observations are however necessary before any definite decision can be made. The observed random variability in the infrared (current work) and in the visual may be attributed not only to the flare activity of the cooler component of the system but also, by analogy with the Sun, to coronal holes. By analogy of the starspots with sunspots, the existence of starspots must be associated with locally strong magnetic fields. The existence of a strong magnetic field at least in HR 1099, which has been extensively observed in the last five years (section 5.1) has been detected indirectly from strong circular polarisation observed from the system at radio wavelengths.

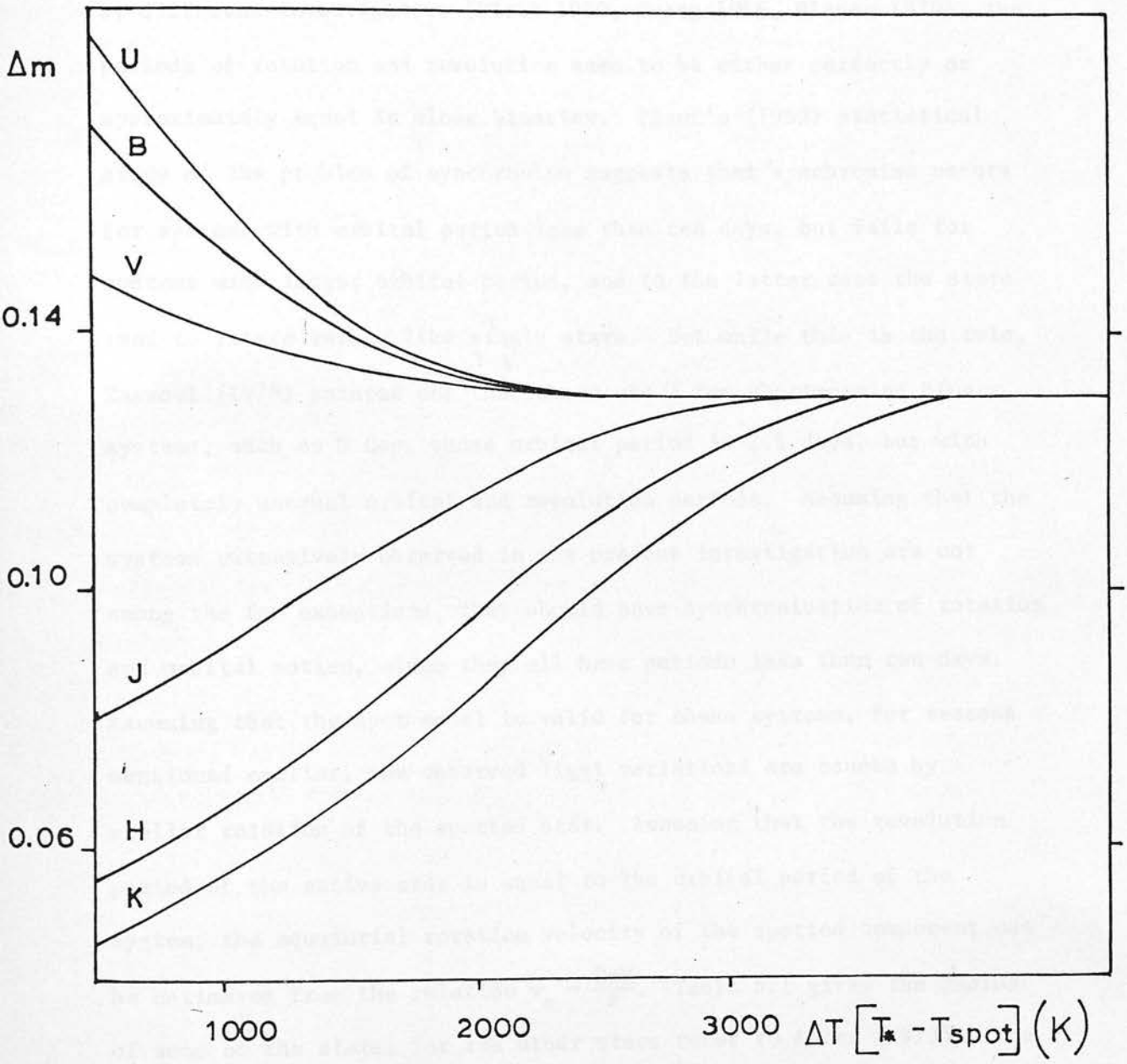

Figure 6.3 The expected visual and infrared light variations (using the spot model) of HR 1099, which satisfies the variations observed at $\lambda = 0.6563$ μm.

Another point worth mentioning is that the active components of the RS CVn systems seem to have equatorial velocities higher than expected for their spectral types. As has been found and discussed by different investigators (Plaut 1959, Huang 1966, Plavec 1970), the periods of rotation and revolution seem to be either perfectly or approximately equal in close binaries. Plaut's (1959) statistical study of the problem of synchronism suggests that synchronism occurs for systems with orbital period less than ten days, but fails for systems with longer orbital period, and in the latter case the stars tend to rotate rather like single stars. But while this is the rule, Tassoul (1978) pointed out that there are a few short-period binary systems, such as U Cep, whose orbital period is 2.5 days, but with completely unequal orbital and revolution periods. Assuming that the systems extensively observed in the present investigation are not among the few exceptions, they should have synchronisation of rotation and orbital motion, since they all have periods less than ten days. Assuming that the spot model is valid for these systems, for reasons mentioned earlier, the observed light variations are caused by stellar rotation of the spotted star. Assuming that the revolution period of the active star is equal to the orbital period of the system, the equatorial rotation velocity of the spotted component can be estimated from the relation $v_e = \frac{2\pi R}{P}$. Table 5.1 gives the radius of some of the stars; for the other stars refer to Allen (1973). The estimated v_e for the different systems is given in Table 6.2. As is obvious from Table 6.2 and Allen (1973, p. 210), the active component of the RS CVn systems rotates faster than single stars of the same spectral type. Kraft (1967) discovered that main-sequence field stars with CaII emission lines have higher axial rotational velocity

TABLE 6.2

Estimated Equatorial Rotational Velocity
of the Spotted Component

Star	Sp T*	R km* x 10^5	P	V_e km/s
HR 1099	K3IV	20.88	$2^d.83782$	53.50
SZ Psc	K1IV	38.97	3.96534286	71.74
TY Pyx	G5V	11.48	3.198584	26.11

* of the spotted component

than expected from their spectral types. This may be a possible explanation for the large equatorial rotation velocities of the active, cool companion; it is worth mentioning here that spectroscopic observations of RS CVn-type systems have shown that the CaII lines are emitted from the active component in most systems and only rarely from both components.

Another observational fact of the present project is the non-existence of apparent infrared excess from fourteen RS CVn systems randomly selected for observation. This fact was the opposite of what was expected, as some of the observed systems are known to show period changes, e.g. SZ Psc, AR Lac, AD Cap (section 2.3.3), and for AR Lac there is photometric evidence for the existence of circumstellar matter (Catalano 1973). If the period changes are real, and not spurious as a consequence of the wave-like light variations, then mass exchange between the two components or mass loss from the system would be expected. Then interstellar or circumstellar matter would exist in the systems that show period variations, and if the density and temperature of the matter were high enough the systems would show infrared excess. But the current observations do not show detectable infrared excess. Let us discuss the case of SZ Psc as the system with the most pronounced period variation. For SZ Psc it has been found (Jakate et al. 1976) that the period decreases at a rate of $\dot{P} = 6 \times 10^{-8}$ days/day; this suggests (using the expression relating period variation to mass loss, given by Plavec 1968) a mass loss rate of 1×10^{-6} $M_{\odot}$ per year. If this mass loss rate is correct, then infrared excess would be expected; the current observations do not however show that. Thus, there is a conflict between the expected

and observed properties. An explanation is that the reported period changes are not real, but are spurious consequences of the observed wave-like light variations outside eclipse and its migration (section 5.3). Another explanation is, as has been mentioned earlier, that the density and temperature of matter are not high enough to be detectable in the near infrared. The mass loss rate of 10^{-6} $M_{\odot}$ per year for SZ Psc, derived from a theoretical relation between period change and mass loss, may be wrong. Another approach to the problem is the following. Let us assume that mass transfer exists from one component to the other in the form of a stream which, because of the inclination of the orbital plane, is visible only for certain orbital phases. But the differential colour diagram (Figure 5.3.2) in combination with the diagram giving the light variations outside eclipse (Figure 5.3.4) shows that the system is redder when the wave has its minimum. This shows that the system is redder when the postulated spotty area of the active component is facing the Earth. No indications of the existence of any mass stream between the two components can be seen in the colour diagram of SZ Psc. If we assume that the postulated stream is probably not visible from the Earth, it is very implausible to make the same assumption for the other systems which show period changes (AR Lac, AD Cap). It seems more likely that the observed period changes are not real (as has been mentioned earlier). It has been mentioned earlier also that Catalano (1973) has reported photometric evidence of circumstellar matter in AR Lac. Catalano came to this conclusion from the light curve of AR Lac; but it is more probable that the distortion of its light curve can be attributed to the existence of the wave-like light variations, a common characteristic of RS CVn binaries, rather than to the presence of circumstellar matter in the system.

A brief review of several workers' suggestions about the evolutionary stage of RS CVn-type binary systems is given in section 2.6.2. The problem is still unsolved. The RS CVn systems do not fit into any currently held theories of either pre- or post-main-sequence evolution.

The pre-main-sequence scenario is supported by the spectral similarities of these systems to the T Tauri stars: CaII emission, Hα emission, MgII emission. Chromospheric activity is a common characteristic of the cooler components of the RS CVn systems. Wilson (1963) and Wilson and Skumanich (1964) have studied the relation between the chromospheric activity, and especially the H and K emission lines, and the age of a single star. T Tauri stars showed the greatest emission, and the strength of the emission weakened as older and older main sequence stars were observed. More work on this subject confirmed the above relation: the younger the system, the stronger the H and K emission line intensity (Wilson and Woolley 1970, Skumanich 1972). The intensity of the H and K emission in the RS CVn systems may imply an age somewhere between T Tauri stars and the Sun (Weiler 1976). This is in agreement with the average age of these systems determined by Mowtle (1973). He fixed the averaged kinematical age of the RS CVn class by studying both the mean heights above and below the galactic plane and their dispersion of velocity components perpendicular to the plane. The mean age derived was 1-3 x 10^8 years. This age makes any post-main-sequence evolution unlikely because the time that stars of one solar mass (like the components of the RS CVn systems) would spend on the main sequence would be of the order of 10^9-10^{10} years.

As has been mentioned earlier, there is a correlation between the age of a star and the strength of the H and K emission. Weiler (1976) uses this correlation to support his suggestion that RS CVn systems must have an age between T Tauri stars and our Sun. For this conclusion, as he mentions in his thesis, he does not use the binary nature of the RS CVn systems. Another fact that has not been taken into account is the influence of rotation on the degree of chromospheric activity (it has been shown earlier in this chapter that the more active components of the RS CVn systems are fast rotators).

The evolutionary status problem of the RS CVn systems can be approached in another way. It is known that at least two of the RS CVn systems are members of triple systems (HR 1099, WW Dra) with the third component a main-sequence star which is less massive than either of the other two components of the system. If the fission theory is accepted as the most plausible theory about the origin of these systems, the three components have a common history, and according to evolutionary theory the least massive component is the least evolved. Thus, if the least massive component is a main-sequence star, the other two components of the triple system, which constitute our binary systems, cannot be pre-main-sequence stars.

One of the most important common properties of the RS CVn-type binary systems is that both components have approximately the same mass (about one solar mass) with the secondary component a little more massive than the other; a consequence of this is the fact that the secondary appears to be more evolved. The secondary also is the more active component with strong chromospheric activity, and not the other component, which is the younger. Thus chromospheric activity

does not seem to be related to the age of the two components. It seems that other parameters influence chromospheric activity, such as the speed of rotation of the cooler component and its possible strong magnetic field. Another reason for the secondaries' strong chromospheric activity may be their position in the H-R diagram. It seems very likely that the secondary is just leaving the main sequence and thus at a stage of instability. Because of this instability, where both nuclear and dynamical energies exist in the star, the star shows a strong chromospheric activity which settles down when the star becomes a helium-burning star. For the above mentioned reasons it seems that the most plausible evolutionary status of the RS CVn systems is main-sequence to post-main-sequence with the less massive component a main-sequence star and the active, more massive star just leaving the main-sequence.

The time that a system spends in an unstable evolutionary stage must be very short. As is known also, the mass ratio of the components of the RS CVn systems is very close to one. From the theory of evolution of close binary systems (section 2.6) this situation must last only a very short time. The above considerations, however, are in conflict with the estimated space density, which is given by Hall (1976) as of the order of 1×10^{-6} systems/pc^3, without taking into account the non-eclipsing systems. This density is remarkably high if we recall that the space density of the W UMa binaries, believed to be the commonest type of binary, is also 1×10^{-6} systems/pc^3, including the non-eclipsing systems. At this stage we have to discuss the significance of selection effects.

In the case where both the components have approximately the same mass and the same luminosity the possibility of detecting the

binary system is much higher than in any other cases. Therefore it is possible that the observed high density of RS CVn systems is the result of selection effects.

CHAPTER VII

MISCELLANEOUS INFRARED OBSERVATIONS

7.1 Infrared Observations of Wolf-Rayet Stars

In this section a joint project with Dr. P.M. Williams, undertaken in order to study the infrared properties of the WR systems, will be discussed.

Wolf-Rayet stars have very broad emission lines of HeI and HeII, C, N , and O at different stages of ionisation in their spectra. The emission lines are so broad that they overlap considerably the underlying continuum of the star. These characteristic lines attracted the curiosity of the two French astronomers Wolf and Rayet (1867) when they were making a survey of the spectra of stars in Cygnus. The study of these objects today is very important, from the point of view of the physics of stellar atmospheres and of the theory of the evolution of binary systems.

Beals (1938) has classified the Wolf-Rayet (WR) stars into two sequences: the carbon sequence (WC) with predominant carbon and oxygen lines, and the nitrogen sequence (WN) with the nitrogen lines dominating their spectra. Both sequences show strong lines of HeII. It is known today that the spectra are not the only systematic difference between the WN and WC sequences. Allen et al. (1972) found that the WC stars are systematically redder at 2.2 μm than the WN sequence. Smith (1973) also noted another systematic difference between WN and WC for WR stars belonging to binary systems; she pointed out that according to observational data the separation between the two stars of a binary system in which one of the components is WC, is always

greater than 65 $R_\odot$, while the opposite is the case for binaries with a WN component.

Most workers in the field of WR stars believe today that our Galaxy contains three types of object exhibiting WR spectra. Two of these belong to population I. One of the latter comprises those WR that belong to binary systems; their masses are approximately 10 $M_\odot$ and the other component of the system is an O or B type star with mass $\sim$ 30 $M_\odot$ and temperature comparable to that of the WR star. It has been suggested by Paczynski (1967) that the WR binaries are the results of systems which have undergone mass exchange of type known as "case B" (section 2.6.1). The other type of WR star belonging to population I consists of single young and very massive objects with masses of the order of 40 $M_\odot$, which occur in ring nebulae; these WR stars appear to be always WN type and also appear to be always single (van den Heuvel, 1978). WR stars of the third type belong to the disk population and are the central stars of planetary nebulae, with masses close to 1 $M_\odot$. Only WC stars (Cohen et al. 1975) have been found to be nuclei of planetary nebulae. Paczynski (1973) suggested that the nuclei of planetary nebulae may also be population I, e.g. BD +30° 3639; Underhill (1973) also pointed out that MI-67 has a WN8 nucleus. There are also indications of the duplicity of these WR stars with very faint companions of the late stage of evolution of WR binary systems. This stage according to van den Heuvel (1976) occurs when the secondary of the binary system is a helium burning star with extended atmosphere (WR star) and the primary is a compact object.

The presence of absorption lines, displaced shortwards in the spectra of WR stars, and also the extreme broadness of the emission

lines, show that these stars have expanding atmospheres. The expansion velocities can be estimated from the displacement of the absorption lines and also from the width of the emission lines. It is known today that these velocities may be a few hundred km s^{-1} to 2500 km s^{-1}, comparable with the ejection velocities of novae. These high expansion velocities observed in the atmospheres of the WR stars, and the evidence of mass loss from them, lead us to the conclusion that these stars are unstable.

It is well established that the WR stars are losing mass with a typical mass loss rate of 10^{-5} $M_{\odot}$ per year. A highly ionised and expanding circumstellar shell surrounds them. The presence of a highly ionised gas envelope around the WR stars is indicated by the strong emission lines of ionised and excited atoms in both WC and WN spectra. Underhill (1968) noted that free-free emission might be expected from these stars because of the presence of a hot ionised gas envelope around them. The first infrared observations of WR stars at wavelengths longward of 1 μm were made by Woolf (1969), who included some WR stars in a broad band photometry project at 11.5 μm. Allen et al. (1972), knowing that the WR stars are losing mass and that Geisel (1970) had found infrared excess in stars undergoing mass loss, undertook to observe 40 northern WR stars expecting infrared excess from them. In fact they found the infrared excess they expected and also they discovered a significant, systematic difference of the H-K colours between WN and WC. Their observations show that the WC stars are systematically redder than the WN ones, as has been mentioned earlier. This has been confirmed by other infrared observational astronomers, e.g. Cohen et al. (1975). No systematic difference has however been found by Hackwell et al. (1974) in the H-L colours of the

two subclasses. This has been explained by assuming that the WC stars have extra emission lines in the K window, so extra line emission radiation is expected in K but not in L. The above explanation has been confirmed by Williams et al. (1980) using near infrared spectrometry.

Excess infrared radiation has been variously ascribed to free-free emission from hot gas surrounding the star but emission from circumstellar dust has been found in many late-type members of the WC sequence (Allen et al. 1972; Hackwell et al. 1974; Gehrz and Hackwell 1974; Cohen et al. 1975; Hackwell et al. 1976; Hartmann 1978).

The most interesting result of the present infrared observation of WR systems was the discovery of an increase of brightness of HD 193793, a WC7 +05 system, by $2^{m}.4$ in L' (λ_o = 3.8 μm) between June 1976 and August 1977. This has been attributed to the condensation of grains in the star's circumstellar shell sometime between June 1976 and August 1977. In order to study the evolution of the shell, the star has been reobserved in May and August 1978. The shell has been found to be fainter since its discovery.

The infrared observations of HD 193793 and the results of this investigation are summarised in two papers which are given in the Appendix (papers 1 and 2).

7.2 Other Infrared Observations

During the early observing runs, concerned firstly with the RS Canis Venaticorum-type binary systems and secondly with Wolf-Rayet

stars, infrared observations of various objects were made, which have not been used in this thesis because they are too limited to yield scientific conclusions at present. The data are given in the following list with the exact date because these observations may be useful to other workers. The errors do not exceed $0^{m}.05$.

List of infrared observations of various objects during 1977-1979

JD 2440000 +	Star	J	H	K
3387.50	GP Cep			7.18
3388.40	BF Cyg		6.68	
3389.48	GP Cep			7.43
3390.57	GP Cep		7.69	7.30
3390.65	HD 18552		6.14	6.09
3391.45	DV Aqr	5.67	5.57	5.58
3395.49	GP Cep		7.68	7.41
3395.67	HD 18552	6.15	6.13	6.06
3396.41	BF Cyg	7.40	6.66	6.26
3396.44	DV Aqr	5.46	5.37	5.36
3396.58	GP Cep	7.83	7.64	7.42
3396.75	V471 Tau		3.40	3.25
3397.42	DV Aqr		5.33	5.32
3397.71	HD 18552	6.13	6.11	6.04
3398.44	DV Aqr	5.72	5.58	5.56
3398.47	GP Cep		7.66	7.44
3401.50	GP Cep	7.76	7.62	7.41
3402.46	GP Cep		7.83	7.52
3793.28	DV Aqr	5.56	5.44	5.40
3794.26	DV Aqr	5.49	5.42	5.38
3795.28	DV Aqr	5.45	5.39	
4144.26	HD 156385	6.28	6.11	5.57
4144.27	HD 156385	6.28	6.11	5.60
4145.24	DV Aqr	5.66	5.56	5.49

JD 2440000 +	Star	J	H	K
4202.55	HD 62910	8.56	8.35	7.96
4202.60	HD 62910	8.56	8.32	7.93
4203.56	HD 62910	8.55	8.35	7.98
4204.58	HD 76536	7.44	7.15	6.60
4218.55	HD 76536	7.43	7.16	6.59
4218.56	HD 76536	7.44	7.15	6.59
4226.49	HD 63099	8.54	8.19	7.69
4226.51	HD 63099	8.51	8.21	7.65
4226.55	HD 62910	8.59	8.35	7.98
4227.47	HD 63099	8.53	8.22	7.68
4228.60	HD 96548	6.59	6.48	6.15
4234.58	HD 96548	6.61	6.51	6.20
4234.61	HD 97152	7.95	7.87	7.37
4236.55	HD 88500	9.78	9.83	9.28
4236.59	HD 92740	5.77	5.65	5.46
4236.60	HD 93162	6.29	5.95	5.72
4237.55	HD 92740	5.74	5.65	5.45
4237.57	HD 92809	7.98	7.72	7.13
4237.59	HD 93131	6.15	6.07	5.90
4238.54	HD 93131	6.16	6.08	5.91
4238.55	HD 93162	6.32	5.99	5.73
4238.56	HD 92740	5.77	5.64	5.45
4238.57	HD 92809	7.97	7.72	7.13
4238.61	HD 97152	7.95	7.90	7.37

CONCLUDING REMARKS

1. No apparent excess in the near infrared has been detected from fourteen RS CVn-type binary systems.

2. Wave-like light variations outside eclipse, similar to those observed in the visual, have been detected in the near infrared from at least the three systems HR 1099, SZ Psc and TY Pyx (for the other RS CVn systems more observations are required before any definite decision can be made). The amplitude of the light variation for the three systems has been found to decrease with increasing wavelength. For HR 1099, which has been observed at more than one epoch, variation of the amplitude of the wave, and also migration of the wave towards increasing phase, has been detected; for this system, a combination of visual with the current infrared observations shows that the wave does not migrate towards one direction only but to both increasing or decreasing phase, and that the speed of the migration is not constant.

3. The wave-like light variations, in all the three systems where they were detectable, seem to decrease slowly while rising steeply.

4. Irregular light variations in the infrared have been observed in HR 1099, UV Psc, SZ Psc and TY Pyx; these irregular variations have also been observed in the visual and can be attributed to flare activity of the systems (or/and probably to coronal holes); flare activity of the above systems has also been detected in the radio and X-ray region of the electromagnetic spectrum.

The maximum brightness of the above systems varies in the visual and apparently also in the infrared.

5. The current infrared observations of RS CVn systems support the spot model. The cooler component of the systems, which is also the more massive and with strong chromospheric activity, is supposed to carry the spot complex. The hypothesis of the existence of dark spots explains the light variability outside eclipse and the observed relation between the amplitude of the variation and the wavelength (decrease of the amplitude with increasing wavelength). It also explains other observational properties of the systems such as flare activity and the existence of strong magnetic fields (observations of polarisation at radio wavelengths).

6. An estimate of the temperature and the effective area of the spot is given, assuming that both the star and the spot emit like black bodies.

Though the spot model is not well understood and the knowledge of the origin of the spots is very poor, it is very likely that this is the most plausible model for the RS CVn systems. It seems that these systems, and actually the more active components, have the characteristics of our Sun on a large scale. In order to study and to give a precise explanation for the light variations outside eclipse, their nature and their physical characteristics, long term, very accurate, and simultaneous observations in different regions of the electronomagnetic spectrum are desirable.

7. Assuming that the existence of dark spots on the active component (secondary) is the reason for the wave-like light variations outside eclipse and that the rotational period of the secondary and the orbital period of the system are synchronised, it follows that the secondary is a fast rotator.

8. Current infrared observations of UV Psc show irregular light variations and also variations of the depth of its primary minimum; wave-like light variations outside eclipse have not been confirmed. The shapes of the "shoulders" at least of the primary mimimum change on a remarkably short time scale ($\sim$ 10 days).

9. Infrared observations of AD Cap and HD 5303 do not show apparent infrared excess but they do show light variability. The light variations look similar to those observed from HR 1099. More observations are required before any definite decision can be made about the nature of the light variability. An estimate of the periods of the light variation of both the above systems are given.

10. The spectral types of the components of the seven extensively observed RS CVn systems have been estimated using the current photometric data.

11. Near infrared photometry of HD 193793 (WC7+05) showed that the brightness of the system increased by $2\overset{m}{.}4$ in L' (λ_o = 3.8 μm) between June 1976 and August 1977. This magnitude change was not detectable in the visual. The above increase of the system's brightness in the infrared has been attributed to the conden-

sation of grains in the star's circumstellar shell some time between June 1976 and August 1977.

APPENDIX

PUBLISHED PAPERS

1. "Condensation of a shell around HD 193793"
   P.M. Williams, D.H. Beattie, T.J. Lee, J.M. Stewart and E. Antonopoulou, 1978, MNRAS 185, 467.

2. "Cooling of the newly condensed shell around HD 193793"
   P.M. Williams and E. Antonopoulou, 1979, MNRAS 187, 183.

3. "Infrared photometry of the RS CVn binary HR 1099"
   E. Antonopoulou and P.M. Williams, 1980, Ap. Space Sci. 67, 469.

4. "Infrared photometry of HR 1099 during late 1979"
   E. Antonopoulou, 1980, IBVS No.1816.

Mon. Not. R. astr. Soc. (1978) 185, 467–472

Communications
from the
Royal Observatory
Edinburgh
No. 296

Condensation of a shell around HD 193793

P. M. Williams, D. H. Beattie, T. J. Lee and
J. M. Stewart *Royal Observatory, Blackford Hill, Edinburgh EH9 3HJ*
E. Antonopoulou *Astronomy Department, Edinburgh University, Blackford Hill, Edinburgh EH9 3HJ*

Received 1978 April 14; in original form 1978 February 10

Summary. Infrared photometry of the Wolf–Rayet binary HD 193793 shows that grains condensed in its circumstellar shell between 1976 June and 1977 August. The observations can be fitted by an optically thin shell of $4 \times 10^{-8} M_{\odot}$ of graphite grains at a temperature of about 900 K. A spectrum in the 2-μm atmospheric window reveals an emission feature near 2.04 μm. We have found the same feature in the W–R system γ^2 Vel and provisionally ascribe it to the 2.058-μm He I line.

1 Introduction

HD 193793 is a Wolf–Rayet binary system (WC6 + O6) in which the O-type component is the brighter by 1.2 mag in the visible (MacDonald 1949). It has been reclassified WC7p + O5 (Smith 1968) but this should not affect the estimated luminosity difference, which is similar to that of the well-known W–R system γ^2 Vel (1.4 mag, Conti & Smith 1972). Infrared observations show that HD 193793 has an infrared excess attributable to free–free radiation from a circumstellar shell (Hackwell, Gehrz & Smith 1974; Cohen, Barlow & Kuhi 1975). The infrared flux and 'excess' were observed to have decreased over 1970–75 by Hackwell *et al.* (1976), who interpreted this in terms of a secular decrease in the size of the circumstellar shell and the mass-loss rate. Shortly before the publication of that paper, we observed HD 193793 to be slightly fainter than its published brightness and we have lately observed it to have brightened considerably in the infrared (Williams *et al.* 1977).

2 Broad-band photometry

The observations were made using the SRC 1.5-m Flux Collector at the Cabezon Observatory of the Instituto Astrofisica de Canarias on Tenerife using photometers developed at the Royal Observatory, Edinburgh. The magnitudes, on the system in which Vega has zero magnitudes, are given in Table 1. The first three observations were made in 1976 May–June and the remainder in 1977 September. The data from the first and last nights are included

Table 1. Journal of infrared observations of HD 193793.

JD	*J*	*H*	*K*	[3.8]	[11.5]	Remarks
2442926		5.7:	5.5:	5.3:		poor night, cirrus
2442930			5.0:		2.9:	bolometer
2442939			5.24	4.89		
2443389		4.98	4.03	2.50		
2443394		4.96	4.01	2.51		also CVF spectrum
2443395	5.50	4.97	4.02	2.51		also CVF spectrum
2443401	5.52	5.01	4.07	2.57		doubtful night
2443402	5.7:	5.1:	4.3:	2.6:		bad night

for completeness only, being very uncertain owing to poor weather. The bolometer observations on the second night are also less accurate than the remaining data, which are believed to be accurate to better than 0.05 mag. The night to night agreement in 1977 September is certainly encouraging. The 1976 data are insufficient to tell us the conditions in the shell at that time, but indicate that HD 193793 was continuing the decline discussed by Hackwell *et al.* (1976). By 1977 September, the system was brighter and redder in the infrared than it had ever been observed to be.

The new flux distribution is shown in Fig. 1. The *BVRI* data were obtained by Fernie (1978) in 1977 October and show no significant differences from earlier photometry by Demers & Fernie (1964). The photometry was dereddened using the visual extinction given by Cohen *et al.* (1975) and a standard reddening curve. To estimate the flux distribution of the circumstellar shell, a 40 000 K blackbody was fitted to the *BVRI* dereddened data and a difference spectrum was formed. This relies on the assumption that the infrared flux distribution of the underlying stars can be extrapolated from that in the visible following a hot blackbody. Owing to their extended regions of formation, the infrared continua of Wolf–Rayet stars probably lie above the blackbody extrapolations, thus reducing the infrared 'excesses' attributable to circumstellar shells. In particular, Cassinelli & Hartman (1975) have calculated a model atmosphere for the W–R star HD 50896, finding the continuum to lie about 1.4 mag above the blackbody extrapolation in the *K*-band and by

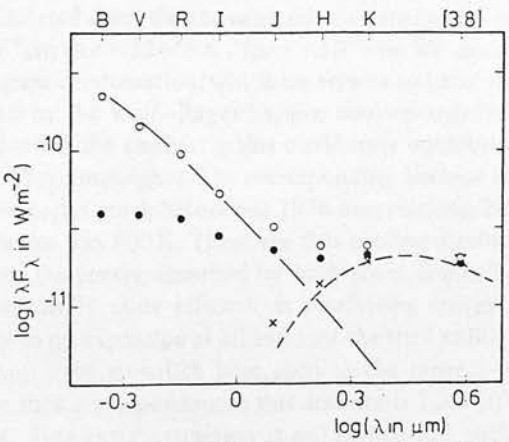

Figure 1. Flux distribution of HD 193793 in 1977 September as observed (filled circles) and corrected for reddening (open circles). The crosses represent the flux distribution attributed to the circumstellar shell, assuming the infrared stellar continuum follows the blackbody extrapolation (broken line) fitted to the *BVRI* points.

more at longer wavelengths, accounting for much of the infrared 'excess'. This effect is likely to be much less important in the case of HD 193793, whose continuum is dominated by that of the O-type star in the visible at least. We therefore regard our difference spectrum as a reasonable representation of the flux distribution of the circumstellar shell around HD 193793 in 1977 September. It can be approximated by a blackbody of about 1300 K, but a graphite grain model seems more realistic given the supposed carbon-richness of WC-type W–R atmospheres and the lack of 10-μm spectral features in other WC stars surrounded by circumstellar grains (e.g. Cohen *et al.* 1975).

3 A model for the shell

The fact that the visible flux was not reduced by the condensation of the shell implies either that the grains have condensed in a disk which we see at a low inclination angle, or, if the shell is spherical, that it must be optically thin in the visible and therefore in the infrared. If we adopt the second alternative, we can calculate the temperature of the grains from their emissivity. The opacities of graphite grains in the *J*, *H* and *K* bands were taken from Gilman (1974) whose data were interpolated amongst for the [3.8] band and extrapolated for the visual region. With these data, the observations are best fitted by grains at a temperature of 900 ± 50 K. The shell is powered by absorption of stellar radiation in the visual and ultraviolet, where both the grain opacity and the stellar radiation are greatest. By requiring a balance between the energies absorbed and reradiated by the grains, we can estimate the radius of the shell from the grain temperature and the stellar radiation. We assume this to be dominated by that from the O-type component, for which we have adopted an effective temperature of 40 000 K and a radius of $18 R_\odot$. The distance, r, in stellar radii, at which spherical grains of temperature T_g are in equilibrium with radiation from a star of effective temperature T can be found from:

$$4r^2 \bar{Q}(a, T_g)\, T_g^4 = \bar{Q}(a, T)\, T^4$$

where $\bar{Q}(a, T)$ are the Planck mean absorption cross-sections. These are the absorption cross-sections, $Q(a, \lambda)$ for grains of radius a averaged over a Planck function for temperature T. Following Clayton & Wickramasinghe (1976), we approximated these by:

$$\bar{Q}(a, T) = \min\,[1, 3.22\, a\, (T/10)^{1.65}].$$

The equilibrium distance calculated from the above equations depends on grain size, ranging from $r = 1344 R_*$ for $a = 10^{-4}$ cm to $r = 22\,608 R_*$ for $a = 10^{-7}$ cm. We can narrow this range by considering the onset of grain condensation, which we assume to have occurred when the expanding shell of matter lost by the Wolf–Rayet became cool enough for grains to form. This can only have occurred when the smallest grains could have equilibrium temperatures near 2000 K (*cf.* Clayton & Wickramasinghe). The corresponding distance is about $2370 R_*$. The condensation cannot have begun much before our 1976 observations. No more than 450 days later, the grain temperature was 900 K. There are two cooling mechanisms. First, the expansion of the shell reduces the energy absorbed by each grain. Secondly, growth of the grains leads to their being relatively more efficient at reradiating energy in the infrared. If we assume that there has been no expansion at all and that the shell radius is still $2370 R_*$, we can deduce that the grains have grown to have radii in the range $3–4 \times 10^{-5}$ cm. The column mass of grains in the shell corresponding to this distance is 7.3×10^{-7} g cm^{-2} and the visual extinction is 0.04 mag. This extra extinction is not compatible with Fernie's observation that the *UBV* magnitudes of HD 193793 have not been affected by the condensation of the shell. This adds to the dynamical arguments against a static shell and we assume that

it is still expanding. We do not know the velocity of this expansion. Spectroscopic observations show that HD 193793 has been losing mass with a velocity near 2500 km/s for many years (e.g. Underhill 1962; Hackwell *et al.* 1976). If we adopt this as an upper limit on the shell velocity, the shell radius cannot have increased by more than $7700R*$ between our 1976 and 1977 observations. The maximum shell radius is then some $10\,000R*$ and the corresponding grain size, column mass and visual extinction are then 1.7×10^{-6} cm, 3.9×10^{-8} g cm^{-2} and 0.002 mag respectively. This last is certainly compatible with the *UBV* photometry.

The radius of the shell is therefore believed to lie in the range $2370–10\,000R*$, or $42\,700–180\,000R_\odot$. This is large compared with the likely separation of the stars, even if this is as great as the $1000–2000R_\odot$ implied by Conti's (1973) estimate of a year or a few years for the orbital period of the system. If HD 193793 owes its Wolf–Rayet nature to mass-exchange in the system, it is probable that the separation is very much smaller. If the mass ratio is similar to that of other WC-type W–R binaries, the separation must be about four times the radius of the critical Roche lobe around the WC component. If that radius is comparable to that of the free–free shell around HD 193793 considered by Cohen *et al.*, the separation is only about $360R_\odot$ and the period near 40 day. Unless the period is many years, the grain shell surrounds the system completely.

For any radius in the above range, the mass of grains in the shell is about $4 \times 10^{-8}M_\odot$. To estimate the total mass of the shell, we need to know its composition and the fraction of the carbon that condensed. For the composition, we used the abundance ratio Ne/N(C III) = 400 found for γ^2 Vel by Castor & Nussbaumer (1972) and assume it to hold in the matter shed by HD 193793. Assuming also that half the carbon was in the form of C III and that the electrons were donated by hydrogen, and guessing that 1 per cent of the carbon has now condensed, we get a total shell mass of about $7 \times 10^{-5}M_\odot$. This is about 10 000 times the mass of the interstellar medium, assuming a density of 1 atom cm^{-3}, enclosed by the maximum size of shell. Even if these mass estimates are wrong by an order of magnitude, it appears unlikely that the shell expansion was significantly slowed down by its sweeping up interstellar matter.

If we adopt the disk model, we cannot be sure that the grains are optically thin and so cannot determine their temperature or distance from the stars. The orbital motion in HD 193793 may have resulted in a non-spherical distribution of circumstellar material if it passed through the Lagrangian points. On the other hand, the existence of grains implies that the shell must have been fairly dense until it was far enough from the stars for condensation to occur. It seems likely that most of the mass was shed in a single event more or less isotropically. Polarimetry may help us to distinguish between the disk and shell geometries. Knowledge of the size of the orbit will also be helpful in understanding the mass loss. Certainly, this system is worth continued monitoring at infrared and other wavelengths.

4 The CVF spectrum

We also scanned the spectrum of HD 193793 in the two-micron atmospheric window at 0.04-μm intervals using a 3 per cent continuously variable filter (CVF). To determine and monitor the atmospheric transmission, standard stars were observed several times each night at different air masses. The first of these spectra of HD 193793 is shown in Fig. 2. The standard used for conversion of the observations to fluxes was α Ari, whose flux distribution was calculated from a model atmosphere characterized by $T_e = 4480$ K, $g = 300$ cm s^{-2} (Williams 1971) taking account of the CO absorption. Apart from greater photometric errors on the individual points, our second spectrum of HD 193793 is essentially similar to

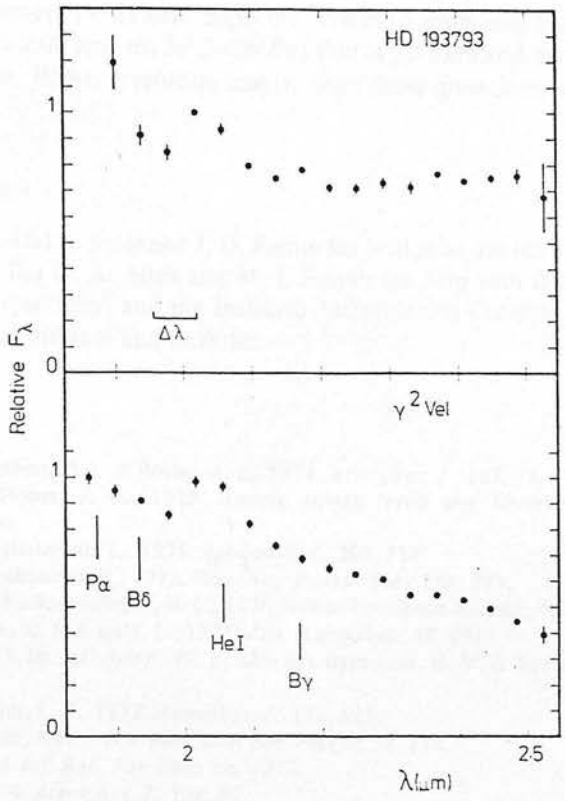

Figure 2. CVF spectra of HD 193793 and γ^2 Vel. The error bars represent ± 1 se and the resolution and expected positions of H and He I lines are marked. We were able to observe γ^2 Vel over a longer wavelength range owing to its greater brightness.

the one presented here with respect to the emission feature near 2.04 μm and the flattened continuum at longer wavelengths due to the grain emission. For comparison, the spectrum of the WC8 type Wolf–Rayet system γ^2 Vel is also given in Fig. 2. This was observed with the same equipment on the Anglo–Australian telescope (AAT) in 1977 April. This also shows the emission feature, but no continuum rise attributable to circumstellar grains. This is compatible with the interpretation of the broad-band photometry (e.g. Cohen *et al.* 1975). Of two other spectra obtained with the AAT at the same time, that of CV Serpentis (another WC8 type Wolf–Rayet) shows the same emission feature, while that of ζ Puppis (O4f) does not.

We did not resolve the emission feature with the filter wheel and know of no other published spectra of Wolf–Rayet stars in this region which might help with its identification. Barnes, Lambert & Potter (1974) have published high-resolution spectra of γ^2 Vel and ζ Pup in the 0.9–1.7 μm region and have identified H, He I–II and C II–IV lines in the W–R star. The positions of the strongest H and He I lines in the 2-μm window are marked on Fig. 2. There may be an emission feature in the spectrum of HD 193793 near Bγ which might be this or the He II (8–14) line, but the only certain feature is that near 2.04 μm. We ascribe this to the 2^1P–2^1S He I line at 2.058 μm. The triplet equivalent of this is the 1.083-μm line, which is conspicuous in emission in both HD 193793 (Kuhi 1968) and γ^2 Vel (Barnes *et al.* 1974). We did not observe the emission feature in ζ Pup nor did Barnes *et al.* find the 1.083-μm line. To search for possible lines of C II–IV, the energy levels for these ions given

by Bashkin & Stoner (1975) were inspected. The most promising lines are the $3p^2P-3d^2D$ of C IV at 2.07 and 2.08 μm, the $5s^1S-5p^1P$ of C III at 2.11 μm and the triplet equivalent of the latter at 2.32 μm. Higher-resolution spectra than those given here will be needed to identify these lines.

Acknowledgments

We are very grateful to Professor J. D. Fernie for letting us use his *UBVRI* data in advance of publication, to Drs D. A. Allen and M. J. Smyth for help with the AAT and Flux Collector observations respectively, and the Instituto Astrofisica de Canarias and the Anglo-Australian Observatory for assistance and facilities.

References

Barnes, T. G., Lambert, D. L. & Potter, A. E., 1974. *Astrophys. J.*, 187, 73.
Bashkin, S. & Stoner, J. O., 1975. *Atomic energy levels and Grotrian diagrams,* North-Holland, Amsterdam.
Cassinelli, J. P. & Hartmann, L., 1975. *Astrophys. J.*, 202, 718.
Castor, J. I. & Nussbaumer, H., 1972. *Mon. Not. R. astr. Soc.*, 155, 293.
Clayton, D. D. & Wickramasinghe, N. C., 1976. *Astrophys. Space Sci.*, 42, 463.
Cohen, M., Barlow, M. J. & Kuhi, L., 1975. *Astr. Astrophys.*, 40, 291.
Conti, P. S., 1973. In *IAU Symp. 49,* p. 225, eds Bappu, M. K. V. & Sahade, J., D. Reidel, Dordrecht, Holland.
Conti, P. S. & Smith, L. F., 1972. *Astrophys. J.*, 172, 623.
Demers, S. & Fernie, J. D., 1964. *Publ. astr. Soc. Pacific.* 76, 350.
Fernie, J. D., 1978. *Inf. Bull. Var. Stars No. 1377.*
Gilman, R. C., 1974. *Astrophys. J.*, 188, 87.
Hackwell, J. A., Gehrz, R. D. & Smith, J. R., 1974. *Astrophys. J.*, 192, 383.
Hackwell, J. A., Gehrz, R. D., Smith, J. R. & Strecker, D. W., 1976. *Astrophys. J.*, 210, 137.
Kuhi, L. V., 1968. In *Wolf–Rayet stars,* p. 103, eds Gebbie, K. G. & Thomas, R. N., N.B.S. Special Publication 307.
MacDonald, J. K., 1949. *Publ. Dom. Astr. Obs.*, 7, 311.
Smith, L. F., 1968. *Mon. Not. R. astr. Soc.*, 138, 109.
Underhill, A. B., 1962. *Astrophys. J.*, 136, 15.
Williams, P. M., 1971. *Mon. Not. R. astr. Soc.*, 153, 171.
Williams, P. M., Stewart, J. M., Beattie, D. H. & Lee, T. J., 1977. *IAU Circ. 3107.*

Mon. Not. R. astr. Soc. (1979) 187, 183–185

Cooling of the newly condensed shell around HD 193793

P. M. Williams *Royal Observatory, Blackford Hill, Edinburgh EH9 3HJ*
E. Antonopoulou *Astronomy Department, Edinburgh University, Blackford Hill, Edinburgh EH9 3HJ*

Received 1978 September 26; in original form 1978 July 14

Summary. New infrared observations of the Wolf–Rayet system HD 193793 in 1978 show that the new dust shell discovered in 1977 has cooled from 900 K to about 810 K in May and 780 K in 1978 August as a consequence of its expansion.

1 Introduction

Infrared photometry of Wolf–Rayet stars shows that many of the late-type members of the WC sequence are surrounded by circumstellar dust shells (e.g. Cohen, Barlow & Kuhi 1975) plausibly as a consequence of the stars' prodigious mass loss. The actual formation of a dust shell around one Wolf–Rayet, the WC7 + O5 system HD 193793, some time between 1976 June and 1977 September was detected by infrared photometry (Williams *et al.* 1978, Paper I). We have re-observed this system this year to study the evolution of the shell.

2 Observations

The observations were made in 1978 May and August using the 1.2-m telescope of the Greek National Observatory at Kryonerion and the SRC 1.5-m flux collector at the Cabezon Observatory of the Instituto Astrofisica de Canarias on Tenerife. We used the same cryostat and filters as for the 1977 observations except on JD 2443726, when we used a different cryostat with *JHK* and L' ($\lambda_0 = 3.8\,\mu$m) filters from the same set as those used for the other observations and an *M* filter. The magnitudes, again relative to Vega, are given in Table 1 and are expected to be accurate to within 0.05 mag. These show that the system is fading and we attribute this to reduced radiation from the circumstellar shell.

3 Discussion

As in Paper I, we seek to model our observations with an appropriate combination of an optically thin shell of graphite grains and a 40 000 K blackbody to represent the O-type star. The mass and temperature of the grains are adjusted to give the best fit to the infrared

Table 1. Infrared photometry.

JD	J	H	K	L'	M
2443641	5.57	5.24	4.62	3.04	
2443726	5.54	5.30	4.70	3.14	2.60
2443733	5.61	5.38	4.73	3.22	
2443737	5.57	5.32	4.75	3.25	

colours. This matching also requires knowledge of the system's interstellar reddening. In Paper I, we used the extinction ($A_v = 1.43$) given by Cohen *et al.* Very recently, Willis & Wilson (1978) have revised the reddening determinations of a number of Wolf–Rayet stars, including HD 193793, using ultraviolet observations from the *TD-1* satellite. The extinction of HD 193793 corresponding to their value of the reddening is $A_v = 2.38$ and we prefer this value owing to the greater sensitivity of the ultraviolet wavelength region to interstellar reddening. Re-analysis of the data in Paper I using this value of the extinction does not change the grain temperature derived, because this comes primarily from the HKL' photometry, but it does reduce the mass of the shell required from $4 \times 10^{-8} M_\odot$ to $2.4 \times 10^{-8} M_\odot$. Similar analysis of the observations given in Table 1, combined again with Fernie's (1978) visible photometry, yields a grain temperature of 810 K and mass of $2.3 \times 10^{-8} M_\odot$ for the May observation and 780 K and the same grain mass in August. Comparison of the observed colours for the two epochs of observation with simulated colours for different grain temperatures is made in Table 2, from which the uncertainties in the temperatures can be assessed. Most weight was placed on fitting the infrared colours and no allowance was made for emission lines from the Wolf–Rayet star.

The similarity of the shell masses derived from the 1977 and 1978 observations implies that the cooling of the grains was caused by the expansion of the shell rather than by the growth of the grains. This is in keeping with the discussion of grain growth in an expanding nova shell by Clayton & Wickramasinghe (1976). For a constant grain size and stellar radiative flux, the ratio of the shell radii in 1977 September (r_1), 1978 May (r_2) and August (r_3) can be determined from the ratio of the grain temperatures by considering the radiative equilibria on the grains. The temperature ratio is much less uncertain than the grain temperatures themselves as it is independent of the grain emissivity, and its relative error is estimated at 2 per cent from the photometry. For grains in the size range estimated in Paper I, the Planck mean absorption cross-sections are proportional to $T^{1.65}$ (Clayton & Wickramasinghe) so that we have

$$\left(\frac{r_2}{r_1}\right)^2 = \frac{\bar{Q}(T_1)\, T_1^4}{\bar{Q}(T_2)\, T_2^4} = \left(\frac{T_1}{T_2}\right)^{5.65}$$

yielding

$$r_2 = (1.35 \pm 0.1)\, r_1$$

Table 2. Comparison of observed and computed colours.

T_g	$(V-L')$	$(R-L')$	$(I-L')$	$(J-L')$	$(H-L')$	$(K-L')$	$(L'-M)$	Observed
820	3.82	3.33	2.88	2.57	2.31	1.57	0.53	
	3.83	*3.29*	*3.02*	*2.53*	*2.20*	*1.58*		*May*
800	3.71	3.22	2.77	2.47	2.24	1.57	0.55	
	3.67	*3.13*	*2.86*	*2.37*	*2.13*	*1.53*	*0.54*	*August*
780	3.59	3.10	2.65	2.35	2.16	1.56	0.56	

and, similarly,

$r_3 = (1.50 \pm 0.1)\, r_1$.

The simplest model of the motion of the shell is that it expands with a constant velocity equal to that of the mass loss (2500 km/s). In this case, the ratio of the times of our observations, measured since the detachment of the shell, should be approximately equal to that of the radii. Given the differences between these times, this implies that the shell was shed between 550 and 840 day before our 1977 observations. In Paper I we estimated that condensation occurred when the shell radius was about $2370\, R_*$, which would have been the case about 138 day after detachment or between 1975 May and 1976 July in this constant velocity model. This is just compatible with our 1976 June observation that the system was faint in the infrared, but we consider this to be fortuitous as the shell dynamics have probably been more complicated. More observations are needed to study these and to see whether shell formation is even a recurrent phenomenon.

Acknowledgments

We are very grateful for observing time at the Greek National Observatory, to Mr J. Zaharopoulos and Mr G. Dimou for assistance at that telescope and to Dr A. J. Longmore and Mr M. Tapia with assistance with the Tenerife observations.

References

Clayton, D. D. & Wickramasinghe, N. C., 1976. *Astrophys. Space Sci.*, 42, 463.
Cohen, M., Barlow, M. J. & Kuhi, L. V., 1975. *Astr. Astrophys.*, 40, 291.
Fernie, J. D., 1978. *Inf. Bull. Var. Stars No. 1377.*
Williams, P. M., Beattie, D. H., Lee, T. J., Stewart, J. M. & Antonopoulou, E., 1978. *Mon. Not. R. astr. Soc.*, 185, 467.
Willis, A. J. & Wilson, R., 1978. *Mon. Not. R. astr. Soc.*, 182, 559.

INFRARED PHOTOMETRY OF THE RS CVn BINARY HR 1099 (V711 TAU)

E. ANTONOPOULOU
Astronomy Dept., Edinburgh University, Blackford Hill, Edinburgh, Scotland

and

P. M. WILLIAMS
Royal Observatory, Blackford Hill, Edinburgh, Scotland

(Received 22 June, 1979)

Abstract. Infrared observations in *J*, *H* and *K* of the RS CVn-type binary HR 1099 (V711 Tau) show apparent light variations similar to those in the visible. The phase shift towards increasing phase is confirmed. There is no conspicuous infrared excess attributable to circumstellar emission. The amplitudes of the infrared variation are compatible with the spot model proposed for RS CVn and enable plausible limits on a characteristic spot temperature and effective spot area to the set.

1. Introduction

HR 1099 (=ADS 2644A, =V711 Tau) is a double-lined spectroscopic binary (Bopp and Fekel, 1976) and a member of the class of RS CVn systems (Landis and Hall, 1976). The observed light variations of the binary system in the visual (Bopp *et al.*, 1977; Landis *et al.*, 1978) have shown that HR 1099 does not eclipse. We included this system in our observing list because if we can reach an understanding of the reasons for light variations of a non-eclipsing RS CVn system such as HR 1099, it will be easier to understand the light variations outside eclipses of the eclipsing RS CVn systems.

Hall (1972) proposed a model for the out-of-eclipse light variations of RS CVn in which there is a region of tremendous spot activity darkening the surface of one of the stars, and our discussion of HR 1099 will begin with a similar model. Support for a spot model for HR 1099 comes from the strong and variable chromospheric activity presumably responsible for the radio flaring and emission spectrum.

2. Observations

The observations of the HR 1099 were made in the *J*, *H* and *K* photometric bands (and occasionally in *L*) during 1978, October 10–30, using the MK II infrared photometer similar to that described by Glass (1973) on the 0.75 m telescope at the SAAO station at Sutherland, South Africa. The photometric measures included both the components of the visual pair ADS 2644 AB and were relative to the same comparison star used for the visual observations (10 Tau). All the differential magnitudes are given in Table I

Astrophysics and Space Science 67 (1980) 469–476. 0004–640X/80/0672–0469$01.20

TABLE I

Differential magnitudes (HR 1099 -- 10 Tau)

JD	ϕ	ΔJ	ΔH	ΔK
2440000+				
3792.50	0.697	0.73	0.41	0.33
3792.52	0.704	0.72	0.48	0.35
3792.58	0.721	0.74	0.48	0.34
3792.60	0.728	0.73	0.46	0.35
3792.63	0.744	0.72	0.42	0.31
3793.49	0.044	0.70	0.40	0.33
3793.51	0.054	0.70	0.40	0.34
3793.56	0.070	0.74	0.49	0.35
3793.58	0.074	0.72	0.41	0.34
3793.63	0.094	0.71	0.41	0.34
3794.50	0.401	0.65	0.36	0.29
3794.54	0.414	0.65	0.46	0.29
3794.56	0.424	0.68	0.39	0.30
3794.60	0.440	0.67	0.38	0.30
3794.62	0.444	0.68	0.37	0.30
3795.44	0.733	0.71	0.37	0.29
3795.46	0.736	0.72	0.37	0.31
3795.49	0.750	0.71	0.43	0.37
3795.51	0.754	0.96	0.62	0.51
3796.44	0.084	0.73	0.42	0.33
3796.46	0.094	0.72	0.41	0.34
3801.43	0.844	0.75	0.42	0.33
3801.46	0.854	0.74	0.45	0.36
3801.47	0.859	0.73	0.45	0.36
3801.58	0.894	0.72	0.44	0.34
3801.60	0.904	0.72	0.44	0.35
3801.62	0.910	0.75	0.44	0.36
3802.48	0.213	0.66	0.37	0.30
3802.49	0.217	0.67	0.37	0.30
3802.52	0.224	0.63	0.35	0.26
3802.54	0.234	0.65	0.36	0.30
3802.57	0.244	0.64	0.36	0.30
3802.59	0.254	0.66	0.37	0.28
3802.61	0.259	0.64	0.34	0.27
3806.44	0.609	0.67	0.40	0.33
3806.45	0.614	0.67	0.39	0.33
3806.47	0.620	0.72	0.37	0.30
3806.50	0.630	0.67	0.37	0.28
3806.55	0.647	0.68	0.41	0.31
3806.57	0.655	0.70	0.40	0.30
3807.55	0.984	0.74	0.44	0.36
3807.57	0.004	0.73	0.46	0.36
3807.59	0.014	0.72	0.44	0.37
3807.60	0.024	0.73	0.45	0.35
3809.38	0.645	0.70	0.42	0.36
3809.42	0.659	0.68	0.41	0.33

Table I (Continued)

JD	ϕ	ΔJ	ΔH	ΔK
3809.54	0.694	0.69	0.41	0.31
3809.56	0.704	0.67	0.40	0.31
3809.58	0.714	0.69	0.42	0.32
3810.46	0.024	0.71	0.43	0.34
3810.50	0.039	0.72	0.44	0.34
3810.52	0.044	0.72	0.43	0.33
3810.57	0.064	0.71	0.41	0.33
3810.59	0.069	0.73	0.41	0.34
3810.61	0.074	0.72	0.41	0.33

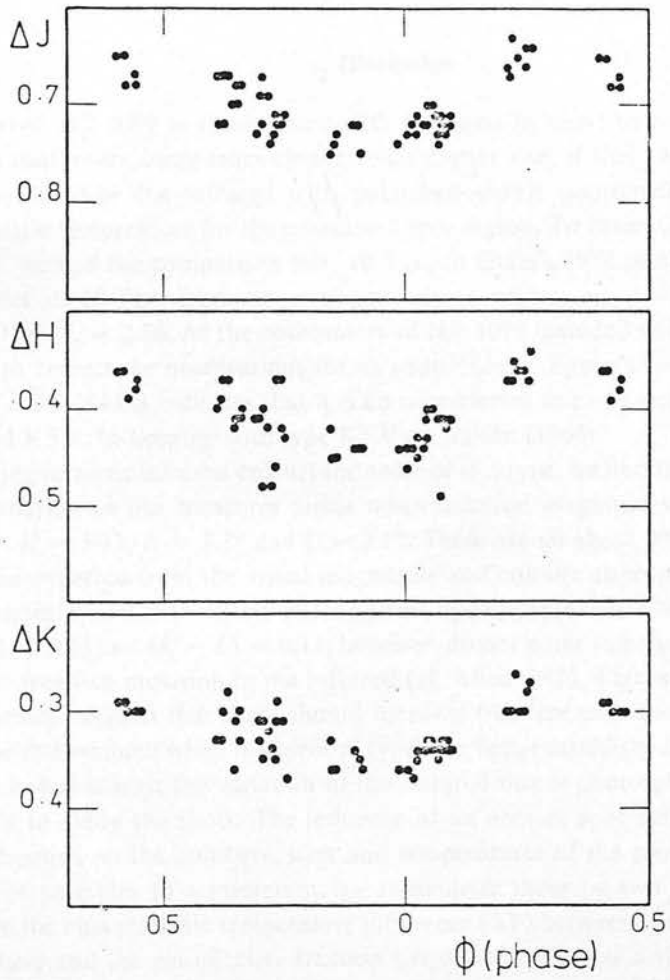

Fig. 1. The differential magnitude ΔJ, ΔH and ΔK of HR 1099 with respect to 10 Tau against orbital phase.

and Figure 1. The first column in Table I contains the Julian date and the second the phase, computed from the elements

$$T_0\,(\mathrm{JD}) = 2442766.069 + 2^{d}83782E,$$

where the period is the spectroscopically determined orbital period (Bopp and Fekel, 1976) and the zero phase corresponds to conjunction with the more active component, believed to carry the spot complex, in front. The spectroscopic and photometric periods differ slightly but the phase shift over the three weeks of our observations should be negligible. The last three columns contain the differential J, H and K magnitudes of HR 1099 with respect to 10 Tau.

3. Discussion

We observed HR 1099 in the infrared with two aims in view: to search for 'excess' radiation that might come from circumstellar matter and, if there was no significant excess, to combine the infrared with published visible photometry to estimate a characteristic temperature for the postulated spot region. To determine the colours of HR 1099, we tied the comparison star, 10 Tau, to Glass's 1974 standards. The mean magnitudes of 10 Tau, from observations on ten nights, are $J = 3.24$, $H = 2.97$, $K = 2.90$ and $L = 2.86$. As the photometry of HR 1099 included its faint companion, we have to correct the observations for its contribution. Eggen's (1968) UBV photometry of ADS 2644 B indicates that it is an unreddened star of spectral type between K2 V and K5 V, in keeping with type K3 V of Wilson (1964).

Adopting intrinsic infrared colours for a star of this type, we find that subtraction of its contribution to our measures yields mean infrared magnitudes for HR 1099 of $J = 3.99$, $H = 3.43$, $K = 3.28$ and $L = 3.17$. These are all about $0^{m}5$ to $0^{m}6$ brighter than those expected from the visual magnitude and colours appropriate to the composite spectral type (G5 IV + K0 IV) suggested by Popper (1978). The infrared colours $(H - K) = 0.15$ and $(K - L) = 0.11$, however, do not point to a significant contribution from free-free radiation in the infrared (cf. Allen, 1973, Figure 1). The emission line spectrum suggests that there should be some free-free emission and the colours should be re-examined when the spectral types are better established. For the present, we believe that at least the variation of the infrared flux is photospheric and that we can use it to study the spots. The influence of an area of spot activity on the light output depends on the numbers, sizes and temperatures of the spots. To reduce the number of variables to a minimum, we summarize these by two parameters only. These are the characteristic temperature difference (ΔT) between the spots and stellar photosphere and the net effective fraction (A) of the projected surface of both stars covered by the spot region. The amplitudes of light variation in different wavebands will put slightly different constraints on possible values of A and ΔT, and a comparison of light curves observed in different colours should help us to solve for A and ΔT. For

TABLE II

Band	Amplitude	ϕ_{min}	R.M.S. residual
J	$0^m086 \pm 0.008$	0.895 ± 0.011	0^m018
H	$0^m087 \pm 0.010$	0.885 ± 0.015	0^m023
K	$0^m064 \pm 0.008$	0.903 ± 0.015	0^m018

simplicity, we assume the spots and stars to radiate like blackbodies and the two stars to have the same effective temperature, 4500 K, corresponding to the colours.

To obtain unbiased measures of the amplitudes of variation in J, H and K, we fitted our data with truncated Fourier series. The amplitudes, phases of minima and residuals are given in Table II.

We calculated values of A and ΔT to give the derived amplitudes $\Delta J \pm 1$ s.d. and $\Delta K \pm 1$ s.d. We did not use the H amplitude because the negative hydrogen ion opacity minimum, which falls in the H band, makes our blackbody assumption less reliable in H than in J and K. The bands in the $(A, \Delta T)$ field satisfying the infrared observations are shown in Figure 2. The observations alone are unable to constrain A and ΔT very tightly and we had intended to make use of the visual amplitude $\Delta V = 0.12$ found by Bopp *et al.* (1977) and Landis *et al.* (1978). However, while the infrared observations

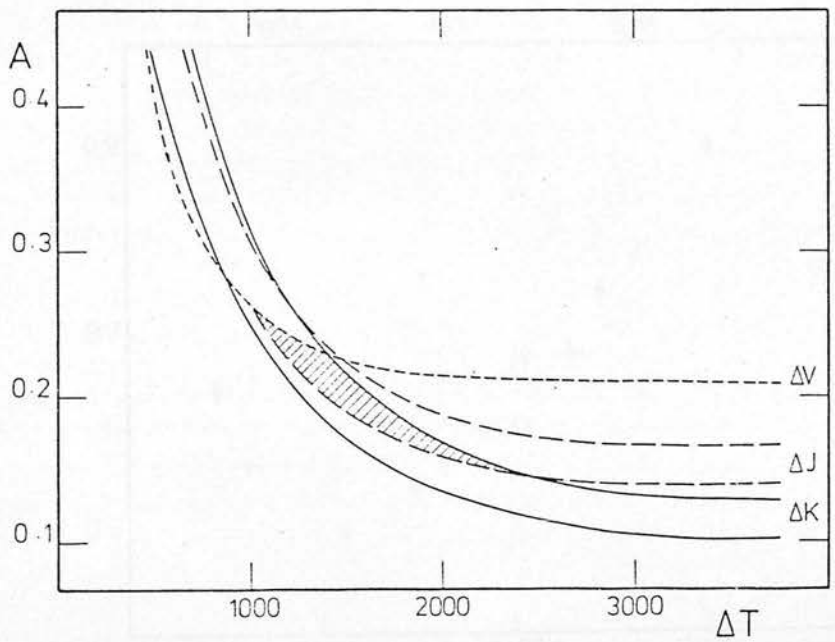

Fig. 2. Relation between the fraction of the projected area of both stars covered by the spots and the temperature difference ($\Delta T = T_* - T_{spot}$) which satisfies the amplitudes $\Delta J \pm 1$ s.d., $\Delta K \pm 1$ s.d. and $\Delta V = 0^m12$ (upper limit).

TABLE III

JD	ϕ_{min}	References
2440000+		
2748–2809	0.644 ± 0.010	Bopp *et al.* (1977)
2816–2837	0.569 ± 0.009	Bopp *et al.* (1977)
3046–3067	0.502 ± 0.017	Landis *et al.* (1978)
3176–3212	0.547 ± 0.009	Landis *et al.* (1978)
3409–3437	0.680 ± 0.016	Bartolini *et al.* (1978)
3484–3551	0.681 ± 0.016	Bartolini *et al.* (1978)
3560–3590	0.744 ± 0.014	Chambliss *et al.* (1978)

were being made in October 1978, Bartolini *et al.* (1978) and Chambliss *et al.* (1978) reported new observations indicating that the V amplitude was only about 0^m07 in late 1977 and early 1978. We do not know the visual amplitude in October 1978 and recognize that simultaneous optical and infrared observations will be needed to determine characteristic parameters for the star spots.

If the visual amplitude at the time of the infrared observations was no greater than 0^m12 (the typical value observed so far), we can constrain the permitted values of A

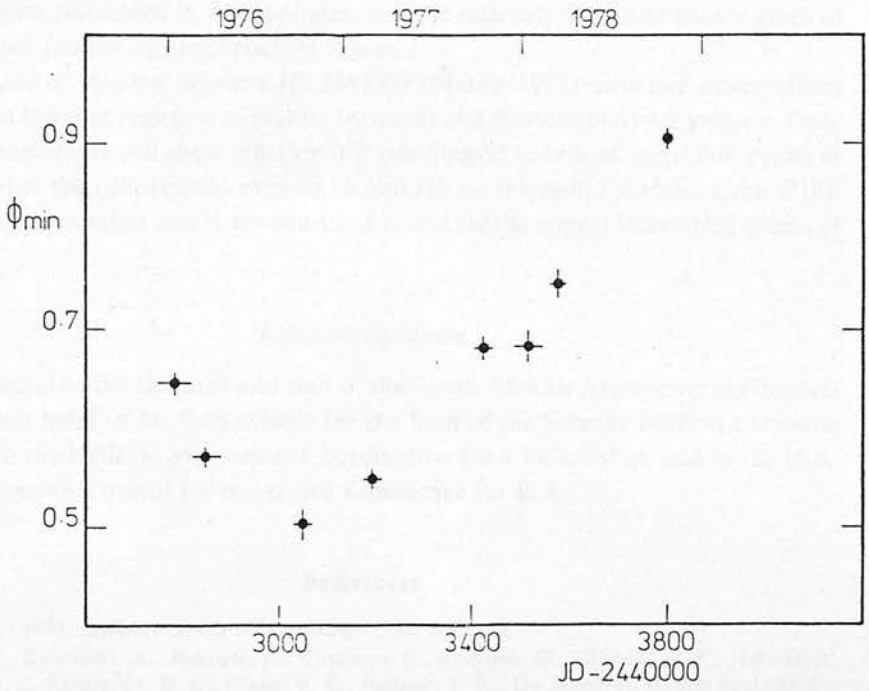

Fig. 3. The calculated phase of minima against epoch, the horizontal lines giving the interval covered by each set of observations.

and ΔT as shown in Figure 2. The smallest visual amplitude that would still be consistent with both the infrared data and our simple model is $\Delta V = 0^{m}08$.

The results are plausible; the spots are between 1000° and 2300° cooler than the photosphere and cover between 0.14 and 0.26 of the projected area of the stars, or between one-quarter and half the hemisphere of the active component assuming the two components to be of the same size. For a more realistic model, we need to know the effective temperatures of the two components and their relative brightnesses. In order to bracket the stellar temperatures, we repeated our calculations assuming an effective temperature of 5500 K and found similar constraints on A and ΔT except that the spots could be up to 800° cooler. In any event, this simple model shows that the visual and infrared variability of this star can be explained by a patch of star spots.

The phases of minima given in Table II do not differ significantly from one another and we adopt a mean phase of 0.895 from our observations. This phase differs from any reported previously. These have been determined from photometry in V but we do not expect the infrared and visible light variation to show minima at different times given the great similarity of the phases of minima at 1.2 and 2.2 μm. We believe this phase difference to reflect migration of the region of spot activity. The first intensive study by Landis *et al.* (1978) yielded a retrogade migration at a rate of 1 cycle in 13 years, but more recent studies (e.g., Chambliss *et al.*, 1978) suggest that the situation is more complicated. We have re-examined all the published B data and redetermined phases of minima using truncated Fourier series and splitting longer runs into two where the data warranted it. These phases, and the intervals they refer to, are given in Table III and plotted against epoch in Figure 3.

The phases of minima between JD 2443200 (March 1977) and our observations suggest that the spot region is migrating forwards at a rate of about 4.8 yr/cycle. Only further observations will show whether it is meaningful to talk of migration cycles at all or whether the spot regions migrate to and fro on the stellar surface. Even if this system were not a radio and X-ray source, it would still be a most interesting object of study.

Acknowledgements

We are grateful to the Director and staff of the South African Astronomical Observatory for their help, to Dr R. S. Stobie for the loan of his Fourier analysis computer program, to the Hellenic Ministry of Coordination for a Fellowship, and to the U.K. Science Research Council for travel and subsistence for E.A.

References

Allen, D. A.: 1973, *Monthly Notices Roy. Astron. Soc.* **161**, 145.

Bartolini, C., Guarnieri, A., Piccioni, A., Catalano, S., Rodono, M., Brooke, A. F., Hall, D. S., Landis, H. J., Sarma, M. B. K., Olson, E. C., Renner, T. R., De Bernardi, C. and Scaltriti, F.: 1978, *Astron. J.* **83**, 1510.

Bopp, B. W. and Fekel, F.: 1976, *Astron. J.* **81**, 771.
Bopp, B. W., Espenak, F., Hall, D. S., Landis, H. J., Lovell, L. P. and Rencroft, S.: 1977, *Astron. J.* **82**, 47.
Chambliss, C. R., Hall, D. S., Landis, H. J., Louth, H., Olson, E. C., Renner, T. R. and Skillman, D. R.: 1978, *Astron. J.* **83**, 1514.
Eggen, O. J.: 1968, *Roy. Obs. Bull.*, No. 137.
Glass, I. S.: 1973, *Monthly Notices Roy. Astron. Soc.* **164**, 155.
Glass, I. S.: 1974, *Monthly Notes Astron. Soc. South Africa* **33**, 53.
Hall, D. S.: 1972, *Publ. Astron. Soc. Pacific* **84**, 323.
Landis, H. J. and Hall, D. S.: 1976, *Inform. Bull. Var. Stars*, No. 1113.
Landis, H. J., Lovell, L. P., Hall, D. S., Henry, G. W. and Renner, T. R.: 1978, *Astron. J.* **83**, 176.
Popper, D. M.: 1978, *Astron. J.* **83**, 1522.
Wilson, O. C.: 1964, *Publ. Astron. Soc. Pacific* **76**, 238.

COMMISSION 27 OF THE I. A. U.
INFORMATION BULLETIN ON VARIABLE STARS
Number 1816

Konkoly Observatory
Budapest
1980 July 14

INFRARED PHOTOMETRY OF HR 1099 DURING LATE 1979

The RS CVn type double-lined spectroscopic binary system HR 1099 (≡ V711 Tau ≡ADS2644A) was observed in the near infrared (mainly J, K and L) at the South African Astronomical Observatory from 1979 November 17 - December 31. The observations were made with the 0.75 m telescope, using the MkII Infrared Photometer similar to that described by Glass (1973).

The photometric measures included both the components of the visual pair ADS 2644 AB and were relative to the same comparison star (10 Tau) used for the visual and our previous infrared observations (Antonopoulou and Williams 1980, Paper I). The effects of atmospheric extinction were allowed for using mean coefficients, but were not significant because of the angular proximity of the comparison star to the variable. A total of 137 observations was obtained in each colour in 24 nights.

The phase of each observation was computed according to the elements:

$$T_o(JD) = 2442766^d.069 + 2^d.83782 \cdot E,$$

where the period is the spectroscopically determined orbital period (Bopp and Fekel 1976) and zero phase corresponds in conjunction with the more active component, believed to carry the spot complex, in front.

The differential observations, taken as variable minus comparison, are plotted against phase and are shown in the Figure.

It is clearly seen that the phase of the minimum is at phase 0.95 in agreement with the phase of the minimum given by the visual data taken at around the same time (Guinan et al. 1979). This means that the phase of the minimum has shifted by 0.055 forwards, comparing these observations with the ones we took one year earlier (Paper I).

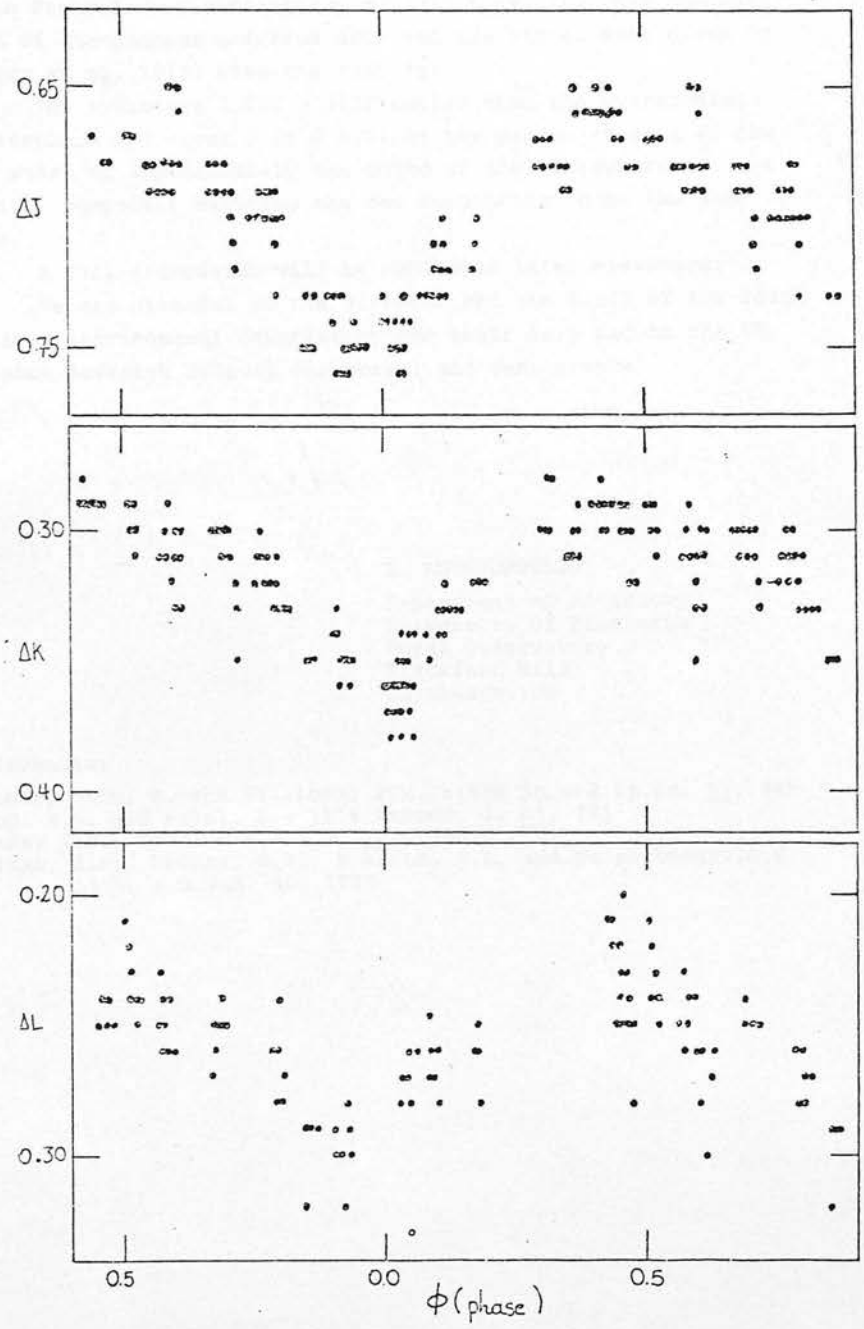
0.65
ΔJ
0.75
0.30
ΔK
0.40
0.20
ΔL
0.30
0.5
0.0
0.5
φ (phase)

The amplitudes of the light variation in J, K and L are about 0.09 mag, 0.07 mag and 0.06 mag, respectively.

Assuming the simplified spot model for HR 1099 as described in Paper I, our preliminary calculations, from the combination of the present infrared data and the visual data given by Guinan et al. 1979, give the results:

The spots are 1250K ± 100K cooler than the surrounding photosphere and cover 0.16 ± 0.02 of the projected area of the two stars or approximately one third of the hemisphere of the active component assuming the two components to be the same size.

A full discussion will be published later elsewhere.

We are grateful to the Director and the Staff of the South African Astronomical Observatory for their help and to the UK Science Research Council for travel and subsistence.

E. ANTONOPOULOU

Department of Astronomy
University of Edinburgh
Royal Observatory
Blackford Hill
Edinburgh, UK

References:

Antonopoulou, E. and Williams, P.M.,:1980 Ap.and Sp.Sc. 67, 469
Bopp, B.W. and Fekel, F.: 1976 Astron. J. 81, 771
Glass, I.S.: 1973, M.N.R.A.S. 164, 155
Guinan, E.F., McCook, G.P., Fragola, J.L. and Weisenberger,A.G.: 1979, I.B.V.S. No. 1723

REFERENCES

Abrami, A. and Cester, B., 1963, Osserv. Astr. di Trieste No. 320

Agrawal, P.C., Riegler, G.R. and Garmire, G.P., 1980, MNRAS 192, 725

Aitken, D.K., 1978, Observatory 98, 99

Aitken, D.K. and Jones, B., 1973, Ap. J. 184, 127

Allen, C.W., 1973, "Astrophysical Quantities", University of London, The Athlone Press

Allen, D.A., 1972, Ap. J. 172, L55

Allen, D.A., 1973, MNRAS 161, 145

Allen, D.A., 1975, "Infrared, the New Astronomy"

Allen, D.A., Harvey, P.M. and Swings, J.P., 1972, Astron. Ap. 20, 333

Aller, H.D., Rugare, T.J. and Hodge, P.E., 1978, Astron. J. 83, 1485

Al-Naimiy, H.M., 1978, IBVS No. 1481

Andersen, J. and Popper, D.M., 1975, Astron. Ap. 39, 131

Antonopoulou, E. and Williams, P.M., 1980, Ap. Space Sci. 67, 469

Arnold, C.N. and Hall, D.S., 1973, IBVS No. 843

Atkins, H.L. and Hall, D.S., 1972, PASP 84, 638

Babaer, B., 1971, Astr. Circ. (U.S.S.R.) No. 628, 5

Bakos, G.A. and Heard, J.F., 1958, Astron. J. 63, 302

Barning, F.J.M., 1963, BAN 17, 22

Bartolini, C., Guarnieri, A., Piccioni, A., Catalano, S., Rodono, M., Brooke, A.F., Hall, D.S., Landis, H.J., Sarma, M.B.K., Olson, E.C., Renner, T.R., De Bernardi, C. and Scaltriti, F., 1978, Astron. J. 83, 1510

Barton, J.R., and Allen, D.A., 1980, PASP 92, 368

Batten, A.H., 1970, PASP 82, 574

Beals, C.S., 1938, Trans, IAU No. 6, 248

Becklin, E.E. and Neugebauer, G., 1967, Ap. J. 147, 799

Becklin, E.E. and Neugebauer, G., 1968, Ap. J. 151, 145

Bessell, M.S., 1979, PASP 91, 589

Bidelman, W.P. and MacConnell, D.J., 1973, Astron. J. 78, 687

Biermann, P. and Hall, D.S., 1976, IAU Symp. No. 73, p. 381

Bond, H.E., 1970, PASP 82, 321

Bond, H.E., 1976, IAU Circ. 2987

Bopp, B.W., 1973, BAAS 5, 399

Bopp, B.W., 1976, IBVS No. 1175

Bopp, B.W. and Evans, D.S., 1973, MNRAS 164, 343

Bopp, B.W. and Fekel, F. Jr., 1976, Astron. J. 81, 771

Bopp, B.W. and Talcott, J.C., 1978, Astron. J. 83, 1517

Bopp, B.W. and Talcott, J.C., 1980, Astron. J. 85, 55

Bopp, B.W., Espenak, F., Hall, D.S., Landis, H.J., Lovell, L.P. and Reucroft, S., 1977, Astron. J. 82, 47

Brown, R.L. and Crane, P.C., 1978, Astron. J. 83, 1504

Burbidge, G.R. and Stein, W.A., 1970, Ap. J. 160, 573

Carr, R.B., 1967, Ph.D. thesis, University of Florida

Cash, W., Bowyer, S., Charles, P.A., Lampton, M., Garmire, G. and Riegler, G., 1978, Ap. J., 223, L21

Castle, K.G., 1977, PASP 89, 862

Catalano, S., 1973, IAU Symp. No. 51, p. 61

Catalano, S. and Rodonò, M., 1967, Mem. Astron. Soc. Ital. 38, 395

Catalano, S. and Rodonò. M., 1969, in "Non-Periodic Phenomena in Variable Stars" ed. L. Detre, p. 435

Catalano, S. and Rodonò, M., 1974, PASP 86, 390

Chambliss, C.R. and Detterline, P.J., 1979, IBVS No. 1591

Chambliss, C.R., Hall, D.S., Landis, H.J., Louth, H., Olson, E.C., Renner, T.R. and Skillman, D.R., 1978, Astron. J. 83, 1514

Chisari, D. and Lacona, G., 1965, Mem. Astron. Soc. Ital. 36, 463

Chugainov, P.F., 1966, IBVS No. 122

Cohen, M., 1973a, MNRAS 161, 85

Cohen, M., 1973b, MNRAS 161, 97

Cohen, M., 1973c, MNRAS 161, 105

Cohen, M., 1974, MNRAS 169, 257

Cohen, M., 1976, Ap. J. 203, 169

Cohen, M. and Barlow, M.J., 1974, Ap. J. 193, 401

Cohen, M. and Kuhi, L.V., 1979, Ap. J. Sup. Series 41, 743

Cohen, M., Barlow, M.J. and Kuhi, L.V., 1975, Astron. Ap. 40, 291

Contopoulos, G. and Banos, C., 1976, Sky and Telescope 51, 154

Cousins, A.W.J., 1963, MNASSA 22, 58

Dupree, A.K., Hartmann, L. and Raymond, J.C., 1980, IAU Symp. No. 88, 39

Dyck, H.M. and Milkey, R.W., 1972, PASP 84, 597

Eaton, J.A., 1977, IBVS No. 1297

Eaton, J.A. and Hall, D.S., 1979, Ap. J. 227, 907

Eggen, O.J., 1968, ROB 137

Ennis, D., Becklin, E.E., Beckwith, S., Elias, J. Gatley, I. Matthews, K., Neugebauer, G. and Willner, S.P., 1977, Ap. J. 214, 478

Epstein, E.E. and Briggs, F.H., 1978, Astron. J. 83, 1487

Evans, D.S., 1971, MNRAS 154, 329

Evans, C.R. and Hall, D.S., 1974, IBVS No. 945

Fahrbach, U., Haussecker, K. and Lemke, D., 1974, Astron. Ap. 33, 265

Feldman, P.A. and Smith. P.M., 1980, IAU Circ. No. 3487

Feldman, P.A., Gregory, P.C., Taylor, A.R. and Seaquist. E.R., 1978a, IAU Circ. No. 3176

Feldman, P.A., Taylor, A.R., Gregory, P.C., Seaquist, E.R., Balonek, T.J. and Cohen, N.L., 1978b, Astron. J. 83, 1471

Feldman, P.A., MacLeod, J.M. and Andrew, B.H., 1979, IAU Circ. No. 3385

Fellgett, P.B., 1951, MNRAS 111, 537

Fernie, J.D., 1979, IBVS No. 1609

Field, J.V., 1969, MNRAS 144, 419

Flannery, B.P. and Ulrich, R.K., 1977, Ap. J. 212, 533

Fraquelli, D.A., 1978, Astron. J. 83, 1535

Gallagher, J.S., 1977, Astron. J. 82, 209

Gallagher, J.S. and Ney, E.P., 1976, Ap. J. 204, L35

Gehrz, R.D., 1971, Ph.D. thesis, University of Minnesota

Gehrz, R.D., 1972, Ap. J. 178, 715

Gehrz, R.D. and Hackwell, J.A., 1974, Ap. J. 194, 619

Gehrz, R.D. and Woolf, N.J., 1971, Ap. J. 165, 285

Gehrz, R.D., Hackwell, J.A. and Jones, T.W., 1974, Ap. J. 191, 675

Geisel, S.L., 1970, Ap. J. 161, L105

Geisel, S.L., Kleinmann, D.E. and Low, F.J., 1970, Ap. J. 161, L101

Gibson, D.M. and Hjellming, R.M., 1974, PASP 86, 652

Gibson, D.M., Hicks, P.D. and Owen, F.N., 1978, Astron. J. 83, 1495

Gillett, F.C. and Forrest, W.J., 1973, Ap. J. 179, 483

Gillett, F.C., Low, F.J. and Stein, W.A., 1968, Ap. J. 154, 677

Gillett, F.C., Merrill, K.M. and Stein, W.A., 1971, Ap. J. 164, 83

Gillett, F.C., Merrill, K.M. and Stein, W.A., 1972, Ap. J. 172, 367

Gillett, F.C., Forrest, W.J., Merrill, K.M., Capps, R.W., and Soifer, B.T., 1975, Ap. J. 200, 609

Gillett, F.C., Dereniak, E.L. and Joyce, R.R., 1977, Opt. Eng. 16, 544

Gilman, R.C., 1969, Ap. J. 155, L185

Gilman, R.C., 1974, Ap. J. 188, 87

Glass, I.S., 1972a, Observatory 92, 140

Glass, I.S., 1972b, Nature Phy. Sci. 237, 7

Glass, I.S., 1973, MNRAS 164, 155

Glass, I.S., 1974, MNASSA 33, 53

Glass, I.S., 1978, "Operating Notes for MkII Infrared Photometer", SAAO

Golay, M.J.E., 1947, Rev. Sci. Instruments 18, 357

Grasdalen, G.L., Strom, K.M. and Strom, S.E., 1973, Ap. J. 184, L53

Gratton, L., 1950, Ap. J. 111, 31

Gray, D.F. and Desikachary, K., 1973, Ap. J. 181, 523

Guinan, E.F., McCook, G.P., Fragola, J.L. and Weisenberger, A.G., 1979, IBVS No. 1723

Hackwell, J.A., 1971, Observatory, 91, 33

Hackwell, J.A., Gehrz, R.D. and Woolf, N.J., 1970, Nature 227, 822

Hackwell, J.A., Gehrz, R.D. and Smith, J.R., 1974, Ap. J. 192, 383

Hackwell, J.A., Gehrz, R.D., Smith, J.R. and Strecker, D.W., 1976, Ap. J. 210, 137

Hall, D.N.B., Aikens, R.S., Joyce, R. and McCurnin, T.W., 1975, Appl. Opt. 14, 450

Hall, D.S. 1972, PASP 84, 323

Hall, D.S., 1975, Acta Astron. 25, 225

Hall, D.S., 1976, IAU Colloq. No. 29, Part I, p. 287

Hall, D.S. and Haslag, K.P., 1976, IAU Colloq. No. 29, Part II, p. 331

Hall, D.S. and Neff, S.G., 1979, Acta Astron. 29, 93

Hall, D.S., Kreiner, J.M. and Shore, S.N., 1980, IAU Symp. No. 88, p. 383

Hardie, R.H., 1962, "Stars and Stellar Systems" 2, 178

Hartmann, L., 1978, Ap. J. 221, 193

Heard, J.F. and Bakos, G.A., 1968, J.R. Astron. Soc. Can. 62, 67

Hearnshaw, J.B., 1979, IAU Coll. No. 46, p. 371

Hearnshaw, J.B. and Oliver, J.P., 1977, IBVS No. 1342

Herschel, Sir W., 1800, Phil. Trans. Roy. Soc. London, Pt. II 90, 255

Hill, G., Hilditch, R.W., Younger, F. and Fisher, W.A., 1975, Mem. R. astr. Soc. 79, 131

Hiltner, W.A., 1947, Ap. J. 106, 481

Hobbs, R.W., Kondo, Y. and Feibelman, W.A., 1978, Astron. J. 83, 1525

Hoffmann, M., 1978, IBVS No. 1489

Hoffmann, W.F. and Aannestad, P.A., 1974, NASA TMX-62, 367

Hoffmann, W.F., Frederick, C.L. and Emery, R.J., 1971, Ap. J. 170, L89

Horn, J., 1970, Ap. Space Sci. 6, 492

Horn, J., 1971, BAC 22, 37

Houk, N, 1978, "Michigan Spectral Catalogue" Vol. 2

Houk, N. and Cowley, A.P., 1975, "Michigan Spectral Catalogue" Vol. 1

Huang, S.-S., 1966, Sky and Telescope 31, 215

Huang, S.-S., 1973, BAAS 5, 41

Humphrey, J.N., 1965, Appl. Opt. 4, 665

Humphreys, R.M., 1976, Ap. J. 206, 122

Humphreys, R.M. and Ney, E.P., 1974a, Ap. J. 187, L75

Humphreys, R.M. and Ney, E.P., 1974b, Ap. J. 190, 339

Humphreys, R.M., Strecker, D.W. and Ney, E.P., 1971, Ap. J. 172, 75

Huth, H., 1959, MVS 424

Hyland, A.R. and Neugebauer, G., 1970, Ap. J. 160, L177

Hyland, A.R., Becklin, E.E., Neugebauer, G. and Wallerstein, G., 1969, Ap. J. 158, 619

Jakate, S.M., 1979, IBVS No. 1578

Jakate, S.M., 1980, IAU Symp. No. 88, p. 415

Jakate, S., Bakos, G.A., Fernie, J.D. and Heard, J.F., 1976, Astron. J. 81, 250

Jameson, R.F. and Longmore, A.J., 1976, MNRAS 174, 217

Jameson, R.F., Longmore, A.J., McLinn, J.A. and Woolf, N.J., 1974, Ap. J. 190, 353

Johnson, H.L., 1962, Ap. J. 135, 69

Johnson, H.L., 1964, Bol. Obs. Ton. Tacub. 3, 305

Johnson, H.L., 1965a, Ap. J. 141, 923

Johnson, H.L., 1965b, Commun. Lun. Plan. Lab. 3, 73

Johnson, H.L., 1966, Ann. Rev. Astron. Ap. 4, 193

Johnson, H.L. and Morgan, W.W., 1953, Ap. J. 117, 313

Johnson, H.L., Mitchell, R.I., Iriate, B. and Wisniewiski, W.Z., 1966, Commun. Lun. Plan. Lab. 4, 99

Johnson, H.L., MacArthur, J.W. and Mitchell, R.I., 1968, Ap. J. 152, 465

Jones, T.W. and O'Dell, S.L., 1977a, Ap.J. 214, 522

Jones, T.W. and O'Dell, S.L., 1977b, Ap. J. 215, 236

Jorden, P.R., Long, J.F., MacGregor, A.D. and Selby, M.J., 1976, Astron. Ap. 49, 421

Joy, A.H., 1941, Ap. J. 94, 407

Joy, A.H., 1942, PASP 54, 35

Kippenhahn, R., 1969, Astron. Ap. 3, 83

Kippenhahn, R. and Weigert, A., 1967, Z. Ap. 65, 251

Kippenhahn, R., Kohl, K. and Weigert, A., 1967, Z. Ap. 66, 58

Koch, R.H., Plavec, M. and Wood, F.B., 1970, PUPAS 10

Kopal, Z., 1955, Ann. Ap. 18, 379

Kraft, R.P., 1967, Ap. J. 150, 551

Kriz, S., 1968, BAC 19, 248

Kriz, S., 1969, BAC 20, 127

Kron, G.E., 1947, PASP 59, 261

Kron, G.E., 1952, Ap. J. 115, 301

Kruse, P.W., McGlauchlin, L.D. and McQuistan, R.B., "Elements of Infrared Technology", New York 1962

Krzeminski, W., 1969, "Low Luminosity Stars" p. 57, ed. S. Kumar

Kuiper, G.P., Wilson, W. and Cashman, R.J., 1947, Ap. J. 106, 243

Landis, H.J. and Hall, D.S., 1976, IBVS No. 1113

Landis, H.J., Lovell, L.P., Hall, D.S., Henry, G.W.and Renner, T.R., 1978, Astron. J. 83, 176

Lauterborn, D., 1970, Astron. Ap. 7, 150

Lee, T.A., 1970, Ap. J. 162, 217

Léna, P. 1978, "Infrared Astronomy" eds. G. Setti and G.G. Fazio, p. 231

Lesh, J.R. and Aizenman, M.L., 1978, Ann. Rev. Astron. Ap. 16, 215

Linden Van der, Th. J., 1980, IAU Symp. No. 88, p. 109

Linsky, J.L., Ayres, T.R., Basri, G.S., Morrison, N.D., Boggess, A., Schiffer, F.H., Holm, A., Casatella, A., Heck, A., Machetto, F., Strickland, D., Wilson, R., Blanco, G., Dupree, A.K., Jordan, C. and Wing, R.F., 1978, Nature 275 389

Lockwood, G.W., Dyck, H.M. and Ridgway, S.T., 1975, Ap. J. 195, 385

Low, F.J., 1961, JOSA 51, 1300

Low, F.J. and Johnson, H.L., 1964, Ap. J. 139, 1130

Low, F.J. and Krishna Swamy, K.S., 1970, Nature 227, 1333

Low, F.J. and Rieke, G.H., 1974, "Methods of Experimental Physics" 12[A], 415

Mendoza, E.E.V., 1966, Ap. J. 143, 1010

Mendoza, E.E.V., 1968, Ap. J. 151, 977

Milone, E.F., 1976, Ap. J. Supp. Ser. 31, 93

Montle, R.E., 1973, Master Thesis, Vanderbilt University

Morgan, J.G. and Eggleton, P.P., 1979, MNRAS 187, 661

Morton, D.C., 1960, Ap. J. 132, 146

Mullan, D.J., 1974, Ap. J. 187, 621

Mutel, R.L. and Weisberg, J.M., 1978, Astron. J. 83, 1499

Nations, H.L. and Ramsey, L.W., 1980, Astron. J. 85, 1086

Neugebauer, G. and Leighton, R.B., 1969, "The Two-Micron Sky Survey" NASA SP-3047

Neugebauer, G., Becklin, E.E. and Hyland, A.R., 1971, Ann. Rev. Astron. Ap. 9, 67

Nikulina, T.G., 1958, Astron. Circ., State University of Kazan (U.S. S.R.) 194, 26

Northcott, R.J. and Bakos, G.A., 1956, Astron. J. 61 188

Northcott, R.J. and Bakos, G.A., 1967, Astron. J. 72, 89

Okazaki, A., 1979, IBVS No. 1560

Oliver, J.P., 1974, Ph.D. thesis, University of California, Los Angeles

Oliver, J. 1974a, BAAS 6, 37

Owen, F.N., 1976, IAU Circ. 2929

Owen, F.N. and Gibson, D.M., 1978, Astron. J. 83, 1488

Owen, F.N., Jones, T.W. and Gibson, D.M., 1976, Ap. J. 210, L27

Paczynski, B. 1965, Acta Astron. 15, 89

Paczynski, B. 1966, Acta Astron. 16, 231

Paczynski, B., 1967, Comm. Obs. Roy. Belg, Uccle, Ser. B, No. 17, p. 111

Paczynski, B., 1971, Ann. Rev. Astron. Ap. 9, 183

Paczynski, B., 1973, IAU Symp. No. 49, p. 143

Panagia, N., 1974, "HII Regions and the Galactic Centre" Eighth ESLAB Symp. p. 163

Persson, S.E., Frogel, J.A. and Aaronson, M., 1976, Ap. J. 208, 753

Pettit, E. and Nicholson, S.B., 1928, Ap. J. 68, 279

Piazzi Smyth, C., 1858, Report on the Tenerife Astronomical Experiment of 1856, London 1858

Plaut, L., 1959, PASP 71, 167

Plavec, M., 1960, BAC 11, 152

Plavec, M., 1964, BAC 15, 165

Plavec, M., 1967, Comm. Obs. Roy. Belg., Uccle, Ser. B, No. 17, p. 111

Plavec, M., 1968, Adv. Astron. Ap. 6, 201

Plavec, M., 1970, "Stellar Rotation" ed. A. Slettebak, p. 133

Plavec, M. and Grygar, J., 1965, Kleine Veroff. Remeis Sternw. Bamberg 4, No. 40, p. 213

Plavec, M. and Smetanova, M., 1959, BAC 10, 192

Plavec, M., Smetanova, M. and Penky, Z., 1961, BAC 12, 117

Plavec, M., Kriz, S. and Horn, J., 1969, BAC 20, 41

Popper, D.M., 1969, BAAS 1, 257

Popper, D.M., 1970, IAU Colloq. No. 6, p. 13

Popper, D.M., 1976, IBVS No. 1083

Popper, D.M., 1977, "Highlights of Astronomy" Vol. 4, Part II, p. 397

Popper, D.M., 1978, Astron. J. 83, 1522

Popper, D.M. and Dumont, P.J., 1977, Astron. J. 82, 216

Popper, D.M. and Ulrich, R.K., 1977, Ap. J. 212, L131

Price, S.D., 1968, Astron. J. 73, 431

Price, S.D. and Walker, R.G., 1976, "The AFGL Four Color Infrared Sky Survey" AFGL-TR-76-0208

Refsdal, S. and Weigert, A., 1969, Astron. Ap. 1, 167

Rosse, 1869, "On the Radiation of Heat from the Moon", Proc. Roy. Soc. London 17, 436

Rydgren, A.E., Strom, S.E. and Strom, K.M., 1976, Ap. J. Supp. Ser. 30, 307

Ryle, M. 1976, IAU Circ. 2972

Sadik, A.R., 1979, Ap. Space Sci. 63, 319

Sahade, J., 1960, in "Stellar Atmospheres" (Stars and Stellar Systems VI), ed. J.L. Greenstein, p. 466, Chicago University Press

Schild, R., Peterson, D.M. and Oke, J.B., 1971, Ap. J. 166, 95

Schmitz, M., Brown, L.W., Mead, J.M. and Nagy, T.A., 1978, "Merged Infrared Catalogue" NASA-TM-79683

Skumanich, A., 1972, Ap. J. 171, 565

Smith, L.F., 1973, IAU Symp. No. 49, 228

Smyth, M.J. and Nandy, K., 1978, MNRAS 183, 215

Smyth, M.J., Stobie, R.S. and Shobbrook, R.R., 1975, MNRAS 171, 143

Soifer, B.T. and Pipher, J.L., 1978, Ann. Rev. Astron. Ap. 16, 335

Spangler, S.R., 1977, Astron. J. 82, 169

Spangler, S.R., Owen, F.N. and Hulse, R.A., 1977, Astron. J. 82, 989

Stein, W.A. and Gillett, F.C., 1969, Ap. J. 155, L197

Stobie, R.S. and Shobbrook, R.R., 1976, IAU Colloq. No. 29, Part II, p. 249

Stoy, R.H., 1963, MNASSA 22, 157

Strohmeier, W., 1967, IBVS No. 217

Strohmeier, W., Knigge, R., 1960, Veroff. Remeis-Sternw. Bamberg V (5)

Strohmeier, W. Knigge, R. and Ott, H., 1957, Kleine Veroff. Remeis-Sternw. Bamberg, No. 18

Strohmeier, W., Knigge, R. and Ott, H., 1965, IBVS No. 100

Strom, S.E., 1972, PASP 84, 745

Struve, O., 1946, Ann. Ap. 9, 1

Struve, O., 1950, "Stellar Evolution" (Princeton University Press) Chap. 3

Surendiranath, R., Vivekananda Rao, P. and Sarma, M.B.K., 1978, Acta Astron. 28, 231

Tassoul, J.-L., 1978, "Theory of Rotating Stars" (Princeton University Press)

Thomas, H.C., 1977, Ann. Rev. Astron. Ap. 15, 127

Thomas, J.A., Hyland, A.R. and Robinson, G., 1973, MNRAS 165, 201

Thomas, J.A., Robinson, G. and Hyland, A.R., 1976, MNRAS 174, 711

Torres, C.A.O., Ferraz Mello, S. and Quast, G.R., 1972, Ap. Letters 11, 13

Tsesevich, V.P., 1954, Izv. Astron. Obs. Odesskii gos. Univ., 4, 168

Tümer, O., Kurutac, M., Tunca, Z., Evren, S., Ertan, A.Y. and Ibanoglu, C., 1980, IBVS No. 1741

Underhill, A.B., 1968, An. Rev. Astron. Ap. 6, 39

Underhill, A.B., 1973, IAU Symp. No. 49, p.237

Valtier, J.C., 1972, Astron. Ap. 16, 38

van den Heuvel, E.P.J., 1976, IAU Symp. No. 73, p. 35

van den Heuvel, E.P.J., 1978, IAU Symp. No. 83, p. 491

Walker, R.G. and Price, S.D., 1975, AFCRL-TR-95-0373

Wallerstein, G., 1971, Ap. J. 166, 725

Walter, F., Charles, P. and Bowyer, S. 1978a, Ap. J. 225, L119

Walter, F., Charles, P. and Bowyer, S., 1978b, Nature, 274, 569

Walter, F., Charles, P. and Bowyer, S., 1978c, Astron. J. 83, 1539

Walter, F., Charles, P. Bowyer, S. and Garmire, G., 1978d, IAU Circ, No. 3173

Wehlau, W. and Leung, K.-C., 1964, Ap. J. 139, 843

Weiler, E.J., 1976, Ph.D. thesis, Northwestern University, Evanston, Illinois

Weiler, E.J., 1977, IAU Circ. No. 3089

Weiler, E.J., 1978a, MNRAS 182, 77

Weiler, E.J., 1978b, Astron. J. 83, 795

Weiler, E.J. and Stencel, R.E., 1979, Astron. J. 84, 1372

Weiler, E.J., Owen, F.N., Bopp, B.W., Schmitz, M., Hall, D.S., Fraquelli, D.A., Piirola, V., Ryle, M. and Gibson, D.M., 1978, Ap. J. 225, 919

White, N.E., Sanford, P.W. and Weiler, E.J., 1978, Nature, 274, 569

Williams, P.M., Beattie, D.H. and Stewart, J.M., 1976, Observatory, 96, 184

Williams, P.M., Beattie, D.H. and Stewart, J.M., 1977, Observatory, 97, 76

Williams, P.M., Beattie, D.H., Lee, T.J., Stewart, J.M. and Antonopoulou, E., 1978, MNRAS 185, 467

Williams, P.M., Adams, D.J., Arakaki, S., Beattie, D.H., Born, J., Lee, T.J., Robertson, D.J. and Stewart, J.M., 1980, MNRAS 192, 25P

Willner, S.P., 1976, Ap. J. 206, 728

Wilson, O.C., 1963, Ap. J. 138, 832

Wilson, O.C., 1964, PASP 76, 238

Wilson, O.C. and Skumanich, A., 1964, Ap. J. 140, 401

Wilson, O.C. and Woolley, R., 1970, MNRAS 148, 463

Wolf, C.J.E. and Rayet, G., 1867, Compt. Rend. Acad. Sci. Paris, 65, 292

Wolfe, W.L. and Zissis, G.J., 1978, "The Infrared Handbook", Washington DC 1978

Wood, F.B., Oliver, J.P., Florkowski, D.R. and Koch, R.H., 1980, "A Finding List for Observers of Interacting Binary Stars" Fifth Edition, University of Pennsylvania Press

Woolf, N.J., 1969, Ap. J. 157, L37

Woolf, N.J., 1973, IAU Symp. No. 52, p. 485

Woolf, N.J. and Ney, E.P., 1969, Ap. J. 155, L181

Woolf, N.J., Stein, W.A. and Strittmatter, P.A., 1970, Astron. Ap. 9, 252

Wright, A.E. and Barlow, M.J., 1975, MNRAS 170, 41

Wynn-Williams, C.G. and Becklin, E.E., 1974, PASP 86, 5

Wynn-Williams, C.G., 1977, IAU Symp. No. 75, p. 105

Wyse, A.B., 1934, Lick Obs. Bull. 17, 37

Ziółkowski, J., 1969, Ap. Space Sci. 3, 14

Ziółkowski, J., 1970, Acta Astron. 20, 213

ACKNOWLEDGMENTS

There are many people to whom I am indebted for their continual encouragement and assistance throughout the period of my research in Edinburgh. I would like to thank my supervisor Dr P.M. Williams for his help and for the initial suggestion of the subject of this thesis. To Prof. H. A. Brück, I extend special thanks for accepting me as a research student and for his support and aid. It is also a sincere pleasure to acknowledge the unwavering help and kindness of Dr M.J. Smyth and Dr M.T. Brück and the concern, faith and guidance of Mrs Mary Smyth who has been a real friend all the time I spent in Edinburgh.

Many others have been involved in many ways, and to them also I must express my special thanks; to Drs I.S. Glass, A.J. Longmore, R.S. Stobie, M. Tapia and Mr J. Harris; and to Mrs Alice Walkingshaw who typed this thesis.

I wish also to address my thanks to the Director and the staff of the South African Astronomical Observatory for being so helpful and hospitable during my observing runs at SAAO.

My thanks are also due to my director in Greece, Prof. G. Contopoulos, for his help, and also to Prof. D. Kotsakis, Prof. M. Moutsoulas and Dr C. Banos for being helpful and understanding.

I was supported while working on this project for one year by a grant from the British Council and for the rest of the time by a scholarship from the Hellenic Ministry of Coordination and Planning. I would also like to thank the PATT Committee for telescope time and the U.K. Science Research Council for travel and subsistence for the observing runs necessary for the observational material of this thesis.